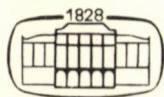


ACTA TECHNICA

ACADEMIAE SCIENTIARUM HUNGARICAE

EDITOR: P. MICHELBERGER

VOLUME 99
NUMBERS 1-2



AKADÉMIAI KIADÓ, BUDAPEST 1986

ACTA TECHN. HUNG.

ACTA TECHNICA

A JOURNAL OF THE HUNGARIAN ACADEMY OF SCIENCES

EDITORIAL BOARD

K. GÉHER, O. HALÁSZ, J. PROHÁSZKA, T. VÁMOS

MANAGING EDITORS

P. CSONKA, GY. CZEGLÉDI

Acta Technica publishes original papers, preliminary reports and reviews in English, which contribute to the advancement of engineering sciences.

Acta Technica is published by

AKADÉMIAI KIADÓ

Publishing House of the Hungarian Academy of Sciences
H-1450 Budapest, Alkotmány u. 21.

Subscription information

Orders should be addressed to

KULTURA Foreign Trading Company
H-1389 Budapest P.O. Box 149

or to its representatives abroad

Acta Technica is indexed in *Current Contents*

Acta Technica is abstracted/indexed in Applied Mechanics Reviews, Current Contents-Engineering, Technology and Applied Sciences, GeoRef Information System, Science Abstracts.

© Akadémiai Kiadó, Budapest

CONTENTS

<u>Barta, J.</u> : On the minimum of strain energy in elastostatics	3
<u>Chhangani, O.P.-Lenkei, P.</u> : Graphical presentation of compressive membrane action in one-way slabs	221
<u>Chhangani, O.P.-Lenkei, P.</u> : Short-time deflections of two-way slabs ..	233
<u>van Dac, Iran</u> : On the dynamics of a man-machine system	249
<u>Dulácska, E.</u> : The safety factor to be applied in shell buckling analysis	9
<u>Ecsedi, I.</u> : Some comments on the twist problem of shells of circular-arc centreline	31
<u>Ecsedi, I.</u> : Torsion of a thin-walled, anisotropic, bent rod of circular-arc centreline	65
<u>Ecsedi, I.</u> : Bounds of the numerical value of rotational flexibility ..	273
<u>Füzy, J.</u> : Simulation of the timber lattice shell without "in-plane" shear capacity by double-layer cosserat surface	287
<u>Gáspár, L.</u> : State conservation of highways	77
<u>Györgyi, J.</u> : Calculation for the vibration of structures: a partial eigenvector problem solution	103
<u>Hankó, Z.</u> : Qualification of interdependence or independence within any pair of variables involved in multiple linear regression	125
<u>Kalischky, S.-Knébel, I.</u> : Optimum design of plastic bar structures for shakedown and dynamic loading	297
<u>Kämpfe, B.-Michel, B.</u> : A new approach to X-ray diffraction analysis of stress states in surface layers	313
<u>Kollár, L.P.</u> : Buckling analysis of coupled shear walls by the multi-layer sandwich model	317
<u>Matsikoudi-Iliopoulou, M.</u> : Elastic membranes reinforced by cords: non-linear axisymmetric deformation with twist	147

<u>Paláncz, B.:</u> Analysis of a closed circuit cryogenic wind-tunnel	163
<u>Reményi, K.:</u> Use of low-grade coal as fuel of power plans	193
<u>Risteski, Ice B.:</u> Mathematical method for determination of thermal contact resistance between solidifying metal and mold	333
<u>Szidarovszky, J.:</u> The analysis of single-cell box beams by the hinged model	349
<u>Szidarovszky, J.:</u> Cross sectional characteristics of single-cell box beams with a cross section of rectangular elements	383
<u>Szidarovszky, J.:</u> Relationship between Saint-Venant's principle and Bernoulli-Navier's theorem as well as Bredt's formulae and warping	397
<u>Vásárhelyi, A.-Lógó, J.:</u> Design of steel frames by multicriterion optimization	413

BOOK REVIEWS

<u>Franz, G. (editor):</u> Beton-Kalender 1986	215
<u>Horváth, K.Z.:</u> The selection of load-bearing structures for buildings	419
<u>Herpy, M.-Berka, J.C.:</u> Active RC filter design	217
<u>Joan, A.:</u> Cavitatia II.	216
<u>Márkus, Gy.:</u> Kreis- und Kreisringplatten unter periodischer Belastung	420
<u>Reinelt, G.:</u> 'The Linear Ordering Problem: Algorithms and Applications'	421
<u>Vértes, Gy.:</u> Structural Dynamics	422
<u>Wischers, B. (editor):</u> Reports on concrete technics 1984/95	218

CONTENTS

<u>Barta, J.:</u> On the minimum of strain energy in elastostatics	3
<u>Dulácska, E.:</u> The safety factor to be applied in shell buckling analysis	9
<u>Ecsedi, I.:</u> Some comments on the twist problem of shells of circular-arc centreline	31
<u>Ecsedi, I.:</u> Torsion of a thin-walled, anisotropic, bent rod of circular-arc centreline	65
<u>Gáspár, L.:</u> State conservation of highways	77
<u>Györgyi, J.:</u> Calculation for the vibration of structures: a partial eigenvector problem solution	103
<u>Hankó, Z.:</u> Qualification of interdependence or independence within any pair of variables involved in multiple linear regression	125
<u>Matsikoudi-Iliopoulou, M.:</u> Elastic membranes reinforced by cords: non-linear axisymmetric deformation with twist	147
<u>Paláncz, B.:</u> Analysis of a closed circuit cryogenic wind-tunnel	163
<u>Reményi, K.:</u> Use of low-grade coal as fuel of power plants.....	193

BOOK REVIEWS

<u>Franz, G. (editor):</u> Beton-Kalender 1986 (P. Csonka)	215
<u>Joan, A.:</u> Cavitatia II. (J.J. Varga)	216
<u>Herpy, M.—Berka, J.C.:</u> Active RC filter design (K. Géher)	217
<u>Wischers, B. (editor):</u> Betontechnische Berichte 1984/85 (T. Gyengő) ..	218

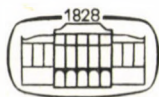
PRINTED IN HUNGARY
Akadémiai Kiadó és Nyomda, Budapest

ACTA TECHNICA

ACADEMIAE SCIENTIARUM HUNGARICAE

EDITOR: P. MICHELBERGER

VOLUME 99



AKADÉMIAI KIADÓ, BUDAPEST 1986

ON THE MINIMUM OF STRAIN ENERGY IN ELASTOSTATICS

J. Barta*

(Received 28 May 1985)

This paper deals with the equilibrium of a body in case the stress-strain state is caused by active forces applied at given points. It is proved that, considering statically equivalent active forces, minimum strain energy is associated with the values of active forces which result in displacement of the application points as if the motion taking place were that of a rigid body.

Discussed in the paper are two theorems, theorem I of I. Ecsedi [1], and theorem II which is a generalisation of theorem I. The purpose of the present paper is to prove theorem II.

The usual assumptions of elastostatics are accepted. It is assumed that only statical effects arise, that is, neither dynamical nor thermal effects take place. The structure assumed to be is free from initial stresses (supposition α). Assumed are also linear elasticity, and the validity of the principle of superposition.

Let us consider an elastic bar (Fig. 1) of a circular cross-section of variable diameter. The material of the bar is homogeneous and isotropic. The bar has a built-in lower end preventing the cross-section of the lower end from displacing in any direction, while the upper end is free, and is subjected to distributed axisymmetric active forces of intensity $\tau(r)$ in the upper end cross-section. We stipulate that these active forces be statically equivalent to a given torque M . Now, according to

Theorem I: The minimum strain energy of the bar (Fig 1) is associated with active forces $\tau(r)$ which result in rotation of the upper end cross-section as a rigid body. (As a result of axisymmetry, this rotation takes place around the bar axis).

Now, let us consider an elastic body (Fig. 2) for ex. bar, plate, truss, frame, continuous body. Frictionless joints and rigid supports prevent the body from moving. The supporting forces do not work. The body and its support are statically determinate or statically indeterminate. The material of

*J. Barta, H-1085 Budapest, József körút 35, Hungary

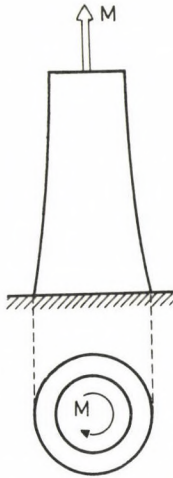


Fig. 1. Torsion of the bar

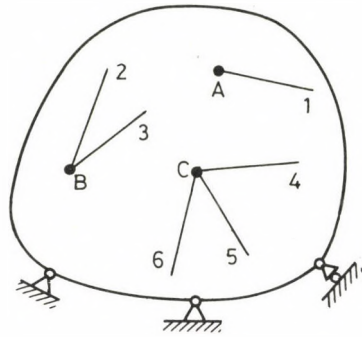


Fig. 2. Application points and action lines of the active forces

the body is homogeneous or heterogeneous, and isotropic or anisotropic. A, B, are given points of the body and are the application points of the active forces. The magnitude of the active forces is denoted by F_1, \dots, F_n . As to the directions of active forces, we distinguish the cases

- (a) the action line of the active force is determined, for ex. in point A of Fig. 2, or
- (b) the action plane of the active force is determined by two directions, for ex. in point B of Fig. 2, or
- (c) the direction of the active force is not determined and three non-complanar directions are therefore used, for ex. in point C of Fig. 2.

We stipulate that the active forces be statically equivalent to the combination of a given force R and a given torque M (stipulation β). It is assumed that stipulation β can be fulfilled*. Then the following theorem holds.

Theorem II: The minimum strain energy of the body (Fig 2). is associated with values F_1, \dots, F_n of active forces for which the displacements of points A, B, ... are such as if points A, B, ... were points of a rigid body.

*It is easy to examine for given R, M, A, B, \dots whether or not stipulation β can be fulfilled. Description of such an examination seems to be superfluous in this paper.

STRAIN ENERGY IN ELASTOSTATICS

Proof of theorem II. From among cases a, b, c case a will be considered for the time being. In the proof, F_1, \dots, F_n are written instead of A, B, The body is characterized by influence numbers

$$\begin{matrix} a_{11}, \dots, a_{1m}, \\ \dots\dots\dots \\ a_{n1}, \dots, a_{nn}. \end{matrix} \tag{1}$$

Explanation: \underline{d}_i is the displacement vector of application point P_i . d_i is the component of \underline{d}_i in direction i , (Fig. 3). a_{ij} is the value of d_i for $F_j = 1$. Directions $1, \dots, n$ determine unit vectors $\underline{u}_1, \dots, \underline{u}_n$. Therefore, products $\underline{u}_1 F_1, \dots, \underline{u}_n F_n$ are equal to the vectors of active forces. Equation

$$a_{i1} F_1 + \dots + a_{in} F_n = d_i \tag{2}$$

expresses a fundamental property of influence numbers. Instead of (2)

$$a_{i1} F_1 + \dots + a_{in} F_n = \underline{d}_i \underline{u}_i \tag{3}$$

can be written. We denote the strain energy of the body by U . Formula

$$\begin{aligned} U = \frac{1}{2} F_1 (a_{11} F_1 + \dots + a_{1n} F_n) \\ \dots\dots\dots \\ + F_n (a_{n1} F_1 + \dots + a_{nn} F_n) \end{aligned} \tag{4}$$

is well known. Stipulation β yields equations

$$\begin{aligned} \phi_1 \equiv R - \underline{u}_1 F_1 - \dots - \underline{u}_n F_n = D, \\ \phi_2 \equiv M - \underline{r}_1 \times \underline{u}_1 F_1 - \dots - \underline{r}_n \times \underline{u}_n F_n = D. \end{aligned} \tag{5}$$

Magnitudes F_1, \dots, F_n have to be chosen in such a way that the strain energy expression (4) will be minimum. At the same time, equation (5) has to be satisfied. Thus the problem is to find a relative minimum.

According to the rule of finding a relative minimum we use function

$$\Phi = U + \lambda_1 \phi_1 + \lambda_2 \phi_2 \tag{6}$$

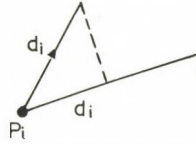


Fig. 3. The displacement vector and its component in given direction

Vectors $\underline{\lambda}_1$ and $\underline{\lambda}_2$ are Lagrange's multipliers. Equations

$$\frac{\delta \Phi}{\delta F_i} = 0 \quad (i=1, \dots, n) \quad (7)$$

read in detail

$$a_{i1}F_1 + \dots + a_{in}F_n - \underline{\lambda}_1 u_i - \underline{\lambda}_2 (\underline{r}_i \times \underline{u}_i), \quad (i=1, \dots, n) \quad (8)$$

Taking into account relation (3) and the rule of mixed product of vectors, we obtain from (8) equations

$$\underline{d}_i u_i - \underline{\lambda}_1 u_i - (\underline{\lambda}_2 \times \underline{r}_i) u_i = 0, \quad (i=1, \dots, n) \quad (9)$$

that is

$$(\underline{d}_i - \underline{\lambda}_1 - \underline{\lambda}_2 \times \underline{r}_i) u_i = 0. \quad (i=1, \dots, n) \quad (10)$$

Equations (10) are fulfilled if

$$\underline{d}_i = \underline{\lambda}_1 + \underline{\lambda}_2 \times \underline{r}_i, \quad (i=1, \dots, n) \quad (11)$$

or

$$(\underline{d}_i - \underline{\lambda}_1 - \underline{\lambda}_2 \times \underline{r}_i) \perp \underline{u}_i, \quad (i=1, \dots, n) \quad (12)$$

Let us follow now the calculation process of relative minimum. Equations (8) and (5) serve for calculating unknowns $F_1, \dots, F_n, \underline{\lambda}_1, \underline{\lambda}_2$. Thus we have n scalar equations and two vector equations. Therefore, equations (8) and (5) include $n+6$ scalar equations with $n+6$ scalar unknowns. After calculating unknowns $F_1, \dots, F_n, \underline{\lambda}_1, \underline{\lambda}_2$, we consider equations (11) and (12). Figs 4 and 5 illustrate relations (11) and (12). \underline{J} is the plane passing

STRAIN ENERGY IN ELASTOSTATICS

through point P_i , perpendicular to direction i . As shown in Figs 4 and 5 (11) allow only one relative minimum while (12) allows more relative minima. Since Fig. 5 comprises Fig. 4, and since the unicity of solution $F_1, \dots, F_n, \lambda_1, \lambda_2$ (as a result of supposition α) is valid, it is possible to use only (11) from among both equations (11) and (12).

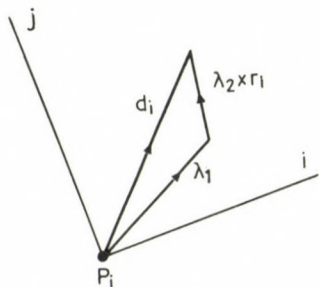


Fig. 4. Relation (11)

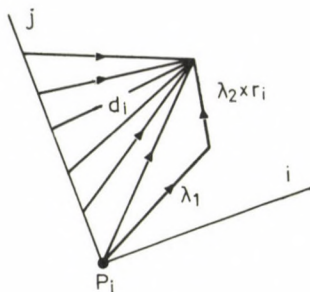


Fig. 5. Relation (12)

According to the rule known from literature, "the necessary and sufficient condition that displacements d_1, \dots, d_n of points P_1, \dots, P_n be such as if points P_1, \dots, P_n were points of a rigid body, is the existence of two vectors d_0 and $\underline{\omega}$ by means of which

$$\underline{d}_i = \underline{d}_0 + \underline{\omega} \times \underline{r}_i, \quad (i=1, \dots, n) \quad (13)$$

can be written". Comparing (13) with (11) it can be seen that $\underline{d}_0 = \underline{\lambda}_1$ and $\underline{\omega} = \underline{\lambda}_2$ are much two vectors. Thus, we have a relative extreme in case a. This relative extreme is a relative minimum since (4) is a positive quadratic form. With this, theorem II is proved for case a. Cases b and c need not be proved since b and c are comprised in a.

Example. Let us consider the torsion problem of a bar with square cross-section. For the sake of comparison two rigorous solutions of torsion problem (Figs 6 and 7) are presented.

A. rigorous solution (Fig. 6) is the classic solution [2]. Here only shear stresses exist in each cross section with the cross sections warping, and the distribution of M is uniform in each cross section.

Another rigorous solution (Fig. 7) comes from theorem II. In this case, the cross-section of the lower end is clamped, all the points of the cross-section of the upper end are considered as given points of applica-

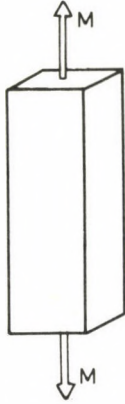


Fig. 6. The lower end cross-section can warp unimpededly

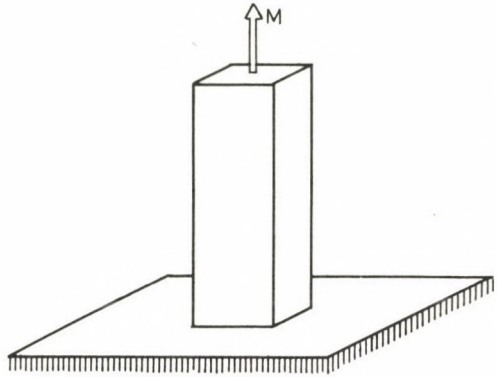


Fig. 7. The lower end cross-section is clamped

tion of active forces, and $R = 0$ is stipulated. Here the upper end cross-section experiences no deformation. Although $R = 0$, normal stresses exist in the upper end cross-section.

REFERENCES

1. Ecsedi, I.: A comment on the torsion of bars having a circular cross-section of variable diameter. *Acta Techn. Hung.* 95 (1982), 13-19.
2. See for ex.: Sokolnikoff, I.S. *Mathematical Theory of Elasticity*, First Ed., McGraw-Hill, New York, London 1946, 149.

THE SAFETY FACTOR TO BE APPLIED IN SHELL BUCKLING ANALYSIS

E. Dulácska*

(Received 3 September 1985)

The paper deals with the necessary safety factor against buckling of shell structures. Using probability theory in an approximate way we propose safety factors for both elastic buckling and failure, and, provide a simplified method of analysis, suggesting a unique safety factor. We also evaluate the values of the safety factors according to the principles of various building codes.

1. INTRODUCTION

In our previous paper /1/ we briefly dealt with the safety factor to be used in buckling analysis of reinforced concrete shells. As we have promised there, we investigate now the problem of the safety factor in shell buckling in general.

The necessary safety of a structure can be achieved in several ways: we can use a unique or a split safety factor. In addition, the level of safety can also be different. The codes of practice of the different countries regulate the required safety in various ways.

In the present paper we recommend a safety factor which is different for elastic buckling and for failure without buckling, but which can be reduced into a unique safety factor. We investigate the values of the safety factors on the basis of the Hungarian (MSz) and German (DIN) codes, and on the basis of the recommendations of CEB and ACI. Finally, we compare the safety of several erected shell domes with the safety factors proposed in the present paper.

2. PRINCIPLES OF DETERMINATION OF THE SAFETY FACTOR

The safety factor

$$\gamma = \frac{P_{CR}}{P} \quad (1)$$

*Dr.Dulácska Endre, H-1022 Budapest, Kitaibel Pál u. 12, Hungary

determining the safety with respect to critical load, depends

- on the accuracy of the theory used in computing the critical load;
- on sudden or gradual character of buckling (decreasing, increasing or constant post-critical load bearing capacity);
- on deviations between theoretical model and actual shell in
 - material quality,
 - material characteristics,
 - load values,
 - dimensions and
 - shape;
- on the standard deviation of these effects and on the simultaneity and coincidence of these effects and standard deviations; and, finally,
- on the risk that we are willing to take with respect to failure.

All these effects manifest themselves in different ways in the determination of elastic critical load $p_{cr,el}$ and in the determination of plastic failure load p_{pl} . On the one hand, the variation of the radius of curvature R due to initial geometric imperfections influences elastic critical load $p_{cr,el}$ according to law $1/R^2$, since this expression appears in the formula for the critical load of a perfect sphere, while it influences the plastic failure load according to $1/R$, since $p_{pl} = 2 \eta_{pl}/R$. On the other hand, we have shown in our paper /2/ that the plastic failure load always has a decreasing character as a function of displacement w , while the elastic postcritical load bearing capacity can have an increasing character, as well as is the case with hyper shells supported along their straight generatrices /3/.

Due to these circumstances, we obtain two different safety factors, γ_{el} and γ_{pl} , for the elastic critical load and for the plastic failure load respectively. With the aid of these we can write the critical limit load, $p_{cr,H}$, using e.g. the "ellipse of Dunkerley" as suggested in /2/, as follows:

$$\left(\frac{p_{cr,H} \cdot \gamma_{el}}{p_{cr,el}^{upper}} \right)^2 + \left(\frac{p_{cr,H} \cdot \gamma_{pl}}{p_{pl}} \right)^2 = 1. \quad (2)$$

Expressing $p_{cr,H}$ we obtain:

THE SAFETY FACTOR TO BE APPLIED IN SHELL BUCKLING ANALYSIS

$$P_{cr,H} = \frac{p_{cr,el}^{upper}}{\gamma_{el}} \sqrt{\frac{1}{1 + \left(\frac{\gamma_{pl}}{\gamma_{el}} \frac{p_{cr,el}^{upper}}{p_{pl}} \right)^2}} \quad (3)$$

Using the "parabole of Dunkerley" we arrive at

$$\frac{P_{cr,H} \cdot \gamma_{el}}{p_{cr,el}^{upper}} + \left(\frac{P_{cr,H} \cdot \gamma_{pl}}{p_{pl}} \right)^2 = 1, \quad (4)$$

from which

$$P_{cr,H} = \frac{p_{cr,el}^{upper}}{\gamma_{el}} \left[\sqrt{\frac{1}{4} A^4 + A^2} - \frac{1}{2} A^2 \right], \quad (5)$$

where

$$A = \frac{\gamma_{el}}{\gamma_{pl}} \cdot \frac{p_{pl}}{p_{cr,el}^{upper}}$$

In the above formulas $p_{cr,el}^{upper}$ denotes the upper, i.e. "snapping" critical load of the shell considered as elastic in the case of given (or assumed) initial imperfection w_0 , which has to be determined, in case of reinforced concrete shells, taking cracks and reinforcement into consideration, and w_0 is the mean value of the imperfection amplitudes $1/l$.

It is possible, for the sake of simplicity, to use a unique safety factor $\gamma_{el,pl}$, but this will provide a transition to the failure without buckling with some approximations only.

The safety of a shell against buckling can be kept on an appropriate level in the simplest way if we take the most onerous, extreme value of every effect, determine the critical load with the aid of these values, and reduce it by the safety factor. This method, which may be called the multiplication of partial safeties, is certainly safe but uneconomical, because it does not take into consideration that, as a rule, the most onerous values of the various effects do not appear simultaneously.

Another possibility is to exactly or approximately apply the rules of probability theory /4/, /5/, /6/. We choose this method in the present paper. However, we have to check the evaluations of the probability theory

by the safety value to be computed from practical data. That is, the methods of the probability theory yield appropriate results in case of a great number of events, but failure of shells by buckling cannot, by any standard, be considered as a mass event, because every individual shell has to have a sufficient degree of safety. Hence, in addition to the evaluation of material qualities and model tests, we are compelled to make certain estimates when assuming the various parameters. The correctness of these estimated values can be checked by comparing our computed safety factor to that derived from the data of erected structures which show no sign of failure.

In applying the probability theory, we assume that the individual random variables are independent of each other, so that we have to deal with one-dimensional distributions, and can use the rule of addition of the variances (the variance law). It follows from this principle that the resultant standard deviation is smaller than that obtained by leaving out the standard deviation of one variable of the computation of the resultant standard deviation and adding it separately to the latter one. So, for example, if we denote the resultant coefficient of variation by v_R , we have

$$v_1 + \sqrt{v_2^2 + v_3^2} \geq \sqrt{v_1^2 + v_2^2 + v_3^2} = v_R.$$

We follow this rule in determining the material characteristics. That is, we determined the characteristic or nominal values by the national codes, as lower fractile from the mean values with the aid of the standard deviation, taking a certain frequency into account. In stability analysis we use these nominal values of the material characteristics. In our investigations we use the random deviations with respect to these values, which are certainly independent of each other.

We assume that the distribution of every random variable has one peak and that their skewness can be neglected. Consequently, they can be replaced by the normal distribution. This represents the roughest approximation in case of meteorological loads (snow, wind). However, their most onerous values are set by the various codes, and by so doing they more or less consider their skewness as well. We only use these determined values here.

Let us check by a rough comparison how the normal distribution approximates a skew one. Let the frequency function be a triangle with variable angles, as shown in Fig. 1, and let us determine the 2.5 % and 97.5 % fractile from the triangular and from the normal distribution.

THE SAFETY FACTOR TO BE APPLIED IN SHELL BUCKLING ANALYSIS

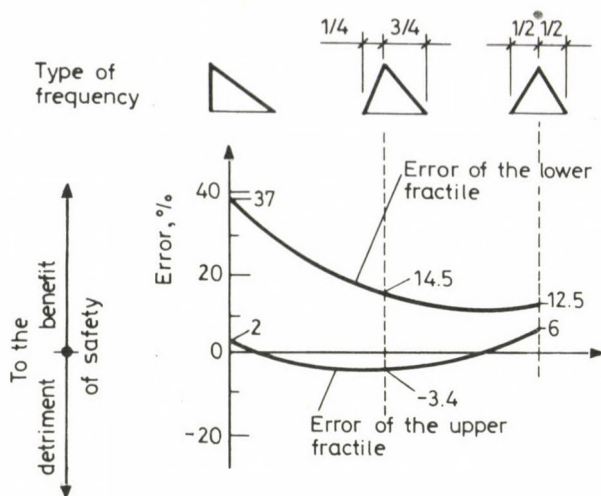


Fig. 1. Error caused by the skewness of distribution

We have plotted the results in Fig. 1. It can be seen that the error in the upper fractiles (loads) is negligibly small. In the lower fractiles (resistances) the error is greater, but always lies on the safe side. Moreover, the central limit theorem of the probability theory states that the distribution of the sum of several non-normal distributions rapidly approaches the normal distribution. Consequently, we can safely use the normal distribution.

Summing up, we can compute the characteristic value of critical load, to be used in design, by subtracting the resultant standard deviation multiplied by α from the mean value of experimental results, or from the critical load computed from the mean values of the resistances.

Here α is a numerical value depending on the quantile belonging to the risk taken. If we accepted a quantile of order 2.5 %, we can take

$\alpha = 2.0$ provided we had a sufficiently large number of samples.

The safety factor can thus be computed from expression

$$\gamma = \frac{\gamma_0}{1 - \alpha \nu_R} \quad (6)$$

Here γ_0 denotes the level of safety which has to account for accessory effects not taken into consideration, for small errors in computation, and,

moreover, for the fact that the required level of safety is higher than that of the level of the nominal value and, consequently, the upper and lower characteristic values of loads and resistances, respectively, have to be shifted apart from each other. Adding these partial safeties together as vectors, we obtain in the Hungarian code of practice $\gamma_0 = 1.1$, in ACI and in CEB Recommendation 1.12 and 1.16 respectively, and in DIN 1.25, as we shall see later. If we use an approximate computation model or an approximate way of analysis, we shall increase the value of γ_0 .

In case of elastic buckling the resultant coefficient of variation, v_R shall be computed from the sum of squares of coefficient of variations as follows:

$$v_R^{el} = \sqrt{v_{load}^2 + v_E^2 + v_\phi^2 + v_{cr}^2} \quad (7)$$

Here v_{load} is the coefficient of variation of average load;

v_E is the coefficient of variation of critical load of concrete or plastic shells, taking the dispersion of modulus of elasticity E beyond the limit of nominal strength. Since the critical load is linearly proportional to E , v_E is, in fact, the coefficient of variation of E ;

v_ϕ is the coefficient of variation of critical load due to the coefficient of variation of modulus of creep ϕ of the shell material;

v_{cr} is the coefficient of variation of critical load due to the change in the radius of curvature R caused by the coefficient of variation of imperfection amplitude w_0 .

3. ESTIMATE OF THE COEFFICIENTS OF VARIATION

Estimate of the coefficients of variation of load and of plastic failure load of the structure, v_{load} and v_{pl} , respectively

In case of failure without buckling the resultant coefficient of variation becomes:

$$v_R^{pl} = \sqrt{v_{load}^2 + v_{pl}^2} \quad (8)$$

Let us determine the component coefficients of variation using the

THE SAFETY FACTOR TO BE APPLIED IN SHELL BUCKLING ANALYSIS

principles of the Hungarian building code /7/.

The safety factor of the dead load of thin concrete structures is $\gamma_{\text{dead}} = 1.2$, that of the service load is $\gamma_{\text{serv}} = 1.3$. On the average we can take $\gamma_{\text{load}} = 1.25$. Since we can write

$$\gamma_{\text{load}} = \frac{1}{1-2 v_{\text{load}}} = 1.25,$$

from this relation we can compute the coefficient of variation of the average load:

$$v_{\text{load}} = 0.1 \quad . \quad (9)$$

The safety factor (i.e. the ratio of mean strength to nominal or characteristic strength) of steel material is $\gamma_{\text{steel}} = 1.2$, that of concrete is 1.4. Since failure mainly depends on reinforcement, we may take the average safety factor of reinforced concrete material as $\gamma_{\text{material}} = 1.25$, i.e. closer to that of steel.

From the formula

$$\gamma_{\text{material}} = \frac{1}{1-2 v_{\text{pl}}} = 1.25$$

we can determine the coefficient of variation of the material, i.e. of plastic failure as

$$v_{\text{pl}} = 0.1 \quad . \quad (10)$$

Applying Eq./6/ to the failure without buckling we can write

$$\gamma_{\text{pl}} = \frac{\gamma_0}{1-2 \sqrt{v_{\text{load}}^2 + v_{\text{pl}}^2}} = \gamma_{\text{material}} \quad \gamma_{\text{load}} = 1.35,$$

from which we obtain

$$\gamma_0 = 1.1 \quad . \quad (11)$$

Estimate of the excess coefficient of variation of the modulus of elasticity, v_E

The results of several thousand measurements of EMPA /11/ are very suitable for assessing the coefficient of variation of v_E , since the formulas for computing the modulus of elasticity are also based on these data. The limit curves and the data to be used can be seen in Fig. 2.

According to the Hungarian building code /7/, the nominal strength of concrete, $f'_{c,min}$, is 70 % of the mean strength, f'_c . We thus can write

$$\gamma_{\text{concrete}} = \frac{1}{1-2 v_{\text{concrete}}} = \frac{1}{0.7} \approx 1.4,$$

from which $v_{\text{concrete}} = 0.15$ is obtained.

Hence the ratio of the nominal cylinder strength, $f'_{c,min}$ to the mean strength, f'_c is also 0.7, i.e.: $f'_{c,min} = 0.7 f'_c$.

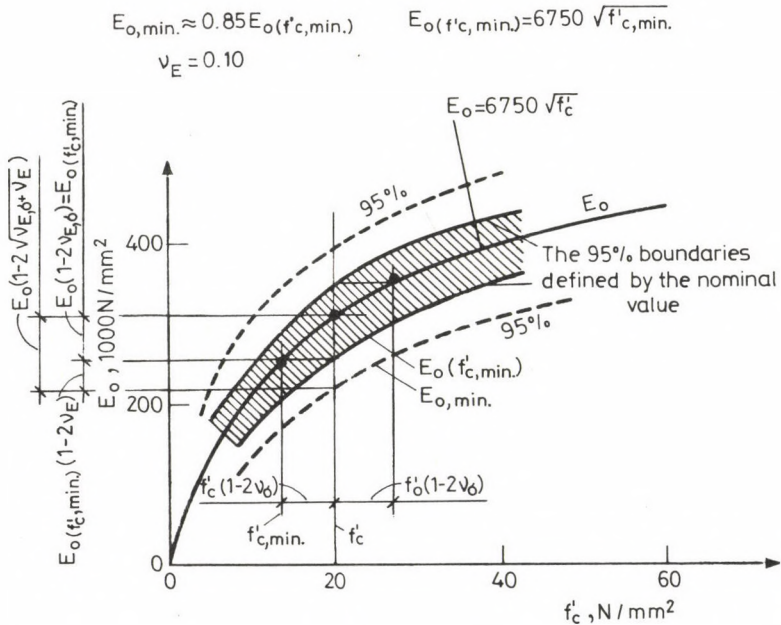


Fig. 2. Estimate of the excess coefficient of variation caused by the coefficient of variation of the modulus of elasticity

THE SAFETY FACTOR TO BE APPLIED IN SHELL BUCKLING ANALYSIS

Thus from formulas for E_0 , given in Fig. 2, the curve of $E_0(f'_{c,min})$ can be determined and plotted as shown in the figure.

Reading the data of the figure we have

$$\frac{E_0(f'_{c,min})}{E_0} \approx 0.86 = 1 - 2 v_{E,\sigma},$$

from which

$$v_{E,\sigma} = 0.07.$$

We can also read off the figure that

$$\frac{E_{0,min}}{E_0} \approx 0.75 = 1 - 2 \sqrt{v_{E,\sigma}^2 + v_E^2}.$$

This yields for the excess coefficient of variation the value

$$v_E = \sqrt{\left(\frac{1 - 0.75}{2}\right)^2 - 0.07^2} = 0.104 \approx 0.1 \quad (12)$$

Estimate of the coefficient of variation of creep, v_ϕ

Vandepitte et al. performed a great number of experiments to explore the influence of the creep of concrete on the critical load of shell domes /12/. From the creeping models they obtained a coefficient of variation $v_{\phi,exp} = 0.20$, while from the quick loading experiments, where creep played no role, they found

$$v_{\phi,exp} = \frac{0.150 + 0.085}{2} \approx 0.12$$

as an average coefficient of variation.

Since we can write

$$v_{\phi,exp} = \sqrt{v_{exp}^2 + v_\phi^2}$$

we have

$$v_\phi = \sqrt{v_{\phi,exp}^2 - v_{exp}^2} = \sqrt{0.20^2 - 0.12^2} \approx 0.16 \quad (13)$$

Estimate of the coefficient of variation of the elastic critical load, v_{cr}

Stability investigations for cylindrical and spherical shells with snap-through character have been made by several researches on metal models. We evaluated their results several years ago /13/ and obtained a coefficient of variation of $v_{exp} = 0.30$. We now revised this result and found that it was unrealistically high. The reason for this is that we also took into account the critical loads of shells that had such a high R/h-ratio (radius of curvature to shell thickness) which certainly would not occur in practice, and, moreover, we computed the coefficient of variation without regression, so that the decreasing trend of the critical load with an increasing ratio R/h also appeared as coefficient of variation.

We think that shells with $R/h > 1300$ do not occur in practice. On the other hand, plasticity reduces the critical load if $R/t < 300$. We could not evaluate this latter effect due to incomplete experimental data so that this regular (systematic) deviation of the experimental results also appeared as a coefficient of variation. We thus proceeded in the new evaluation in the following way:

We evaluated the experiments in the range of $300 < R/h < 1300$. Here we divided the experimental results by the values of the regression curve,

$$\frac{\rho_{cr,el}^{upper}}{\rho_{cr}^{lin}} = \rho_{hom} = \frac{1}{1 + \sqrt{3} \frac{R}{1000h}}$$

for all the experiments. (Here ρ_{cr}^{lin} is the "classical" critical load of shells, determined by the linear buckling theory.)

We then computed the coefficient of variation of the values thus obtained, separately for every researcher's model tests. (These values lay around 1.0.) We only evaluated test series on more than 10 models. From among the coefficients of variation obtained in this way we considered the highest one to be relevant. We compiled the results in Table I. So, finally, we took value

$$v_{cr} = 0.23 \quad (14)$$

THE SAFETY FACTOR TO BE APPLIED IN SHELL BUCKLING ANALYSIS

for the coefficient of variation of the elastic critical load.

Table 1. Standard deviations of shell model tests

Kind of shell	Reference	Researcher	No. of models	R/h	Relative standard deviation
Cylindrical shells	/13/	Lundquist	29	650- 900	0.172
		Weingarten-Morgan Seide	24	500-1000	0.226
		Kanemitsu-Nojima	19	760-1250	0.210
		Harris-Sver-Skene -Benjamin	20	400- 800	0.192
Domes	/13/	Litle	23	500- 800	0.113
		Seaman	20	500-1200	0.203
		Klöppel-Jungbluth	35	300-1300	0.234

Explanation of the comparatively high value of the coefficient of variation of the elastic critical load of shells, v_{cr}

In model tests, the critical load computed from wall thickness h , modulus of elasticity E , and the actual strength are compared with the experimental critical load. Since all these data are actually measured values, their coefficients of variation are small, and do not account for the great coefficient of variation of the critical load. Indeed, we neglected these coefficients of variation in our investigation. On the other hand, initial imperfections influence the radius of curvature, R , according to relation

$$R = \frac{l_0^2}{8/f_0 + w_0/}$$

Here l_0 is the buckling length, f_0 is the rise of the shell on length l_0 , computed from planned radius of curvature R_0 , and w_0 is the maximum amplitude of the initial imperfection.

Evaluation of the various theoretical investigations shows that f_0 is inferior to the wall thickness. Consequently, $w_0 = h$ can already mean a plane point on the shell. According to theoretical investigations, the critical load hardly depends on the buckling length of imperfection, but de-

pendes essentially on w_0 . Hence we shall investigate the influence of w_0 only.

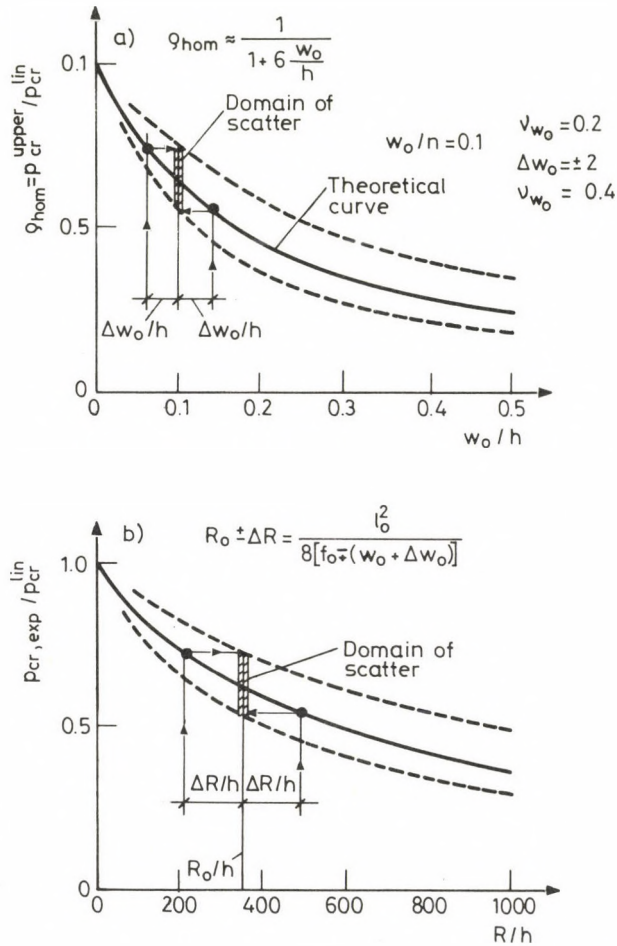


Fig. 3. How the scatter of imperfection causes scatter of the critical load

We plotted in Fig. 3a a curve ρ_{hom} , which approximated the theoretical results. If w_0 deviated from the calculated value, we shift to the right or to the left along the curve by value Δw_0 . Thus a smaller or greater w_0 and, correspondingly, a greater or smaller critical load becomes possible. If we refer these values to the original w_0 , and project them to the vertical line corresponding to w_0 , they appear as coefficient of variation of the critical load.

THE SAFETY FACTOR TO BE APPLIED IN SHELL BUCKLING ANALYSIS

The situation will be similar when evaluating test results, if we plot the critical load as a function of R/h . Here w_0 causes R to change by ΔR , which changes also the critical load. Referring these changes to the original R_0 , i.e. projecting them into the vertical line passing through R_0 , results in the coefficient of variation of the critical load.

4. THE SAFETY FACTORS OF SHELLS WITH SNAP-THROUGH CHARACTER

The proposed values of the safety factors

The data to be used for calculating the safety factor have been obtained previously as $\gamma_0 = 1.1$; $\alpha = 2.0$; $v_{load} = 0.1$; $v_{pl} = 0.1$; $v_\phi = 0.16$; $v_{cr} = 0.23$.

The safety factor of failure without buckling will be for reinforced concrete and metal shells, taking Eqs/6/ and /8/ into consideration:

$$\gamma_{pl} = \frac{\gamma_0}{1 - 2\sqrt{v_{load}^2 + v_{pl}^2}} = 1.55 \quad (15)$$

We obtain for the safety factor of elastic buckling, in case of reinforced concrete shells, from Eqs/6/ and /7/:

$$\gamma_{el}^{concrete} = \frac{\gamma_0}{1 - 2\sqrt{v_{load}^2 + v_E^2 + v_\phi^2 + v_{cr}^2}} = 2.955 \approx 3.0 \quad (16)$$

For metal shells we can assume $v_\phi = v_E = 0$. We thus obtain

$$\gamma_{el}^{metal} = \frac{\gamma_0}{1 - 2\sqrt{v_{load}^2 + v_{cr}^2}} = 2.207 \approx 2.2 \quad (17)$$

If we do not want to separate the plastic and the elastic safety factors, but we want to introduce a unique safety factor instead, the values v_{pl}^2 and v_{cr}^2 also have to appear under the root sign, but diminished to such an extent as corresponds to the role played by them in elastic-plastic buckling.

If we write values v_{pl} and v_{el} into the equation of the

Dunkerley-ellipse applied to plastic critical load, and equate this to another into which we wrote $\gamma_{el,pl}$, we can determine:

$$\gamma_{el,pl} = \gamma_{el} \frac{(\gamma_{pl}/\gamma_{el})^2 + (p_{pl}/p_{cr,el})^2}{1 + (p_{pl}/p_{cr,el})^2} \quad (18)$$

If we assume that $p_{pl}/p_{cr,el} \approx p_p/p_{cr}^{lin}$, we will obtain for the unique safety factor the expression

$$\gamma_{el,pl} \approx \gamma_{el} \sqrt{\frac{(\gamma_{pl}/\gamma_{el})^2 + (p_p/p_{cr}^{lin})^2}{1 + (p_p/p_{cr}^{lin})^2}} \quad (19)$$

Some values for $\gamma_{el,pl}$ are found in Table II. Here p_p denotes the plastic failure load p_{pl} valid in case $w_0 = 0$.

Table 2. The unique safety factor $\gamma_{el,pl}$ for buckling and plastic failure

Material of the shell	Proposal		According to prin- ciples of DIN/CEB/		According to prin- ciples of ACI	
	Concrete	Metal	Concrete	Metal	Concrete	Metal
$p_p/p_{cr}^{lin} = 0$	1.50	1.50	1.75	1.75	2.10	2.10
$= 0.5$	1.90	1.70	2.18	1.92	2.23	2.10
$= 1.0$	2.35	1.90	2.70	2.16	2.98	2.42
$= 2.0$	2.75	1.97	3.14	2.37	3.40	2.59
$= \infty$	3.00	2.20	3.40	2.50	3.65	2.70

The safety factor shall be increased if

- the theory applied is approximative,
- the computation model deviates from the actual structure,
- the material characteristics are not reliable.

The values of the safety factor established according to the principles of DIN

DIN gives a factor of safety $\gamma_{pl} = 1.75$ for structures not exposed to buckling /8/. It determines the failure load from the nominal strength.

THE SAFETY FACTOR TO BE APPLIED IN SHELL BUCKLING ANALYSIS

With values $\nu_{pl} = 0.1$ and $\nu_{load} = 0.1$ we have

$$\gamma_{pl} = \frac{\gamma_0}{1 - 2 \sqrt{\nu_{load}^2 + \nu_{pl}^2}} = 1.75 \quad (20)$$

from which we obtain $\gamma_0 = 1.25$. The safety factor of elastic buckling becomes in the case of reinforced concrete shells:

$$\begin{aligned} \gamma_{el}^{concrete} &= \frac{\gamma_0}{1 - 2 \sqrt{\nu_{load}^2 + \nu_E^2 + \nu_\phi^2 + \nu_{cr}^2}} = \\ &= \frac{1.25}{1 - 2 \sqrt{0.1^2 + 0.1^2 + 0.16^2 + 0.23^2}} = 3.357 \approx 3.4 \end{aligned} \quad (21)$$

The IASS-Recommendations /14/ accepted this level of safety for buckling analysis of reinforced concrete shells, because it gave $\gamma_{pl} = 1.75$ and $\gamma_{el} = 3.5$.

For metal shells we obtain with $\nu_\phi = \nu_E = 0$:

$$\gamma_{el}^{metal} = \frac{1.25}{1 - 2 \sqrt{0.1^2 + 0.23^2}} = 2.508 \approx 2.50 \quad (17)$$

The values of unique elastic-plastic safety factor $\gamma_{el,pl}$, computed from Eq.(19), are tabulated in Table II.

Safety factor according to the principles of the CEB Recommendation

According to the CEB Recommendations /9/ $\gamma_{steel} = 1.15$; $\gamma_{concr} = 1.50$; and we can assume $\gamma_{material} = 1.25$. From these we obtain the value $\nu_{pl} = 0.1$. The Recommendations specify for the loads $\gamma_{dead} = 1.35$ and $\gamma_{live} = 1.5$. These yield an average value of $\gamma_{load} = 1.4$, which results in $\gamma_{load} = 0.15$. We thus have

$$\gamma_{pl} = \gamma_{material} \gamma_{load} = 1.25(1.4) = 1.75 \quad (22)$$

We can write

$$\gamma_{pl} = \frac{\gamma_0}{1 - 2\sqrt{\nu_{load}^2 + \nu_{pl}^2}} = 1.75$$

which yields $\gamma_0 = 1.12$. The safety factor of elastic buckling is, in case of reinforced concrete shells:

$$\begin{aligned} \gamma_{el}^{concrete} &= \frac{\gamma_0}{1 - 2\sqrt{\nu_{load}^2 + \nu_E^2 + \nu_\phi^2 + \nu_{cr}^2}} = \\ &= \frac{1.12}{1 - 2\sqrt{0.15^2 + 0.1^2 + 0.16^2 + 0.23^2}} = 3.36 \approx 3.4 \quad (23) \end{aligned}$$

and in case of metal shells (assuming $\nu_\phi = \nu_E = 0$):

$$\gamma_{el}^{metal} = \frac{1.12}{1 - 2\sqrt{0.15^2 + 0.23^2}} = 2.48 \quad (24)$$

That is, the safety factors computed according to the principles of CEB essentially coincide with those yielded by the DIN.

Safety factors according to the principles of American Code ACI

According to ACI /10/ $\gamma_{dead} = 1.4$; $\gamma_{live} = 1.7$. We thus can assume $\gamma_{load} \approx 1.5$, which yields a coefficient of variation $\nu_{load} = 0.167$. In case of eccentric compression $\gamma_{material} = 1.4$, from which $\gamma_{material} = 0.15$ can be computed.

The safety factor of plastic failure becomes

$$\gamma_{pl} = 1.5 (1.4) = 2.1 \quad (25)$$

We can write

$$\gamma_{pl} = \frac{\gamma_0}{1 - 2\sqrt{\nu_{material}^2 + \nu_{load}^2}} = 2.1,$$

from which $\gamma_0 = 1.16$ can be computed.

THE SAFETY FACTOR TO BE APPLIED IN SHELL BUCKLING ANALYSIS

Hence we obtain for the safety factor of elastic buckling of reinforced concrete shells:

$$\begin{aligned} \gamma_{el}^{\text{concrete}} &= \frac{\gamma_0}{1 - 2\sqrt{\nu_{\text{load}}^2 + \nu_E^2 + \nu_\phi^2 + \nu_{cr}^2}} = \\ &= \frac{1.16}{1 - 2\sqrt{0.167^2 + 0.1^2 + 0.16^2 + 0.23^2}} = 3.65 \end{aligned} \quad (26)$$

and of metal shells, taking $\nu_\phi = \nu_E = 0$:

$$\gamma_{el}^{\text{metal}} = \frac{1.16}{1 - 2\sqrt{0.167^2 + 0.23^2}} = 2.688 \approx 2.7 \quad (27)$$

We present the values of unified elastic-plastic safety factor $\gamma_{el,pl}$, computed from Eq./19/, in Table II.

5. SAFETY FACTORS OF SHELLS WITH INCREASING OR CONSTANT POST-BUCKLING LOAD BEARING CAPACITY

If we require the same level of safety against buckling failure of shells in every case, we shall apply safety factors of different magnitude in case of decreasing and increasing post-buckling load bearing capacities. This is essentially due to the circumstance that in case of increasing load bearing capacity, it is plastic failure load rather than critical load which characterizes failure. This phenomenon is schematically illustrated in Fig.4, where we represented the decreasing and increasing load bearing capacities by inclined, broken straight lines, disregarding the difference in coefficient of variation between both cases.

We obtain, as shown in the figure, for a structure with decreasing load bearing capacity

$$\gamma_2 = \frac{p_{cr}}{p_{pl}} \gamma_1,$$

with γ_1 as the safety factor determined in case of decreasing load bearing capacity. Since increasing load bearing capacity is characterised by relation $p_{cr}/p_{pl} < 1$, in this case we shall have $\gamma_2 < \gamma_1$. Following the proposed way of analysis we have

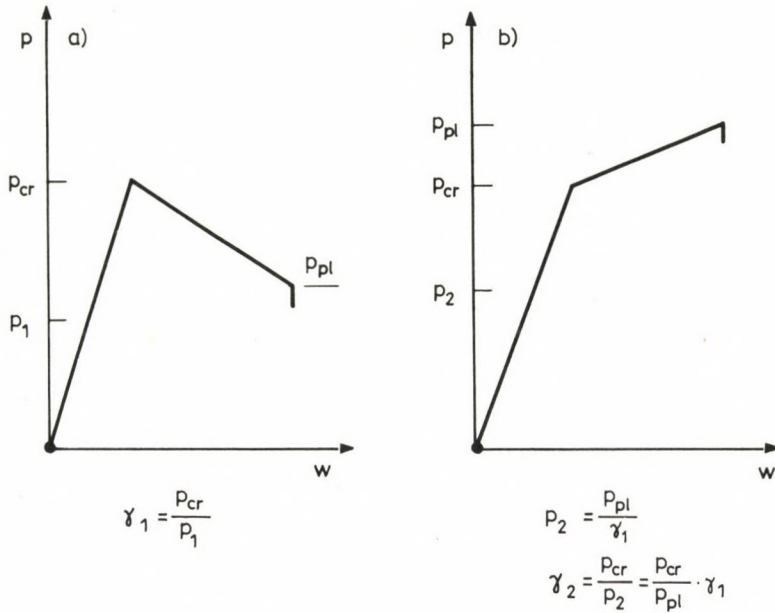


Fig. 4. Decreasing and increasing load bearing capacity

$$\gamma_o = 1.1; \quad \alpha = 2.0; \quad \nu_{load} = 0.1; \quad \nu_{pl} = 0.1; \quad \nu_E = 0.1; \quad \nu_\phi = 0.16.$$

and the evaluation of tests made on bars with constant post-buckling load bearing capacity yields

$$\nu_{cr} = \nu_{exp} = 0.18.$$

We thus obtain the resultant variation-coefficient $\nu_R = 0.28$ for reinforced concrete shells and $\nu_R = 0.23$ for metal shells, and the following safety factors can be computed (omitting subscript el):

$$\gamma_{constant}^{rc} = \frac{\gamma_o}{1 - 2 \nu_R} = \frac{1.1}{1 - 2(0.28)} = 2.5, \quad (28)$$

$$\gamma_{constant}^{metal} = \frac{1.1}{1 - 2(0.23)} \approx 2.05. \quad (29)$$

In case of investigations according to the principles of DIN:

$$\gamma_{constant}^{rc} \approx 2.85, \quad \gamma_{constant}^{metal} \approx 2.30.$$

THE SAFETY FACTOR TO BE APPLIED IN SHELL BUCKLING ANALYSIS

In case of investigations according to the principles of CEB:

$$\gamma_{\text{constant}}^{\text{rc}} = 2.80, \quad \gamma_{\text{constant}}^{\text{metal}} = 2.10.$$

In case of investigations according to the principles of ACI:

$$\gamma_{\text{constant}}^{\text{rc}} = 3.05, \quad \gamma_{\text{constant}}^{\text{metal}} = 2.28.$$

In case of shells which have a snap-through character, but the slope of the falling curve is less than in cases of axially compressed cylinder and radially compressed sphere, it seems reasonable to use an intermediate safety factor γ_{intermed} , which lies between $\gamma_{\text{decreasing}}$ and γ_{constant} . The value of this safety factor can be approximated by the following interpolation formula, using $\rho_{\text{hom}}(0.5)$, the value of the ratio $\rho_{\text{hom}} = \rho_{\text{cr}}^{\text{upper}} / \rho_{\text{cr}}^{\text{lin}}$ assumed at $w_0/h = 0.5$, characteristic of the slope of the curve of decreasing load bearing capacity

$$\gamma_{\text{intermed}} = \gamma_{\text{constant}} + (\gamma_{\text{decreasing}} - \gamma_{\text{constant}}) \frac{1 - \rho_{\text{hom}}(0.5)}{0.75}. \quad (30)$$

Note that in cases of axially compressed cylindrical and radially compressed spherical shells $\rho_{\text{hom}}(0.5) = 0.25$, while in case of a radially compressed very long cylinder $\rho_{\text{hom}}(0.5) = 1.00$. Introducing the values into formula (30) for various $\rho_{\text{hom}}(0.5)$, we obtain the values of Table 3. according to the different building codes.

Also, note that the safety factor for elastic buckling of shells with decreasing post-buckling load bearing capacity is twice the safety factor valid in the case of failure without buckling.

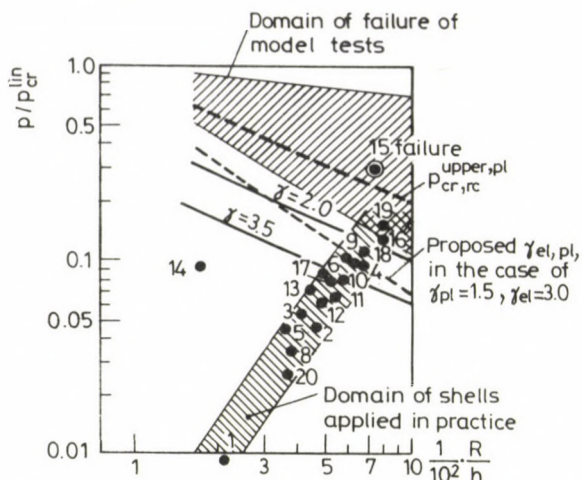
Table 3. Values of the intermediate safety factors

	$\rho_{\text{hom}}(0.5) =$	$\gamma_{\text{el, intermed.}}$				γ_{pl}
		0.25	0.50	0.75	1.00	
Concrete and r.c. shells	proposal	3.00	2.83	2.67	2.50	1.55
	according to DIN	3.40	3.22	3.03	2.85	1.75
	according to CEB	3.40	3.20	3.00	2.80	1.75
	according to ACI	3.65	3.45	3.25	3.05	2.10
Metal shells	proposal	2.20	2.15	2.10	2.05	1.55
	according to DIN	2.50	2.43	2.37	2.30	1.75
	according to CEB	2.48	2.36	2.23	2.10	1.75
	according to ACI	2.70	2.56	2.42	2.28	2.10

6. COMPARISON WITH ERECTED DOMES OF LARGE SPAN

We computed the critical load of several erected reinforced concrete domes with the aid of the method outlined in /1/, and compared them with their actual loads in Fig.5. On the basis of this comparison we think that computation of the critical load with the method outlined in /1/, assuming the value of the safety factor at about $\gamma_{\text{el}} = 3.0$, which gives $\gamma_{\text{el,pl}} \approx 2.4$ at $R/h = 500$, yields a safety level corresponding to the practice followed until now. Only three erected shells with a safety factor less than two were found. One of these actually buckled, and the other two were extremely slender. The figure also suggests that elliptic shells (i.e. those with positive Gaussian curvature) having a slenderness ratio $R/h < 500$ will most likely exhibit a sufficient degree of safety against buckling. However, for hyperbolic surfaces (those with negative Gaussian curvature) prone to develop inextensional deformation, this limit value may lie considerably lower, e.g. the collapsed cooling towers of Ferrybridge had a slenderness ratio of about $R/h \approx 200$.

THE SAFETY FACTOR TO BE APPLIED IN SHELL BUCKLING ANALYSIS



- | | |
|-------------------------------|----------------------------|
| 1. Jena, Germany | 11. Belgrade, Yugoslavia |
| 2. Jena, Germany | 12. Algeciras, Spain |
| 3. Matsuyama, Japan | 13. Novosibirsk, SU |
| 4. Ingoviscosa Works, Germany | 14. Rome, Italy |
| 5. Hilling, USA | 15. Gödöllő, Hungary |
| 6. Hamburg, Germany | 16. Thessaloniki, Greece |
| 7. Windward, USA | 17. Puerto Rico, USA |
| 8. Wales, Great Britain | 18. Cleadon, Great Britain |
| 9. Albuquerque, USA | 19. Lyon, France |
| 10. Belgrade, Yugoslavia | 20. Massachusetts, USA |

Fig. 5. Comparison of actual safety of erected domes with our proposal

7. SUMMARY

The paper dealt with the necessary safety factor against buckling of shell structures. Using probability theory in an approximate way we proposed safety factors for both elastic buckling and failure, and, to provide simplified method of analysis, we suggested a unique safety factor. We also evaluated the values of the safety factors according to the principles of various building codes. We proposed a unique safety factor $\gamma_{pl} = 1.5$ for failure without buckling while $\gamma_{el}^{concr} = 3.0$ for pure elastic buckling of concrete and reinforced concrete shells, and $\gamma_{el}^{metal} = 2.2$ in case of metal shells.

1. Dulácska, E.: Explanation of the chapter on stability of the "Recommendations for reinforced concrete shells and folded plates" and a proposal to its improvement. IASS Bulletin No. 77 (1982), 3-18.
2. Dulácska, E.: Buckling of Elastic-Plastic Shells. IASS Bulletin No. 68 (1979), 15-20.
3. Kollár, L.—Dulácska, E.: Buckling of Shells. Wiley, London (1984).
4. Korn, G.A.—Korn, Th.M.: Mathematical Handbook for Scientists and Engineers. 2nd Ed. McGraw-Hill, New York.
5. Burington, R.S.—May, D.C.: Handbook of Probability and Statistics. 2nd Ed. McGraw-Hill, New York 1967.
6. Sicherheit von Betonbauten. Beiträge zur Arbeitstagung Berlin 7/8 Mai 1973. Deutscher Beton-Verein, Wiesbaden.
7. MSz 15022/1.: Vasbetonszerkezetek. (Building Code for Reinforced Concrete Structures) Magyar Szabványügyi Hivatal, Budapest 1971.
8. DIN 1045.: Bestimmungen für Ausführung von Bauwerken aus Stahlbeton. Deutscher Betonverein, Wiesbaden 1972.
9. CEB—FIP: Model Code for Concrete Structures. CEB—FIP International Recommendation. 3rd Ed. 1978.
10. ACI—Standard 318: Building Code Requirement for Reinforced Concrete. American Concrete Institute, Detroit-Michigan (1977).
11. Roš, M.: Die materialtechnischen Grundlagen und Probleme des Eisenbetons im Hinblick auf die zukünftige Gestaltung der Stahlbeton-Bauweise. EMPA Bericht, No. 162, 1950.
12. Vandepitte, D.—Rathé, J.—Weymeis, G.: Experimental Investigations into the Buckling and Creep Buckling of Shallow Spherical Caps—subjected to Uniform Radial Pressure. Proceeding IASS World Congress, Vol. 1 Madrid, Spain, 1979, 1.1-1.15.
13. Kollár, L.—Dulácska, E.: Schalenbeulung, Theorie und Ergebnisse der Stabilität gekrümmter Flächentragwerke. Werner, Düsseldorf (1975).
14. IASS: Recommendations for Reinforced Concrete Shells and Folded Plates. Madrid (1979).

SOME COMMENTS ON THE TWIST PROBLEM OF SHELLS
OF CIRCULAR-ARC CENTRELINE

I. Ecsedi*

(Received 3 September 1985)

SUMMARY

This study discusses the uniform torsion of thin-walled shells of circular arc centreline, made of homogeneous, isotropic, linearly elastic material. The meridian section of the shell of circular arc centreline is a multiply connected planar domain. The proof of the three inequality relations concerning torsional rigidity is fundamentally based on considerations of J. Barta, exposed in 1955.

NOTATION

$\underline{r}, \phi, \underline{z}$	cylindrical coordinates
$\underline{e}_r, \underline{e}_\phi, \underline{e}_z$	unit vectors
s, ϕ, ξ	orthogonal non-straight coordinates
$\underline{e}_s, \underline{e}_\xi$	tangent to curve γ or its normal unit vector
h	wall thickness
G	shear modulus of elasticity
$\tau_s = \tau_\phi, \tau_{\phi\xi} = \tau_{\xi\phi}$	shear stresses
$N_{\phi s}, N_{s\phi}$	shear stress resultants
Q_ϕ	shear stress resultant
$M_{\phi s}, M_{s\phi}$	shear stress resultant force couples
γ_{rz}	planar curve, meridian section of the central surface of the shell
R_s, R_ϕ	main radius of curvature of central surface
g_s, g_ϕ	main curvatures of central surface
$\underline{F} = F \underline{e}_z$	force
\underline{M}	momentum
$\underline{\rho}/s = R/s \underline{e}_r + Z/s \underline{e}_z$	equation of curve γ
$\nabla = \frac{\delta}{\delta r} \underline{e}_r + \frac{\delta}{\delta z} \underline{e}_z$	Hamilton's differential operator in plane rz
$\underline{u} = u \underline{e}_r + v \underline{e}_\phi + w \underline{e}_z$	displacement vector

*Ecsedi I., H-3524 Miskolc, Klapka Gy. u. 36, Hungary

$\epsilon_s, \epsilon_\phi$	specific elongation
$\gamma_{s\phi}$	specific angular change
$\Psi = \psi/s/$	auxiliary function
\underline{S}	torsional rigidity
α_i	symbol of field i
γ_i	boundary curve of field i
e_i	tangential unit vector of curve γ_i
\underline{n}_i	normal unit vector of curve γ_i
$\underline{C}_i, \underline{D}_i, (i=1, 2, \dots, h)$	constants
$\underline{N}_{ij} (i \neq j, i, j=1, 2, \dots, n; \emptyset)$	tangential stress resultant
γ_{ij}	section of curve γ_i separating field α_i and α_j
γ_{i0}	'free' boundary section of curve γ_i
\underline{A}_i	area of field α_i
"."	symbol of scalar product of two vectors
"x"	symbol of vectorial product of two vectors,

other quantities and variables being defined in the text.

1. INTRODUCTION

Problems like "determine the system of internal forces and the strain of a rod upon which given forces and force couples applying twist to the rod are acting" have often been discussed in the mathematical theory of elasticity. A rigorous solution to this problem has been derived by P. Blaise /8/ for a thin-walled hollow rod while an upper and a lower bound to the rigorous solution by J. Barta /7/.

P1. Blaise's and J. Barta's argumentations apply to a rod a straight centreline. All these considerations are generalized for the case of a rod of circular arc centreline on the basis of P. Blaise's argumentation in Chapter 2 and 3 and in accordance with J. Barta's argumentation in Chapter 4 of this work.

2. FUNDAMENTAL RELATIONSHIPS

2.1 Figure 1 shows a thin-walled shell of circular arc centreline, made of elastic material. Central surface \underline{H} of the thin-walled shell of circular arc centreline is brought about by rotating meridian curve γ falling

THE TWIST PROBLEM OF SHELLS

within plane \underline{rz} around axis \underline{z} , the magnitude of rotation being ϑ ($0 < \vartheta < 2\pi$) while lateral surfaces H_1 and H_2 of the shell are obtained by rotating curves γ_1 and γ_2 falling within meridian plane \underline{rz} around axis \underline{z} , the magnitude of rotation being now ϑ ($0 < \vartheta < 2\pi$). Equation of closed curve γ non-intersecting axis of rotation \underline{z} :

$$\underline{\rho}/s = R/s/e_{\underline{r}} + Z/s/e_{\underline{z}}. \tag{2.1}$$

Equations of curves γ_1 and γ_2 , similarly closed and nonintersecting axis of rotation \underline{z} :

$$\underline{\rho}_1 = \underline{\rho}/s + 0.5 h e_{\underline{\xi}}. \tag{2.2}$$

$$\underline{\rho}_2 = \underline{\rho}/s - 0.5 h e_{\underline{\xi}}. \tag{2.3}$$

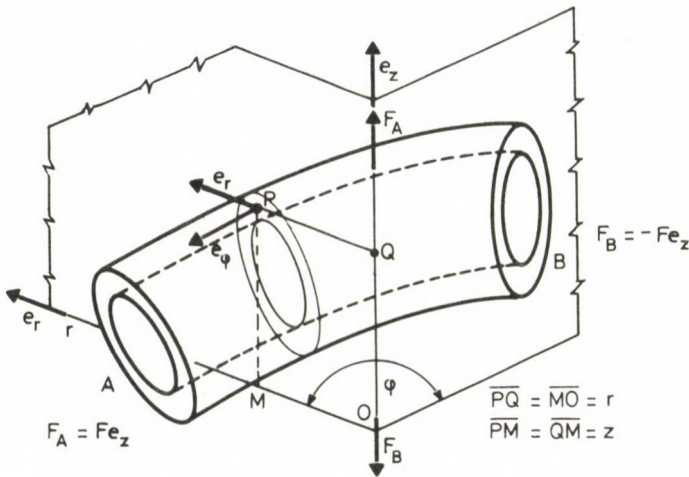


Fig. 1. Shell of circular arc centreline

In the formulas given above,

- \underline{s} arc co-ordinates measured along curve γ
- $\underline{h} = h/s/$ wall thickness of the shell
- \underline{e}_ξ normal unit vector of curve γ .

Statically, the stress resultants and stress resultant force couples acting

upon any central curve falling within the meridian section are equivalent to a force the line of action of which is axis \underline{z} . The movement of the rims of the shell having a closed meridian curve is not hindered by any external constraint. The problem outlined above is called the problem of uniform twist of a shell of circular arc centreline with closed meridian curve /2/, /3/.

Figure 2 shows the meridian section of the shell, falling within an arbitrary meridian plane. The meridian curve of the central section of the shell is designated γ . In the calculations, the role of orthogonal non-straight co-ordinate system \underline{s}, ϕ, ξ is predominant. The position of point \underline{P} is given by polar angle ϕ of the meridian plane including point \underline{P} , by arc co-ordinate \underline{s} of point \underline{P}_{γ} associated with point \underline{P} , as well as by signed distance (co-ordinate) $\xi = \overrightarrow{P_{\gamma}P} \cdot \underline{e}_{\xi}$ (Fig. 2). Here \underline{P}_{γ} designates a point of curve γ for which $\overrightarrow{P_{\gamma}P} \cdot \underline{e}_{\xi} = 0$.

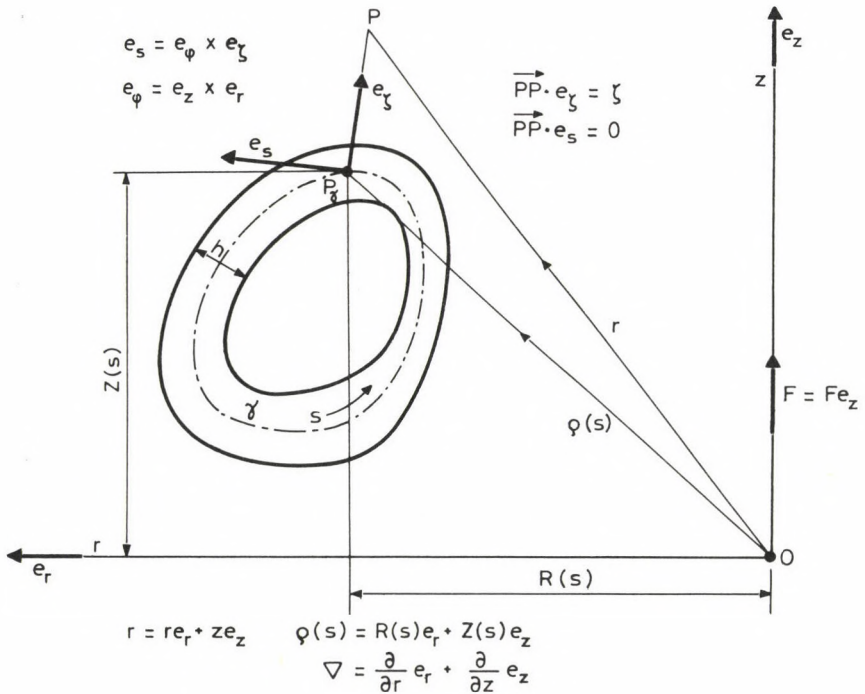


Fig. 2. Meridian section

THE TWIST PROBLEM OF SHELLS

All scalar co-ordinates of stress tensor $\underline{\underline{I}}$ of rods of circular arc centreline experiencing uniform twist, written in co-ordinate system s, ϕ, ξ are identically zero except for tangential stresses

$$\tau_{s\phi}(s, \xi) = \tau_{\phi s}(s, \xi),$$

and

$$\tau_{\xi\phi}(s, \xi) = \tau_{\phi\xi}(s, \xi)$$

(/1/,/2/,/3/).

Accordingly only the following stress resultants and force couples from among those characteristic of the internal system of forces of the shell will identically differ from zero:

$$N_{\phi s} = \int_{-h/2}^{h/2} \tau_{\phi s} (1 + g_{\phi\xi}) ds, \quad (2.4)$$

$$N_{s\phi} = \int_{-h/2}^{h/2} \tau_{s\phi} (1 + g_{s\xi}) ds, \quad (2.5)$$

$$Q_{\phi} = \int_{-h/2}^{h/2} \tau_{\xi\phi} (1 + g_{s\xi}) ds, \quad (2.6)$$

$$M_{\phi s} = \int_{-h/2}^{h/2} \xi \tau_{\phi s} (1 + g_{\phi\xi}) d\xi \quad (2.7)$$

$$M_{s\phi} = \int_{-h/2}^{h/2} \xi \tau_{s\phi} (1 + g_{s\xi}) d\xi. \quad (2.8)$$

Using the usual approximations of the theory of shells,

$$1 + g_{s\xi} \approx 1, \quad 1 + g_{\phi\xi} \approx 1, \quad (-h/2 \leq \xi \leq h/2),$$

we obtain that

$$N_{\phi s} = N_{s\phi} = \int_{-h/2}^{h/2} \tau_{s\phi} d\xi, \quad (2.9)$$

$$M_{\phi s} = M_{s\phi} = \int_{-h/2}^{h/2} \xi \tau_{s\phi} d\xi, \quad (2.10)$$

$$Q_{\phi} = \int_{-h/2}^{h/2} \tau_{\xi\phi} d\xi. \quad (2.11)$$

The non-identically fulfilled equations of equilibrium concerning stress resultants and stress resultant force couples are, as follows /4/, /5/:

$$\frac{d}{ds} RN_{\phi s} + \frac{dR}{ds} N_{s\phi} + \frac{dZ}{ds} Q_{\phi} = 0 \quad (2.12)$$

$$\frac{d}{ds} RM_{\phi s} + \frac{dR}{ds} M_{s\phi} - RQ_{\phi} = 0, \quad (2.13)$$

$$\frac{\phi s}{R_s} - \frac{s\phi}{R_{\phi}} - (N_{s\phi} - N_{\phi s}) = 0. \quad (2.14)$$

With the value of tangential stress $\tau_{\xi\phi}$ perpendicular to the central surface of the shell neglected we obtain

$$Q_{\phi} = 0. \quad (2.15)$$

As a result of such an approximation, it follows from equations (2.9), (2.10), (2.11), (2.12), (2.13), (2.14) that

$$N_{\phi s} = N_{s\phi} = \frac{C_N}{R^2}, \quad (2.16)$$

$$M_{\phi s} = M_{s\phi} = \frac{C_M}{R^2}. \quad (2.17)$$

Stress resultants and stress force couples of positive sign are shown in Fig. 3.

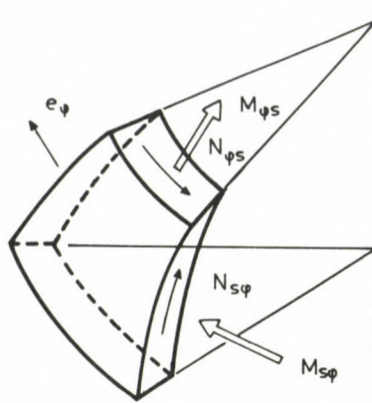


Fig. 3. Illustration of stress resultants and stress resultant couples

The value of constants C_N and C_M can be defined on condition of existence of equations (2.18) and (2.19) resulting from the conditions of mechanical equilibrium:

$$\oint_{\gamma} N_{s\phi} e_{-s} ds = F e_{-z} , \quad (2.18)$$

$$\oint_{\gamma} (\rho \times N_{s\phi} e_{-s} + M_{s\phi} e_{-\phi}) ds = 0 . \quad (2.19)$$

Using the well known relationships of vector analysis, we obtain equation (2.20), (Fig. 2):

$$\begin{aligned} \oint_{\gamma} N_{\phi s} e_{-s} ds &= e_{-\phi} \times \oint_{\gamma} N_{\phi s} e_{-s} ds = e_{-\phi} \times \oint_{\gamma} \frac{C_N}{R^2} e_{-\xi} ds = e_{-\phi} \times \int_A \frac{C_N}{r^2} \nabla dA = \\ &= -2 e_{-\phi} \times e_{-r} \int_A \frac{C_N}{r^3} dA = \left(2 C_N \int_A \frac{dA}{r^3} \right) e_{-z} \end{aligned} \quad (2.20)$$

In the above equation, \underline{A} designates the domain in plane rz , defined within closed curve γ . The combination of equations (2.18) and (2.20) yields formula

$$C_N = \frac{F}{2 \int_A \frac{dA}{r^3}} . \quad (2.21)$$

Note that formula (2.21) can be rewritten as

$$C_N = \frac{F}{\oint_Y \frac{1}{R^2} \frac{dZ}{ds} ds} \quad (2.22)$$

by the use of relationship

$$2 \int_A \frac{dA}{r^3} = \oint_Y \frac{1}{R^2} \frac{dZ}{ds} ds . \quad (2.23)$$

On the basis of relationship

$$\begin{aligned} & \oint_Y (\underline{\rho} \times N_{S\phi} \underline{e}_S + M_{S\phi} \underline{e}_\phi) ds = \\ & = \oint_Y \left[\underline{\rho} \times (\underline{e}_\phi \times \underline{e}_\xi) N_{S\phi} + M_{S\phi} \underline{e}_\phi \right] ds = \\ & = \underline{e}_\phi \left[\oint_Y (N_{S\phi} \underline{\rho} \cdot \underline{e}_\xi + M_{S\phi}') ds \right] = \\ & = \underline{e}_\phi \left[\int_A \left(\frac{C_N}{R^2} \underline{r} \right) \cdot \underline{\nabla} dA + \oint_Y M_{S\phi} ds \right] = \\ & = \underline{e}_\phi \left\{ C_N \int_A \left[\frac{\partial}{\partial r} \frac{1}{r} + \frac{\partial}{\partial z} \frac{z}{r^2} \right] dA + \right. \\ & \left. + C_M \oint_Y \frac{ds}{R^2} \right\} = \underline{e}_\phi C_M \oint_Y \frac{ds}{R^2} \end{aligned} \quad (2.24)$$

it can be understood that equation of equilibrium (2.19) for momentum can be fulfilled only if

$$C_M = 0 . \quad (2.25)$$

Notation

$$\underline{r} = r \underline{e}_r + z \underline{e}_z \quad (2.26)$$

was used in writing relationship (2.24).

It follows from equation (2.25) that

$$M_{S\phi}' = M_{\phi S} = 0 , \quad (2.27)$$

THE TWIST PROBLEM OF SHELLS

while from the latter equation and equations

$$N_{s\phi} = N_{\phi s} \quad (2.28)$$

that also equation of equilibrium (2.14) is fulfilled in case of fulfilment of condition $Q_{\phi} = 0$.

In the present case, condition $Q_{\phi} = 0$ results in a stressed state of the shell membrane.

The value of C_N is determined by the magnitude of load F :

$$C_N = \frac{F}{\int \frac{1}{R^2} \frac{dZ}{ds} ds} \quad (2.29)$$

2.2 The use of Hooke's law in the theory of shell membranes leads to equations (2.30), (2.31), (2.32):

$$\epsilon_s = \frac{1}{Eh} (N_s - \nu N_{\phi}) = 0, \quad (2.30)$$

$$\epsilon_{\phi} = \frac{1}{Eh} (N_{\phi} - \nu N_s) = 0, \quad (2.31)$$

$$\gamma_{s\phi} = \frac{N_{s\phi}}{Gh} = \frac{C_N}{GhR^2}. \quad (2.32)$$

On the basis of /4/, /5/, we can write

$$\frac{dw}{ds} \frac{dZ}{ds} + \frac{du}{ds} \frac{dR}{ds} = \epsilon_s, \quad (2.33)$$

$$\frac{1}{R} \left(u + \frac{dv}{d\phi} \right) = \epsilon_{\phi}, \quad (2.34)$$

$$\frac{dv}{ds} + \frac{1}{R} \left[\frac{dw}{d\phi} \frac{dZ}{ds} + \left(\frac{du}{d\phi} - \nu \right) \frac{dR}{ds} \right] = \gamma_{s\phi}(s). \quad (2.35)$$

A combination of equations (2.30), (2.31), (2.32), (2.33), (2.34), (2.35) yields

$$u = 0, \quad (2.36)$$

$$w = k\phi \quad (2.37)$$

and that function $v = v(s)$ satisfies ordinary differential equation

$$\frac{dv}{ds} + \frac{1}{R} \left(k \frac{dZ}{ds} - v \frac{dR}{ds} \right) = \frac{C_N}{GhR^2} \quad (2.38)$$

In writing formulas (2.36) and (2.37), the terms relating to rigid-body motion uninteresting in the present case has been disregarded.

Let $v(s) = R(s) \psi(s)$. (2.39)

A combination of equations (2.38) and (2.39) leads to equation (2.40):

$$\frac{d\psi}{ds} - \frac{k}{R^2} \frac{dZ}{ds} + \frac{C_N}{GhR^3} = 0 \quad (2.40)$$

Due to the univalence of the displacement field, also $\psi = \psi(s)$ is univalent that is equation

$$k \int_Y \frac{1}{R^2} \frac{dZ}{ds} ds = C_N \int_Y \frac{ds}{GhR^3} \quad (2.41)$$

exists.

On the basis of the above relationship, constant k can be calculated as a function of constant C_N or load F .

Mechanically, constant k can be obviously defined as the displacement of a meridian section, falling within two meridian sections including unit angle, in the direction of the axis of rotation. The quantity defined by rule

$$S = \frac{F}{k} \quad (2.42)$$

is called the torsional rigidity of the shell of circular arc centreline, twisted uniformly. A combination of formulas (2.22) and (2.23), (2.41), (2.42) yields

$$S = 4 \frac{\left(\int_Y \frac{dA}{R^3} \right)^2}{\int_Y \frac{ds}{GhR^3}} \quad (2.43)$$

Using relationship (2.22), formula (2.43) can also be written as

$$S = \frac{\left(\int_Y \frac{1}{R^2} \frac{dZ}{ds} ds \right)^2}{\int_Y \frac{ds}{GhR^3}} \quad (2.44)$$

THE TWIST PROBLEM OF SHELLS

The points of the shell surface, falling within a meridian section, are shifted at a uniform rate in the direction of axis \underline{z} in the meridian section, and they also displace at right angles to the meridian plane. This latter displacement is a function of co-ordinate \underline{s} . By integration of equation (2.40) we obtain

$$\psi(s) = \psi(0) - k \int_0^s \frac{1}{R^2} \frac{dZ}{ds} ds + C_N \int_0^s \frac{ds}{GhR^3} . \quad (2.45)$$

Transformation of equation (2.45) can be continued by the use of formulas (2.29), (2.31):

$$\psi(s) = \psi(0) + \frac{F}{\int_Y \frac{1}{R^2} \frac{dZ}{ds} ds} \left[\frac{\int_Y \frac{ds}{GhR^3}}{\int_Y \frac{1}{R^2} \frac{dZ}{ds} ds} \cdot \int_0^s \frac{1}{R^2} \frac{dZ}{ds} ds + \int_0^s \frac{ds}{GhR^3} \right] . \quad (2.46)$$

For displacement at right angles to the meridian plane, the following result can be written:

$$v(s) = \frac{R(s)}{R(0)} v(0) + \frac{FR(s)}{\int_Y \frac{1}{R^2} \frac{dZ}{ds} ds} \left[\frac{\int_Y \frac{ds}{GhR^3}}{\int_Y \frac{1}{R^2} \frac{dZ}{ds} ds} \cdot \int_0^s \frac{1}{R^2} \frac{dZ}{ds} ds + \int_0^s \frac{ds}{GhR^3} \right] . \quad (2.47)$$

The mechanical meaning of quantity $\psi = \psi(\underline{s})$ is obvious. The motion of points along the parallel circle of central surface \underline{H} determined by arc co-ordinate \underline{s} can be divided into two parts. On the one hand, these points move at a variable rate in the direction of axis \underline{z} while on the other hand, the points of the parallel circle displace like a rigid body around axis \underline{z} through an angle of $\psi = \psi(\underline{s})$ (Fig. 4).

Since in general $\psi = \psi(\underline{s}) \neq \text{constant}$, the shape of curve γ falling within a definite meridian section will experience distortion (warpage, swell) due to angular displacements of different values like a rigid body,

associated with the different points of curve γ .

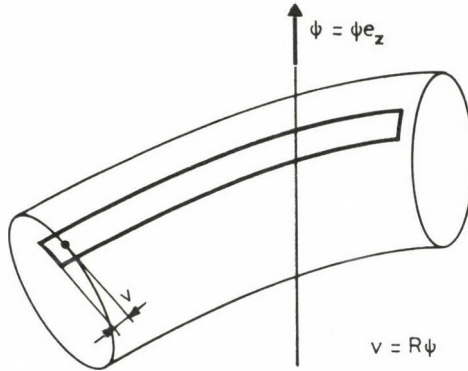


Fig. 4. Definition of ψ

2.3 No distortion of the curve occurs along that section of meridian curve γ where

$$\frac{d\psi}{ds} = 0 \quad (2.48)$$

in the points of the curve.

On the basis of equation (2.40), it is understandable that equation (2.48) will exist only if

$$GhR \frac{dZ}{ds} = \text{constant} . \quad (2.49)$$

It can be gathered from equation (2.49) that $\psi = \text{constant}$ along constant curve section \underline{Z} .

Let

$$\frac{dZ}{ds} \neq 0 . \quad (2.50)$$

The section of curve γ satisfying condition (2.49), (2.50) in case $\underline{h} = \text{constant}$ can be defined by the use of equations

$$R \frac{dZ}{ds} = D = \text{constant} , \quad (2.51)$$

$$\left(\frac{dR}{ds}\right)^2 + \left(\frac{dZ}{ds}\right)^2 = 1 \quad (2.52)$$

Somewhat tiresome but elementary calculations result in

$$R = \sqrt{s^2 + D^2}, \quad (2.53)$$

$$Z = D \operatorname{arsh} \frac{s}{D}. \quad (2.54)$$

(2.53), (2.54) are the parametric equation of curve section γ that displaces angularly like a rigid body. By eliminating parameter s we arrive from equations (2.53), (2.54) to equation

$$R = D \operatorname{ch} \frac{Z}{D}. \quad (2.55)$$

On the basis of what has been said so far, the meridian curve of the shell of a central surface not being distorted in case $h = \text{constant}$ is illustrated by curve γ given in Fig. 5.

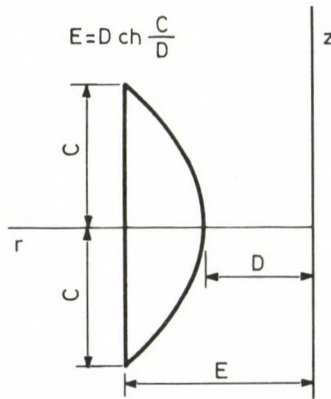


Fig. 5. Non-warping meridian section

2.4 Tangential stress $\tau_{s\phi}$ can be defined on the basis formula (2.56) derived by combination of equations (2.16), (2.21):

$$\tau_{s\phi} = \frac{F}{2R^2 h \int_A \frac{dA}{r^3}} \quad (2.56)$$

Formula (2.56) can also be written as

$$\tau_{s\phi} = \frac{F}{R^2 h \oint_{\gamma} \frac{1}{R^2} \frac{dZ}{ds} ds} \quad (2.57)$$

$\tau_{s\phi}$ will be constant if the wall thickness of the shell changes according to relationship

$$h(s) = \frac{D}{R^2} \quad (2.58)$$

where D : positive constant.

3. CIRCULAR-ARC CENTRELINE SHELL OF MULTIPLY CONNECTED MERIDIAN SECTION

The meridian section of the central surface of the thin-walled shell of circular-arc centreline, falling within a meridian plane of arbitrary position, is shown in Fig. 6. The meridian section is set up of fields (cells) of number n . Field α_i is confined by closed curve γ_i . Curve γ_i is considered to be a union of curves $\gamma_{i0}, \gamma_{i1}, \dots, \gamma_{in}$. Counterclockwise direction is considered to be positive for each curve. The tangential unit vector of curve γ_i is designated \underline{e}_i while its normal unit vector $\underline{n}_i, \underline{n}_i$ pointing always away from the area enclosed by curve γ_i .

On the basis of Fig. 6, one can write

$$\underline{e}_i(P) = \underline{e}_{i0}(P), \quad P \in \gamma_{i0}, \quad (3.1)$$

$$\underline{e}_i(P) = \underline{e}_{ij}(P), \quad P \in \gamma_{ij}, \quad (3.2)$$

with γ_{i0} the free boundary section of field α_i , and γ_{ij} the common boundary line of fields α_i and α_j . Considering that the sense of positive direction is identical for each field, equation

$$\underline{e}_{ij} + \underline{e}_{ji} = \underline{0} \quad (3.3)$$

exists. In the points of curve γ_i , tangential stress resultant $N_{s\phi}$ is designated briefly N_{ij} , the sign of N_{ij} being related to the position of vec-

tor \underline{e}_{ij} . Accordingly, \underline{N}_{ij} will be positive if the direction of the vector of tangential stress resultant $\underline{F}_{ij} = \underline{N}_{ij} \underline{e}_{ij}$ complies with the direction of vector \underline{e}_{ij} .

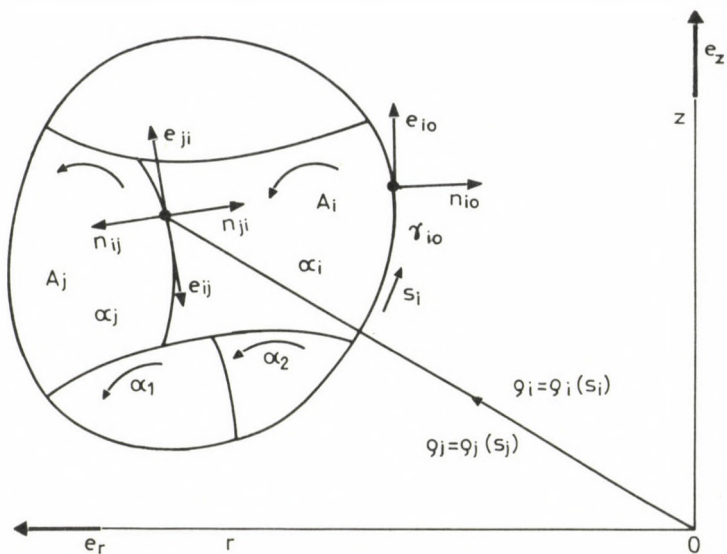


Fig. 6. Multiply connected meridian section

Tangential stress resultant \underline{N}_{ij} is derived in the following way:

A constant \underline{C}_i ($\underline{i} = 1, 2, \dots, n$) is assigned to each field (cell) α_i ($\underline{i} = 1, 2, \dots, n$). Using constants \underline{C}_i , the value of tangential stress resultant \underline{N}_{ij} is obtained on the basis of formula

$$N_{ij}(P) = \frac{C_i - C_j}{R_{ij}^2} P \in \gamma_{ij} \quad (3.4)$$

while the value of tangential stress resultant \underline{N}_{io} can be calculated by means of formula

$$N_{io} = \frac{C_i}{R_{ij}^2}, \quad P \in \gamma_{io} \quad (3.5)$$

Evidently, tangential stress resultants $\underline{N}_S \phi = \underline{N} \phi_S$ defined on the basis of formulas (3.4), (3.5) satisfy equation of equilibrium (2.12), provided $\underline{Q} \phi = 0$.

The tangential stress resultants defined on the basis of formulas (3.4), (3.5) automatically satisfy also the conditions of equilibrium applying to the points of 'fit' of the different shells. On the basis of analysis of the moment equation written for axis \underline{z} , expressing the equilibrium of the shell section associated with 'node' \underline{P}_{124} , it is possible to demonstrate that the above statement is correct.

Part of 'shell elements' \underline{H}_{21} , \underline{H}_{42} , \underline{H}_{14} interconnected in node \underline{P}_{124} is shown in Fig. 7.

One of the necessary conditions for the equilibrium of configuration Ω_{124} obtained by cutting shell elements \underline{H}_{21} , \underline{H}_{42} , \underline{H}_{14} is expressed by equation

$$m_z = 0 \quad (3.6)$$

where \underline{m}_z — moment of all the forces and force couples acting upon configuration Ω_{124} , calculated for axis \underline{z} . Developed in detail, moment equation (3.6) yields the following relationship:

$$\Phi R^2 N_{21} + \Phi R^2 N_{42} + \Phi R^2 N_{14} = 0, \quad (3.7)$$

that is

$$(C_2 - C_1) + (C_4 - C_2) + (C_1 - C_4) = 0. \quad (3.8)$$

Actually, this latter equation exists in any case independently of the value of constants \underline{C}_i .

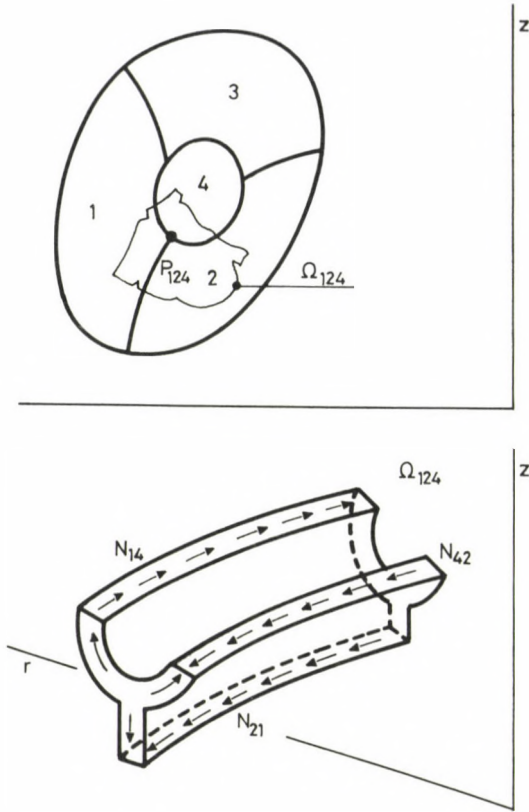


Fig. 7. Schematic illustration to write the equilibrium equation

Let us define now resultant vector \underline{F} of tangential stress resultants associated with the section falling within an arbitrary meridian plane as well as moment vector \underline{m}_O calculated for point O .

$$\begin{aligned} \underline{F} &= \sum_{\substack{i,j \\ i \neq j}} \int N_{ij} \frac{\underline{e}_{ij}}{\gamma_{ij}} ds = \sum_{i=1}^n C_i \frac{\underline{e}_i}{R_i^2} \oint ds = \\ &= \underline{e}_\phi \times \left[\sum_{i=1}^n C_i \oint \frac{n_i}{\gamma_i R_i^2} ds \right] = \end{aligned}$$

$$\begin{aligned}
 &= \underline{e}_\phi \times \left[\sum_{i=1}^n C_i \int_{A_i} \left(\frac{1}{r^2} \right) \underline{\nabla} dA \right] = \\
 &= \left(2 \sum_{i=1}^n C_i \int_{A_i} \frac{dA}{r^3} \right) \underline{e}_z, \tag{3.9}
 \end{aligned}$$

$$\begin{aligned}
 \underline{m}_o &= \sum_{\substack{i,j \\ i \neq j}} \int_{\gamma_{ij}} \underline{\rho}_{ij} \times N_{ij} \underline{e}_{ij} ds = \\
 &= \underline{e}_\phi \left[\sum_{\substack{i,j \\ i \neq j}} \int_{\gamma_{ij}} N_{ij} \underline{\rho}_{ij} \cdot \underline{n}_{ij} ds \right] = \\
 &= \underline{e}_\phi \left[\sum_{i=1}^n C_i \oint_{\gamma_i} \frac{1}{R_i^2} \underline{\rho}_i \cdot \underline{n}_i ds \right] = \\
 &= \underline{e}_\phi \left[\sum_{i=1}^n C_i \int_{A_i} \left(\frac{r}{r^2} \right) \cdot \underline{\nabla} dA \right] = \\
 &= \underline{e}_\phi \left[\sum_{i=1}^n C_i \int_{A_i} \left[\frac{\partial}{\partial r} \left(\frac{1}{r} \right) + \frac{\partial}{\partial z} \left(\frac{z}{r^2} \right) \right] dA \right] = \underline{0}. \tag{3.10}
 \end{aligned}$$

Equations (3.9), (3.10) suggest that statically, the tangential stress resultants acting upon the central curve (meridian section of the central surface) falling within any meridian section of the shell are equivalent to a force the line of action of which being axis \underline{z} . The relation between force \underline{F} loading the meridian section and constants $\underline{C}_1, \underline{C}_2, \dots, \underline{C}_n$ is given by formula (3.11) from equation (3.9):

$$F = 2 \sum_{i=1}^n C_i \int_{A_i} \frac{dA}{r^3} . \quad (3.11)$$

Relationship (3.11) can also be written as

$$F = \sum_{i=1}^n C_i \oint_{\gamma_i} \frac{1}{R_i^2} \frac{dZ_i}{ds} ds \quad (3.12)$$

using identity

$$2 \oint_{A_i} \frac{dA}{r^3} = \oint_{\gamma_i} \frac{1}{R_i^2} \frac{dZ_i}{ds} ds . \quad (3.13)$$

The value of constants C_i ($i = 1, 2, \dots, n$) can be determined on condition that displacement $\underline{v} = \underline{v}(s)$ of the central surface of the shell be a univalent function. Function $\underline{v} = \underline{v}(s)$ will be univalent if function $\psi = \psi(s)$ defined by rule $\psi(s) = \underline{v}(s)/R(s)$ is univalent while function $\psi = \psi(s)$ will be univalent if for any possible closed curve g

$$\oint_g \frac{d\psi}{ds} ds = 0 . \quad (3.14)$$

This latter condition will be certainly fulfilled in the present case if equation

$$\oint_{\gamma_i} \frac{d\psi}{ds} ds = 0 \quad (3.15)$$

exists for all closed curves γ_i .

It follows from shape

$$u = 0 , \quad v = R(s) \psi(s) , \quad (3.16)$$

$$(3.17)$$

$$w = k \phi \quad (k = \text{constant}) \quad (3.18)$$

of the displacement field that

$$\frac{d\psi}{ds} = - \frac{k}{R^2} \frac{dZ}{ds} + \frac{N_s \phi}{GhR} . \quad (3.19)$$

By combination of equations (3.4), (3.5), (3.15), (3.19), the lin-

ear equation system serving to define constants \underline{C}_i is obtained:

$$a_{i0} C_i + a_{i1} (C_i - C_1) + a_{i2} (C_i - C_2) + \\ + a_{i3} (C_i - C_3) + \dots = k f_i, \quad (i=1,2,\dots,n). \quad (3.20)$$

In the above equation,

$$a_{ij} = \int_{\gamma_{ij}} \frac{ds}{G h_i R_i^3}, \quad (i \neq j; i, j = 0, 1, 2, \dots, n); \quad (3.21)$$

$$f_i = \oint_{\gamma_i} \frac{1}{R_i^2} \frac{dZ_i}{ds} ds = 2 \int_{A_i} \frac{dA}{r^3}, \quad (3.22)$$

Let

$$C_i = G k D_i, \quad (i = 1, 2, \dots, n). \quad (3.23)$$

Changes \underline{D}_i introduced by formula (3.23) result in

$$F = 2kG \sum_{i=1}^n D_i \frac{dA}{r^3} = kG \sum_{i=1}^n D_i \oint_{\gamma_i} \frac{1}{R_i^2} \frac{dZ_i}{ds} ds. \quad (3.24)$$

The torsional rigidity, \underline{S} , of the shell experiencing uniform twist is defined by the following formula:

$$S = \frac{F}{k}. \quad (3.25)$$

A combination of formulas (3.24) and (3.25) yields

$$S = G \sum_{i=1}^n D_i f_i. \quad (3.26)$$

Constants \underline{D}_i ($i=1, 2, \dots, n$) are defined by the use of a system of equations (3.20). On the basis of equations (3.20) and (3.23), one can write

$$a_{i0} D_i + a_{i1} (D_i - D_1) + a_{i2} (D_i - D_2) + a_{i3} (D_i - D_3) + \dots = f_i, \\ (i=1, 2, \dots, n). \quad (3.27)$$

THE TWIST PROBLEM OF SHELLS

It follows from formulas (3.4), (3.5) as well as from equation (3.23) that

$$N_{ij} = G \frac{F}{S} \frac{D_1 - D_j}{R_{ij}^2}, \quad (3.28)$$

$$N_{i0} = G \frac{F}{S} \frac{D_1}{R_{i0}^2}. \quad (3.29)$$

4. SOME INEQUALITIES CONCERNING TORSIONAL RIGIDITY

4.1 On the basis of equation system (3.27), it can be written that

$$\begin{aligned} f_1 D_1 + f_2 D_2 + f_3 D_3 + \dots &= a_{10} D_1^2 + \\ &+ a_{12} (D_1 - D_2)^2 + a_{13} (D_1 - D_3)^2 + \dots \\ &+ a_{20} D_2^2 + a_{23} (D_2 - D_3)^2 + \dots \\ &\cdot \\ &\cdot \\ &\cdot \\ &+ a_{n0} D_n^2. \end{aligned} \quad (4.1)$$

It follows from this relationship that

$$\begin{aligned} S = G \left[a_{10} D_1^2 + a_{12} (D_1 - D_2)^2 + a_{13} (D_1 - D_2)^2 + \right. \\ \left. \dots + a_{20} D_2^2 + \dots + a_{n0} D_n^2 \right]. \end{aligned} \quad (4.2)$$

while from formula (4.2) one can read that \underline{S} can never be negative. We have used when writing relationship (4.1) that

$$a_{ij} = a_{ji}, \quad (i \neq j, i, j = 1, 2, \dots, n). \quad (4.3)$$

4.2 Theorem:

Let

$$b_1^2 + b_2^2 + \dots + b_n^2 \neq 0. \quad (4.4)$$

There exists the following inequality relation:

$$S \geq G \frac{(b_1 f_1 + b_2 f_2 + \dots + b_n f_n)^2}{U(b_1, b_2, \dots, b_n)}, \quad (4.5)$$

where

$$U(b_1, b_2, \dots, b_n) = a_{10} b_1^2 + a_{12}(b_1 - b_2)^2 + a_{13}(b_1 - b_3)^2 + \dots + a_{20} b_2^2 + \dots + a_{n0} b_n^2. \quad (4.6)$$

Proof:

On the basis of the Schwarz inequality relation we can write that

$$\underline{b}^* \underline{U} \underline{b} \geq (\underline{b}^* \underline{U} \underline{D})^2 \quad (4.7)$$

where

$$\underline{b}^* = [b_1, b_2, \dots, b_n], \quad (4.8)$$

$$\underline{D}^* = [D_1, D_2, \dots, D_n], \quad (4.9)$$

$$\underline{U} = \begin{bmatrix} a_{11} & -a_{12} & -a_{13} \\ -a_{21} & a_{22} & -a_{23} \\ -a_{31} & -a_{32} & a_{33} \\ \vdots & \vdots & \vdots \\ a_{i1} & a_{i2} & a_{i3} \\ \vdots & \vdots & \vdots \\ a_{n1} & a_{n2} & a_{n3} \end{bmatrix} \quad (4.10)$$

$$a_{ii} = a_{i0} + a_{i1} + a_{i2} + \dots + a_{in}, \quad (4.11)$$

(i = 1, 2, ..., n).

"*" in formulas (4.8), (4.9) designates transposition.

Matrix \underline{U} defined by (4.10) is a positive definite symmetric matrix, its symmetry being obvious while its positive definite nature follows from formula

$$\underline{b}^* \underline{U} \underline{b} = U(b_1, b_2, \dots, b_n) \quad (4.12)$$

applying to arbitrary vector

$$\underline{b}^* = (b_1, b_2, \dots, b_n) .$$

On the basis of equations (3.26), (4.9), (4.10) it can be written that

$$\underline{U} \underline{D} = \underline{f} , \tag{4.13}$$

where

$$\underline{f} = (f_1, f_2, \dots, f_n)^* . \tag{4.14}$$

By combination of inequality (4.7) and equation (4.13), we obtain the formula resulting from formula (4.2):

$$S = GU / (D_1, D_2, \dots, D_n) = G \underline{D}^* \underline{U} \underline{D} , \tag{4.15}$$

that is the inequality relation (4.5) to be proved.

4.3 Theorem:

With numbers $X_{10}, X_{12}, \dots, X_{1n}; X_{21}, X_{20}, \dots, X_{2n}; X_{31}, X_{32}, X_{30}, X_{34}, \dots, X_{3n}; \dots, X_{n1}, X_{n2}, \dots, X_{no}$; satisfying condition

$$\begin{aligned} X_{10} + X_{12} + X_{13} \sim \dots &= f_1 , \\ X_{21} + X_{20} + X_{23} \sim \dots &= f_2 , \\ X_{31} + X_{32} + X_{30} \sim \dots &= f_3 , \\ \cdot & \\ \cdot & \\ \cdot & \end{aligned} \tag{4.16}$$

$$\begin{aligned} X_{12} + X_{21} &= 0 , \\ X_{13} + X_{31} &= 0 , \\ X_{23} + X_{32} &= 0 , \\ \cdot & \\ \cdot & \end{aligned} \tag{4.17}$$

but otherwise arbitrary real numbers, inequality relation

$$S \leq G \left[\frac{X_{10}^2}{a_{10}^2} + \frac{X_{12}^2}{a_{12}^2} + \frac{X_{13}^2}{a_{13}^2} + \dots + \frac{X_{1n}^2}{a_{1n}^2} + \frac{X_{20}^2}{a_{20}^2} + \frac{X_{23}^2}{a_{23}^2} + \dots + \frac{X_{2n}^2}{a_{2n}^2} \dots + \frac{X_{no}^2}{a_{no}^2} \right] \tag{4.18}$$

will exist.

Proof: Considering real numbers $X_{10}, X_{12}, X_{13}, \dots$ satisfying (4.16), (4.17), written in the following form:

$$\begin{aligned}
 X_{10} &= a_{10} D_1 + x_{10} \\
 X_{12} &= a_{12} (D_1 - D_2) + x_{12} , \\
 X_{13} &= a_{13} (D_1 - D_3) + x_{13} , \\
 &\cdot \\
 &\cdot \\
 &\cdot \\
 X_{21} &= a_{21} (D_2 - D_1) + x_{21} , \\
 X_{20} &= a_{20} D_2 + x_{20} , \\
 X_{23} &= a_{23} (D_2 - D_3) + x_{23} , \\
 &\cdot \\
 &\cdot \\
 &\cdot \\
 X_{no} &= a_{no} D_n + x_{no} , \\
 &\cdot \\
 &\cdot \\
 &\cdot
 \end{aligned}
 \tag{4.19}$$

it is easy to verify that numbers

$$X_{10}, X_{12}, X_{13}, \dots ;$$

$$X_{21}, X_{20}, X_{23}, \dots ; \dots$$

according to (4.18) will automatically satisfy conditions (4.16), (4.17), provided numbers

$$x_{10}, x_{12}, x_{13}, \dots ;$$

$$x_{21}, x_{20}, x_{23}, \dots ;$$

satisfy conditions

$$x_{10} + x_{12} + x_{13} + \dots + x_{1n} = 0 ,$$

$$x_{21} + x_{20} + x_{23} + \dots + x_{2n} = 0 ,$$

$$x_{31} + x_{32} + x_{30} + \dots + x_{3n} = 0 ,$$

\cdot
 \cdot
 \cdot

$$x_{12} + x_{21} = 0 ,$$

$$x_{13} + x_{31} = 0 ,$$

$$x_{23} + x_{32} = 0 ,$$

\cdot
 \cdot
 \cdot

$$\begin{aligned}
 G \left(\frac{x_{10}^2}{a_{12}} + \frac{x_{12}^2}{a_{13}} + \frac{x_{13}^2}{a_{13}} + \dots + \frac{x_{20}^2}{a_{20}} + \frac{x_{23}^2}{a_{23}} + \frac{x_{24}^2}{a_{24}} + \dots + \frac{x_{30}^2}{a_{30}} + \frac{x_{34}^2}{a_{34}} + \dots \right) = \\
 = S + G \left(\frac{x_{10}^2}{a_{10}} + \frac{x_{12}^2}{a_{12}} + \frac{x_{13}^2}{a_{13}} + \dots + \frac{x_{20}^2}{a_{20}} + \frac{x_{23}^2}{a_{23}} + \frac{x_{24}^2}{a_{24}} + \dots + \frac{x_{30}^2}{a_{30}} + \frac{x_{34}^2}{a_{34}} + \frac{x_{35}^2}{a_{35}} + \right. \\
 \left. + \frac{x_{no}^2}{a_{no}} \right). \quad (4.25)
 \end{aligned}$$

It can be read in formula (4.25) that the theorem to be verified is correct.

4.4 Solution \underline{D} to linear equation system

$$\underline{U} \underline{D} = \underline{f} \quad (4.26)$$

of matrix of coefficients \underline{U} , symmetric and positive definite, is formed on the basis of rule

$$\begin{aligned}
 a_{11} D_1^{/i+1/} &= a_{12} D_2^{/i/} + a_{13} D_3^{/i/} + \dots + f_1, \\
 a_{22} D_2^{/i+1/} &= a_{21} D_1^{/i+1/} + a_{23} D_3^{/i/} \dots + f_2, \\
 a_{33} D_3^{/i+1/} &= a_{31} D_1^{/i+1/} + a_{32} D_2^{/i+1/} + \dots + f_3 \\
 &\cdot \\
 &\cdot \\
 &\cdot
 \end{aligned} \quad (4.27)$$

when the Gauss-Seidel iteration process is used.

It has been proved /6/ that, in case of a positive definite, symmetric matrix of coefficients, \underline{U} , elements $D_k^{/i/}$ of sequence of iteration (4.27) will converge to solution D_k of system of equations (3.26) for arbitrary starting values D_k . Using this theorem, it can be seen that unknowns D_1, D_2, \dots, D_n of system of equations (3.27) are non-negative in any case, that is

$$D_k \geq 0, \quad (k = 1, 2, \dots, n). \quad (4.28)$$

The correctness of relationship (4.28) follows from the fact that

THE TWIST PROBLEM OF SHELLS

the terms of sequences of iteration with starting value $D_k^{/0/}=0(k=1,2,\dots,n)$ defined by (4.27) are non-negative, and because non-negative numbers have been multiplied and added, non-negative numbers $D_k(k=1,2,\dots,n)$ will obviously be obtained necessarily also as limit values. With equation (3.27) and inequality (4.28) combined, it may be written that

$$D_i \geq \frac{f_i}{a_{ii}}, \quad (4.29)$$

$$D_i \leq \frac{\sum_{i=1}^i f_i}{a_{i0}}, \quad (4.30)$$

(i = 1,2,..., n) .

Using the above inequalities, the following upper and lower bounds can be derived for the numerical value of torsional rigidity S:

$$S \geq G \sum_{i=1}^n \frac{f_i^2}{a_{ii}}, \quad (4.31)$$

$$S \leq G f \sum_{i=1}^n \frac{f_i}{a_{i0}}. \quad (4.32)$$

4.5 Theorem:

Let

$$K = G \sum_{i=1}^n L_i f_i, \quad (4.33)$$

$$\beta_i = \frac{1}{f_i} \left\{ a_{i1}(L_i - L_1) + a_{i2}(L_i - L_2) + \dots + a_{i0}L_i + \dots + a_{in}(L_i - L_n) \right\}, \quad (4.34)$$

$$b = \min_i \beta_i, \quad (i = 1,2,\dots, n), \quad (4.35)$$

$$B = \max_i \beta \quad (i = 1,2,\dots, n). \quad (4.36)$$

There exist the following inequality relationships:

$$b S \leq K, \quad (4.37)$$

$$B S \geq K. \quad (4.38)$$

Proof:

Essentially, the verification complies with the proof of J. Barta /7/ where an analogous result has been proved for the torsional rigidity of thin-walled multi-field prismatic rod of straight centreline, definable on the basis of the Saint-Venant theory. It follows from the symmetry of matrix \underline{U} that the following relationship is correct:

$$\begin{aligned} \underline{L}^* \underline{f} &= \underline{L}^* \underline{U} \underline{D} = \underline{D}^* \underline{U} \underline{L} = \\ &= L_1 f_1 + L_2 f_2 + \dots + L_n f_n = D_1 \left[a_{10} L_1 + a_{12} (L_1 - L_2) + \dots \right. \\ &+ \left. a_{1n} (L_1 - L_n) \right] + D_2 \left[a_{21} (L_2 - L_1) + a_{20} L_2 + a_{23} (L_2 - L_3) + \dots \right] \\ &+ D_n \left[a_{n1} (L_n - L_1) + a_{n2} (L_n - L_2) + a_{no} L_n \right] = \beta_1 f_1 D_1 + \beta_2 f_2 D_2 + \dots \\ &+ \beta_n f_n D_n . \end{aligned} \quad (4.39)$$

On the basis of relationship (4.39), considering that quantities D_i are non-negative and the definition of b, B , it may be written that

$$G(f_1 L_1 + f_2 L_2 + \dots \dots + f_n L_n) \leq BS , \quad (4.40)$$

$$G(f_1 L_1 + f_2 L_2 + \dots \dots + f_n L_n) \geq bs . \quad (4.41)$$

It can be directly read from inequalities (4.40) and (4.41) that the theorem to be verified is correct.

5. COMMENTS ON INEQUALITY RELATIONS

5.1 A short discussion concerning inequality (4.5) is enough to show that the sign of equality in the formula applies only in case

$$\begin{aligned} b_i &= \lambda D_i , \\ (i &= 1, 2, \dots, n) , \end{aligned} \quad (5.1)$$

where λ is arbitrary but non-zero real constant.

5.2 In the special case when there is (there are) a quantity (or more quantities) of zero value among quantities a_{i0} (like in the case shown

in Fig. 8), upper bound

$$S < \infty \tag{5.2}$$

of no interest results from relation (4.32).

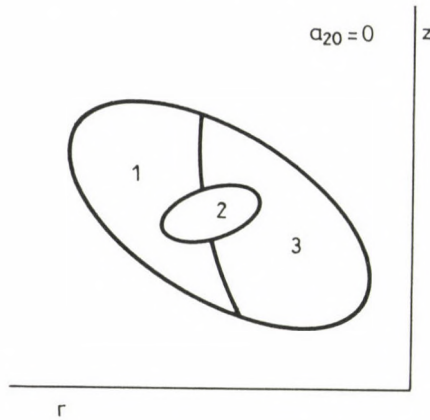


Fig. 8. A special case

5.3 It can be read from equations (4.18) and (4.25) that in relation (4.18), the sign of equality will apply only if

$$X_{ij} = a_{ij}(D_i - D_j) , \tag{5.3}$$

$$(i \neq j; i, j = 0, 1, 2, \dots, n, D_0 = 0) .$$

5.4 A short discussion as a completion of the derivation of inequalities (4.37) and (4.38) helps to show that in these formulas the sign of equality will apply only if

$$b = B \tag{5.4}$$

that is if

$$\beta_1 = \beta_2 = \dots = \beta_n . \tag{5.5}$$

Considering the definition of quantities β_i , the sequence of inequalities given in (5.5) can be fulfilled only if

$$\begin{aligned} L_i &= \lambda D_i , \\ (i &= 1, 2, \dots, n) , \end{aligned} \tag{5.6}$$

where λ arbitrary but non-zero real constant.

6. EXAMPLES

6.1 By selection of

$$b_1 = b_2 = \dots = b_n = 1 \quad (6.1)$$

from inequality relation (4.5), lower bound

$$S \geq G \frac{\left(\sum_{i=1}^n f_i \right)^2}{\sum_{i=1}^n a_{i0}} \quad (6.2)$$

can be derived for the numerical value of torsional rigidity S.

6.2 From inequality relation (4.18), by substituting

$$X_{12} = X_{21} = X_{13} = X_{31} = X_{23} = X_{32} = \dots \quad \dots = 0, \quad (6.3)$$

lower bound

$$S \leq G \sum_{i=1}^n \frac{f_i^2}{a_{i0}} \quad (6.4)$$

can be obtained for torsional rigidity S.

6.3 With

$$L_1 = L_2 = L_3 = \dots \quad \dots = L_n = 1 \quad (6.5)$$

in inequality relation (4.37) and (4.38),

$$\beta_i = \frac{a_{i0}}{f_i}, \quad (6.6)$$

$$(i = 1, 2, \dots, n).$$

Obviously

$$B = \max_i \beta_i = \max_i \frac{a_{i0}}{f_i} = A, \quad (6.7)$$

$$b = \min_i \beta_i = \min_i \frac{a_{i0}}{f_i} = a. \quad (6.8)$$

On the basis of relations (4.37), (4.38), it is possible to write that

THE TWIST PROBLEM OF SHELLS

$$G(f_1 + f_2 + \dots \dots + f_n) \leq AS , \quad (6.9)$$

$$G(f_1 + f_2 + \dots \dots + f_n) \geq aS . \quad (6.10)$$

In the special case when some a_{i0} is equal to zero, $a = b = 0$, result

$$G(f_1 + f_2 + \dots \dots + f_n) \geq 0 \quad (6.11)$$

follows from relation (6.10), which is of no interest in the present case.

6.4 Figure 9 illustrates the meridian section of the central surface of a shell of circular arc centreline, the wall thickness of which is constant, range A being set up of three elementary fields (cells).

In the present problem, definition of unknowns D_1, D_2, D_3 requires that linear equation system

$$\begin{aligned} a_{10}D_1 + a_{12}(D_1 - D_2) + a_{13}(D_1 - D_3) &= f_1 , \\ a_{21}(D_2 - D_1) + a_{20}D_2 + a_{23}(D_2 - D_3) &= f_2 , \\ a_{31}(D_3 - D_1) + a_{32}(D_3 - D_2) + a_{30}D_3 &= f_3 \end{aligned} \quad (6.12)$$

be solved, where

$$a_{10} = \left(\frac{2c}{R_1^3} + \frac{R_1^2 - R_2^2}{R_1^2 R_2^2} \right) \frac{1}{h} , \quad (6.13)$$

$$a_{12} = a_{21} = a_{13} = a_{31} = \frac{c}{R_2^3 h} , \quad (6.14)$$

$$a_{23} = a_{32} = \frac{1}{2} \frac{R_2^2 - R_3^2}{R_2^2 R_3^2 h} , \quad (6.15)$$

$$a_{20} = a_{30} = \frac{1}{2} \left(\frac{R_2^2 - R_3^2}{R_2^2 R_3^2} + \frac{c}{R_3^2} \right) \frac{1}{h} \quad (6.16)$$

$$f_1 = 2c \frac{R_1^2 - R_2^2}{R_1^2 R_2^2} , \quad (6.17)$$

$$f_2 = f_3 = c \frac{R_2^2 - R_3^2}{R_2^2 F_3^2} \quad (6.18)$$

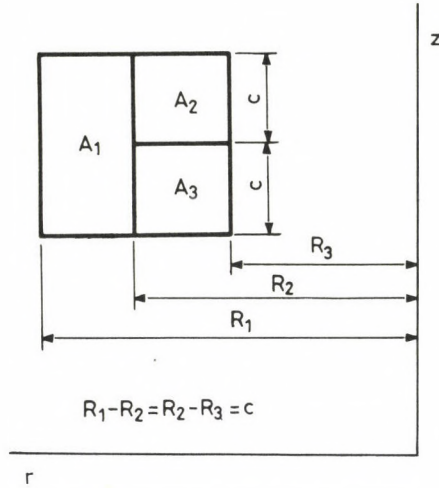


Fig. 9. Example for calculation of torsional rigidity

Calculating with values

$$R_1 = 4c, \quad R_2 = 3c, \quad R_3 = 2c \quad (6.19)$$

we will obtain

$$D_1 = 0.970712 \text{ ch} , \quad (6.20)$$

$$D_2 = 0.39763 \text{ ch} , \quad (6.21)$$

$$D_3 = 0.39763 \text{ ch} \quad (6.22)$$

from linear equation system (6.5).

Using the values given in (6.19) in calculation result

$$S = 0.167328 \text{ Gh} \quad (6.23)$$

can be derived from formula (3.26) for the numerical value of torsional rigidity.

6.5 Figure 10 shows the meridian section of the central surface of a shell of circular arc centreline, set up of congruent quadratic cells,

THE TWIST PROBLEM OF SHELLS

the wall thickness of the shell being constant.

Using the data of Fig. 9 in calculation, it may be written that

$$a_{10} = a_{n0} = \left(\frac{1}{2} \frac{R_1^2 - R_2^2}{R_1^2 R_2^2} + \frac{c}{R_1^3} + \frac{c}{R_2^3} \right) \frac{1}{h} \quad (6.24)$$

$$a_{12} = a_{21} = a_{23} = a_{32} = \dots = \frac{1}{2} \frac{R_1^2 - R_2^2}{R_1^2 R_2^2} \frac{1}{h} , \quad (6.25)$$

$$a_{20} = a_{30} = \dots = \left(\frac{c}{R_1^3} + \frac{c}{R_2^3} \right) \frac{1}{h} , \quad (6.26)$$

$$f_1 = f_2 = \dots = f_n = c \frac{R_1^2 - R_2^2}{R_1^2 R_2^2} . \quad (6.27)$$

Of course

$$c = R_1 - R_2 . \quad (6.28)$$

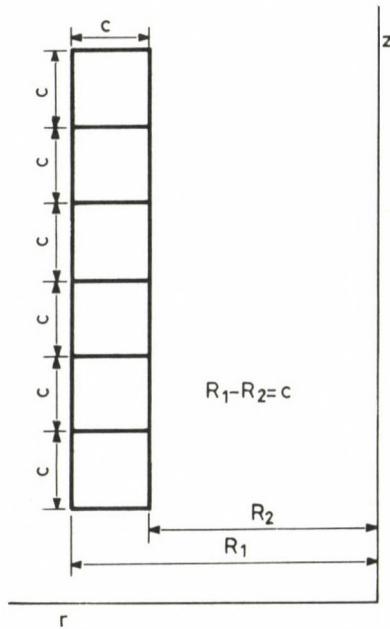


Fig. 10. Meridional section set up of quadratic cells

Let

$$R_1 = (\lambda + 1)c , \quad R_2 = \lambda c . \quad (6.29)$$

(6.30)

Using inequality relations (6.9) and (6.10) in this example, the following lower and upper bounds are obtained for the numerical value of torsional rigidity S:

$$S \geq \text{Ghn}m(\lambda), \quad (6.31)$$

$$S \leq \text{Ghn}M(\lambda), \quad (6.32)$$

where

$$m(\lambda) = \frac{\left(\frac{1}{\lambda^2} - \frac{1}{(\lambda+1)^2}\right)^2}{\frac{1}{\lambda^2} - \frac{1}{(\lambda+1)^2} + \frac{1}{(\lambda+1)^3} + \frac{1}{\lambda^3}}, \quad (6.33)$$

$$M(\lambda) = \frac{\left(\frac{1}{\lambda^2} - \frac{1}{(\lambda+1)^2}\right)^2}{\frac{1}{(\lambda+1)^3} + \frac{1}{\lambda^3}}. \quad (6.34)$$

REFERENCES

1. Timoshenko, S.P., Goodier, I.N.: Teoria uprogusti. Izd. Nauka. Phys. — Math. — Literature. Moscow 1975, 430-433.
2. Lehnitski, S.G.: Krutsherie anisotrophih krivogo bruse. Prik. Meth. Mech. 24/1960/.
3. Ecsedi, I.: Contribution to the twist problem of rods of circular arc centre-line. Műszaki Tudomány 60 (1980), 93-109.
4. Flügge, W: Stresses in shells. Springer Verlag, Berlin-Göttingen-Heidelberg 1960.
5. Goldenveizer, A.L.: Theory of elastic thin shells (translated by G.Hermann) Pergamon Press, Oxford-London-New York 1961.
6. Ralston, A.: Introduction to numerical analysis. Műszaki Könyvkiadó, Budapest 1969. Chapter 9.3, 431.
7. Barta, J.: Sur l'estimation de la rigidité de torsion des prismes multicellulaires à parois minces. Acta Techn.Hung. 12(1955), 333-338.
8. Blaise, O.: La torsion des prismes multicellulaires à parois minces. Annales des Ponts et Chaussées. 122, (1952), 601.
9. Blaise, P.: Sur la resolution numerique du problème de la torsion des prismes multicellulaires à parois minces. Acta Techn. Hung., 12 (1955), 333.

TORSION OF A THIN-WALLED, ANISOTROPIC, BENT ROD OF
CIRCULAR-ARC CENTRELINE

I. Ecsedi*

(Received 25 February 1986)

This work deals with the problem of uniform torsion of a thin-walled, anisotropic, linearly elastic, rod of circular-arc centreline and homogeneous material, generalizing the relationships derived by E. Reissner for an isotropic, linearly elastic rod of homogeneous material.

SYMBOLS

r, ϕ, z	cylindrical co-ordinates
$\underline{e}_r, \underline{e}_\phi, \underline{e}_z$	unit vectors
g	closed curve in plane rz
A	single-connected domain in plane rz confined by curve g
g_1, g_2	closed curves in plane rz
T	double-connected domain in plane rz confined by curves g_1 and g_2
s	arc co-ordinate defined over curve g
$\underline{\rho} = \underline{\rho}(s)$	equation of curve g
\underline{e}	tangential unit vector of curve g
\underline{n}	normal unit vector of curve g
" \times "	vectorial product of two vectors
" "	scalar product of two vectors
$\nabla = \frac{\partial}{\partial r} \underline{e}_r + \frac{\partial}{\partial z} \underline{e}_z$	Hamiltonian differential operator
$h = h(s)$	wall thickness
F	force
M	moment
$\epsilon_r, \epsilon_\phi, \epsilon_z$	specific elongation
$\gamma_{r\phi} = \gamma_{\phi r}, \gamma_{\phi z} = \gamma_{z\phi}$	specific angular changes
$\gamma_{rz} = \gamma_{zr}$	
$\sigma_r, \sigma_\phi, \sigma_z$	normal stresses
$\tau_{r\phi} = \tau_{\phi r}, \tau_{\phi z} = \tau_{z\phi}$	
$\tau_{rz} = \tau_{zr}$	shearing stresses,

*Dr. István Ecsedi, H-3526 Miskolc, Klapka Gy.u.36., Hungary

$$\begin{aligned}
 a_{11}, a_{12} &= a_{21}, \\
 a_{13} &= a_{31}, \\
 a_{15} &= a_{51}, \\
 a_{22}, a_{23} &= a_{32}, \\
 a_{25} &= a_{52}, \\
 a_{33}, a_{35} &= a_{53}, \\
 a_{44}, a_{46} &= a_{64}, \\
 a_{66}
 \end{aligned}$$

elasticity constants of anisotropic material

$$\psi = \psi(r, z)$$

$$\rho_{\underline{n}} = \underline{\rho} \cdot \underline{n}, u, v, w$$

auxiliary function
displacements

k

relative rigid-body displacement in the direction of the z-axis

\underline{S}

torsional rigidity

Other quantities and variables are defined in the text accordingly.

1. Figure 1 illustrates a closed curve g in plane rz . The z -axis is not intersected by curve g . Equation of curve g in the rz co-ordinate system of origin O :

$$\underline{\rho}(s) = R(s) \underline{e}_r + Z(s) \underline{e}_z. \quad (1)$$

With distance $h/2$ measured in both directions along normal n in point P of curve g we obtain points P_1 and P_2 for curves g_1 and g_2 running parallel with curve g , respectively (Fig. 1).

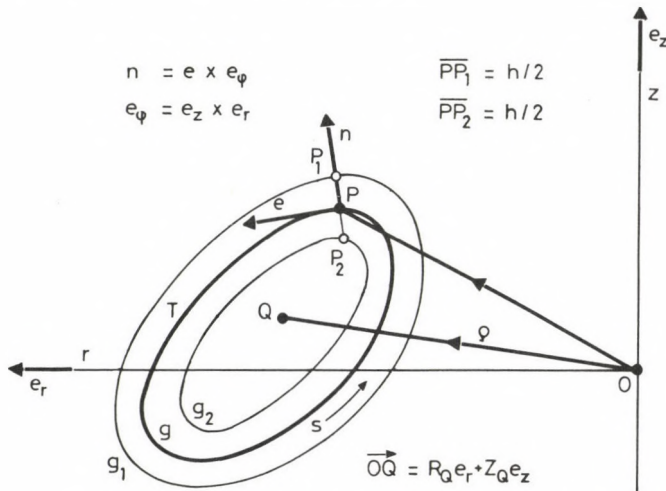


Fig. 1. Meridian section

TORSION OF A BENT ROD

Let the centre of gravity of annular domain T confined by closed curves g_1 and g_2 falling within plane rz be denoted Q . By displacing domain T angularly through angle α ($0 < \alpha < 2\pi$) around the z -axis we obtain the thin-walled rod of circular-arc centreline. The centreline of the rod is the arc of a circle of radius R_Q , determined by central angle α (Fig. 2).

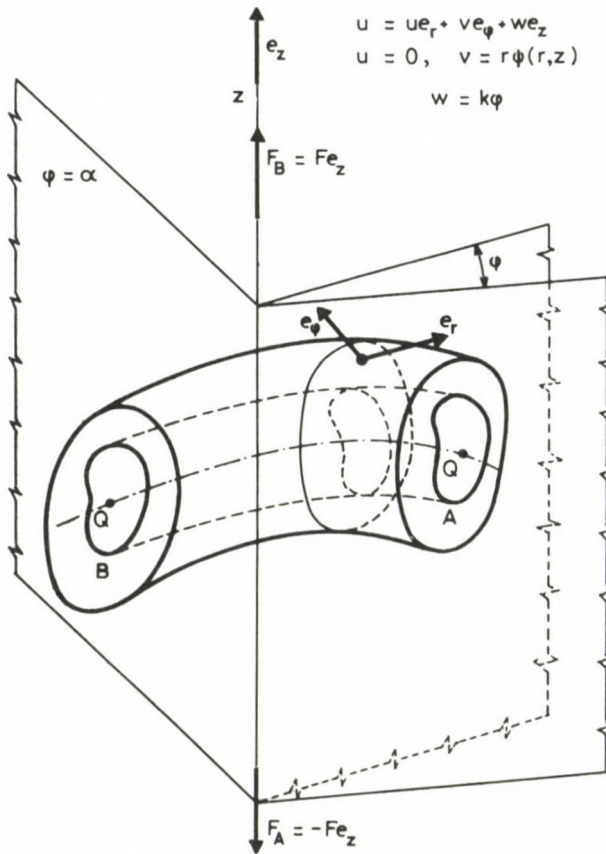


Fig. 2. Bent rod of circular-arc centreline

The wall thickness of the rod is essentially the width of domain T , $h=h(s)$, measurable in meridian plane rz . Acting upon marginal cross sections A and B of the thin-walled rod are forces

$$\underline{F}_A = -F_e_z \quad \text{and} \quad \underline{F}_B = F_e_z,$$

respectively, the line of action of forces F_A and F_B being the z-axis. The stress acting upon any cross section of the rod is a force of magnitude F falling within the cross sectional plane with the z-axis being its line of action. In the literature, the problem outlined above is called the uniform torsion of incomplete tores /2/, /3/, /4/.

A solution to the problem of uniform torsion of thin-walled, isotropic rods of closed cross section was given by E. Reissner /1/.

This work is designed to generalize the results of E. Reissner for the case of an anisotropic rod.

2. In the case investigated, the anisotropy of a thin-walled, closed cross section rod of circular-arc centreline in uniform torsion is described in the $r_\phi z$ co-ordinate system schematically illustrated in Fig.2 by Hook's law /4/, /5/:

$$\begin{aligned}
 \epsilon_r &= a_{11} \sigma_r + a_{12} \sigma_\phi + a_{13} \sigma_z + a_{15} \tau_{rz} , \\
 \epsilon_\phi &= a_{12} \sigma_r + a_{22} \sigma_\phi + a_{23} \sigma_z + a_{25} \tau_{rz} , \\
 \epsilon_z &= a_{13} \sigma_r + a_{23} \sigma_\phi + a_{33} \sigma_z + a_{35} \tau_{rz} , \\
 \gamma_{rz} &= a_{15} \sigma_r + a_{25} \sigma_\phi + a_{35} \sigma_z + a_{55} \tau_{rz} , \\
 \gamma_{z\phi} &= a_{44} \tau_{z\phi} + a_{46} \tau_{r\phi} , \\
 \gamma_r &= a_{64} \tau_{r\phi} + a_{66} \tau_{r\phi} .
 \end{aligned}
 \tag{2}$$

From the literature, it is well known that, independently of whether the rod of circular-arc centreline is isotropic or anisotropic, the stressed state of the rod displays the following properties /6/:

- a) The stressed state is independent of polar angle ϕ .
- b) In each point of the rod, normal stresses $\sigma_r, \sigma_\phi, \sigma_z$ and shearing stress $\tau_{rz} = \tau_{zr}$ are zero i.e.

$$\sigma_r = \sigma_\phi = \sigma_z = \tau_{rz} = 0 .
 \tag{3}$$

TORSION OF A BENT ROD

Accordingly, it can be written that

$$\tau_{z\phi} = \tau_{z\phi}(t,z), \quad \tau_{r\phi} = \tau_{r\phi}(r,z).$$

Assume that

$$\underline{\tau}\phi = \tau_{r\phi} \underline{e}_r + \tau_{z\phi} \underline{e}_z. \quad (4)$$

For a thin-walled rod of closed cross section, assume that tangential stress $\tau\phi$ is not changing along the cross sectional thickness of the rod and that $\tau\phi$ is parallel with tangential unit vector \underline{e} of curve g that is

$$\underline{\tau}\phi = \tau\phi(s) = \tau_{s\phi}(s) \underline{e}. \quad (5)$$

On the basis of a comparison of equations (1), (3), (4), it may be written that

$$\tau_{r\phi} = \tau_{s\phi} \frac{dR}{ds}, \quad \tau_{z\phi} = \tau_{s\phi} \frac{dZ}{ds}, \quad (6) (7)$$

since

$$\underline{e} = \frac{dR}{ds} \underline{e}_r + \frac{dZ}{ds} \underline{e}_z. \quad (8)$$

By testing the mechanical equilibrium of rod section AA'BB'CC'DD', we obtain on the basis of the equation of moment written for the z-axis the following relationship:

$$\tau_{s\phi} R^2 h = \tau_{s\phi}(0) R_2(0) h(0) = C = \text{constant}. \quad (9)$$

Using this relationship, it may be written that

$$\begin{aligned} \underline{F} &= \int_T \underline{\tau}\phi dT = \int_g \tau_{s\phi} \underline{e} h ds = \underline{e}\phi \times \int_g \tau_{s\phi} h \underline{n} ds = \underline{e}\phi \times \int_g \frac{C}{R^2} \underline{n} ds = \\ &= \underline{e}\phi \times \left[\int_A \left(\frac{C}{R^2} \right) \nabla dA \right] = \left(2C \int_A \frac{dA}{R^3} \right) \underline{e}_z. \end{aligned} \quad (10)$$

In the derivation of relationship (10), also the integral theorem of Gauss has been used. Using identity

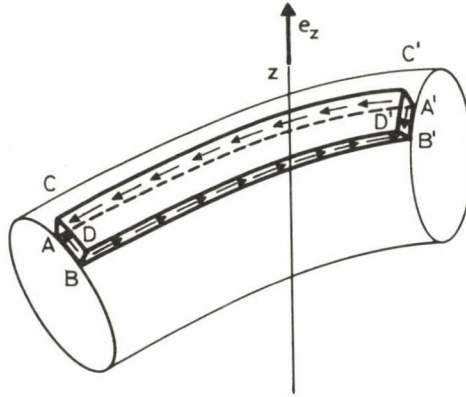


Fig. 3. Derivation of the equilibrium equation

$$2 \int_A \frac{dA}{r^3} dA = - \int_A \frac{\partial}{\partial r} \left(\frac{1}{r^2} \right) dA = - \int_g \frac{n_r}{R^2} ds = \int_g \frac{1}{R^2} \frac{dZ}{ds} ds = \int_g \frac{dZ}{R^2}, \quad (11)$$

formula (9) can be further transformed and written in the following shape:

$$\underline{F} = C \left(\int_g \frac{dZ}{R^2} \right) \underline{e}_z. \quad (12)$$

In the derivation of relationship (11),

$$\underline{n} = n_r \underline{e}_r + n_z \underline{e}_z = - \frac{dZ}{ds} \underline{e}_r + \frac{dR}{ds} \underline{e}_z$$

has been taken into consideration.

Formula (12) reads that

$$C = \frac{F}{\int_g \frac{dZ}{R^2}} \quad (13)$$

The moment of shearing stresses $\underline{\tau}_\phi = \tau_{s\phi} \underline{e}_\phi$ acting upon a cross-section in any arbitrary meridian plane $0 \leq \phi \leq \alpha$ can be determined for starting point 0, the origin of the coordinate system on the basis of formula

$$\underline{M} = \left(\int_A \tau_{s\phi} h \rho_n ds \right) \underline{e}_\phi \quad (14)$$

TORSION OF A BENT ROD

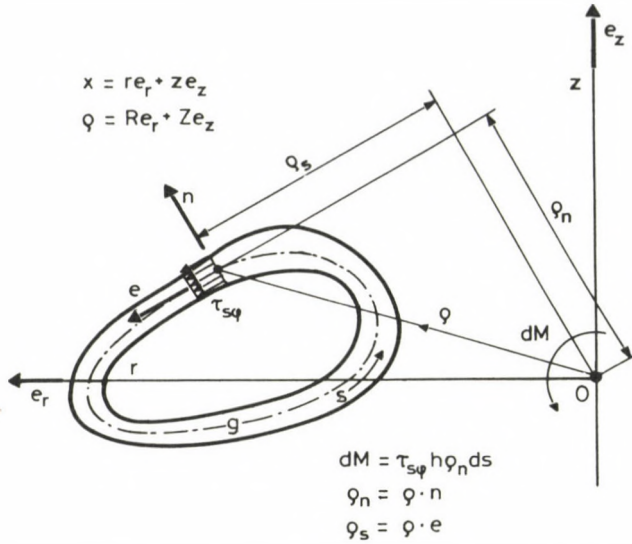


Fig. 4. Calculation of the moment of shearing stresses

where

$$\rho_n = \underline{\rho} \cdot \underline{n} \quad (15)$$

Considering that

$$\underline{M} = M \underline{e}_\phi \quad (16)$$

and

$$M = \int_g \frac{C}{R^2} \rho_n ds = C \int_g \frac{\underline{\rho} \cdot \underline{n}}{R^2} ds = C \int_A \left(\frac{\underline{x}}{r^2} \right) \cdot \nabla dA = 0 \quad (17)$$

since

$$\underline{x} = r \underline{e}_r + z \underline{e}_z \quad (18)$$

and

$$\left(\frac{\underline{x}}{r^2} \right) \cdot \nabla = \frac{\partial}{\partial r} \left(\frac{1}{r} \right) + \frac{\partial}{\partial z} \left(\frac{z}{r} \right) = -\frac{1}{r^2} + \frac{1}{r^2} = 0 \quad (19)$$

Relationships (9) (12), (17) read that shearing stresses determined on the basis of formula

$$\tau_{s\phi} = \frac{F}{\int_g \frac{dZ}{R^2} ds} \frac{1}{R^2 h} \quad (20)$$

distributed in the plane of the cross-section, are equivalent to a force of magnitude F , the line of action of which being the z -axis.

3. A combination of equations (2), (3), (5), (6) permits writing

$$\varepsilon_r = \varepsilon_\phi = \varepsilon_z = \gamma_{rz} = 0, \quad (21)$$

$$\gamma_{z\phi} = \gamma_{z\phi}(r, z), \quad (22)$$

$$\gamma_{r\phi} = \gamma_{r\phi}(r, z). \quad (23)$$

It has been proved in [3], [7] that a displacement field of a geometry

$$u = 0, \quad (24)$$

$$v = r \psi(r, z), \quad (25)$$

$$w = k\phi, \quad (k = \text{constant}) \quad (26)$$

is associated with the above deformation (specific elongations and angular distortions) in the $r\phi z$ cylindrical co-ordinate system.

Kinematically, the implication of quantity k in formula (26) is quite obvious: k is the displacement of two cross sections falling within the meridian plane, including unit angle, as compared with each other in the direction of the z -axis.

Using the geometric equations, we obtain on the basis of equations (24), (25), (26) the following formulae:

$$\gamma_{r\phi} = r \frac{\partial \psi}{\partial r}, \quad (27)$$

$$\gamma_{z\phi} = r \frac{\partial \psi}{\partial z} + \frac{k}{r}. \quad (28)$$

Specific angular change $\gamma_{s\phi}$ in the points of curve g can be determined on the basis of formula

$$\begin{aligned} \gamma_{s\phi} &= \gamma_{r\phi} \frac{dR}{ds} + \gamma_{z\phi} \frac{dZ}{ds} = R \frac{\partial \psi}{\partial r} \frac{dR}{ds} + R \frac{\partial \psi}{\partial z} \frac{dZ}{ds} + \frac{k}{R} \frac{dZ}{ds} = \\ &= R \frac{\partial \psi}{\partial s} + \frac{k}{R} \frac{dZ}{ds}. \end{aligned} \quad (29)$$

A combination of formulae (1), (5), (6) yields

$$\gamma_{R\phi} = a_{66} \tau_{R\phi} + a_{46} \tau_{z\phi} = \left(a_{66} \frac{dR}{ds} + a_{46} \frac{dZ}{ds} \right) \tau_{s\phi}, \quad (30)$$

$$\gamma_{z\phi} = a_{46} \tau_{R\phi} + a_{44} \tau_{z\phi} = \left(a_{46} \frac{dR}{ds} + a_{44} \frac{dZ}{ds} \right) \tau_{s\phi}. \quad (31)$$

Formulae (32), (33) can be derived by the use of formulae (29), (30), (31):

$$\gamma_{s\phi} = \left[a_{66} \left(\frac{dR}{ds} \right)^2 + 2 a_{46} \frac{dR}{ds} \frac{dZ}{ds} + a_{44} \left(\frac{dZ}{ds} \right)^2 \right] \tau_{s\phi}, \quad (32)$$

$$\frac{\partial \psi}{\partial s} = -\frac{k}{R^2} \frac{dZ}{ds} + \frac{1}{R} \left[a_{66} \left(\frac{dR}{ds} \right)^2 + 2 a_{46} \frac{dR}{ds} \frac{dZ}{ds} + a_{44} \left(\frac{dZ}{ds} \right)^2 \right] \tau_{s\phi}. \quad (33)$$

Considering that the displacement field is unique, there exists relationship

$$k \int_g \frac{1}{R^2} \frac{dZ}{ds} ds = C \int_g \frac{1}{R^3 h} \left[a_{66} \left(\frac{dR}{ds} \right)^2 + 2 a_{46} \frac{dR}{ds} \frac{dZ}{ds} + a_{44} \left(\frac{dZ}{ds} \right)^2 \right] ds \quad (34)$$

as a result of equation

$$\int_g \frac{\partial \psi}{\partial s} ds = 0. \quad (35)$$

In writing the above relationship, also equation (8) has been used.

4. The torsional rigidity of a thin-walled rod of circular-arc centreline and of closed cross section in uniform torsion is defined by formula

$$S = \frac{F}{k} \quad (36)$$

/1/, /4/, /7/.

Using formula (13), (34), /36/, we obtain relationship

$$S = \frac{\left(\int_g \frac{1}{R^2} \frac{dZ}{ds} ds \right)^2}{\int_g \frac{1}{R^3 h} \left[a_{66} \left(\frac{dR}{ds} \right)^2 + 2 a_{46} \frac{dR}{ds} \frac{dZ}{ds} + a_{44} \left(\frac{dZ}{ds} \right)^2 \right] ds} \quad (37)$$

for the numerical value of torsional rigidity S . Relationship (37) can be transformed by means of formula (10) to obtain formula

$$S = \frac{\left(2 \int_A \frac{dA}{r^3} \right)^2}{\int_g \frac{1}{R^3 h} \left[a_{66} \left(\frac{dR}{ds} \right)^2 + 2 a_{46} \frac{dR}{ds} \frac{dZ}{ds} + a_{44} \left(\frac{dZ}{ds} \right)^2 \right] ds} \quad (38)$$

The formula derived by E. Reissner /1/ for the torsional rigidity of an isotropic rod follows directly from formula (37) with the following substitutions:

$$a_{46} = a_{64} = 0, \quad a_{44} = a_{66} = 1/G.$$

5. Finally, the displacement of curve g , the mid curve of the meridian plane, at right angles to the meridian plane is determined. The vector coordinate of the displacement in question in direction \underline{e} , i.e. function $v = v(s)$, is obtained on the basis of a relationship written as a combination of formulae (36), (37):

$$v(s) = \frac{v(0)}{R(0)} R(s) + \frac{FR}{\int_g \frac{1}{R^2} \frac{dZ}{ds} ds} \left\{ \frac{\int_0^S \frac{1}{R^2} \frac{dZ}{ds} ds}{\int_g \frac{1}{R^2} \frac{dZ}{ds} ds} \int_g \frac{1}{R^3 h} \left[a_{66} \left(\frac{dR}{ds} \right)^2 + \right. \right. \\ \left. \left. + 2 a_{46} \frac{dR}{ds} \frac{dZ}{ds} + a_{44} \left(\frac{dZ}{ds} \right)^2 \right] ds + \int_0^S \frac{1}{R^3 h} \left[a_{66} \left(\frac{dR}{ds} \right)^2 + \right. \right. \\ \left. \left. + 2 a_{46} \frac{dR}{ds} \frac{dZ}{ds} + a_{44} \left(\frac{dZ}{ds} \right)^2 \right] ds \right\}. \quad (39)$$

Constant $v(0)$ in formula (39) is a quantity in relation with the rigid body displacement around the z -axis.

TORSION OF A BENT ROD

REFERENCES

1. Reissner, E.: Note on the problem of twisting of circular ring sector. *Quart. Appl. Math. and Mech.* 7 (1949), 342-347.
2. Michell, I.H.: Uniform torsion flexure of incomplete tores. *Proceedings of the London Mathematical Society* 31 (1899), 140-141.
3. Freiburger, W.: The uniform torsion of an incomplete tore. *Australian J. Scient. Res. Ser. A.* 2(1949), 354-375.
4. Lehnickij, S.G.: *Krutschenie anisotropnih i nesgorodnih stershnei.* Izd. Nauka Fiz-Mat. Literaturi. Moscow 1971, 211-215.
5. Lehnickij, S.G.: *Teoria uprugosti anisotropnovo tela.* Izd. Nauka Fiz-Mat. Literaturi. Moscow 1977, 346.
6. Ecsedi, I.: Comments on the problem of torsion of rods of circular-arc centreline. *Műszaki Tudomány* 66. (1980), 93-109. (in Hungarian)
7. Timoshekno, S.P., Goodier, I.N.: *Teoria uprugosti.* Izd. Nauka Fiz-Mat. Literaturi. Moscow (1975), 430-433.

STATE CONSERVATION OF HIGHWAYS

L. Gáspár Jr.*

(Received 23 July 1985)

The change in the state of highways is affected by several parameters. Owing to recent restrictions in the finances, the conservation of the current state of roads above an acceptable standard has become a task which can be fulfilled only with difficulty and only to the detriment of the earlier larger-scale evolution. Knowing the current state of highways in Hungary, the author makes a suggestion concerning the selection of the most convenient intervention types available for maintenance. The basic principles are outlined together with the first steps of a comprehensive work the main objective of which is to develop an economical system for the conservation of the state of the road. The sequence of future interventions is given, which might be applied considering their practicability as well as a system of index numbers to characterize the state of pavements and a method for the technico-economic comparison of the different road maintenance techniques.

1. INTRODUCTION

In satisfying the ever increasing demand of the country's economy on transport – a tendency manifesting itself throughout the world – road transport takes an increasing share, wherefore, as a matter of course undisturbed road traffic has a great significance from the point of view of the economy. However, for an undisturbed road traffic, a pavement of appropriate quality is needed. The significant reduction of the financial means available for road engineering which has taken place lately, makes it particularly timely to find an economical way of the conservation of the road network having a value of several thousand million forints, a considerable sum in Hungarian economy. In the following, some research activities undertaken in Hungary in this field will be reported.

2. CHANGE IN THE STATE OF THE HIGHWAY NETWORK

Let us briefly survey the process in the course of which the condition of a road undergoes changes.

After having completed a new road construction or immediately after the completion of the pavement structure, both the pavement and the drainage

*Dr. L. Gáspár, H-1158 Budapest, Doktor S. u. 2, Hungary

system are in a very good condition. This "initial condition" is primarily influenced by the level of design for the contract, the properties of the building material used and by the standard of the construction work /1/.

The quality estimation of the completed project is part of the procedure of acceptance. (In general, quality estimation is aided by quality control during construction.) The quality grading, in the acceptance record has also to establish the degree of the approximation of the high quality specified in advance. Although this classification follows universal rules based on professional knowledge, because certain parameters can be estimated only by inspection, also the subjectivity of the persons carrying out the classification may affect the value of the estimation.

Consequently, the decision on the quality grade might be considered as a joint result of — for the most part objective measurements and to a lesser part subjective factors. However, it seems necessary to emphasize that the terms "objective" and "subjective" are by no means equivalent with values of judgement or with the terms "reliable" and "unreliable". Namely, the keen observation of specifications, engineering directives, standards, etc., might be considered objective activities, while the decisions made by the representatives of the investor on the basis of the consideration of other field circumstances of their expert's knowledge and experiences can be considered subjective ones.

In the course of the engineering acceptance examinations, the guarantee period, which at present is a minimum of one year, may be extended. This might occur in the following cases: (a) severe damage can develop after a few years initiated by minor defects of the pavement; (b) hidden damages may arise on the surface (or may be activated within a short time; (c) in cases when one of the quality parameters approaches the acceptance limit, the contractor agrees to a guarantee period of 2 or 3, incidentally 5 years in hope of an advantageous evaluation during the acceptance procedure. The extension of the guarantee period can have the following advantageous economic effects:

- the damages occurring within this period will be repaired at a professional level and without legal dispute;
- the contractor is motivated to do a good job;
- voluntary acceptance of a lengthened guarantee period can serve, in the ever increasing market competition, as a means to justify its reliability.

STATE CONSERVATION OF HIGHWAYS

Although roads are meant for life, so to say to be everlasting, the state of the pavement, deteriorates mainly under traffic and atmospheric influences. This process can be slowed down significantly by appropriate maintenance, while incidental non-proper use can cause rapid deterioration. The deterioration process can produce several types of defect, in some instances a series of defects, of which the most significant ones are as follows:

- linear cracks,
- hair cracks, mosaic cracking, pavement disintegration,
- ravelling, peeling, potholing,
- rutting,
- bleeding, development of a slippery surface,
- wear of chipping grains, development of slippery surface,
- longitudinal waves.

Some of these defects deteriorate approximately linearly with time, others have a progressive or degressive character. It may also occur that a defect, e.g. rutting, due to the causes responsible for the damages may develop in several different ways depending on the predominant accelerating or decelerating factor (deformation and wear or postcompaction, respectively).

The state of the road showing gradual deterioration is subjected to systematic investigation. The expert staff responsible for the maintenance and operation obtain visual information during the periodic highway state surveys. (In their activities the persons responsible are aided by a list of defects with photo illustrations.) /2/ In addition, countries with a higher standard of highway management, mainly on highways with heavy traffic also carry out state surveys using different measuring instruments of high performance and rapid operation. (The parameters measured most frequently are: load bearing capacity, riding comfort, friction coefficient, rut depth, surface soundness.) The time for performing measurements is of great significance in the case of parameters the actual value of which is significantly affected by the season or weather. The time series obtained from the data on the state of the road sections give information about the process of deterioration. From the regularities of deterioration characteristic of the given type of road (performance models) and from the extrapolation of condition data the residual service life can be predicted. However, generally this activity is of limited exactness due to the facts listed below:

- the performance models taken as a basis can only be approximate and generalized,

- the deterioration process can be changed by unexpected conditions (e.g. extreme weather),
- the extrapolation can be carried out only based on a single state parameter, but the value of this may be strongly influenced by other parameters owing to their mutual interaction,
- the future traffic volume can only be estimated with a rather uncertain approximation.

If one of the state parameters, namely the critical one, deteriorates to an extent approaching the threshold value, intervention is needed in order to carry out repair work. (This activity otherwise exerts a more or less strong influence on parameters which have not yet reached the critical level.)

The optimal moment of an intervention of higher significance (e.g. strengthening the pavement structure) is not always determined by the change of a single parameter to the threshold value but also by the comparatively low value of several condition parameters. It often occurs that due to some constraints (lack of financial means, mechanical equipment, or manpower, etc.) repair works cannot be carried out at the optimal time. This unfavourable circumstance usually causes significant losses.

It is to be noted that the establishment of the threshold values calling for intervention is a complex technico-economic task. Obviously in case of very limited financial resources even the standard of state still tolerable will be further reduced. It sometimes occurs that warning limits are given which notify in advance of the approach of the term of intervention, i.e. the need for planning condition improving activities.

It may occur that the different parameters (load capacity, surface soundness, need of maintenance work, etc.) on a road section are not in agreement with one another. In such cases before a decision is made on the intervention each value has to be revised and, if it is found that the first data have been correct, and the "contradiction" still exists, different compromise-based solutions can be applied.

3. THE CONDITION OF THE PAVEMENT AND THE TYPE OF INTERVENTION NEEDED

The suitability survey carried out in 1979 practically extended to the entire road network of the country furnished reliable information on the actual state of the roads /3/. The continuous updating of the information

STATE CONSERVATION OF HIGHWAYS

mentioned above as well as the repetition in 1984 of the comprehensive survey already permitted the determination of several time series. On the other hand, a comparatively large number of condition improving (maintenance) techniques are available several of which might be considered energy saving and environment protecting.

The compilation of a design guideline became necessary containing information for the selection of the most appropriate intervention technique for a given pavement condition. Namely, it is evident, that among several variations there is to be found one which, if applied at the appropriate time, can be considered more effective than the others. This guideline has been published on behalf of the Road Transport Department of the Ministry of Transport by the Institute for Transport Sciences at the beginning of the year 1985 /4/.

The purpose of this publication can be summarized as follows. It contains information on the types and number of interventions to be carried out on the pavement based on the rating notes connected directly or indirectly with the condition of the pavement and obtained mainly from the suitability survey. The suitability surveys performed on the highway network are based as it is known, on the separate evaluation of several parameters. However, the actual values of these parameters together determine a single "road condition" and, correspondingly, a single most suitable method of intervention. The design guideline worked out illustrates this kind of interrelation.

The design guideline is intended mainly to assist the experts of the highway directorates. It helps to determine the extent of the improvement interventions to be performed on a network in a given condition based on the consideration of the technical and economic information available. The choice of the work to be carried out is helped by the simultaneous consideration of the techniques described in the design guideline and the road traffic volume. However, the road engineers, in possession of local knowledge and practical experience, take other factors into account (e.g. hydrologic or soil conditions, the different maintenance principles, financial possibilities) and came to the final decision relating the condition improving intervention and to the kind of the work to be carried out on a "subjective basis". Prior to the actual measure economic calculations should be made.

It is worth while to note that the design guideline can be effectively utilized, in addition to the purposes mentioned above, also to work out

nation-wide examination programs (e.g. to support the ratios and quantities of the interventions, to help the distribution of the financial means, etc.).

The publication of the design guideline might be considered the first step towards the complex state evaluation and towards an economical highway management.

When compiling the design guideline parameters have been considered which are associated with the actual or future condition of the pavement. On the basis of the above considerations the following parameters have been selected for use:

- (a) load bearing capacity of the pavement (measured by the Lacroix deflectograph or the Benkelman beam),
- (b) soundness of the pavement surface (by unified visual state classification or with the aid of the state surveying guide-book),
- (c) drainage of the pavement (by unified visual state classification, with the aid of the state surveying guide-book),
- (d) unevenness of the pavement (measured with the Bump Integrator or, where such measurement results are not available, by visual estimation).

To make the manual work easier, the number of the (mathematically possible) variations have been strongly reduced to

- 3 groups of load bearing capacity
- 3 groups of surface soundness, and to
- 2 groups of surface unevenness; but there are no special groups for drainage. The measures to be undertaken in case of inadequate drainage should only be mentioned on the different unit sheets (it should be noted that for the evaluation of the load bearing capacity, the soundness and evenness of the surface 5 scores for each and 3 scores for the drainage are available, but on grounds of experience the reduction carried out seems to be justified);

– the number of variations could be decreased by the "condition variations" which require no intervention within 5 years;

– in the selection of definite validity, the state variants to be assigned as individual alternatives, also the actual occurrence frequency observed in the course of the latest country-wide survey, i.e. the total of the km-lengths have been taken into account and the variants of less frequent occurrence which did not reach the length of 50 to 100 km, have been omitted;

STATE CONSERVATION OF HIGHWAYS

— the asphalt concrete and macadam-type pavements (of void content decreasing under effect of the traffic load) ought to be classified (due to the fact that the type of the wearing course affects the type of the intervention techniques to be applied) into a special group, but the techniques to be used have not been separated according to the load applied on the road and to the category of the road with the implicit assumption that the asphalt concrete pavement has been constructed on main roads or on secondary roads with dense traffic while the macadam-like pavement has been applied on secondary roads with light traffic. The unit sheets should be used in cases differing from those assumed.

The design guideline does not apply to repairs of defects due to thawing damages.

Drafting of the design guideline consisting of 22 sheets, is demonstrated in Fig. 1. The technological variants suggested by this paper take into account to a certain extent also the combined effects of the different defects. Under the title "Realization" the most significant rules of the planning, the implementation and the quality control of condition improving interventions are given, for brevity's sake, only in the form of referentions. The design guideline calls attention to the possibility of the application of hydraulic binders if this can come into question at all.

For sections of asphalt concrete pavement only asphalt concrete layers, in extreme cases partly with hydraulically bound ones, while for sections with macadam-like pavements either macadam-like layers or those of asphalt concrete character are suggested for strengthening. (This latter solution comes only into the foreground in case of heavy traffic.)

As to the case of intervention urgency, three grades are suggested depending on the condition improvement needed within one, three or five years. In some instances prior to the final decision control measurements are suggested to permit the consideration or the elimination of eventual changes in the meantime.

Later when sufficient empirical knowledge will be available, the design guideline can be further developed and in the distant future, its validity can be extended to the road network managed by local authorities.

In Table 1 the types of intervention intended for certain combinations having sufficiency notes or of state images as well as the urgency of the implementation are indicated. The symbols in Table 1 denote the condition parameters as follows: T = load bearing capacity, F = soundness of surface, E = surface evenness.

VARIANT OF CONDITION IMPROVING TECHNIQUE		No. 14.				
FUNDAMENTALS	ROAD SECTION	STATE NOTES OF SUITABILITY SURVEY				
	type, traffic	wearing course	load capacity	surface soundness	drainage	surface unevenness
	-----	macadam type pavement	T 1-3	F 4-5	V 1-3	E 1-3
	CHARACTERISTIC FEATURES					
TYPE	Surface dressing					
PRIMARY OBJECTIVE(S)	Repair of surface soundness					
NEED OF URGENCY	Within one year					
REALIZATION	<p>It is recommended to repair within one year the impermeability and skid resistance of the hard cover surface by application of bitumen emulsion surface dressing. To determine the quality and quantity of the material to be used to this end, the engineering recommendations No. MI-07 3403/5-85 are decisive. The incidental pothole elimination should be realized two months prior to the surface dressing. After finishing the seal coat traffic is not permissible to use for three hours. On macadam-like asphalt pavements the surface of which is rich in binder, the cutback surface dressing is to be preferred (according to the recommendations No. MI-07 3403/5-85). On a strongly cracked pavement surface dressing must not be applied. In case where this condition is not fulfilled, within one year a levelling course is to be constructed. In this case penetration macadam levelling course can be applied (technical recommendations No. MI-07 3403/5-85). For such a purpose also asphalt emulsion can be used if the necessary materials and machinery are available (technical recommendations MI-07 3215/2 J). Within one year shoulder and drainage ditch repairs have to be carried out in case where the suitability note is V2-3.</p>					
NOTE	The selection of the binder of the surface dressing is also influenced by the longitudinal and cross fall of the highway section.					

Fig. 1 Example to the Technique Unit Sheet

Table 1. Types of interventions to be applied in case of different "condition patterns"

No. Suitability notes	Intervention types						Drainage ³
	Strengthening over 10 equivalent cm		Strengthening under 10 equivalent cm		Surface interventions		
	Asphalt concrete (AC)	Hydr.bound with thin AC	Asphalt concrete	Penetration macadam or emulsion asphalt	Levelling course	Surface dressing	
<u>Pavement of asphalt concrete types</u>							
1.T3	F1-2	E4-5				III	/III/
2.T1-3	F3	E4-5				III	/III/
3.T1-3	F4-5	E1-3				I ⁵	/I/
4.T1-3	F4-5	E4-5				I	/I/
5.T4	F1-2	E1-3				III	/I/
6.T4	F1-3	E4-5		III			/I/
7.T4	F3	E1-3		V			/I/
8.T4	F3	E4-5		III			/I/
9.T4	F4-5	E1-3		III			/I/
10.T4	F4-5	E4-5		I			/I/
11.T5	F1-2	E1-5		I			/I/
12.T5	F3-5	E1-5	I ^{4,1}	I ^{4,1}	I ⁴		/I/

Table 1. Types of interventions to be applied in case of different "condition patterns"(cont.)

No. Suitability notes	Intervention types						Drainage ³
	Strengthening over 10 equivalent cm		Strengthening under 10 equivalent cm		Surface interventions		
	Asphalt concrete (AC)	Hydr.bound with thin AC	Asphalt concrete	Penetration macadam or emulsion asphalt	Levelling course	Surface dressing	
<u>Macadam-type pavements</u>							
13. T1-3 F3 E4-5					III		/I/
14. T1-3 F4-5 E1-3						I ⁵	/I/
15. T1-3 F4-5 E4-5					I		/I/
16. T4 F1-2 E4-5					V	III	/I/
17. T4 F3 E4-5					V	III	/I/
18. T4 F3 E1-5						III	/III/
19. T4 F4-5 E1-5			V ²	V ²			/I/
20. T5 F1-2 E1-5			III ²	III ²			/III/
21. T5 F3-5 E1-3	III ^{4,1}	III ^{4,1}	III ²	III ²			/I/

Legends: I = to be carried out within one year; III = to be carried out within three years; V = to be carried out within five years; 1 = in case of a strengthening need over 30 equivalent cm the construction of a hydraulically bound (conveniently fly-ash concrete) pavement with a thin AC wearing course should be investigated; 2 = over the value of $F_{100} = 500\ 000$ an asphalt concrete type pavement should be constructed; 3 = the values between parentheses are valid only in case where the suitability note of the drainage is V3 or V2 and it occurs together with T4-5 and/or with F4-5; 4 = the fact whether a thin or a thick strengthening is to be applied, depends on the extent in lack of bearing capacity (see also note 1.); 5 = surface dressing can be applied in case where the pavement surface is not strongly cracked or deformed

4. ECONOMIC CONSERVATION OF HIGHWAYS

Demands on road traffic are growing but, at the same time, the financial means available for road construction and for their state conservation are decreasing. The ever increasing gap between demands and financial possibilities imperatively requires the endeavour to greatly increase the economy of the condition conservation activities. In the following, a method for trying to realize the above objective will be summarized.

In optimizing the activities for conservation of the road network, in connection with the interventions to be realized on certain road sections, in the first line the questions "where", "when" and "what" should be answered. The strategy of road maintenance can be based on several kinds of principles; the possibility of the grouping of these principles is furnished by the extent of their theoretical or empirical character. The method of approach described in the following, uses empirical data almost exclusively. A method has been worked out for collecting and processing accessible data concerning actual condition improving interventions carried out on the domestic network and has led to conclusions and plotting graphs which could serve as a basis for the actual planning of conservation activities. The main parts of the system under development are as follows: data collection, planning the service life of the condition improving interventions, comparison of alternative interventions, determination of the scale of intervention which may come into question as could be applicable.

4.1 Data collection

Considering that the procedure is based on the actual domestic situation, a preliminary, detailed and largely extended data collection has a decisive significance. This is an essential condition because, in general, at present no data base is available for co-ordinated nation-wide information.

From among the activities related to this subject, the following groups of information might be utilized:

— a study made by the Hungarian Institute for Transport Sciences (KTI) in connection with the data relating to the quality of pavement structure strengthenings carried out on the Hungarian road network from 1976 to 1983;

– a KTI study co-ordinated by the so-called "Service-life Commission" on roads concerning their service life, commenced in country Fejér, and extended thereafter to the whole country;

– data collection in the UTORG related to the condition of the road network of the country, with the results of the suitability surveys, and the processing of these data;

– the design guideline worked out by KTI, dealing with the condition improving interventions which can conveniently be utilized in case of different combinations of the state notes established by the suitability survey of national highway network;

– the theoretical and practical results obtained so far in connection with the suitability survey of national and local road networks;

– the results, i.e. evaluations contained by the KTI study obtained in the course of following the deterioration process of 30 road sections selected for this purpose between 1973 and 1979;

– publications of KTI' (i.e. of its legal predecessor, Road Research Institute) containing the data of the condition improving interventions carried out in the past on the road network;

– the results obtained by the "rapid" condition evaluation procedure worked out by KTI in 1975;

– experiences obtained by the application of the Dimensioning Code for Flexible Road Pavement Structures (HUMU) published in 1971 and preliminary examinations for its revision;

– results of recent traffic counts on the road networks;

– country-wide or county soil conditions and other information in connection with the soil of earthworks and the hydrologic conditions;

– different regulations for the acceptance of highway construction type projects (ÉKSZ-70 Vol. VI, Ministry of Transport and Communication: Tentative Technical Directives 63/75, M.T.C. (K.P.M.) Tentative Technical Directives 63/77, MSZ-07 3210/83. Sectoral Standard);

– publications of the Central Statistical Office in connection with prices, changes of prices and price indices;

– development of the main characteristics of highway accidents.

For the elaboration of the engineering directives there should be available, in addition to the information sources mentioned above, data associated with the interventions and their specific costs to be found at the District Highway Directorates. This activity may run into difficulties due

STATE CONSERVATION OF HIGHWAYS

to several reasons:

(a) Registrations of data of the different District Directorates differ from each other to a certain extent.

(b) Some of the information sources originating from earlier periods have got lost due to reorganizations carried out in the meantime or in consequence of staff changes.

(c) The changes in numbering and in kilometric marking of roads reduce the reliability of old data;

(d) In some instances the lack of a uniform nomenclature (technical terms) causes difficulties, mainly in cases where interventions carried out earlier are to be evaluated.

Due to these disadvantageous circumstances only part of the engineering and financial data needed are available. There are sections on which absolutely no information is to be found. Accurate information is available only on roads built comparatively recently or in connection with roads which had been handled earlier as high priority roads, mostly main highways designated with a single figure.

Besides, if the data collection is extended to data on traffic, results are obtained at provisional or stationary traffic survey stations. For our examinations the values of the average daily traffic, taking all vehicle types into account, expressed in the measurement unit of unit-vehicle per day are of interest, but the value F_{100} related only to the heavy vehicles and expressed conveniently in a daily average number of converted 100 kN axle load is of greater significance.

Informative data should also be collected on the characteristics of the earthworks of the road sections in question. To achieve this goal beside the soil mechanical and hydrologic maps accessible, soil mechanical expert opinions (if they can be found) as well as further data related to the subject in question to be found in the possession of the Highway Directorates (e.g. individual sampling, data collection initiated by them) might be used. Information is further needed on the quality of the project (new construction or strengthening of the pavement). Beside establishing the quality grade, full information is needed on whether during the acceptance procedure all of the determined quality parameters' data had been obtained. For instance, it is not indifferent whether the quality grad II established had based on the unsuitability of density or of the pavement profile.

All in all, at each road section the main objective is to collect a

Table 2 Data collected about a highway section

Location of highway section	Type of soil	Hydrologic condition	Traffic data
Approach road to Kismarót 0 + 000 – 5 + 700	silt	No danger of humidification	1970 522/day ; 18 heavy axle/day 1975 1217/day; 39 heavy axle/day 1980 1501/day; 74 heavy axle/day

1st intervention				2nd intervention				3rd intervention				4th intervention			
Time	Type	Width of pavement	Quality	Time	Type	Width of pavement	Quality	Time	Type	Width of pavement	Quality	Time	Type	Width of pavement	Quality
1968	20 cm cem. 4 cm AB 10	4.5 m	1st cl	1975	5 cm AB-20	6.0 m	2nd cl (thick- ness)	1980	single emulsion surface dressing	6.0 m	-	1984	single emulsion surface dressing	6.0 m	1st cl

series of data as indicated in Table 2.

4.2 Planning of the service life of condition improving interventions

The term service life of a road means the period during which its behaviour satisfies the demands. It is a difficult task to predict after finishing some construction or maintenance work on it. The service life of a road is predicted. Wanting to approach the problem in a theoretical way, even in the most advantageous case only a few of the actual influential factors can be taken into account, not to mention that in most cases their future development is known only to a limited extent, or is absolutely unknown. Another choice (of practical background) might be to approach the problem on the basis of collecting and evaluating earlier experiences. Although, in the latter case, no doubt, all factors are taken into consideration, however, a number of difficulties are to be reckoned with; e.g. a collection of a great many data extending to vast areas and long periods must be carried out and, it is always hazardous to draw conclusions as to future development from past experiences. Further, the designation of classes considered as being homogeneous is a rather difficult problem.

The procedure mentioned in the second place is selected to be dealt with, with the objective of trying to reduce the difficulties involved. The objective assumed could briefly be summarized as follows: by generalizing the actual practices followed in Hungary in the past, a design guideline will be drafted relating to the service life expectancy of the condition improving interventions by selecting variables like the whole pavement structure, the traffic predictable, the probability of the earthwork getting humid, the width of the pavement, and the quality of each of the interventions.

A fundamental requirement is that the design aid should be easily treated and clearly surveyed. This objective can be attained obviously by graphic representation or by the application of graphs. In this case, anyhow, it is considered necessary, with the view of assuring the possibility of two-dimensional drawings and an acceptable number of diagrams, to strongly restrict the number of the variables actually exhibited (entering on one of the axles of the diagram or as a parameter) and the steps of the variables are to be selected with great care.

As parameters to be depicted, on the basis of the foregoing the fol-

lowing had been selected:

- pavement structure,
- modified traffic volume (modified by the number of all vehicles, by the width of the pavement and by the quality grade of the work carried out),

- expected service life of the intervention.

a) To characterize the pavement structure the expression in terms of equivalent thickness seems to be the most advantageous. However, this simple and widely used method has not been selected for the above-mentioned purpose after all, due to the following reasons:

- in case of a pavement of a given type the assumption of a constant coefficient of equivalence is but a rough approximation (in given instances it depends on the depth of the layer in question, on its age, on the quality of the construction, on the strength conditions of the support layer and weather conditions);

- still greater is the uncertainty of the above coefficients in the case if the pavement has deteriorated to a certain extent and in the overwhelming majority of cases this is the case;

- during the service life of the majority of road sections the pavement has been widened at least once, wherefore the cross section of the pavement structure is, in general, not uniform, not even concerning the equivalent thickness.

The development of the so-called typical pavement has been estimated more advantageous where from the extraordinarily rich varieties of "sandwich" structures of the present highway network the characteristic groupings are selected, and their behaviour is considered taking into account the average domestic construction technique, the interaction of the layers and the changes taking place during the use of several years. After the evaluation of a great number of samples a comparatively realistic picture might be obtained in this way.

The determination of a series of typical pavement structures will take place after completion of the data collection currently going on, however, some preliminary fundamental principles have already been elaborated. These are as follows:

- the number of types should be 10 to 15;
- in case of layers without any binder (unbound) and with hydraulic binders differences in thickness of 5 to 7 cm (e.g. limits of 15 to 20 cm)

STATE CONSERVATION OF HIGHWAYS

might be possible;

– in case of asphalt layers (excluding layers of asphalt-concrete character) 2 to 3 cm differences in thickness (e.g. limits of 8 to 11 cm) might occur;

– the different unbound base courses may be considered as other types only on the basis of their thickness;

– if the pavement has been widened, the part of the structure with the shortest life-time expectancy is to be considered critical;

– some special and, therefore, particularly infrequent variants of pavement structure should not be grouped to either types, they have to be evaluated separately.

b) Taking the traffic into account is perhaps the most intricate problem partly because the traffic load is also to be predicted (other factors, like pavement, soil and the probability of humidification are at the time of the examination known or can at least, be reconstructed), partly because the damaging effects of the different vehicle types are basically different.

The first problem can be solved with the aid of the ratios of the nation-wide traffic-development the exactitude of which meets the requirements of the examination in most cases.

However, the diverse effects exerted on the pavement structure by the different types of vehicles are a far more difficult problem. Namely, the load capacity is not the only condition evaluation parameter considered in this study. As a matter of course, if only the loss in load bearing capacity of the hard cover were considered as a motive for upgrading it, as was prescribed by the Code for Dimensioning Flexible Road-Pavement Structures /5/ published in 1971, the influence exerted by the different types of vehicles on this type of defect could be comparatively easily determined with the aid of the commonly known relationship obtained in the American AASHO Road Test /6/. However, an intervention may become necessary not only as a consequence of the deficiency of the load bearing capacity, but also due to the deformation of the pavement or because the surface has become slippery. In these two latter cases the role of limousines with low axle load in the development of the deficiency cannot be neglected. Consequently, all vehicles passing through the road section in question should be taken into account. The width of the pavement surface, used by the vehicles passing the road examined should also be known, overtakings excluded. This width depends

— beside the different wheel gauges of the vehicles and the slight differences in driving style — essentially on the width of the pavement. Therefore, it is obvious that the load (specific pressure) on the pavement connected with its width should be known because assuming a transversally homogeneous load capacity, the first damages are to be expected here and the state repairing techniques adopted in Hungary, even in case of the deterioration of this comparatively narrow strip, involve the condition improvement of the whole width of the pavement. (The only exceptions are the pavement repairs on a small surface (e.g. patching) which, however, should be applied but only to a limited extent.)

In any form of destruction the traffic volume has a decisive role. But it is absolutely not indifferent in what quality the different pavement layers had been produced, and this fact influences their damage resistance considerably. In predicting the duration expectation, therefore, also the quality parameter is to be calculated with. As a first approximation, the quality classification given during the acceptance procedure seems to be the most convenient. In applying this the following problems arise.

- In the reference period of the data collection several qualification systems were in force with the aid of which the quality class of the project (or its different layers) had been established;
- the different quality parameters (e.g. bitumen content of the wearing course, layer thickness, cross fall) have different roles in affecting the deterioration process;
- establishment of the quality class had in certain cases been influenced, beside the actual values of the quality parameters, also by other factors.

On the basis of what has been mentioned above, it seems to be convenient to take into account for the service life prediction the level of priority of certain parameters with a disadvantageous effect on the deterioration process. Although the selection of such parameters needs further investigations, preliminarily the following should be considered: composition of the material of the wearing course (in the first line its binder content), the density of the surface course, and layer thickness.

In order to reduce the number of the parameters in the diagrams, the heavy traffic load of the road section (the daily average number of the unit axles of 100 kN passing through) is modified in such a way that the number of vehicles circulating on the road section in question, the width of the

pavement, and the quality grade of the last intervention are also involved.

The modified traffic volume may be established accordingly with the aid of the relationship as follows:

$$F'_{100} = m_j \cdot m_{sz} \cdot m_m \cdot F_{100} \text{ (unit axle/day)}$$

wherein

- F'_{100} — modified heavy traffic per day,
- m_j — modifying factor related to the number of all vehicles passing through,
- m_{sz} — modifying factor related to pavement width,
- m_m — factor related to quality of last state improvement intervention,
- F_{100} — heavy traffic volume per day (expressed in number of axles of 100 kN).

Establishment of the series of the modifying factors can take place subsequently, to the evaluating process carried out after ending the data collection in the near future.

c) The kind of soil and its actual water content strongly affects the load capacity of the pavement structure and consequently the loss of load capacity. For this purpose the utilization of the CBR-value is adopted all over the world. However, for the examination dealt with in this study we do not follow this practice for the following reasons:

- determination of the CBR-value in laboratory and mainly in the field often runs into difficulties;
- the CBR-value in case of a given soil varies between rather wide limits in a year; taking into account a single value considered critical theoretically, one cannot rely upon it, and its determination in practice also raises difficult problems;
- in the planning phase the efficiency of drainage is not yet known and is in close connection with the variation of the CBR-value.

Therefore, another solution has been selected according to which the main kinds of soils have been considered in a special group but, for cases where the load bearing capacity of the soil strongly depends on its humidity, two groups have been established:

- granular soils,
- transition soils (of medium cohesiveness) with no serious danger

of humidification,

- cohesive (bound) soils with no serious danger of humidification,
- cohesive (bound) soils with serious danger of humidification.

One should reckon with a serious danger of humidification in case where the earthwork is, according to the experiences of the past, periodically threatened by flood or internal waters, i.e. by a high average ground water table. (Their quantity will be worked out in the near future.)

The earthwork can be classified into different groups in possession of data collected from maps and expert opinions.

d) The anticipated service life of the condition improving interventions represents the dependent variable in this study. In this connection the service life means the period between the end of the repairing intervention and the moment where the necessity of a new condition improvement presents itself.

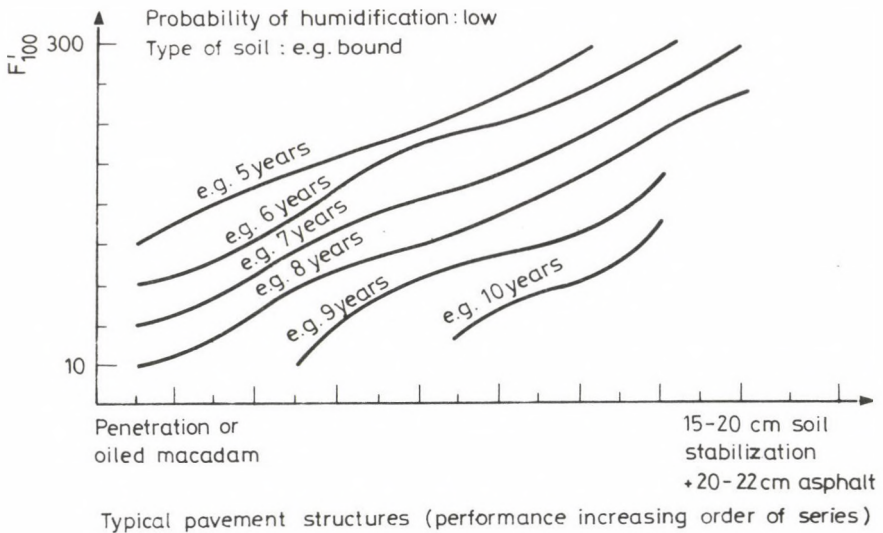


Fig. 2 Principle diagram for the prediction of the service life of the intervention

In the diagrams, as is shown in Fig. 2, the parameter of the set of curves is the service life estimated. Since in the case of pavement structures, on the horizontal axis, only discrete values are defined, the curves are, strictly speaking, equalized polynomials, a point of which may be obtained as follows. The pairs of values constituting associated ones in the

STATE CONSERVATION OF HIGHWAYS

course of data collection (pavement structure, soil drainage, modified traffic volume, service life of interventions) should be classified into such "homogeneous groups" in which the first three variables are common. For these variables the most probable value of the service life should be determined from the subsets to be considered statistically large samples obtained from a great many, incidentally several thousand data surveys, and this is what should be plotted in the diagrams. (With the aid of this procedure the more advantageous and more disadvantageous cases than the average can be omitted because, as a matter of course, a good many factors have not been taken into account at this examination, such as for example, weather influences, level of maintenance, and these factors can bring forth better or worse situations than the country-wide average.)

It is noteworthy that the different variants of pavement structures come into consideration, commonly in restricted traffic regions, and this circumstance, which is readily seen in Fig. 3, reduces the number of variations which are theoretically possible. According to a preliminary calculation, assuming 5 types of soil, 12 varieties of hard cover pavement structures and 4 traffic categories about 240 combinations may occur.

5. DETERMINATION OF THE INTERVENTION SCALE ACTUALLY REALIZABLE IN A SPECIFIC CASE

Starting from the objectives of road maintenance, such as preservation of the state of the road network, which can be attained by techniques of planned preventive maintenance and reconstruction works as well as maintenance and repair works necessitated due to traffic safety, the means serving this objective should briefly be investigated.

In the foregoing such a procedure was presented which, in the case of given inputs hard cover pavement structure, soil, traffic determines the service life of the latest state condition improving intervention. After this period, the structure or at least the pavement surface gets into a state which makes a new, urgent intervention necessary. This state may ensue at different combinations of values of several quality parameters. From this it follows that the most convenient, i.e. the technically and economically most reasonable type of intervention is the function of this state level as well as of the traffic volume (the significance) of the road. This optimal intervention type has a duration (and costs) which comes closest to the interests of the country's economy in respect of travel comfort, low demand on

maintenance, low operation costs, etc. (It is to be noted that, mentioning two extreme types of intervention, the cost of the modernization of a road section of 1 km comes up to about 20 million forints while 1 km surface dressing costs approximately 120 thousand forints or so.)

However, in practice the situation is – and this tendency has recently become ever more prevalent – that the money available for road maintenance is less than would be necessary to carry out the optimal condition improvement on all sections of the highway network. In this exigence the maintenance units are constrained to make the best of the unfavourable situation (to compromise). One solution is that with the aid of some priority ranking some of the road sections will be selected and on these only some state improving interventions will be carried out, only the current maintenance, while on other damaged parts of the roads works will be done until a new plan period comes into operation when also their turn will come. However, this strategy could hardly be considered acceptable because the road sections "left to their fate" further deteriorate, and soon get into such a neglected state that the cost of their reconstruction will be much higher. Therefore, it is more practicable to select the solution according to which on all or nearly all of the sections which need condition improving intervention only some repair work should be performed. By applying such a method, due to limited financial means, in general, one cannot attain the required technical level, however, in most cases it is sufficient to stop further deterioration, i.e. it permits the postponement of subsequent interventions. In case of a given state and traffic density there are among the possible interventions such which are not acceptable due to one or more simultaneously occurring circumstances:

- the service life to be expected seems to be too short (a few weeks or months),
- it does not improve the critical state parameter,
- the operation costs remain at an unacceptable level even after intervention,
- the traffic safety remains at an unacceptable level.

The purpose of the examination to be undertaken is to select the condition improving variant of the minimal technical quality still tolerable for the type of the road, requiring the lowest cost at the same time. The problem can be formulated in such a way that the boundary has to be defined under which a more moderate variant of intervention can already be considered

as money lost.

It is sure that the effects of the different condition improving interventions are rather well-known, however, the estimation to what an extent the actual conditions (such as the characteristic values of the traffic, the level, i.e. the combination of the state defining parameters, the construction and the "antecedents" of the pavement structure, etc.) affect the efficiency of the different types of interventions, is still missing.

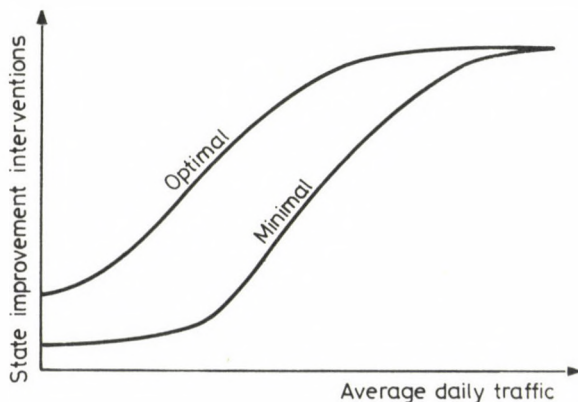


Fig. 3 Conceptual diagram of a convenient intervention-scale to be realized on a road section for a given traffic volume

Note: 1. On the vertical axis the different variants of state improvement interventions entering for engineering claims (and specific cost) increasing upwards; 2. The values of the average daily traffic (horizontal axis) can incidentally be modified by a coefficient depending on the road type

Figure 3 shows the expected issues of the examination concerning its principles. In practice, among others, two significant problems are to be dealt with which are as follows:

- in case of a given traffic volume a great number of "state patterns" are developed which need reparation, accordingly the optimal and minimal intervention types are also different, perhaps a complex state characterizing index could help in solving this problem;

- the type of road (motorway, main road, secondary road), and incidentally the urban or rural character can also affect the type of intervention.

The actual suggestion will be preceded by data collection concerning the actual service life of certain types of interventions carried out in the

past, consultation held with experts as well as economic calculations.

6. TECHNICO-ECONOMIC COMPARISON OF THE DIFFERENT TYPES OF INTERVENTIONS

Deterioration of a road does not necessarily occur but, the marks of at least three deterioration chains, only being in loose connection with each other, present themselves with different intensities. The necessity of the state improving intervention arises in case when intolerable parameters can be measured on any of the deterioration branches. It may, however, also occur that the simultaneous effects of the three kinds of deterioration make immediate intervention necessary. Also the fact mentioned above emphasizes the significance of working out some kind of a complex condition evaluating parameter. In possession of such a parameter the technico-economic comparison of the different state improving interventions can be carried out. The significance of this examination is supported by the fact that its issues could help in selecting from two state improving varieties, the costs of which are of similar magnitude, for a given traffic and road state.

By a methodical consideration the approach will be selected in the framework of which the following circumstances will be examined:

- the influence exerted on the overall quality (and separately on each of the different quality parameters) by the different types of interventions,
- the service life of the different kinds of interventions (and within this the shape of the deterioration curve),
- the preconditions concerning the construction material, machines and weather conditions necessary to implement the interventions in an adequate quality.

The knowledge of the effects of the different condition improving alternatives (variants of techniques) based on detailed and objective data will permit their application at the most convenient moment. (Here the financial restrictions are temporarily not considered.)

The timeliness of this examination is also justified by the domestic practice based mainly on the financial restrictions by which the surface dressing made recently by using bitumen emulsion, binder is considered a general highway conservation activity. However, it occurs frequently that the state of the road section (e.g. strongly deformed, incidentally cracked, surface) or the traffic volume does not justify the economical application of this technique.

STATE CONSERVATION OF HIGHWAYS

7. CONCLUDING REMARKS

The state preservation of the road network in Hungary is one of the most timely and most significant problems. The activities of evolutionary character have been strongly pushed into the background because of restricted financial means. The question what kind of state improvement should be undertaken and at what time, in order to make the optimal utilization of the financial means possible has become a central problem. To realize this assumed objective the present paper wants to contribute by reporting on the ground principles of such a planning method of the state conservation of highways which is based on the estimation of earlier practices and on the generalization of collected informative data. This activity is still at an early stage, however, it is obvious that it can become useful not only in attaining the main objective but also in the realization of the others mentioned in this paper (e.g. determination of the scale of interventions which could be considered realistic, elaboration of a complex parameter characterizing the state of the pavement, technico-economic comparison of the different varieties of maintenance techniques.

REFERENCES*

1. Gáspár, L. Jr.: Changes in State of Highways. Közlekedéstudományi Szemle 8 (1985).
2. Schváb, J.: Catalogue of Asphalt Pavement Deficiencies. Publication No. 2 of the Institute for Transport Sciences (1982).
3. Törőcsik, F.—D. Rósa—E. Tóth: Preparatory Work for the Suitability Survey of Hungarian Highway Network, Characteristics Examined. UTORG. Budapest 1985.
4. Design guideline to Road Condition Improving Works. Ministry of Transport, Highway Transportation Department. Budapest 1985. (Worked out by L. Gáspár Jr.)
5. Dimensioning Code for Flexible Highway Pavement Structures. Ministry of Transport and Communication, Highway Department and Municipal Council Transport Department, 1971.
6. The AASHO Road Test. Highway Research Board. Special Report 61. C. 1962.

* (1-5 in Hungarian)

CALCULATION FOR THE VIBRATION OF STRUCTURES:
A PARTIAL EIGENVECTOR PROBLEM SOLUTION

J. Györgyi*

(Received 11 April 1985)

Solutions to vibration problems where the solution can be written in accordance with the components corresponding to the eigenvector have been studied in this work, and determination of the physical implication of errors resulting from neglect of eigenvectors associated with higher frequencies has been recommended for the case of free vibration, and excitation by periodical forces. To justify this recommendation, numerical examples and experiments have been presented, pointing out that on the basis of data of the numerical experiments, the limits required for practical application, compatible with the errors of starting parameters of the technical problem, can be formulated.

1. INTRODUCTION

Investigation of the vibration of structures by means of the finite element method requires dynamic calculations for systems of a rather high degree of freedom. In vibration calculations, second-degree differential equation systems depending on the description of mass forces and damping conditions, as well as of exciting effects. The first step is to calculate eigenvalues and eigenvectors, and the calculated values are then used to write the general solution. In this work, the general solutions for the different cases are presented in a form where the components associated with the different eigenvectors appear each separately.

In case of large systems, it is not possible to calculate all the eigenvalues and eigenvectors but for a solution of an accuracy required for practical application, it is not necessary either to have all the components. In this work, we investigate what criteria should be taken as a basis for deciding the number of eigenvectors to be used in the calculations, specifying the characteristics of errors the use of which is practicable in engineering calculations for free vibration and excitation by periodical forces.

*Dr. J. Györgyi, H-1221 Budapest, Arany János u. 96/b., Hungary

2. SOLUTIONS TO DIFFERENTIAL EQUATION SYSTEMS IN VIBRATION PROBLEMS

Undamped free vibration

If the usual displacement functions for static calculations are used to calculate mass forces, we will face the problem of solution of a constant-coefficient differential equation system:

$$\underline{M} \ddot{\underline{u}}(t) + \underline{K} \underline{u}(t) = 0, \quad (1)$$

where \underline{K} stiffness matrix, \underline{M} mass matrix of the structure.

In the knowledge of the eigenvectors associated with eigenvalue problem $\underline{K} \underline{v} = \lambda \underline{M} \underline{v}$, provided the eigenvectors were normed for $\underline{V}^* \underline{M} \underline{V} = \underline{E}$, the solution /1/:

$$\underline{u}(t) = \sum_{r=1}^n \underline{v}_r \underline{v}_r^* \underline{M} \left\{ \underline{u}_0 \cos \omega_r t + \frac{1}{\omega_r} \dot{\underline{u}}_0 \sin \omega_r t \right\}, \quad (2)$$

where $\underline{u}_0, \dot{\underline{u}}_0$ are initial displacements and velocities (associated with $t=0$), respectively, $\omega_r = \sqrt{\lambda_r}$ and \underline{v}_r radian eigenfrequency r , and eigenvector r (vibrational mode), respectively.

Undamped vibration excited by periodical force

In this case, the right side of the matrix differential equation (1) can be written as

$$\underline{q}(t) = \underline{q}_0 + \sum_{k=1}^m \underline{q}_{ck} \cos \alpha_k t + \underline{q}_{sk} \sin \alpha_k t \quad (3)$$

The particular solution associated with harmonic components of frequency α_k of an amplitude of \underline{q}_0 and \underline{q}_{ck} , \underline{q} /1/:

$$\underline{u}_q(t) = \sum_{r=1}^n \underline{v}_r \underline{v}_r^* \left(\frac{1}{\omega^2} \underline{q}_0 + \sum_{k=1}^m \frac{1}{\omega_r^2 - \alpha_k^2} (\underline{q}_{ck} \cos \alpha_k t + \underline{q}_{sk} \sin \alpha_k t) \right) \quad (4)$$

A general solution to the inhomogeneous differential equation system can be obtained as the sum of solutions (3) and (4).

Frequency dependent mass matrix

The effect of mass forces on the different elements can be taken into consideration more accurately if displacement functions written as the power function of ω are used /2/. In this case, the radian eigenfrequencies and the associated vibrational modes can be obtained in the solution of homogeneous equation system

$$(\underline{K} - \omega^2 \underline{M}_0 - \omega^4 \underline{M}_2 - \omega^6 \underline{M}_4 \dots - \omega^S \underline{M}_{S-2}) \underline{v} = \underline{0} . \quad (5)$$

The function describing the displacements of the structure can be written as

$$\underline{u}(t) = \sum_{r=1}^n \underline{v}_r (a_r \cos \omega_r t + b_r \sin \omega_r t) \quad (6)$$

also in this case but, as has been shown in /3/, writing the solution in a form similar to (2) is not possible. Integration constants a_r , b_r can be calculated from the initial conditions in the knowledge of all the eigenvectors only. If only a few eigenvectors are taken as a basis to define the solution, the method of least squares shall be used for calculation of constants a_r , b_r . At the same time, again expression (4) is obtained for the description of excitation by periodical forces (with the values of \underline{v}_r and ω_r calculated on the basis of equation (5)).

External damping proportional to velocity

The matrix-differential equation describing free vibrations of the structure is now

$$\underline{M} \ddot{\underline{u}}(t) + \underline{C} \dot{\underline{u}}(t) + \underline{K} \underline{u}(t) = \underline{0} , \quad (7)$$

which can be attributed to first-order differential equation system (4).

$$\underline{A} \dot{\underline{y}}(t) + \underline{B} \underline{y}(t) = \underline{0} , \quad (8)$$

where

$$\underline{A} = \begin{bmatrix} \underline{0} & \underline{M} \\ \underline{M} & \underline{C} \end{bmatrix} \quad \underline{B} = \begin{bmatrix} -\underline{M} & \underline{0} \\ \underline{0} & \underline{K} \end{bmatrix} \quad \underline{y}(t) = \begin{bmatrix} \dot{\underline{u}}(t) \\ \underline{u}(t) \end{bmatrix} . \quad (9)$$

The solution of equation (8) requires that eigenvalue problem

$$\tilde{\lambda} \underline{\underline{A}} \underline{\underline{w}} = - \underline{\underline{B}} \underline{\underline{w}}$$

be solved, where in case of low damping, $\tilde{\lambda}_r$ are eigenvalues and

$$\underline{\underline{w}}_r = \begin{bmatrix} \tilde{\lambda} \\ \underline{\underline{v}}_r \\ \underline{\underline{v}}_r \end{bmatrix}$$

complex eigenvectors while in case of a high damping, both $\tilde{\lambda}_r$ and $\underline{\underline{w}}_r$ are real.

It was shown in /3/ that, in the knowledge of eigenvalues and eigenvectors

$$\tilde{\lambda}_j = -\rho_j + i \omega_{jc} \qquad \underline{\underline{v}}_j = \underline{\underline{v}}_j^v + i \underline{\underline{v}}_j^i$$

and

$\lambda_\ell = -\rho_\ell$ and v_ℓ , respectively, the solution could be written as the sum of solutions associated with the different solutions. Accordingly,

$$\begin{aligned} \underline{\underline{u}}(t) = & \sum_{j=1}^{n_r} 2e^{-\rho_j t} \left[\left\{ \underline{\underline{A}}_j \underline{\underline{M}} \dot{\underline{\underline{u}}}_0 + (\underline{\underline{A}}_j \underline{\underline{C}} - \rho_j \underline{\underline{A}}_j \underline{\underline{M}} - \omega_{jc} \underline{\underline{B}}_j \underline{\underline{M}}) \underline{\underline{u}}_0 \right\} \right. \\ & \left. \cos \omega_{jc} t - \left\{ \underline{\underline{B}}_j \underline{\underline{M}} \dot{\underline{\underline{u}}}_0 + (\underline{\underline{B}}_j \underline{\underline{C}} - \rho_j \underline{\underline{B}}_j \underline{\underline{M}} + \omega_{jc} \underline{\underline{A}}_j \underline{\underline{M}}) \underline{\underline{u}}_0 \right\} \sin \omega_{jc} t \right] + \\ & + \sum_{\ell=2n_r+1}^{2n} \underline{\underline{v}}_\ell^v \underline{\underline{v}}_\ell^{v*} \left\{ \underline{\underline{M}} \dot{\underline{\underline{u}}}_0 + (-\rho_\ell \underline{\underline{M}} + \underline{\underline{C}}) \underline{\underline{u}}_0 \right\} e^{\rho_\ell t} \end{aligned} \quad (10)$$

where

$$\underline{\underline{A}}_j = \underline{\underline{v}}_j^v \underline{\underline{v}}_j^{v*} - \underline{\underline{v}}_j^i \underline{\underline{v}}_j^{i*},$$

$$\underline{\underline{B}}_j = \underline{\underline{v}}_j^i \underline{\underline{v}}_j^{v*} + \underline{\underline{v}}_j^v \underline{\underline{v}}_j^{i*},$$

while n_r is the number of complex pairs of eigenvalues.

VIBRATION OF STRUCTURES

Note that the case where λ_1 is a multiple eigenvalue which is at the same time a multiple root of the minimal polynomial is not included in formula (10). For the sake of completeness, also the solution for a harmonic excitation force of radian frequency α and amplitude q is given below, broken down in accordance with the eigenvector:

$$\begin{aligned}
 \underline{u}(t) = & \sum_{j=1}^{n_r} \frac{-2}{(\rho_j^2 + \alpha^2 - \omega_{jc}^2)^2 + 4\rho_j^2 \omega_{jc}^2} * \\
 & * \left\{ \underline{v}_j^v \left[\underline{v}_j^{v*} q \left[\rho_j (\rho_j^2 + \alpha^2 + \omega_{jc}^2) \cos \alpha t - \alpha (\rho_j^2 + \alpha^2 - \right. \right. \right. \\
 & \left. \left. \left. - \omega_{jc}^2) \sin \alpha t \right] + \right. \right. \\
 & \left. \left. + \underline{v}_j^{i*} q \left[\omega_j (\rho_j^2 - \alpha^2 + \omega_{jc}^2) \cos \alpha t - 2\alpha \rho_j \omega_{jc} \sin \alpha t \right] \right] - \right. \\
 & \left. - \underline{v}_j^i \left[\underline{v}_j^{v*} q \left[-\omega_j (\rho_j^2 - \alpha^2 + \omega_{jc}^2) \cos \alpha t + 2\alpha \rho_j \omega_{jc} \sin \alpha t \right] + \right. \right. \\
 & \left. \left. + \underline{v}_j^{i*} q \left[\rho_j (\rho_j^2 + \alpha^2 + \omega_{jc}^2) \cos \alpha t - \alpha (\rho_j^2 + \alpha^2 - \omega_{jc}^2) \sin \alpha t \right] \right] \right\} + \\
 & + \sum_{\ell=2n_r+1}^{2n} \frac{-\ell}{\rho_\ell^2 + \alpha^2} \underline{v}_\ell \underline{v}_\ell^{*} q (\rho_\ell \cos \alpha t - \alpha \sin \alpha t) \quad (11)
 \end{aligned}$$

Frequency dependent internal damping

In the literature, the damping matrix in the form

$$\underline{C} = a_0 \underline{M}, \quad (12)$$

$$\underline{C} = a_1 \underline{K}, \quad (13)$$

or

$$\underline{C} = a_0 \underline{M} + a_1 \underline{K} \quad (14)$$

is often used to take the damping effect of internal friction into consideration.

With a damping matrix proportional to matrices \underline{M} , \underline{K} assumed, it is possible to write the solution by means of eigenvectors associated with the undamped case.

Low or high damping may be associated with the different vibrational modes depending on whether the value

$$\lambda_j = \frac{\xi_j}{2} + i \sqrt{\omega_j^2 - \frac{\xi_j^2}{4}} = -\rho_j + i \omega_{jc} \quad (15)$$

is complex or real.

Here ω_j is the radian eigenfrequency associated with the undamped case while ξ_j , for the case given in (12),

$$\xi_j = a_0, \quad (16)$$

for (13)

$$\xi_j = a_1 \omega_j^2, \quad (17)$$

while for (14)

$$\xi_j = a_0 + a_1 \omega_j^2. \quad (18)$$

With the values of ξ_j substituted again into the expression given in (15) we obtain that both low and high damping may be associated with given damping characteristic, depending on the magnitude of radian eigenfrequency for given eigenvector.

The solution for the case of free vibration:

$$\begin{aligned} \underline{u}(t) = & \sum_{j=1}^{n_r} \underline{v}_j \underline{v}_j^* \underline{M} e^{-\rho_j t} \left[\underline{u} \cos \omega_{jc} t + \left(\frac{1}{\omega_{jc}} \dot{\underline{u}}_0 + \right. \right. \\ & \left. \left. + \frac{\rho_j}{\omega_{jc}} \underline{u}_0 \right) \sin \omega_{jc} t \right] + \sum_{l=n_r+1}^n \underline{v}_l \underline{v}_l^* \underline{M} \left[e^{-\rho_{l2} t} \left(\frac{\rho_{l1}}{\rho_{l1} - \rho_{l2}} \underline{u}_0 + \right. \right. \\ & \left. \left. + \frac{1}{\rho_{l1} - \rho_{l2}} \dot{\underline{u}}_0 \right) - e^{-\rho_{l1} t} \left(\frac{\rho_{l2}}{\rho_{l1} - \rho_{l2}} \underline{u}_0 + \frac{1}{\rho_{l1} - \rho_{l2}} \dot{\underline{u}}_0 \right) \right] \quad (19) \end{aligned}$$

Here n_r is the length of low-damping components while ρ_{l1} and ρ_{l2}

can be calculated from relationship

$$\rho_{1,2} = -\rho_j \pm \sqrt{\frac{\xi_j^2}{4} - \omega_j^2}$$

for components of high damping.

In case of the proportional damping given in (12) through (15), the solution for harmonic excitation can similarly be calculated on the basis of components according to real eigenvectors, e.g. if $\underline{q} = \underline{q} \cos \alpha t$

$$\underline{u}(t) = \sum_{r=1}^n \underline{v}_r \underline{v}_r^* \frac{1}{\sqrt{(\omega_r^2 - \alpha^2)^2 + \xi_r^2 \alpha^2}} \underline{q} \cos(\alpha t - \nu_r)$$

where

$$\nu_r = \arctan \frac{\xi_r \alpha}{\omega_r^2 - \alpha^2} \quad (20)$$

Frequency independent internal damping

As seen in /5/, the damping matrix can be written in this case as

$$\underline{C} = \frac{\gamma}{\omega \sqrt{1 + \frac{\gamma^2}{4}}} \underline{K},$$

where $\gamma = \frac{\theta}{\pi}$, while θ logarithmic decrement characteristic of the structure.

In this case, low damping is associated with every vibrational mode, and the displacements can be written as the sum of terms associated with the different vibrational modes:

$$\underline{u}(t) = \sum_{r=1}^n \underline{v}_r \underline{v}_r^* \underline{M} e^{-\frac{\gamma}{2} \omega_{rc} t} \left[\underline{u}_0 \cos \omega_{rc} t + \left(\frac{1}{\omega_{rc}} \dot{\underline{u}}_0 + \frac{\gamma}{2} \underline{u}_0 \right) \sin \omega_{rc} t \right], \quad (21)$$

where $\omega_{rc} = \frac{\omega_r}{\sqrt{1 + \frac{\gamma^2}{4}}}$, ω_r radian eigenfrequency of undamped vibration while the particular solution for a harmonic force:

$$\underline{u}(t) = \sum_{r=1}^n \underline{v}_r \underline{v}_r^* \frac{1}{\omega_r^2 \sqrt{\left(1 - \frac{\alpha^2}{\omega_r^2}\right)^2 + \frac{\alpha^2}{\omega_r^2} \frac{4\gamma^2}{4+\gamma^2}}} \underline{q} \cos(\alpha t - \nu_r),$$

where

$$\nu_r = \arctan \frac{\gamma \omega_{rc} \alpha}{\omega_r^2 - \alpha^2}. \quad (22)$$

If the structure consists of elements of different damping characteristics (e.g. superstructure interacting with the ground, structure containing both steel and reinforced concrete elements), the damped vibration can be taken into consideration by using the complex stiffness matrix, the differential equation system of vibration in case of free vibration being

$$\underline{M} \ddot{\underline{u}}(t) + \underline{K} \underline{u}(t) = \underline{0}. \quad (23)$$

Displacements of the structure can be calculated as a real part of complex displacements /6/.

The complex solution can be written in accordance with (2) in the knowledge of complex eigenvectors and complex radian eigenfrequencies obtained as a result of a complex eigenvalue problem. Also the complex initial conditions are required for writing the solution. As has been shown in /3/, the imaginary part of the initial conditions can be produced only after the integration constants that can be calculated in the knowledge of all the eigenvectors having been determined. If we want to obtain the solution with the use of eigenvectors of a certain number only, either the initial conditions shall be specified for places of a reduced number or the integration constants shall be calculated using the method of least squares.

To avoid the above difficulties, production of a damping matrix proportional to the velocity which is equivalent to complex damping has been recommended in /7/. Accordingly, in case of complex stiffness

$$\underline{K} = \underline{K}_U + i \underline{K}_V \quad (24)$$

$$\underline{C} = \sum_{r=1}^n \frac{1}{\omega_{rc}} \underline{v}_r \underline{v}_r^* \underline{K}_V \quad (25)$$

where ω_{rc} and \underline{v}_r can be obtained from the solution of real eigenvalue problem

$$\underline{K}_U \underline{v} = \omega_{rc}^2 \underline{M} \underline{v} . \quad (26)$$

It can be seen that calculation of a damping matrix corresponding to eigenvectors of a definite number is possible because the damping matrix is set up of components according to the eigenvectors.

In the knowledge of this damping matrix, differential equation system

$$\underline{M} \ddot{\underline{u}}(t) + \underline{C} \dot{\underline{u}}(t) + \underline{K}_U \underline{u}(t) = \ddot{\underline{u}} \quad (27)$$

shall be solved where the solution will be obtained according to (10) and, in case of excitation by periodical forces, to (11).

As has been proved in /7/ also by numerical experiments, the deviation between the values calculated for damping characteristics for eigenvectors included in the calculation and the results obtained in calculation with the complex stiffness matrix is negligible. To set up a matrix \underline{C} equivalent to complex stiffness will be especially practicable if there is also a damping proportional to external velocity. Namely, in this case, the matrices containing the two limits can be simply added.

As seen above, the solutions for the different vibration problems can be written as the sum of solutions corresponding to the eigenvectors. Investigations concerning number of eigenvectors to be included in calculations are given in the next Chapter.

3. ERRORS IN A PARTIAL EIGENVALUE PROBLEM SOLUTION

Free vibration

The solution obtained for the undamped case in (2) can be written also in the following form:

$$\underline{u}(t) = \sum_{r=1}^n \underline{v}_r \left\{ z_r \cos \omega_r t + \frac{z_r}{\omega_r} \sin \omega_r t \right\} . \quad (28)$$

Here

$$z_r = \underline{v}_r^* \underline{M} \underline{u}_0 , \quad z_r' = \underline{v}_r^* \underline{M} \dot{\underline{u}}_0 . \quad (29)$$

In the solution, the weight of the eigenvectors is different. E.g. if \underline{u}_0 and some eigenvector coincide, $z_r = 1$ and the other multipliers z_r will be zero. More and more complicated vibrational modes belong to increas-

ingly high frequencies. If the components of the vector of initial condition, found in the basis of the eigenvectors, are determined by means of coordinates z_r , it will be found in the majority of practical cases that the vibrational modes associated with higher frequencies are negligible. The algorithms suited for the calculation of some of the least eigenvalues and eigenvectors can thus be practicably applied (although the order of the matrices may be very high but they are band matrices).

To decide whether the number of the calculated eigenvectors is sufficient, the vectors of initial conditions, obtained by the approximate solution, can be compared with the original vectors:

$$\begin{aligned} \underline{u}'_0 &= \sum_{r=1}^m \underline{v}_r \underline{v}_r^* \underline{M} \underline{u}_0 = \sum_{r=1}^m z_r \underline{v}_r \rightarrow \underline{u}_0, \\ \dot{\underline{u}}'_0 &= \sum_{r=1}^m z_r \dot{\underline{v}}_r \rightarrow \dot{\underline{u}}_0. \end{aligned} \quad (30)$$

It is difficult to set out any criterion for the accuracy of displacements since it is rather the relative displacements that predominate in calculation for stresses.

Vectors

$$\begin{aligned} \underline{q}_0 &= \underline{K} \underline{u}_0, & \underline{q}'_0 &= \underline{K} \underline{u}'_0, \\ \underline{s}_0 &= \underline{M} \dot{\underline{u}}_0, & \underline{s}'_0 &= \underline{M} \dot{\underline{u}}'_0, \end{aligned} \quad (31)$$

can be calculated on the basis of initial conditions, and thus the error in approximate calculation can be determined by comparison of the loads in the nodes. Stresses arise in the structure that can be calculated reliably only if the displacements are very accurate. According to calculational experiences, an accuracy of relative axial displacements of the nodes, required for calculation of normal forces in case of a set of beams consisting of coaxial rods, can be achieved only by calculation of almost all the eigenvectors. The number of eigenvectors required for the calculation can be considerably reduced in this case if the limit of error is specified for the sum of forces acting in the direction of the set of beams. (At the same time, normal forces can be calculated by means of the shear forces of the columns.) The limit of error can be specified also for other combinations of forces (e.g. sum of moments for some point). Thus the error will be

$$\varepsilon_q = \frac{|f(\underline{q}_0) - f(\underline{q}')|}{f(\underline{q}_0)}, \quad (32)$$

$$\varepsilon_s = \frac{|f(\underline{s}_0) - f(\underline{s}')|}{f(\underline{s}_0)}.$$

The physical contents of the two errors are hardly compatible. Therefore, a comparison of energies associated with accurate and approximate initial conditions is recommended:

$$\varepsilon = \frac{|E - E'|}{E}, \quad (33)$$

where

$$E = \frac{1}{2} \left\{ \underline{u}_0^* \underline{K} \underline{u}_0 + \underline{u}_0^* \underline{M} \dot{\underline{u}}_0 \right\},$$

while E' , using the relationships given in 7.7,

$$E' = \frac{1}{2} \sum_{r=1}^m z_r^2 \underline{v}_r^* \underline{K} \underline{v}_r + z_r'^2 \underline{v}_r^* \underline{M} \underline{v}_r = \frac{1}{2} \sum_{r=1}^m z_r^2 \omega_r^2 + z_r'^2, \quad (34)$$

can be calculated by means of the constants associated with the general solution. In energy calculations, the energy of forces acting upon absolute motions in the nodes is calculated and thus a slight inaccuracy of relative displacement has little effect on the sum of energies. A limit for the magnitude of error, applicable to every structure, cannot be specified as it depends on the inaccuracy required in \underline{q} . However, for given type of structures, the limits can be determined on the basis of numerical experiments but in this case the stresses arising after the limits have been fulfilled must by all means be checked.

In the solutions for different damping models, one may proceed in accordance with what has been said, that is the components of initial velocity and displacement vectors per eigenvector (including approximate mechanical energy) can be calculated for time $t = 0$ and the error analysis can be carried out.

Excitation by periodical forces

The relationship given in (4) can be written in case of a harmonic component (e.g. $\underline{q} = \underline{q}_{ck} \cos \omega_k t$) in the following way:

$$\underline{u}_q(t) = \sum_{r=1}^n \frac{v_r v_r^*}{\omega_r^2 - \alpha_k^2} q_{ck} \cos \alpha_k t = \sum_{r=1}^n \mu_{rk} v_r z_{rk}^c \cos \alpha_k t. \quad (35)$$

Here

$$\mu_{rk} = \frac{1}{1 - \frac{\alpha_k^2}{\omega_r^2}},$$

$$z_{rk}^c = \frac{1}{\omega_r^2} v_r^* q_{ck}.$$

The place of the different eigenvectors in the solution depends on the place of the force vector in the basis of the eigenvectors as well as on magnification factor μ_{rk} determined by the relationship between the radian eigenfrequency and the excitation frequency. Should these coincide, μ_{rk} may be infinitely large. This means that in case of the excitation force given in (3), all the radian eigenfrequencies (and the eigenvector associated with them) not exceeding the maximum value of α_k must be calculated. Considering that to make the Fourier series accurate requires that terms of increasingly high frequencies be included, practically the calculation of all the eigenvectors would be necessary. However, the situation will change if the damping always present in the structure is taken into consideration. E.g. in case of a homogeneous structural damping, the solution will be, according to (22):

$$\underline{u}_q(t) = \sum_{r=1}^n \mu_{rk} v_r \frac{1}{\omega_r^2} v_r^* q_{ck} \cos(\alpha_k t - \nu_{rk}),$$

where

$$\mu_{rk} = \frac{1}{\sqrt{\left(1 - \frac{\alpha_k^2}{\omega_r^2}\right)^2 + \frac{\alpha_k^2}{\omega_r^2} \frac{4\gamma^2}{4 + \gamma^2}}}. \quad (36)$$

If the highest excitation frequency lies below the calculated highest eigenfrequency, ω_m , the value of μ_{rk} can be calculated for every value r and k . If any $\alpha_k > \omega_m$, at most resonance will occur and thus $\mu_{rk} \leq \mu_{max}$, where $\mu_{max} \approx \frac{1}{\gamma}$ because of 1. (37)

If all the eigenvectors are not taken into consideration, the error in vector $\underline{u}(t)$ will be

$$\underline{u}_q(t) = \sum_{s=m+1}^n \mu_{sk} \frac{v_s}{\omega^2} \frac{1}{s} \underline{q}_{ck} \cos(\alpha_k t - v_{sk}) . \quad (39)$$

In the knowledge of $\underline{K}^{-1} = \underline{V} \left\langle \frac{1}{\omega^2} \right\rangle \underline{V}^*$,

$$\Delta \underline{u}_q(t) = \mu_{sk} \left[\underline{K}^{-1} \sum_{r=1}^m \underline{v}_r \frac{1}{\omega^2} \underline{v}_r^* \right] \underline{q}_{ck} \cos(\alpha_k t - v_{sk}) .$$

Force can be assigned to the error in displacement:

$$\Delta \underline{q}(t) = \mu_{sk} \left[\underline{q}_{ck} \leftarrow \underline{K} \sum_{r=1}^m \underline{v}_r \frac{1}{\omega^2} \underline{v}_r^* \right] \underline{q}_{ck} \cos(\alpha_k t - v_{sk}) . \quad (39)$$

The error vector can be compared with "static" force vector $\underline{q}_{ck}(\underline{q}_{st})$. In so doing, the length (spherical norm) of the static force vector and the length of force vector $\Delta \underline{q}$ can be compared. With the length of the eigenvectors included in the calculation increased, force vector

$$\underline{q}'_{st} = \underline{K} \sum_{r=1}^m \underline{v}_r \frac{1}{\omega^2} \underline{v}_r^* \underline{q}_{st}$$

written as a combination of the eigenvectors will more and more approach vector \underline{q}_{st} and thus the length or error vector

$$\Delta \underline{q}_{st} = \underline{K}_s \sum_{m+1}^n \underline{v}_s \frac{1}{\omega^2} \underline{v}_s^* \underline{q}_{st}$$

will reduce monotonously with also the length of vector $\Delta \underline{q}(t)$ reducing accordingly:

$$\| \Delta \underline{q} \| = \mu_{sk} \| \Delta \underline{q}_{sk} \| \leq \frac{1}{\gamma} \| \Delta \underline{q}_{sk} \| ,$$

that means to given ϵ , the number of eigenvectors where the error will lie below the specified value i.e.

$$\epsilon_{st} > \frac{\| \Delta \underline{q} \|}{\| \underline{q}_{st} \|} \quad (40)$$

can be assigned.

The "relative" error of dynamic calculation can be estimated by taking the load vector that has already been calculated as a basis for comparison. The load vector:

$$q_{dyn}^* = K \sum_{r=1}^m v_r \frac{1}{\omega_r^2} v_r^* \frac{1}{\sqrt{\left(1 - \frac{\alpha_k^2}{\omega_r^2}\right)^2 + \frac{\alpha_k^2}{\omega_r^2} \frac{4\gamma^2}{4 + \gamma^2}}} \quad (41)$$

$$\epsilon_{dyn} > \frac{\|\Delta q\|}{\|q_{dyn}^*\|} \quad (42)$$

In case of more harmonic components, vectors $q(t)$, q_{st} , q_{dyn}^* can be obtained by appropriate summation and the errors can be defined for the solution vectors.

Note that if the excitation frequency lies below or at the highest radian eigenfrequency that has been calculated that far, the expression given in (37) will take the following shape:

$$\mu_{rk} < \frac{1}{\sqrt{\left(1 - \frac{\alpha_k^2}{\omega_r^2}\right)^2 + \frac{\alpha_k^2}{\omega_r^2} \frac{4\gamma^2}{4 + \gamma^2}}} \quad (43)$$

Derivations for the case of external damping proportional to velocity are given in /3/. Here only the relationships required for calculation of the error vectors are given.

If vector Q is a vector of double size with amplitude q of the actual load vector, $q e^{i\alpha t}$, in the lower part, then, with the symbols used in (9),

$$\|\Delta Q\| \leq R_e \left\| \left\{ \tilde{c} \left[Q - \sum_{r=1}^m \frac{\tilde{w}_r}{-\lambda} \frac{1}{\omega_r} \tilde{w}_r^* Q \right] \right\} \right\| \quad (44)$$

will be obtained, where

$$\tilde{c} = \frac{1}{i\alpha} \frac{1}{-\min(\rho_s) + i\omega_{mc}} \quad (45)$$

VIBRATION OF STRUCTURES

Values ρ_s associated with the omitted eigenvectors should be substituted into expression \tilde{c} . Considering that no conditions have been imposed upon the matrix of damping proportional to velocity, this value could be even zero. At the same time, the structural damping is always present and thus

$$\min(\rho_s) = \frac{\gamma}{2} \omega_{mc} \cdot$$

In the knowledge of vector $\Delta \underline{q}$, $\Delta \underline{q}$ can be obtained in its lower part and thus the error analysis can be carried out in accordance with what has been said above.

Note that the rules set out in (40) and (42) are very strict and require sometimes that almost the entire eigenvector basis be calculated. E.g. in case of rods where axial forces are acting in the so called amplitude direction, the sum of axial forces can be calculated with eigenvectors of a relatively small number taken into consideration but their distribution between the different nodes cannot be calculated in this way. In practical calculations, it is reasonable to proceed in the way described for the case of free vibration, calculating vector $\Delta \underline{q}$ and the expectable error for vector $\Delta \underline{q}$ including the sums of forces calculated in certain selected directions. Examples for this are given in the description of numerical results.

4. NUMERICAL EXPERIENCES

In the foregoing, the solution of the problem of free vibration as a partial eigenvalue problem has been dealt with. It has been recommended to determine the number of the required eigenvectors on the basis of a comparison of the mechanical energies associated with the initial starting conditions and with the starting conditions that can be derived from the approximate solution, as well as on the basis of testing the kinetic equilibrium in the nodes. The rod shown in Fig. 1 has been investigated under starting conditions brought about by force configurations a), b), c), d).

The radian frequencies associated with the different vibrational modes, weight numbers z_r according to (29), and the values for energy ratio (E'/E) are tabulated in Table 1. Considering the weight numbers, the use of the first three eigenvectors seems to be necessary in case of starting conditions a), b) and c) while the use of the first nine eigenvectors in case

of starting condition b) for a solution of appropriate accuracy. If a correspondence of 1 % of the energies is required, then 1, 2, 3 or 15 eigen-vector (s) shall be included in the calculation.

Table 1

r	ω_r [1/s]	a		b		c		d	
		z_r	E_r^2/E	z_r	E_r^2/E	z_r	E_r^2/E	z_r	E_r^2/E
1	11.68	3.3517	<u>0.9944</u>	1.6164	0.9194	0.4064	0.2185	-	-
2	39.43	0.0505	0.0026	0.1320	<u>0.0699</u>	0.1953	0.5754	-	-
3	73.25	<u>0.0253</u>	0.0022	<u>0.0258</u>	0.0092	0.0618	<u>0.1980</u>	-	-
4	121.1	0.0002	-	0.0001	-	0.0001	-	0.0239	0.7046
5	151.9	0.0002	-	0.0002	-	0.0004	-	0.0051	0.0500
6	173.0	0.0004	-	0.0001	-	0.0003	-	0.0061	0.0941
7	209.5	0.0001	-	-	-	-	-	-	-
8	244.4	0.0008	-	0.0017	0.0004	0.0017	0.0017	-	-
9	310.3	0.0003	-	-	-	0.0001	-	<u>0.0039</u>	0.1247
10	350.4	0.0012	0.0001	0.0006	0.0001	0.0001	-	-	-
11	535.7	0.0004	-	0.0001	-	0.0001	-	-	-
12	547.2	0.0016	0.0005	0.0002	-	0.0006	0.0009	0.0001	0.0004
13	610.6	0.0002	-	0.0002	-	0.0001	-	0.0003	0.0029
14	680.5	0.0002	-	0.0001	-	-	-	-	-
15	707.1	0.0001	-	0.0002	-	0.0001	0.0020	0.0005	<u>0.0091</u>
16	802.9	0.0006	0.0001	0.0006	0.0006	0.0001	0.0029	0.0003	0.0042
17	1078	0.0001	-	0.0002	0.0001	0.0001	0.0002	0.0002	0.0033
18	1081	0.0001	-	0.0001	-	0.0001	0.0002	0.0002	0.0048

Indicated in Table 2 are the errors obtained in the displacement of node 7 in direction x, taking into consideration different eigenvectors,

VIBRATION OF STRUCTURES

then the error in relative displacement of nodes 7 and 5 in direction y as well as that in relative displacement of nodes 7 and 8 in direction x, defined in (33). It can be seen that there is a close relationship between the energy ratio and error of displacement for absolute displacement as well as for relative displacement of direction 7-5 while at the same time a result of appropriate accuracy will now be obtained for the relative displacement of direction 7-8 only if all the eigenvectors are included in the calculation.

Table 2

r	a			b			c		
	ϵ_7	ϵ_{7-5}	ϵ_{7-8}	ϵ_7	ϵ_{7-5}	ϵ_{7-8}	ϵ_7	ϵ_{7-5}	ϵ_{7-8}
1	0.008	0.039	1.000	0.081	0.354	1.000	0.354	0.781	1.000
1-3	0.001	0.001	1.000	0.001	0.004	1.000	0.004	0.008	1.000
1-6	0.001		1.000	0.001	0.004	0.997	0.004	0.008	0.997
1-10	-		1.000	0.001	0.002	0.995	0.002	0.006	0.997
1-15	-		0.780	-	0.002	0.860	0.002	0.003	0.955

All this is a confirmation of what has been said earlier. Thus in respect of calculation of the stresses, satisfaction of given limit of error is necessary but not sufficient. In given case, with the first three eigenvectors taken into consideration, the normal force arising in rods of amplitude direction can be calculated to the required accuracy only if the equilibrium in the node is taken as a basis for calculation instead of the relative displacements.

In case of harmonic excitation, the static and dynamic error vectors have been defined in (40) and (42), respectively. Accordingly, after calculation of eigenvectors of a certain number, force vector $\Delta q(t)$ can be calculated as the upper bound of a force vector associated with further eigenvectors, depending on the excitation frequency and damping. The ratio of these vector elements (a certain combination thereof) and the static, or the dynamic force calculated that far is considered to be the limit of error. In the case shown in Fig. 1, the error calculated for load configura-

tion a), b), c), d) and excitation frequency $\alpha = 10, 100, 1000$ l/s has been defined for the sum of forces acting in the direction of the beam (decisive in respect of moments arising in the columns). A value of $\gamma = 0.1$ has been taken into consideration for internal damping. In case of a higher excitation frequency, the additional dynamic load is small and thus the dynamic error is greater than the static error decisive in respect of calculation for the dimensions. At the same time, the dynamic error may be smaller in case of lower excitation frequencies.

The values of static error are tabulated in Table 3.

Table 3

r α	a			b			c			d		
	10	100	1000	10	100	1000	10	100	1000	10	100	1000
1	0.35	1.00	1.00	0.46	2.99	2.99	3.42	9.74	9.74	∞	∞	∞
1-2	0.05	0.47	0.47	0.13	1.27	1.27	0.17	1.70	1.70	∞	∞	∞
1-3	-	0.03	0.03	0.01	0.10	0.10	0.01	0.06	0.06	∞	∞	∞
1-6	-	-	0.03	0.01	0.02	0.10	0.01	0.01	0.06	0.21	0.30	2.13
1-10	-	-	0.01	-	-	0.01	-	-	0.03	0.03	0.03	0.27
1-15	-	-	-	-	-	-	-	-	-	0.01	0.01	0.07

As seen the number of variables to be included in the calculation can be determined depending on excitation frequency and configuration of excitation forces.

A network plotted for the longitudinal wall of a tenstoreyed building made of prefabricated building elements is shown in Fig. 2 (the nodes being plotted as the actual nodes). The first ten radian eigenfrequencies of the system of a degree of freedom of 462 vary in the range of 11.64 to 145.3 l/s. A force is associated with either of load displacements a) and b), the excitation frequency of which being $\alpha = 5, 50, 500$ l/s. The static and dynamic errors have been defined for the displacement of the point of application of the force in the direction of the force, their magnitude being given in Table 4 and 5, respectively. In case a), the error due to partial eigenvector calculation could be identified with 3, 6,

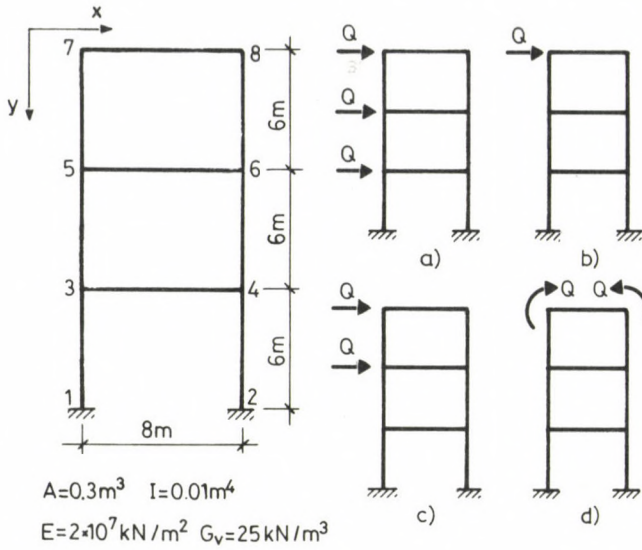


Fig. 1.

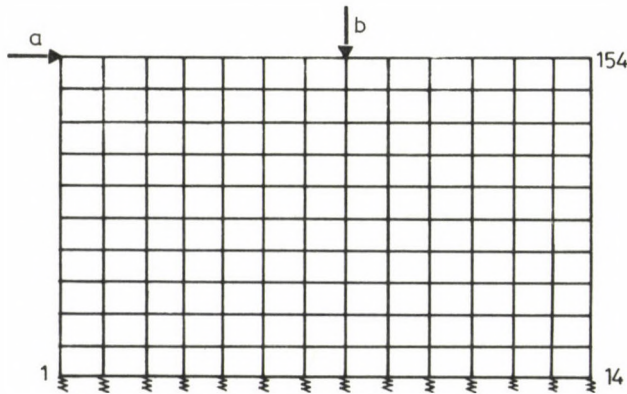


Fig. 2. Network for the longitudinal wall of a 10-storeyed building in Kelenföld

10 eigenvectors having been taken into consideration, depending on the excitation frequency. In calculating the first ten eigenvectors for a frequency of $\alpha = 500 \text{ l/s}$ in case b), an error factor of 2.19 should be taken into consideration which, in given case, would result in the construction of an economically unacceptable structure. For higher excitation frequencies, the

dynamic errors lie above the static errors, a fact indicating that the dynamic displacement calculated by means of eigenvectors of a certain number is small and it is by far not comparable with the accurate value of dynamic displacements. It can be seen on the basis of what has been said that the errors due to partial eigenvalue problem solution can be identified, permitting correct and controlled dynamic calculations to be carried out.

Table 4

$$\epsilon_{st} = \Delta o/o_{st}$$

r α	a			b		
	5	50	500	5	50	500
1	0.11	0.90	0.90	1.22	10.00	10.00
1-2	0.08	0.79	0.79	0.81	7.78	7.78
1-3	0.06	0.61	0.61	0.79	7.78	7.78
1-6	0.03	0.04	0.32	0.49	0.68	4.88
1-10	0.03	0.03	0.30	0.22	0.25	2.19

Table 5

$$\epsilon_{din} = \Delta e/e'_{din}$$

r α	a			b		
	5	50	500	5	50	500
1	0.10	14.38	∞	36.71	∞	∞
1-2	0.07	12.69	∞	3.49	∞	∞
1-3	0.05	8.21	∞	3.43	112.1	∞
1-6	0.03	0.20	∞	0.94	0.72	∞
1-10	0.03	0.15	154.1	0.28	0.19	67.79

As has been reported also in /8/, the convergence can be detected also for the stresses.

VIBRATION OF STRUCTURES

REFERENCES

1. Harris, C.M.—Crede, C.E.: Shock and Vibration Handbook, Vol. 2. McGraw-Hill, London 1961.
2. Przemieniecki, J.S.: Theory of Matrix Structural Analysis, McGraw-Hill, New York 1968.
3. Györgyi, J.: Process for calculation of (beam) structures of frequency dependent mass matrix and of a damping variable per component. Doctor's Thesis, Budapest 1984 (in Hungarian).
4. Hurty, W.C.—Rubinstein, M.F.: Dynamics of structures. Prentice-Hall Inc., Englewood Cliffs, New Jersey 1964.
5. Györgyi, J.: Taking into consideration the internal friction of the material in dynamic calculations for buildings. Építés-Építészettudomány, 10, (1984), 79–92 (in Hungarian).
6. Györgyi, J.: Dynamic Analysis of a Structure with Components of Different Damping Characteristics. Periodica Polytechnica, 23 (1979), 125–134.
7. Györgyi, J.: Viscous and Hysteretic Damping in Vibration of Structures. Periodica Polytechnica, 29 (1985).
8. Györgyi, J.—Lovas, A.: Experiences with the use of the method of finite elements in dynamic calculations. IV Hungarian Conference on Mechanics, Miskolc, Hungary, 1983.

QUALIFICATION OF INTERDEPENDENCE OR INDEPENDENCE WITHIN ANY PAIR OF
VARIABLES INVOLVED IN MULTIPLE LINEAR REGRESSION

A generalized stochastic approach

Z. Hankó*

(Received 21 June 1985)

Supposing joint normal distribution of the sample representing the variables involved in the multiple linear regression relation a stochastic interdependence/independence qualification method within any pair of variables is suggested. The limit significance level of qualification (based on which acceptance decision can be made) may be adopted according to the subject of investigation.

1. INTRODUCTION

In investigating natural / technological/ social phenomena, an ever increasing need can be recognized concerning the determination of the numerical relation of the variables involved. As is well known, the value of readings (measurement results or data) regarding the variables are influenced by not only measurement errors but also random fluctuations, and the variables, therefore, show a stochastic character. The numerical relation between stochastic variables can only be determined by regression analysis.

Fortunately, most of the phenomena and the samples regarding their variables show normal distribution (at least as a good approximation), and even the joint distribution of the samples shows a normal one. The only regression relation between variables of joint normal distribution is the linear one and that is the reason why exceptional attention is paid to multiple linear regression analysis.

Sometimes in practice the regression relation between the dependent variable and one of the independent variables shows a curvilinear feature, indicating that the joint distribution of the variables involved is not a normal one. In similar cases the adoption of a polynomial (power series) of the relevant independent variable often proves to be a reasonable approximation. This solution brings even the bivariable curvilinear regression re-

*Dr.Z.Hankó, H-1122 Budapest, Csaba u. 16/A, Hungary

lation to a multiple linear regression relation.

Taking into consideration also the above thoughts, the questions regarding qualification can be summarized, as follows:

- whether the interdependence between the dependent variable and any of the independent variables is close enough or not (in the presence of the remaining variables involved in the multiple linear regression relation);
- whether the independence within any pair of the independent variables is close enough or not (in the presence of the remaining variables involved in the multiple linear regression relation).

If the interdependence between the dependent variable and any of the independent variables is not close enough, then this independent variable is superfluous in the multiple linear regression relation because it does not worthily decrease the scatter (unbiased standard deviation of residuals), and increase the closeness, of the relation. If any pair of the independent variables does not show a reasonable independence, then one of them is also superfluous in the relation because they exert their effect on the dependent variable via each other (in similar cases that variable of the pair shall be discarded the interdependence of which is looser with the dependent variable). These questions can be answered by the application of the method discussed below.

2. SUBJECT OF QUALIFICATION

The general form of a multiple linear regression relation, based on a sample of size " n " (always discrete and finite) originated from a population of size " N " (either continuous or discrete and either finite or infinite), is

$$Y_{0j} = \bar{Y} + \sum_{\gamma=1}^v b_{y\gamma} (X_{\gamma j} - \bar{X}_{\gamma}), \quad (1)$$

where Y_{0j} = conditional expected value (designated j) of the dependent variable; \bar{Y} = empirical expected value (sample mean) of the dependent variable; $b_{y\gamma} = b_{y\gamma.1,2,\dots,\gamma-1,\gamma+1,\dots,v-1,v}$ = empirical regression coefficient of the independent variable γ where the terms in the subscript following the dot indicate those independent variables which also belong to the relation beyond those indicated before the dot; $X_{\gamma j}$ = the value designated j of independent variable γ ; \bar{X}_{γ} = empirical expected value (sample mean) of inde-

MULTIPLE LINEAR REGRESSION

pendent variable γ .

Actually, independent variable γ can denote different independent variables, each being in a linear relationship with the dependent variable according to preliminary assumption, but it can also denote the different degrees (powers) of a polynomial "Z". For example $X_{\gamma-1} = Z$, $X_{\gamma} = Z^2$ and $X_{\gamma+1} = Z^3$ if a polynomial of third degree is applied; and it is for the qualification procedure to decide whether these assumptions are appropriate or not.

The regression coefficients of a multiple linear regression relation are usually determined by the least squares method which results in the most probable relation between the dependent variable and the independent variable (s) with the possible minimum scatter. For determination of the regression coefficients it is necessary to solve a linear equation system which consists of ν linear equations and contains ν unknown variables. For solving the linear equation system, the Cramer-rule is most often used, e.g. the correlation matrix in the form of matrix equation. Here another solution is proposed (which is neither more time-consuming nor more difficult than the preceding one), creating at the same time the conditions for qualification within each pair of the variables involved in the multiple linear regression relation.

The empirical regression coefficient and its corrected (unbiased) standard deviation, of independent variable γ in the multiple linear regression relation are /1/

$$b_{y\gamma} = R_{y\gamma} \sqrt{\frac{V_{yy}/D_{yy}}{V_{\gamma\gamma}/D_{\gamma\gamma}}}, \quad \text{and} \quad (2)$$

$$\sigma_{by\gamma} = \pm \sqrt{\frac{V_{yy}/D_{yy}}{V_{\gamma\gamma}/D_{\gamma\gamma}} \frac{1 - R_{y\gamma}^2}{m}}, \quad \text{in which} \quad (3)$$

$$-1 < R_{y\gamma} = -\frac{D_{yy}}{\sqrt{D_{yy}D_{\gamma\gamma}}} < +1, \quad \text{furthermore} \quad (4)$$

$$V_{yy} = \frac{[(Y_i - \bar{Y})^2]}{n}; \quad C_{y\gamma} = \frac{[(Y_i - \bar{Y})(X_{\gamma i} - \bar{X}_{\gamma})]}{n}; \quad V_{\gamma\gamma} = \frac{[(X_{\gamma i} - \bar{X}_{\gamma})^2]}{n} \quad (5)$$

and
$$-1 < r_{y\gamma} = \frac{C_{y\gamma}}{\sqrt{V_{yy}V_{\gamma\gamma}}} < +1, \quad (6)$$

where $R_{\underline{y}\underline{y}} = R_{\underline{y}\underline{y}.1,2,\dots,\underline{y}-1,\underline{y}+1,\dots,\underline{v}-1,\underline{v}}$ = empirical multiple partial correlation coefficient between variables \underline{Y} and $\underline{X}_{\underline{y}}$; $V_{\underline{y}\underline{y}}$ and $V_{\underline{y}\underline{y}}$ = empirical variances of variables \underline{Y} and $\underline{X}_{\underline{y}}$, respectively; $C_{\underline{y}\underline{y}}$ = empirical covariance between variables \underline{Y} and $\underline{X}_{\underline{y}}$; $r_{\underline{y}\underline{y}}$ = empirical total correlation coefficient between variables \underline{Y} and $\underline{X}_{\underline{y}}$; $D_{\underline{y}\underline{y}}$, $D_{\underline{y}\underline{y}}$ and $D_{\underline{y}\underline{y}}$ = algebraic subdeterminant of the extended correlation matrix (formed by the empirical total correlation coefficients), \underline{R} , while the subscripts denote the positions of the subdeterminants; $m = n - v - 1$ = number of excess data-groups in the sample (degrees of freedom); n = number of data-groups in the sample; v = number of independent variables (equals the number of the unknown regression coefficients to be determined).

Table 1. Multiple extended correlation matrix

$$\underline{r}_{\underline{y}\delta} = \underline{r}_{\delta\underline{y}}$$

$\underline{R} \equiv$

		\underline{y}										
		\underline{Y}	\underline{X}_1	\underline{X}_2	.	.	$\underline{X}_{\underline{y}}$.	.	.	$\underline{X}_{\underline{v}}$	
δ		0	1	2	.	.	\underline{y}	.	.	.	\underline{v}	
	\underline{Y}	0	1	$r_{\underline{y}1}$	$r_{\underline{y}2}$.	.	$r_{\underline{y}\underline{y}}$.	.	$r_{\underline{y}\underline{v}}$	
	\underline{X}_1	1	1	r_{12}	.	.	$r_{1\underline{y}}$.	.	.	$r_{1\underline{v}}$	
	\underline{X}_2	2	$r_{2\underline{y}}$	r_{21}	1	.	.	$r_{2\underline{y}}$.	.	$r_{2\underline{v}}$	
	1	
	1	
	1	.	.	.	
	\underline{X}_{δ}	δ	$r_{\delta\underline{y}}$	$r_{\delta 1}$	$r_{\delta 2}$.	.	$r_{\delta\underline{y}}$	1	.	.	$r_{\delta\underline{v}}$
	1	.	.
	1	.
$\underline{X}_{\underline{v}}$	\underline{v}	$r_{\underline{v}\underline{y}}$	$r_{\underline{v}1}$	$r_{\underline{v}2}$.	.	$r_{\underline{v}\underline{y}}$.	.	.	1	

The extended correlation matrix, \underline{R} , is shown in Table 1. This matrix is of $(v+1)$ th order, quadratic, real, symmetric and positive definite; it is of $(v+1)$ th order, quadratic and real, symmetric because the num-

MULTIPLE LINEAR REGRESSION

ber of its rows and columns is identical: $(v+1)$; and r_{yy}, r_{yy} , that means that its real elements are symmetrical to the main diagonal of the matrix; positive definite because the value of its determinant exceeds zero ($D > 0$).

As is known, the inverse (reciprocal) matrix, \underline{Q}^{-1} , of the correlation matrix, \underline{Q} , is again of $(v+1)$ th order and symmetric; thus in the position denoted by the subscript the ratio of the corresponding algebraic subdeterminant and the determinant of the correlation matrix occurs. To calculate the empirical regression coefficient (Eq.2), and its empirical standard deviation (Eq.3), only the inverse matrix has to be determined in addition to the fundamental stochastic parameters (empirical variances and covariances, Eq.5, and empirical total correlation coefficients, Eq.6).

Many numerical procedures are known for calculating the inverse of a matrix. From among these the Gauss' elimination procedure is very advantageous for inverting the correlation matrix /2/. The result of the calculation is a matrix the structure of which is similar to the structure of the correlation matrix shown in Table 1, and the elements of which are D_{yy}/D ; D_{yy}/D ; D_{yy}/D etc. In proving the correctness of the inversion procedure: the matrix product of the correlation matrix and the inverted subdeterminant matrix must result in the positive unit matrix.

Knowing the inverse subdeterminant matrix, both the empirical multiple correlation coefficient, R_M , and the empirical corrected (unbiased) residual scatter, σ_{oy} , of the multiple regression relation can be calculated.

R_M is the measure of closeness of the regression relation:

$$0 < |R_M| = + \sqrt{\frac{\sum_{\gamma=1}^v r_{yy} R_{yy} \sqrt{D_{yy}}}{\sqrt{D_{yy}}}} = + \sqrt{1 - \frac{D}{D_{yy}}} < 1, \tag{7}$$

while σ_{oy} is the measure of goodness, by which the various confidence intervals of the conditional expected value of the dependent variable can be estimated:

$$\sigma_{oy} = \pm \sqrt{\frac{n}{m} V_{yy} (1 - R_M^2)} = \pm \sqrt{\frac{n}{m} V_{yy} \frac{D}{D_{yy}}} . \tag{8}$$

Two more remarks are worth remembering.

a) If $v = 1$, then the multiple regression relation will be reduced to a bivariable one. In this case the algebraic subdeterminants of the cor-

relation matrix are, as follows:

$$D_{=yy} = D_{=Y\gamma} = 1 \quad \text{and} \quad D_{=y\gamma} = D_{=Yy} = -r_{yx} = -r_{xy}.$$

This means that

$$R_{y\gamma} = R_M = r_{yx}$$

and this brings everything to the well known bivariable relation.

b) The empirical partial correlation coefficient (Eq.4) can be calculated not only between the dependent variable and one of the independent variables but also within any pair of the independent variables. While the former one is serving for qualification of interdependence, the latter one can be used for qualification of independence.

Each element of the sample consisting of $n(v+1)$ elements incorporates the resultant of those (generally unknown) random effects which are reflected in the relevant numerical value. The fundamental statistical parameters (empirical variances and covariances) sum up and average those random effects which have affected the variables of the sample. This summed up and averaged effect, weighted by the derived statistical parameters (empirical total correlation coefficient, correlation matrix, its subdeterminants and determinant, partial correlation coefficients), will appear in the empirical regression coefficient. The empirical regression coefficient is, therefore, the most characteristic parameter of the multiple linear regression relation, and it also is – in consequence of its derivation – a normally distributed stochastic variable. This is the very fact why the degree of interdependence and/or independence within any pair of variables of a multiple linear regression relation can be estimated by the empirical regression coefficient (and its standard deviation) using appropriate statistical hypothesis.

3. METHOD OF QUALIFICATION

The square root in Eq.(2) of the empirical regression coefficient is always positive. Its multiplier, the empirical partial correlation coefficient, can vary between -1 to $+1$. Value ± 1 indicates functional relation (with 100 per cent probability) within the pair of variables involved,

MULTIPLE LINEAR REGRESSION

while the zero value indicates that there is no-correlation between the variables (in case of really joint normal distribution, it indicates also independence). The intermediate values are approximately linear measures of linear dependence between the variables.

Since the empirical regression coefficient is a normally distributed stochastic variable, therefore the probability of risk can be estimated using a hypothesis test; that is the risk that the actual value ranges between no-correlation (independence) and functional relation (interdependence) as extremes.

Starting from Eqs (2) and (3) at the limit of no-correlation:

$$(b_{yY})_0 = \lim_{|R_{yY}| \rightarrow 0} b_{yY} = 0 \quad \text{and} \quad (2/a)$$

$$(\sigma_{byY})_0 = \lim_{|R_{yY}| \rightarrow 0} \sigma_{byY} = \pm \sqrt{\frac{V_{yy}/D_{yy}}{V_{YY}/D_{YY}}} \frac{1}{m} ; \quad (3/a)$$

while supposing functional relation:

$$(b_{yY})_1 = \lim_{|R_{yY}| \rightarrow 1} b_{yY} = + \sqrt{\frac{V_{yy}/D_{yy}}{V_{YY}/D_{YY}}} \quad \text{and} \quad (2/b)$$

$$(\sigma_{byY})_1 = \lim_{|R_{yY}| \rightarrow 1} \sigma_{byY} = 0 . \quad (3/b)$$

The standard abscissas of the normal probability distribution function for estimating the probability of risk can be formulated as the difference between the actual and the relevant limit value of the empirical regression coefficient, respectively.

The standard abscissa for estimating no-correlation:

$$x_{N0} = \frac{|b_{yY}| - (b_{yY})_0}{\sqrt{\sigma_{byY}^2 + (v_{byY})_0^2}} = + \sqrt{m \frac{R_{yY}^2}{2 - R_{yY}^2}} ; \quad (9)$$

while the standard abscissa for estimating functional relation:

$$x_{N1} = \frac{(b_{yY})_1 - |b_{yY}|}{\sqrt{\sigma_{byY}^2 + \sigma_{byY}^2}} = + \sqrt{m \frac{1 - |R_{yY}|}{1 + |R_{yY}|}} . \quad (10)$$

Subscript \underline{N} denotes normal distribution, while 0 and 1 indicate no-correlation and functional relation, respectively, as limits.

The probability of risk can be calculated, using the standard abscissa, as follows:

$$P_{Nr} = 2 \left(1 - \int_{-\infty}^{w_N} \frac{dx_N}{2\pi \exp x_N^2} \right) = 1 - \sqrt{\frac{2}{\pi \exp x_N^2}} \sum_{k=0}^{\infty} \frac{x_N^{2k+1}}{k! (2k+1)}, \quad (11)$$

where \underline{P}_{Nr0} = probability of risk that the actual empirical regression coefficient is not equal to zero, and thus this is the significance level of no-correlation; \underline{P}_{Nr1} = probability of risk that the actual value of the empirical regression coefficient is not equal to the value of the functional relation, and thus this is the significance level of functional relation. Here again subscript \underline{N} denotes normal distribution, \underline{r} indicates risk-probability, and 0 and 1 refer to the limits of no-correlation and functional relation, respectively.

According to the actual results of the hypothesis tests occurring in practice, a qualification by empirical frequency of occurrence can be added to the value of the risk-probability (significance level), and that serves as a basis for decision. From among the results only those are to be mentioned that permit unambiguous decisions, namely:

with

$$\underline{P}_{Nr} \geq 0.05 (=) 5\% \quad \text{the realization of the hypothesis is practically certain;}$$

with

$$\underline{P}_{Nr} < 0.001 (=) 0.1\% \quad \text{the realization of the hypothesis is practically impossible;}$$

within these two limits, the realization of the hypothesis is doubtful.

It follows from what has been said above that, if $\underline{P}_{Nr0} = \underline{f}_0(x_{N0}) \geq 5\%$, it can be taken for granted that the actual empirical regression coefficient differs from zero only at random and thus there is no-correlation between the variables involved (the variables are independent in case of normal distribution). Similarly, if $\underline{P}_{Nr1} = \underline{f}_1(x_{N1}) < 0.1\%$, then a functional relationship between the variables involved will be practically impossible (the relation being rather non-correlated and thus the variables independent). Contrary to the previous case, if $\underline{P}_{Nr0} = \underline{f}_0(x_{N0}) < 0.1\%$, then no-correlation is practically impossible (as in this case there exists rather a functional relationship and thus the variables are interdependent), while if

MULTIPLE LINEAR REGRESSION

$P_{Nr1} = f_1(x_{N1}) \geq 5\%$, it can be practically taken for granted that the numerical value of the actual empirical regression coefficient differs from the limit value, indicating functional relationship, only at random, so that the variables involved are linearly interdependent.

Both in the definition of risk-probability and in the previous interpretations, the random character has been mentioned repeatedly. In this respect the fact that the parameters involved in the hypothesis test are empirical variables derived from the sample and the sample is only more-or-less truly representing the population from which it is originating shall be taken into consideration. This uncertainty is reflected in the context of the empirical occurrence-qualifications (practically certain or practically impossible) and this is taken into account when the number of excess data-groups, \underline{m} , is used in Eqs (3), (9) and (10) instead of the number of data-groups, \underline{n} .

In case of normal distribution the standard abscissas of the various risk-probabilities (significance levels) are known, e.g. if $P_{Nr} = 5\%$, then $\underline{x}_N = 1.96$, and if $P_{Nr} = 0.1\%$, then $\underline{x}_N = 3.291$, etc. Thus Eqs (9) and (10) can be rearranged:

$$0 < |R_0| = + \sqrt{\frac{2 x_{NO}^2}{\underline{m} + x_{NO}^2}} \leq 1 \tag{9/a}$$

and

$$0 \leq |R_1| = + \frac{\underline{m} - x_{N1}^2}{\underline{m} + x_{N1}^2} < 1. \tag{10/a}$$

$R_0 = 0$ and $R_1 = 1$ can only be reached if $\underline{m} = +\infty$ (if x_N differs from zero), but $\underline{m} = \underline{n} - \nu - 1$ is always finite; and $\underline{m}_{\min} = x_N^2$ (if $x_{N\min}$ exceeds zero). $x_{N\min} = 0$ cannot be assumed because it represents a deterministic functional relationship and this disagrees with the assumption that the variables are stochastic variables affected by random effects.

If decision is made concerning the limit risk-probability (limit significance level), the value of the corresponding standard abscissa is known; and if the number of the excess data-groups is also known, then the limit value of the partial correlation coefficient (Eqs 9/a and 10/a) can be calculated. Comparing the actual partial correlation coefficient with the previous limit value, independence/interdependence between the variables involved with special regard to the multiple relation can be qualified.

To illustrate the methodological results summarized above Fig. 1 shows three-variable relationships

$$\left| R_0 \right| = f_{R0} \left[m; P_{Nr0} = f_0(x_{N0}) \right] \quad (9/b)$$

and

$$\left| R_1 \right| = f_{R1} \left[m; P_{Nr1} = f_1(x_{N1}) \right] \quad (10/b)$$

the application of which will be discussed below.

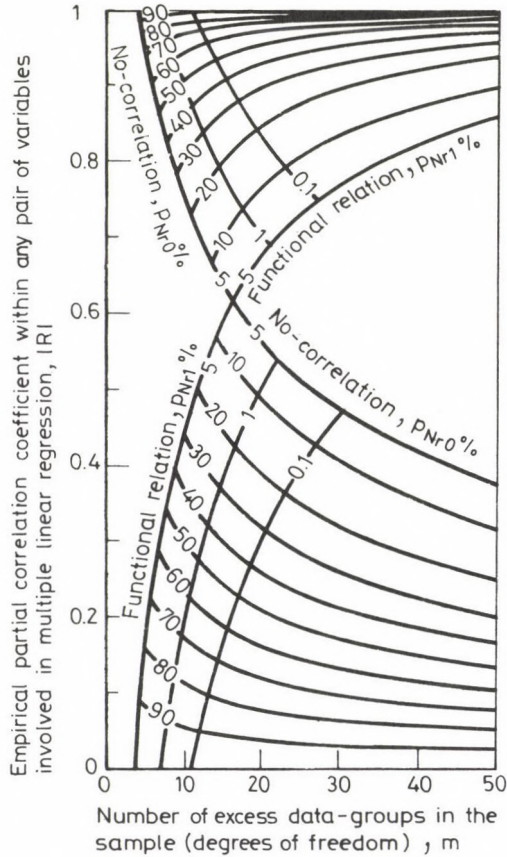


Fig. 1. The partial correlation coefficient as a function of the degrees of freedom; the parameters are: significance level of no-correlation and functional relation; serving for qualification of interdependence (upper triangle; tip downward) and independence (lower triangle; tip upward), respectively, between the variables involved

4. QUALIFICATION OF INTERDEPENDENCE

The graphs of Eqs (9/a,b) and (10/a,b) applying $p_{Nr} = 5\%$ ($x_N=1.96$) as the characteristic third parameter – like diagonals – divide the $0 \leq |R| \leq 1$ and $0 \leq m < +\infty$ rectangular field of Fig. 1 in four subfields resembling triangles. The upper triangle (with tip downwards) serves for qualification of interdependence (between the dependent variable and any of the independent variables).

The triangular subfield for interdependence qualification is bounded from the left by no-correlation relations of various significance levels and from the right by functional relations again of various significance levels. The highest significance level of no-correlation indicated here is $p_{Nr0} = 5\%$, because – as it has been mentioned previously – no-correlation will be practically certain if the significance level exceeds 5%; and this is irrelevant in the case of interdependence qualification. Similarly, the lowest significance level of functional relation is also 5%, because functional relation will be at least doubtful if the significance level is lower than 5%. If the limit significance level of no-correlation decreases and/or that of functional relation increases, the triangular subfield of interdependence qualification will shift to the right and upwards, indicating a closer stochastic linear interdependence between the variables involved.

For practical application of interdependence qualification, the following steps shall be considered:

– decision shall be made in advance concerning limit significance level of

= no-correlation: maximum 5%, and the lower the value, the closer the interdependence; and simultaneously

= functional relation: minimum 5%, and the higher the value, the closer the interdependence;

– using the actual empirical multiple partial correlation coefficient, $R_{y\dot{Y}}$, between the dependent variable and any of the independent variables

= the actual standard abscissa (x_{N0} ; Eq.9) and the relevant actual significance level (p_{Nr0} ; Eq.11) of no-correlation shall be calculated; and if

$$p_{Nr0} \text{ actual} < p_{Nr0} \text{ limit}$$

the condition for no-correlation of interdependence will be fulfilled; and simultaneously

= the actual standard abscissa (\underline{x}_{N1} ; Eq.10) and the relevant actual significance level (P_{Nr1} ; Eq.11) of functional relation shall be calculated; and if

$$P_{Nr1} \text{ actual} > P_{Nr0} \text{ limit}$$

the condition for functional relation of interdependence will be fulfilled.

As can be seen from the foregoing, if the actual significance level of no-correlation relation tends to zero, and simultaneously, that of functional relation to unity, the stochastic linear interdependence of the variables involved will tend to deterministic interdependence; and as a result, the necessary number of the excess data-groups will tend to infinite.

5. QUALIFICATION OF INDEPENDENCE

The lower triangle (with tip upwards) in Fig. 1 serves for qualification of independence (for any pair of the independent variables).

The triangular subfield for independence qualification is bounded from the left by functional relations of various significance levels and from the right by no-correlation relations again of various significance levels. Here the highest significance level of functional relation is $P_{Nr1} = 5\%$, because functional relation will be practically certain if the significance level exceeds 5%; and this is irrelevant in case of independence qualification. Similarly, the lowest significance level of no-correlation is 5%, because no-correlation relation will be at least doubtful if the significance level is lower than 5%. If the limit significance level of functional relation decreases and/or that of no-correlation relation increases, the triangular subfield of independence qualification will shift to the right and downwards, indicating a closer stochastic linear independence between the variables involved.

For practical application of independence qualification, the following steps shall be considered:

– decision shall be made in advance concerning limit significance level of

MULTIPLE LINEAR REGRESSION

= functional relation: maximum 5 %, and the lower the value, the closer the independence; and simultaneously

= no-correlation: minimum 5 %, and the higher the value, the closer the independence;

– using the actual empirical multiple partial correlation coefficient, \underline{R} , for any pair of the independent variables

= the actual standard abscissa (\underline{x}_{N1} ; Eq. 10) and the relevant actual significance level (\underline{p}_{Nr1} ; Eq. 11) of functional relation shall be calculated; and if

$$\underline{p}_{Nr1} \text{ actual} < \underline{p}_{Nr1} \text{ limit}$$

the condition for functional relation of independence will be fulfilled; and simultaneously

= the actual standard abscissa (\underline{x}_{N0} ; Eq. 9) and the relevant actual significance level (\underline{p}_{Nr0} ; Eq. 11) of no-correlation relation shall be calculated; and if

$$\underline{p}_{Nr0} \text{ actual} > \underline{p}_{Nr0} \text{ limit}$$

the condition for no-correlation relation of independence will be fulfilled.

As can be seen from the foregoing, if the actual significance level of functional relation tends to zero, and simultaneously, that of no-correlation relation to unity, then the stochastic linear independence of the variables involved will tend to deterministic independence; and as a result, the necessary number of the excess data-groups will tend to infinite.

6. CONTRADICTORY QUALIFICATION

As illustrated in Fig. 1, the upper and lower triangular subfields serving for interdependence and independence qualification, respectively, are only a small part of the total rectangular $|\underline{R}| \div \underline{m}$ field. The two remaining triangular subfields on the left and right (the tips of which pointing in opposite direction and touching each other horizontally) are contradictory subfields.

The left subfield is bounded from above by no-correlation relation the significance level of which exceeds 5 %, and from below by functional relation the significance level of which also exceeds 5 %. As it has been mentioned earlier, if the significance level exceeds 5 % then the realization of the hypothesis will be practically certain. The relation between the pair of variables, characterized by $|\underline{R}| \div \underline{m}$ coordinates, falling within this

subfield, is contradictory because from above significant no-correlation (independence) and from below significant functional relation (interdependence) are indicated.

Similarly, the right subfield is also contradictory. From above it is bounded by functional relation the significance level of which is lower than 5 %, and from below by no-correlation relation the significance level of which is also lower than 5 %. As is known, if the significance level of the hypothesis test is lower than 5 %, then the realization of the hypothesis will be doubtful and if it is lower than 0.1 %, the realization will be practically impossible. The relation between the variables of any pair, characterized by $\left| \frac{R}{r} \right| \frac{1}{n}$ coordinates, falling within this subfield is, therefore, contradictory, because from above a doubtful/impossible functional relation (which is really independence) and from below a doubtful/impossible no-correlation relation (which is really interdependence) are indicated.

The contradictory qualification can be attributed to three main causes:

- the mathematical form of the multiple linear regression relation is a very rough numerical approximation to the cause-and-effect chain which is intended to be described by it (the joint distribution of the sample differing roughly from normal distribution);

- the sample of one or both of the two variables involved is statistically inadequate because e.g.

- = the elements of the relevant sample are not independent, or homogeneous, or neither,

- = the elements of the sample carry systematic error (trend-like or periodic), etc.

- the number of the excess data-groups is very far from optimum.

To avoid contradictory qualification, different methods can be applied, depending on the cause of the disadvantageous result.

To avoid an inadequate mathematical form, it is advisable to derive the form of the regression relation so as to start from the mathematical description of the phenomenon, and if there is no linear relation between (any of) the variables, then some transformation or power series can be adopted.

The independence and homogeneity of the sample elements must always be checked in advance. Adequate statistical methods are available for this purpose, and for removal of systematic errors from the sample.

As can also be seen in Fig. 1, the optimum number of excess data-groups can be found at the cross-point of no-correlation and functional re-

MULTIPLE LINEAR REGRESSION

lation the significance levels of which have been adopted as limits. E.g. in case of interdependence qualification: if ρ_{Nr0} limit = 0.1 % and ρ_{Nr1} limit = 5 % are adopted, then $m_{\text{optimum}} = 27 \div 28$; or in case of independence qualification: if $\rho_{Nr1} = 0.1$ % and $\rho_{Nr0} = 5$ % are applied, then $m_{\text{optimum}} = 30 \div 31$.

Thus, because the limits adopted above are most advisable in practice, it can be said that the optimum number of the excess data-groups is about 29. It follows from the foregoing that the minimum number of the excess data-groups equals 11 (the corresponding partial correlation coefficient equals unity in case of interdependence while zero in case of independence). In case the above boundary conditions are adopted, the triangular subfields of interdependence and independence qualification, respectively, are not touching each other with their tips but there is a "white gap" between these two subfields the magnitude of which is about $\Delta|R| = 0.753 - 0.474 = 0.279$, and $\Delta m = (30 - 27) \div (31 - 28) = 3$; thus the contradictory subfield is extended.

7. EXAMPLE

An example is given below to illustrate the application of the qualification method introduced. Vágás I. /3/ has elaborated multiple linear regression relations for flood forecasting purposes for various cross-sections of the Tisza River and her tributaries in Hungary. Among these there is a quadruple linear regression relation for estimating the expected value of flood level in the Szeged cross-section of the Tisza River. In his paper he has also published the quadruple data-groups of 31 floods observed between 1876 and 1979. These data will be used here for illustrating the qualification method.

The general form of the quadruple linear regression relation adopted is:

$$Y_{0j} = \bar{Y} + b_{yT}(X_{Tj} - \bar{X}_T) + b_{yM}(X_{Mj} - \bar{X}_M) + b_{yS}(X_{Sj} - \bar{X}_S),$$

where Y_{0j} = expected flood level (gage reading) for Tisza River at Szeged, \bar{Y} = sample mean of the observed reading peaks for Tisza River at Szeged, X_{Tj} = reading peak at Tokaj (up-stream) cross-section of Tisza River, \bar{X}_T = sample mean of the observed reading peaks at Tokaj for Tisza River, X_{Mj} =

reading at Makó cross-section for the Maros River (tributary of the Tisza River), made simultaneously with the Tokaj reading, \bar{X}_M = sample mean of the observed readings at Makó for Maros River, X_{Sj} = the lowest reading which preceded the actual flood at Szeged for Tisza River, \bar{X}_S = sample mean of the observed lowest readings preceding the floods at Szeged for Tisza River.

Using the sample consisting of $n(v+1) = 31(3+1) = 124$ elements, the six different empirical total correlation coefficients, r , have been calculated for use in formulating the quadruple extended correlation matrix, \underline{R}_4 (Table 2). The sample mean and variance of each variable have also been incorporated in this table.

Table 2. Quadruple extended correlation matrix

$$r_{\gamma\delta} = r_{\delta\gamma}$$

$\delta \backslash \gamma$		Y	X_T	X_M	X_S
		0	1	2	$v = 3$
Y	0	1	0.456 322	0.659 804	0.539 480
X_T	1	0.456 322	1	-0.221 989	0.099 780
X_M	2	0.659 804	-0.221 989	1	0.273 517
X_S	$v = 3$	0.539 480	0.099 780	0.273 517	1
sample mean /cm/		822.5806	768.8065	400.8710	660.6452
variance /cm ² /		3354.39	4763.34	9712.41	11380.23

Table 3 illustrates the result of the inversion procedure of the correlation matrix, the inverse subdeterminant matrix, \underline{R}_4^{-1} ; and the matrix product of the two previous matrices, the unit matrix, \underline{E}_4^+ , which shows that the inversion procedure is correct within an acceptable limit of calculation error.

MULTIPLE LINEAR REGRESSION

Table 3. Quadruple inverse matrix and unit matrix

$$\frac{\underline{\underline{D}}_{\gamma\delta}}{\underline{\underline{D}}} = \frac{\underline{\underline{D}}_{\delta\gamma}}{\underline{\underline{D}}}$$

		γ		\underline{Y}	\underline{X}_T	\underline{X}_M	\underline{X}_S	
				0	1	2	$\nu = 3$	
$\underline{\underline{R}}_{\underline{\underline{4}}}^{-1}$	\underline{Y}	0	9.19287	-5.38408	-6.54047	-2.63322		
	\underline{X}_T	1	-5.38408	4.26391	4.12258	1.35425		
	\underline{X}_M	2	-6.54047	4.12258	5.81289	1.52718		
	\underline{X}_S	$\nu=3$	-2.63322	1.35425	1.52718	1.86773		
		δ		\underline{Y}	\underline{X}_T	\underline{X}_M	\underline{X}_S	
				0	1	-4.76×10^{-7}	5.96×10^{-8}	-1.19×10^{-7}
		\underline{X}_T	1	3.87×10^{-7}	0.999999	-3.58×10^{-7}	-2.23×10^{-7}	
		\underline{X}_M	2	-2.98×10^{-7}	-3.87×10^{-7}	1	0	
$\underline{\underline{R}}_{\underline{\underline{4}}}^+$	\underline{X}_S	$\nu=3$	-7.15×10^{-7}	0	1.19×10^{-7}	1		

The results of the qualification calculations are summarized in Tables 4 and 5. Table 4 illustrates the results for interdependence qualifications, and Table 5 can be used for independence qualifications; and both tables contain the results of both bivariable and four-variable relations.

First the bivariable results should be discussed. With the various bivariable actual significance levels in Table 4 checked, it can be seen that none of the $\underline{Y}-\underline{X}_\gamma$ bivariable relations shows acceptable interdependence (each \underline{P}_{Nr0} exceeds 0.1 % and each \underline{P}_{Nr1} is less than 5 %). With the various bivariable actual significance levels in Table 5 checked, it can be seen that each $\underline{X}_\gamma - \underline{X}_\delta$ bivariable relation shows significant independence (each \underline{P}_{Nr1} is less than 0.1 % and each \underline{P}_{Nr0} significantly exceeds 5 %).

Using the quadruple linear regression relation, the significance level within each pair of the variables shows a characteristic modification.

Table 4. Qualification of interdependence

Conditions for acceptable interdependence (limit significance levels)

$$p_{Nr0} < 0.1 \% \text{ and } p_{Nr1} \geq 5 \%$$

Pairs of variables		$\bar{Y} - \bar{X}_T$	$\bar{Y} - \bar{X}_M$	$\bar{Y} - \bar{X}_S$
bi- vari- able m=29	\bar{r}	0.456 322	0.659 804	0.539 480
	\bar{X}_{N0}	1.835 816	2.840 561	2.222 328
	p_{Nr0}	6.64 %	0.45 %	2.63 %
	\bar{X}_{N1}	3.290 343	2.438 008	2.945 345
	p_{Nr1}	0.10 %	1.48 %	0.32 %
four- vari- able m=27	\bar{R}	0.862 703	0.894 720	0.635 484
	\bar{X}_{N0}	4.000 301	4.244 956	2.613 655
	p_{Nr0}	0.01 %	0.00 %	0.90 %
	\bar{X}_{N1}	1.410 719	1.224 848	2.453 110
	p_{Nr1}	15.83 %	22.06 %	1.42 %

Table 5. Qualification of independence

Conditions for acceptable independence (limit significance levels):

$$p_{Nr0} \geq 5 \% \text{ and } p_{Nr1} < 0.1 \%$$

Pairs of variables		$\bar{X}_T - \bar{X}_M$	$\bar{X}_T - \bar{X}_S$	$\bar{X}_M - \bar{X}_S$
bi- vari- able m=29	\bar{r}	0.221 989	0.099 780	0.273 517
	\bar{X}_{N0}	0.855 919	0.380 900	1.061 565
	p_{Nr0}	39.20 %	70.33 %	28.84 %
	\bar{X}_{N1}	4.296 929	4.872 147	4.067 329
	p_{Nr1}	0.00 %	0.00 %	0.00 %

MULTIPLE LINEAR REGRESSION

Table 5. (continued)

Pairs of variables		$\underline{X}_T - \underline{X}_M$	$\underline{X}_T - \underline{X}_S$	$\underline{X}_M - \underline{X}_S$
four- vari- able m=27	R	-0.830 708	-0.481 412	-0.463 486
	\underline{X}_{N0}	3.771 440	1.881 169	1.802 509
	\underline{P}_{Nr0}	0.02 %	5.99 %	7.15 %
	\underline{X}_{N1}	1.580 122	3.074 363	3.146 141
	\underline{P}_{Nr1}	11.41 %	0.21 %	0.17 %

The interdependence (Table 4) within the pairs of $\underline{Y}-\underline{X}_T$ and $\underline{Y}-\underline{X}_M$ is significant (\underline{P}_{Nr0} is less than 0.1 % and \underline{P}_{Nr1} significantly exceeds 5 %), while the interdependence of the $\underline{Y}-\underline{X}_S$ pair is doubtful ($0.1 \% < \underline{P}_{Nr0} < 1 \%$ and $5 \% > \underline{P}_{Nr1} > 1 \%$). The independence (Table 5) within the pairs of $\underline{X}_T-\underline{X}_S$ and $\underline{X}_M-\underline{X}_S$ is more or less acceptable (\underline{P}_{Nr0} exceeds 5 % and \underline{P}_{Nr1} is slightly more than 0.1 % instead of being less), while the independence of $\underline{X}_T-\underline{X}_M$ is completely unacceptable because this relation shows a significant interdependence (\underline{P}_{Nr0} is less than 0.1 % and \underline{P}_{Nr0} exceeds significantly 5 %).

In spite of the unsuccessful qualification results, the closeness of the quadruple relation and the goodness of the expected dependent variable is also shown as an illustration.

The empirical quadruple correlation coefficient (Eq.7), $|R_4| = 0.944\ 0445$ indicates a very close stochastic linear interdependence between the dependent variable and the independent variables; and this is also proved by the significance levels of no-correlation, \underline{P}_{Nr0} , and functional relation, \underline{P}_{Nr1} , respectively (\underline{P}_{Nr0} is practically zero and $\underline{P}_{Nr1} = 37.80\%$, and these indicate significant interdependence).

The empirical corrected (unbiased) residual scatter of the relation (Eq.8) serves for calculation of the confidence interval(s) of particular risk-probability, indicating the goodness of the conditional expected value of the dependent variable. Thus the residual scatter, $\sigma_{oy} = \pm 20.5\text{cm}$, and the calculated confidence interval of 5 % risk-probability, $1.96 \sigma_{oy} = \pm 40 \text{ cm}$, shall be applied. This uncertainty indicates not only large residual scatter but also (in consequence of the foregoing) an unacceptable

result in forecasting flood level.

For correct reference it shall be mentioned that according to Vágás and Simády /4/, this quadruple linear regression relation is only a rough approximation to the physical phenomenon, and they do not advise to use it for practical forecasting purposes. In consequence of this statement, the cause-effect chain has not been mathematically checked; and because the number of excess data-groups is almost optimum, only the statistical adequacy of the sample had to be checked. The result of this investigation showed that the homogeneity of the sample was also questionable.

8. CONCLUSION AND RECOMMENDATION

In case the use of a multiple linear regression relation for numerical interpretation of a phenomenon is intended, the following recommendations shall be taken into consideration:

(a) It is advisable to try to derive the mathematical form (at least approximately) from the phenomenon itself to find the type of relationship between the variables involved. If the relationship between the variables is other than linear, the use of transformation or power series, etc. can help in linearizing the original relationship.

(b) The sample elements shall be checked statistically for independence and homogeneity, and the systematic errors shall be removed from them.

(c) It shall be checked whether the joint distribution of the sample be reliably approximated by normal distribution (at least the marginal distributions should be checked).

(d) The limit significance levels of no-correlation and functional relation, respectively, both for qualification of interdependence between the dependent variable and any of the independent variables, and for qualification of independence within any pair of the independent variables, shall be decided in advance. It is advisable to use 0.1 % as limit significance level for

- no-correlation, p_{NR0} , in case of interdependence qualification and
- functional relation, p_{NR1} , in case of independence qualification.

The limit significance level of functional relation, p_{NR1} , in case of interdependence qualification and that of no-correlation, p_{NR0} , in case of independence qualification must equal or exceed 5 %. The actual value to

MULTIPLE LINEAR REGRESSION

be selected as limit depends on the subject of investigation (Fig. 1).

(e) The sample consisting of $n(v+1)$ elements (n = number of data-groups, v = number of independent variables) involves $v(v+1)/2$ empirical total correlation coefficients. These serve for formulation of the multiple extended correlation matrix (Table 1) the inverse of which is the subdeterminant matrix; and of which the empirical partial correlation coefficients within any pair of the variables (Eq.4) can be calculated. Using Eqs(9), (10) and (11), the actual significance level of no-correlation and that of functional relation can be calculated in case of both interdependence (between the dependent variable and any of the independent variables) and independence (within any pair of independent variables) qualification. It can be decided whether the variables are interdependent/independent by comparison of the actual and limit significance levels.

(f) If the qualification of both interdependence and independence proves to be acceptable, then the closeness of the relation can be checked by the multiple correlation coefficient, $|R_M|$, using Eq.(7); the residual scatter of the expected value of the dependent variable can be estimated on the basis of Eq.(8), and this can serve for estimating the confidence interval of the expected value of the dependent variable. For calculating the empirical regression coefficients, b_{yY} , Eq.(2) can be used and thus the numerical multiple linear regression relation (Eq.1) can be formulated.

REFERENCES

1. Korn, G.A. — Korn, T.M.: Mathematical Handbook for Scientists and Engineers. 2nd ed., McGraw-Hill, New York, Toronto, London 1970.
2. Alcock, D.: Illustrating Basic. Syndicate of the Cambridge University Press; Cambridge 1977.
3. Vágás, I.: Gage Relation Methods of Flood Forecasting (in Hungarian); Hidrológiai Közlöny, Budapest 1980/11.
4. Vágás, I. — Simády, B.: The methods and results of flood forecasting developed at Szeged (in Hungarian). Vízügyi Közlemények, Budapest 1983/3.

ELASTIC MEMBRANES REINFORCED BY CORDS:
NONLINEAR AXISYMMETRIC DEFORMATION WITH TWIST

Maria Matsikoudi-Iliopoulou*

(Received 25 September 1985)

In this paper we develop the equations of axisymmetric deformation of an initially cylindrical membrane composed of an elastic homogeneous, isotropic and incompressible material possessing a strain energy function of Mooney-Rivlin type. The membrane is reinforced by perfectly flexible and inextensible helicoidal cords. Application to a specific boundary-value problem is also given.

NOTATION

$A_{\beta\rho}$	underformed surface metric tensor
$a_{\beta\rho}$	deformed surface metric tensor
$C_{\beta\rho}$	second fundamental form
u^{β}	surface coordinates
$\Gamma_{\mu\rho}^{\beta}$	Cristoffel symbols
R	underformed radius
r	deformed radius
θ	underformed polar angle
ϑ	deformed polar angle
n	arc length of the underformed meridian
ξ	arc length of the deformed meridian
Y	axial coordinate of the underformed state
y	axial coordinate of the deformed state
g	angular displacement
α	constant angle subtended by the cords with the generators of the underformed membrane
ds_0	element of length of the underformed membrane
ds	element of length of the deformed membrane
γ	angle subtended by ds_0 with the generator of the underformed membrane
δ	angle subtended by ds with the generator of the deformed membrane
b	angle subtended by the cords with the meridian of the deformed membrane

*M. Matsikoudi-Iliopoulou, School of Technology, Division of Applied Mechanics, Aristotle University of Thessaloniki, GR-540 06 Thessaloniki, Greece

b^0	angle subtended by the cords with the meridian of the deformed membrane expressed in degrees
$n^{\beta\rho}$	components of stress tensor
τ	the tension in the cords
W	strain energy function
I_1, I_2	strain invariants
$n^{(i)}$	physical stress-resultants
n_i	non-dimensional stress-resultant
p	normal pressure
Δ	distance between adjacent cords in the underformed membrane
$2L_0$	height of the underformed membrane
$2L$	height of the deformed membrane
σ	angle between the tangent to the meridian and the axis of symmetry
$\ell = d\xi/dn$	
$x = r/R$	
$z = \xi/R$	
$\omega = dg/dz$	
$\frac{\partial W}{\partial I_1} = C_1$	
$\frac{\partial W}{\partial I_2} = C_2$	
$\Gamma = C_2/C_1$	
$\lambda = \frac{pR}{2C_1}$	
$T = \frac{\tau}{2C_1\Delta}$	
$h^{1/2} = \sqrt{1-\ell^2\cos^2\alpha}$	

1. INTRODUCTION

The theory of large elastic deformations of reinforced membranes was developed by J.E. Adkins and R.S. Rivlin /1/ and /2/ who also obtained the solutions to a number of boundary-value problems. Most of these solutions are outlined by A.E. Green and J.E. Adkins /3/ who give references to

original sources. Many other authors have given solutions to a number of specific problems of reinforced elastic solids. Apart from their theoretical interest, the deformation of reinforced solids has a technological interest as well, since reinforcement by inextensible cords form a common feature of such manufactured articles, as pneumatic tyres and hose-pipes.

In this paper we considered the axisymmetric deformations of circular cylindrical membranes reinforced by a family of flexible and inextensible helicoidal cords. We assume that the cords form a constant angle with the generators of the underformed cylinder. We also assume that no two cords are brought into contact as a result of the deformation. In section 2 we define "axisymmetric deformation with twist" and study the geometry of the deformation. In section 3 we derive the equations of motion and the constitutive equations for an elastic, isotropic body, made of Mooney-Rivlin material and reinforced by one family of perfectly flexible and inextensible cords. Subsequently, we derive the solution of a circular cylindrical membrane sealed at each end by rigid plugs. In section 4 we develop a numerical method for the solution of the equations of section 3 and discuss a number of numerical examples.

2. FINITE AXISYMMETRIC DEFORMATIONS WITH TWIST OF ELASTIC MEMBRANES

We define as "Axisymmetric deformation with twist" the deformations in which i) both the deformed and underformed membranes are surfaces of revolution, ii) points of constant latitude retain this property but change their angular position and iii) the stretch along and in the direction of a latitude circle remains constant. It is assumed that the meridian C generating the deformed membrane does not intersect the axis of symmetry.

In this paper we consider a membrane as a two dimensional body.

The deformation is described with respect to a fixed cylindrical coordinate system. We denote (R, Θ, Y) the coordinates in the underformed configuration of a point which has coordinates (r, θ, y) in the deformed state. The y -axis coincides with the axis of symmetry of the membrane. If we denote by n and ξ the arc length of the underformed and deformed meridians respectively, we can easily prove that, in the kind of deformation treated here we have the relations:

$$\begin{aligned} r &= r(\xi), \\ y &= y(\xi), \\ \vartheta &= \theta + g(\xi) \end{aligned} \tag{2.1}$$

where g is the angular displacement due to the presence of the cords and possibly an external torque.

We will assume that the curvilinear surface coordinates u^β coincide with the orthogonal system θ, ξ in the deformed membrane so that $u^1 = \vartheta$ and $u^2 = \xi$. The position vector of a particle of the deformed membrane, is given by (Fig. 1).

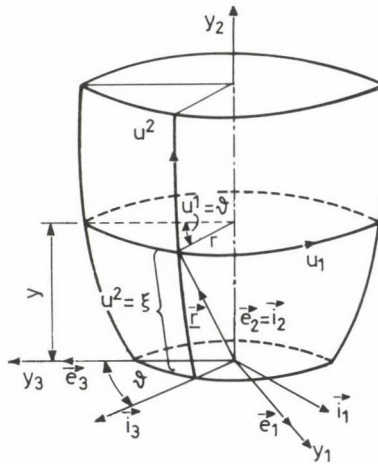


Fig. 1. Surface of revolution defining deformed membrane

$$\vec{r}(u^1, u^2) = y(\xi) \vec{i}_2 + r(\xi) \vec{i}_3(\vartheta) . \tag{2.2}$$

Introducing the notation

$$\frac{\partial}{\partial \xi} = () \tag{2.3}$$

we find the deformed surface metric tensor

$$\left[a_{\beta\rho} \right] = \begin{bmatrix} r^2 & 0 \\ 0 & 1 \end{bmatrix}, \left[a^{\beta\rho} \right] = \begin{bmatrix} r^{-2} & 0 \\ 0 & 1 \end{bmatrix}, a = r^2 \tag{2.4}$$

and the second fundamental form

$$[C_{\beta\rho}] = \begin{bmatrix} -r\sqrt{1-r'^2} & 0 \\ 0 & r''/\sqrt{1-r'^2} \end{bmatrix}. \quad (2.5)$$

The only non zero Christoffel symbols are given by

$$\Gamma_{12}^1 = r'/r, \quad \Gamma_{11}^2 = -rr'. \quad (2.6)$$

Using capital letters for the undeformed state, the position vector of the corresponding particle of the undeformed membrane is given by

$$\vec{R}(u^1, u^2) = Y(\xi) \vec{I}_2 + R(\xi) \vec{I}_3(\vartheta, \xi). \quad (2.7)$$

For this coordinate system we find that the surface metric tensor of the undeformed state is

$$[A_{\beta\rho}] = \begin{bmatrix} R^2 & -R^2 g' \\ -R^2 g' & (R^2 g'^2 + Y'^2 + R'^2) \end{bmatrix}, \quad (2.8)$$

$$[A^{\beta\rho}] = \begin{bmatrix} (1/R^2) + g'^2/(R'^2 + Y'^2) & g'/(R'^2 + Y'^2) \\ g'/(R'^2 + Y'^2) & 1/(R'^2 + Y'^2) \end{bmatrix}, \quad (2.9)$$

$$A = R^2(Y'^2 + R'^2)$$

3. GENERAL EQUATIONS

We consider the axisymmetric deformation with twist, of an initially circular cylindrical membrane, composed of an elastic Mooney-Rivlin material, reinforced by one family of inextensible cords. We assume that the cords form a constant angle with the generators of the undeformed membrane.

We observe that in the coordinate system considered, $R = \text{const.}$, since the undeformed state is cylindrical.

Let the elements of length in the undeformed and deformed configuration be denoted by ds_0 and ds respectively. Let γ and δ be the angle subtended by ds_0 and ds respectively, with the generator of the undeformed and deformed membrane. If dn and $d\xi$ are the elements of length of the

underformed and deformed meridians respectively, we can easily obtain

$$\left(\frac{ds}{ds_0}\right)^2 = \left(\frac{d\xi}{ds_0}\right)^2 + r^2 \left(\frac{d\theta}{ds_0}\right)^2 = \left(\frac{d\xi}{dn}\right)^2 \cos^2 \gamma + \frac{r^2}{R^2} \left(\frac{d\theta}{d\theta} \sin \gamma\right)^2, \quad (3.1)$$

whence

$$\left(\frac{ds}{ds_0}\right)^2 = \lambda^2 \cos^2 \gamma + x^2 \left(\sin \gamma + R \frac{dg}{dn} \cos \gamma\right)^2 \quad (3.2)$$

where we have used Eqs (2.1)₃ and the notation

$$\lambda = d\xi/dn, \quad x = r/R. \quad (3.3)$$

Let β be the angle subtended by the cords with the meridian of the deformed state. Then, since ds_0 and ds are elements of an inextensible cord for $\gamma = \alpha$ and $\delta = \beta$, we have $ds = ds_0$. Eq. (3.2) reduces to

$$\lambda^2 \cos^2 \alpha + x^2 \left(\sin \alpha + R \frac{dg}{dn} \cos \alpha\right)^2 = 1. \quad (3.4)$$

From the above equation and because

$$\cos \beta = \lambda \cos \alpha \quad (3.5)$$

we find that

$$\sin \beta = x \left(\sin \alpha + R \frac{dg}{dn} \cos \alpha\right). \quad (3.6)$$

The components of stress tensor of a reinforced membrane can be resolved into two parts

$$n^{\beta\rho} = n^{\beta\rho} + n^{\prime\prime\beta\rho} \quad (3.7)$$

where $n^{\beta\rho}$ is due to the tension in the cords and $n^{\prime\prime\beta\rho}$ is due to the deformation of the elastic materials and can be expressed in terms of the strain energy function W .

The $n^{\beta\rho}$ components were found by A.D. Kydoniefs /4/ and the $n^{\prime\prime\beta\rho}$ components for a Mooney-Rivlin membrane with strain energy function $W = C_1(I_1 - 3) + C_2(I_2 - 3)$ were found by M. Iliopoulou /5/.

The physical stress-resultants per unit length of the deformed membrane are

$$n_{(1)} = r^2 n^{11}, \quad n_{(2)} = n^{22}, \quad n_{(3)} = r n^{12}. \quad (3.8)$$

Using Eqs (3.3) and introducing the notation

$$z = \xi/R, \quad dg/dz = \omega(z), \quad (3.9)$$

the above non-dimensional stress-resultants take the form

$$\begin{aligned} n_1 &= \frac{\tau}{2C_1 \Delta} \left(\frac{1 - \ell^2 \cos^2 \alpha}{\ell x} \right) + \frac{x}{\ell} \left(1 + \omega^2 \ell^2 - \frac{1}{2x^4} \right) + \frac{\Gamma x}{\ell} \left(\ell^2 - \frac{1}{x^4} \right), \\ n_2 &= \frac{\tau \ell \cos^2 \alpha}{2C_1 \Delta x} + \frac{1}{\ell x} \left(\ell^2 - \frac{1}{\ell^2 x^2} \right) + \frac{\Gamma}{\ell x} \left(x^2 \ell^2 - \omega^2 - \frac{1}{\ell^2} \right), \\ n_3 &= \frac{\tau \cos \alpha \sqrt{1 - \ell^2 \cos^2 \alpha}}{2C_1 \Delta x} + \omega \ell \left(1 + \frac{\Gamma}{\ell^2 x^2} \right), \end{aligned} \quad (3.10)$$

where

$$n_1 = n_{(1)}/2C_1, \quad n_2 = n_{(2)}/2C_1, \quad n_3 = n_{(3)}/2C_1, \quad \Gamma = \frac{C_2}{C_1} \quad (3.11)$$

and Δ denotes the distances between adjacent cords in the underformed membrane. The first term of each of Eqs (3.10) are the components due to the tension in the cords, while the rest of them are due to the deformation of the elastic material.

The equations of equilibrium due to surface forces p , per unit deformed area normal to the deformed membrane are

$$\begin{aligned} n^{\beta\rho} \Big|_{\rho} &= 0, \\ b_{\beta\rho} n^{\beta\rho} + p &= 0. \end{aligned} \quad (3.12)$$

Using Eqs (2.5), (2.6), (3.3), (3.11) and the equation of Mainardi-Codazzi, introducing the non-dimensional notation

$$\lambda = pR/2C_1, \quad (3.13)$$

and taking into account the fact that $n^{\beta\rho}$ is independent of ϑ , equations (3.12)₁ for $\beta = 2$ and (3.12)₂ yield

$$\frac{d(xn_2)}{dx} = n_1, \quad (3.14)$$

$$\frac{n_1 \cos \sigma}{x} + n_2 \frac{d(\cos \sigma)}{dx} = \lambda \quad .$$

Here σ denotes the angle subtended by the tangent to the meridian of the deformed membrane and the axis of symmetry.

From Eqs (3.12)₁ for $\beta = 1$ by integration we derive

$$n_3 = \frac{D}{x^2} \quad (3.15)$$

where D is a non-dimensional integration constant.

The resultant torque that should be applied as an external load to balance the distribution of n_3 and the end sections is equal to (see Ref. /5/).

$$\frac{M}{2C_1} = 2\pi \Gamma^3(o) \frac{n^{12}(o)}{2C_1} = 2\pi R^2 x^2(o) n_3(o) \quad . \quad (3.16)$$

In this paper we will examine the problem in the absence of external torque. Thus, from (3.16) and (3.15) we find that

$$D = 0 \quad , \quad n_3(x) = 0 \quad . \quad (3.17)$$

Let us now consider the deformation under uniform internal pressure p . Then from Eqs (3.10)₃ we find

$$T = - \frac{\omega x \ell}{h^{1/2} \cos \alpha} \left(1 + \frac{\Gamma}{\ell^2 x^2} \right) \quad (3.18)$$

where

$$T = \frac{\tau}{2C_1 \Delta} \quad (3.19)$$

is the non-dimensional tension in the cords and

$$h^{1/2} = \sqrt{1 - \ell^2 \cos^2 \alpha} \quad . \quad (3.20)$$

From Eqs (3.4) using Eqs (3.3)₁, (3.9)₁ and (3.9)₂ we find

$$\ell^2 \cos^2 \alpha + x^2 (\sin \alpha + \omega \ell \cos \alpha)^2 = 1 \quad . \quad (3.21)$$

From the above equation and (3.20) we obtain

$$\omega = \frac{h^{1/2}}{x\ell\cos\alpha} - \frac{\tan\alpha}{\ell} \quad (3.22)$$

Substituting (3.18) and (3.22) into (3.10)₁ and (3.10)₂ we find

$$\begin{aligned} x n_2 = & \frac{x\ell\sin\alpha}{h^{1/2}} - \frac{1}{x^2\ell^3} + \Gamma(\ell x^2 - \frac{1}{x^2\ell^3\cos^2\alpha} - \frac{1}{\ell^3\cos^2\alpha} + \\ & + \frac{2\sin\alpha}{x\ell^3 h^{1/2}\cos^2\alpha} - \frac{\sin\alpha}{x\ell h^{1/2}}) \quad (3.23) \end{aligned}$$

$$\begin{aligned} n_1 = & -\frac{h^{1/2}\sin\alpha}{\ell\cos^2\alpha} + \frac{x}{\ell\cos^2\alpha} - \frac{1}{x^3\ell^3} + \Gamma(\frac{h^{1/2}\sin\alpha}{x^2\ell^3\cos^2\alpha} - \\ & - \frac{1}{x^3\ell^3\cos^2\alpha} + x\ell) \quad (3.24) \end{aligned}$$

Differentiating Eqs (3.23) and substituting this result together with n_1 from (3.24) into Eqs (3.14)₁ after some lengthy algebra we find

$$\begin{aligned} \left\{ \frac{x\sin\alpha}{h^{3/2}} + \frac{3}{x^2\ell^4} + \Gamma\left(\frac{3(x^2+1)}{x^2\ell^4\cos^2\alpha} + x^2 - \frac{2\ell^4\cos^4\alpha - 9\ell^2\cos^2\alpha + 6}{x\ell^4 h^{3/2}\cos^2\alpha}\right)\sin\alpha \right\} \frac{d\ell}{dx} = \\ - \frac{\sin\alpha}{\ell h^{1/2}\cos^2\alpha} - \frac{3}{x^3\ell^3} + \frac{x}{\ell\cos^2\alpha} + \Gamma\left(\frac{3-2\ell^2\cos^2\alpha}{x^2\ell^3 h^{1/2}\cos^2\alpha}\right)\sin\alpha - x\ell - \frac{3}{x^3\ell^3\cos^2\alpha} \quad (3.25) \end{aligned}$$

Thus, we have reduced the constitutive equations, together with the differential equations of equilibrium to a first order differential equation.

Let us now consider the following problem. A cylindrical membrane with initial length $2L_0$ and initial radius R sealed at both ends by rigid plugs of radius R , is subjected to an axisymmetric deformation with twist due to uniform internal pressure p . Since the deformed membrane is symmetric about the plane of $y_2 = 0$ we consider only the upper half of the membrane (Fig. 2).

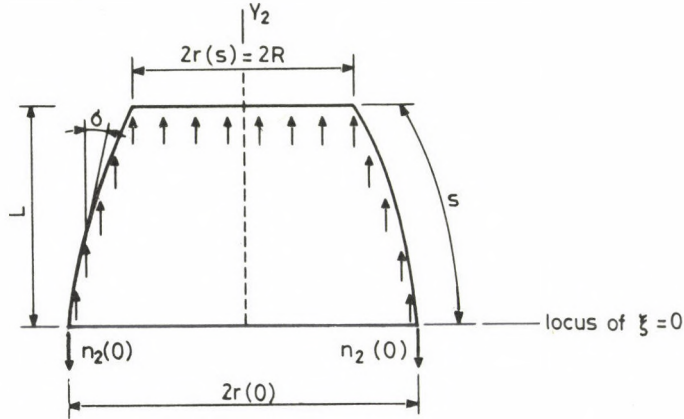


Fig. 2. Forces in y_2 -direction subjected to the upper half of the deformed membrane

From the conditions of equilibrium of the forces in y_2 -direction we obtain for $z = 0$ that

$$n_2(0) = \frac{\lambda x(0)}{2} . \quad (3.26)$$

The boundary conditions for this problem at $z = 0$ are

$$\sin \sigma (0) = 0 ,$$

$$n_2(0) = \frac{\lambda x(0)}{2} , \quad (3.27)$$

while at $z = s/R$ we have

$$x(s/R) = 1 . \quad (3.28)$$

From the two equations (3.14) we can derive

$$\frac{d(xn_2 \cos \sigma)}{dx} = \lambda x . \quad (3.29)$$

Integrating the above equation, for constant pressure λ , we find

$$\cos \sigma = \frac{\lambda x^2 + B}{2xn_2} \quad (3.30)$$

ELASTIC MEMBRANES REINFORCED BY CORDS

where B is an integration constant. Because for $z = 0$, $\sigma = 0$, taking into account (3.27)₂ we conclude that $B = 0$. Substituting n_2 from Eqs (3.23) in (3.30) we find

$$\cos \sigma = \frac{\lambda x}{2} / \left\{ \frac{\ell \sin \alpha}{h^{1/2}} - \frac{1}{x^3 \ell^3} + \Gamma \left(\ell x - \frac{1}{x^3 \ell^3 \cos^2 \alpha} - \frac{1}{x \ell \cos^2 \alpha} + \frac{2 \sin \alpha}{x^2 \ell^3 h^{1/2} \cos^2 \alpha} - \frac{\sin \alpha}{x^2 \ell h^{1/2}} \right) \right\}. \quad (3.31)$$

From this equation with the boundary conditions $z = 0$, $\cos \sigma = 1$, we can derive

$$\lambda = 2 \left(\frac{\ell(0) \sin \alpha}{x(0) h^{1/2}(0)} - \frac{1}{x^4(0) \ell^3(0)} + \Gamma \left(\ell(0) - \frac{1}{x^4(0) \ell^3(0) \cos^2 \alpha} + \frac{1}{x^2(0) \ell^3(0) \cos^2 \alpha} + \frac{2 \sin \alpha}{x^3(0) h^{1/2}(0) \ell^3(0) \cos^2 \alpha} - \frac{\sin \alpha}{x^3(0) \ell(0) h^{1/2}(0)} \right) \right). \quad (3.32)$$

From Fig. (3.1) and Eqs (3.3), (3.9) it follows that the non-dimensional underformed and deformed length of the membrane and the angular displacement due to twist are respectively

$$\frac{2L_0}{R} = -2 \int_{x(0)}^1 \frac{dx}{\ell \sin \sigma}, \quad (3.33)$$

$$\frac{2L}{R} = -2 \int_{x(0)}^1 \tan^{-1} \sigma dx, \quad (3.34)$$

$$g = - \int_{x(0)}^1 \frac{\omega dx}{\sin \sigma}. \quad (3.35)$$

Negative sign is chosen because x is a decreasing function of z .

4. NUMERICAL EXAMPLES

We solve the differential Eqs (3.25) with the associated boundary conditions (3.27) and (3.28) numerically. The heights of the underformed

and deformed membrane and the angular displacement g are given by Eqs (3.33), (3.34) and (3.35). The tension in the cords is given by Eqs (3.18) and the stress-resultants by Eqs (3.10).

We consider that the constant angle subtended by the cords with the generators of the underformed membrane is $\alpha = \pi/3$. The angle b that the cords make with the meridian of the deformed membrane using (3.5) and (3.6) is given by Eq. (3.20) as

$$\sin b = h^{1/2} = \sqrt{1 - \lambda^2 \cos^2 \alpha} . \quad (4.1)$$

From the above equation it is obvious that the value of λ should not exceed 2 for the given angle $\alpha = \pi/3$, because in that case the cords would become parallel to the axis of rotation.

The following data were considered in our computer program:

- (i) $\Gamma = 0.2$, $\alpha = \pi/3$, $\lambda = 2.0, 2.2, 2.4, 2.6, 2.8, 3.0$.

The results for these data are shown in Figs 3 and 4.

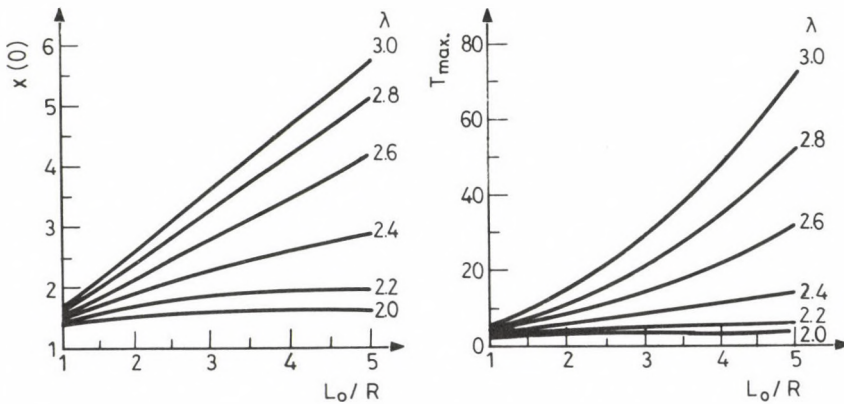


Fig. 3. Deformed radius, $x(0)$, at $z = 0$ vs. underformed height of the membrane, L_0/R , for $\Gamma = 0.2$ and $\alpha = \pi/3$

Fig. 4. Maximum tension in the cords vs. underformed height of the membrane, L_0/R , for $\Gamma = 0.2$ and $\alpha = \pi/3$

ELASTIC MEMBRANES REINFORCED BY CORDS

Figure 3 has been produced from Fig. 11 by reassigning the two axis (λ , $x(0)$) and using the underformed height as a parameter. The maximum tension in the cords develops at $z = 0$.

(ii) $\Gamma = 0.2$, $\alpha = \pi/3$, $L_0/R = 3$, $\lambda = 2.6$.

The results of these data are shown in Figs 5., 6., 7., 8. and 9.

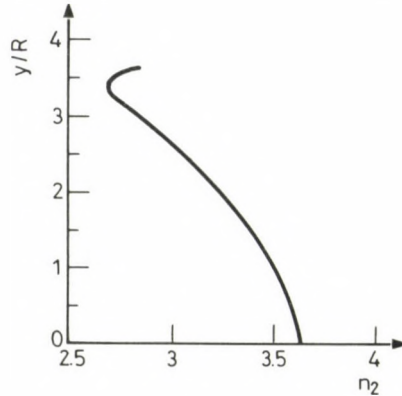
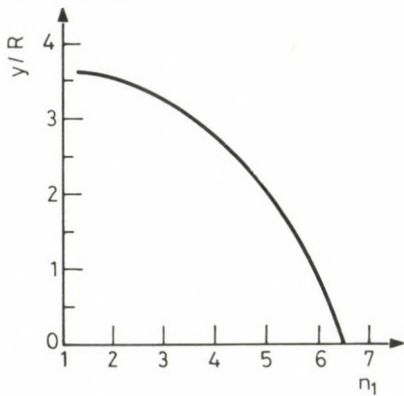


Fig. 5. Distance from the surface $z = 0$, Y/R , vs. stress resultant n_1 for $\Gamma = 0.2$, $\alpha = \pi/3$, $L_0/R = 3$ and $\lambda = 2.6$

Fig. 6. Distance from the surface $z = 0$, Y/R , vs. stress resultant n_2 for $\Gamma = 0.2$, $\alpha = \pi/3$, $L_0/R = 3$ and $\lambda = 2.6$

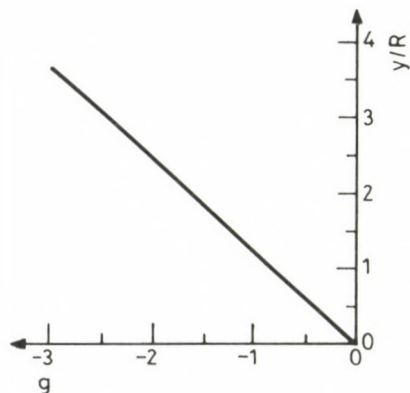
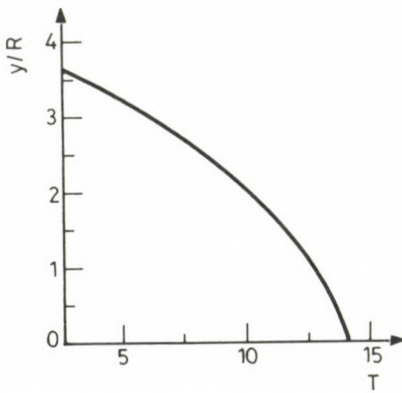


Fig. 7. Distance from the surface $z = 0$, Y/R , vs. tension in the cords, T , for $\Gamma = 0.2$, $\alpha = \pi/3$, $L_0/R = 3$ and $\lambda = 2.6$

Fig. 8. Distance from surface $z = 0$, Y/R , vs. angular displacement, g , for $\Gamma = 0.2$, $\alpha = \pi/3$, $L_0/R = 3$ and $\lambda = 2.6$

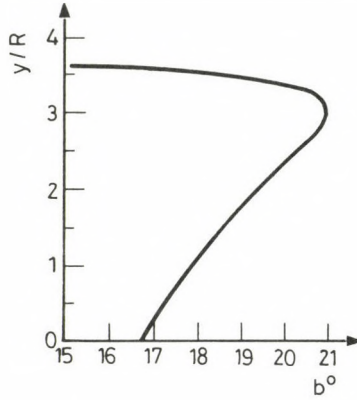


Fig. 9. Distance from surface $z = 0$, Y/R , vs. the angle subtended by the cords with the meridian of the deformed membrane expressed in degrees, b^0 , for $\Gamma = 0.2$, $\alpha = \pi/3$, $L_0/R = 3$ and $\lambda = 2.6$

(iii) $\Gamma = 0.2$, $\alpha = \pi/3$, $L_0/R = 3$, $x(0) = 1.5, 2, 3, 5$.

The results of these data are shown in Fig 10.

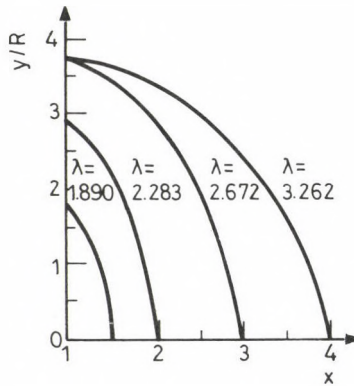


Fig. 10. Upper right quarter of the deformed meridians for $\Gamma = 0.2$, $\alpha = \pi/3$
 $L_0/R = 3$

The solution of the problem is subjected to the following constraints:

- (1) The stress-resultants n_1 , n_2 and the tension T in the cords must be positive.

ELASTIC MEMBRANES REINFORCED BY CORDS

- (2) The value of $h = 1 - \lambda^2 \cos^2 \alpha$ must be positive in order to yield real values of the quantities considered here. This constraint limits the extent of the curves shown in Fig. 11.

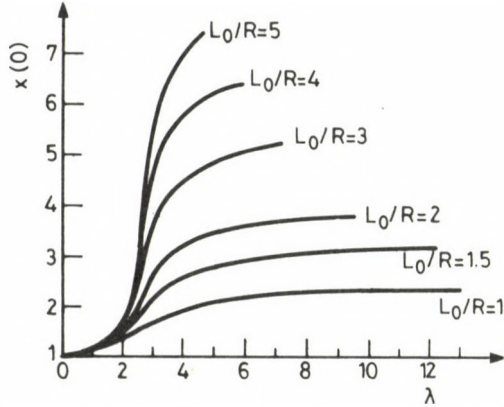


Fig. 11. Deformed radius, $x(0)$, at $z = 0$, vs. pressure, λ , for $L_0/R = 1, 1.5, 2, 3, 4, 5$

For instance, for the value of the underformed length $L_0/R = 2$, the pressure factor λ cannot exceed 9.652 and for $L_0/R = 4$ it cannot exceed 5.868. At these limiting values of the pressure factor λ , the value of λ tends to 2 and from Eqs (4.1) the value of the angle b that the cords subtend with the meridian of the deformed membrane, is almost zero.

REFERENCES

1. J.E. Adkins and R.S. Rivlin: Phil. Trans. Royal Soc. A 248, (1955), 201.
2. J.E. Adkins: Phil. Trans. Royal. Soc. A 249 (1956), 125.
3. A.E. Green and J.E. Adkins: Large Elastic Deformation. Claredon Press (1954).
4. A.D. Kydonieffs: Lett. in Appl. Eng. Sci. 5, (1977), 63.
5. M. Matsikoudi-Iliopoulou and G. Lianis: Acta Mechanica 42, (1982), 153.

ANALYSIS OF A CLOSED CIRCUIT CRYOGENIC WIND-TUNNEL

B. Paláncz*

(Received 24 May 1985)

An analysis focusing on heat and mass transfer processes of the steady-state and transient performance of a closed circuit cryogenic wind-tunnel, in which the recycled tunnel gas is cooled down by liquid nitrogen injection, is presented. A simplified mathematical model is developed in order to determine the relation between LN_2 injection rate and the distribution of gas temperature as well as LN_2 concentration along the tunnel circuit. Optimal steady-state characterized by the tunnel wall temperature, at which the total cost of the process is minimum can be defined. Stability condition developed from linear dynamical analysis indicates the possibility of instability caused by recycling flow. The findings of this analysis can be applied to other types of cryogenic closed cooling circuits, too.

SYMBOLS

a	cost coefficient ($\$ kg^{-1}s$)
A_c	cross-sectional area (m^2)
A_e	evaporation surface of droplets (m^2)
b	cost coefficient ($\$$)
c	LN_2 concentration ($kg m^{-3}$)
c_p	specific heat capacity of GN_2 at constant pressure ($kJ kg^{-1}K^{-1}$)
d	droplet diameter (m)
d_0	initial droplet diameter at $x = 0$ (m)
dA_e	surface of droplets in a control volume $A_c dx$ (m^2)
dn	number of droplets in the control volume $A_c dx$
D	diameter of the tunnel (m)
K	dissipation coefficient (dimensionless)
K_t	total cost ($\$$)
L	liquid flow rate ($kg s^{-1}$)
L_0	injection rate ($kg s^{-1}$)
L_c	length of the tunnel circuit (m)
N	droplet evaporation rate ($kg m^{-2}s^{-1}$)

*B. Paláncz, H-1085 Budapest, Salétrom u. 9., Hungary

PALÁNCZ, B.

\dot{n}	inlet rate of droplets for a unit of time (number s^{-1})
Q	dissipation heat (W)
r_e	evaporation heat of LN_2 ($kJ\ kg^{-1}$)
s	variable of the Laplace-transformation
t	time (s)
t_c	circuit time of the recycling flow in the tunnel circuit (s)
T	temperature (K)
T_e	saturation temperature of N_2 at the operation pressure (K)
T_{wo}	optimal wall temperature
\dot{V}	volumetric flow rate of gas phase ($m^3\ s^{-1}$)
w	linear gas velocity ($m\ s^{-1}$)
x	length coordinate (m)
Y	solution vector of system (48-49)

Greek Letters

α_c	heat transfer coefficient between liquid and gas phases ($W\ m^{-2}\ K^{-1}$)
α_w	heat transfer coefficient between gas phase and tunnel wall ($W\ m^{-2}\ K^{-1}$)
δ	thickness (m) or Dirac-delta
η, ξ	dimensionless length variables
λ	heat conduction coefficient of gas phase ($W\ m^{-1}\ K^{-1}$)
μ	dynamic viscosity of gas phase ($kg\ m^{-1}\ s^{-1}$)
ν	kinematic viscosity ($m^2\ s^{-1}$)
Ω	resolvent matrix
ρ	density ($kg\ m^{-3}$)

Indices

a	ambient
i	insulation
L	liquid phase
G	gas phase
w	wall

CLOSED CIRCUIT CRYOGENIC WIND-TUNNEL

INTRODUCTION

In the last years a worldwide effort of developing high Reynolds number facilities using closed circuit cryogenic wind tunnels can be noted. This concept proved to be the most promising amongst many techniques /1/.

Operational experiences with these facilities have shown, that cryogenic operation of their tunnel gases is a practical method for obtaining high Reynolds number flows without any dynamical pressure penalty and with savings in fan power.

A cryogenic wind tunnel is an endless pressure duct of varying cross sectional area, which has in addition to the regular components of a closed circuit tunnel, a liquid nitrogen injection section and a gas bleed section. In order to get the necessary low temperature in the tunnel, LN_2 is injected into the tunnel circuit. The evaporating LN_2 compensates the fan power as well as the heat flow through the insulated wall of the tunnel. This insulation of the cold test gas from the ambient presents heat gains and associated energy waste, and improves the controllability of the process. To maintain the tunnel resident gas – to keep the static pressure constant in the tunnel – it is necessary to remove gaseous nitrogen (GN_2) from the circuit. A typical cryogenic closed circuit wind tunnel can be seen in Fig. 1. LN_2 is injected through the nozzles located downstream of the fan. This arrangement utilizes the high turbulence of the flow existing behind the fan and ensures a long distance for LN_2 droplet evaporation before the test section, where one phase flow and uniform velocity, temperature and static pressure profiles are expected.

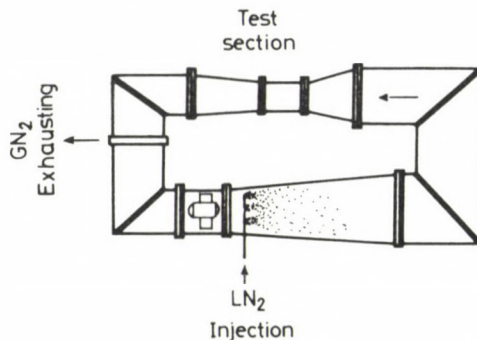


Fig. 1. Simplified sketch of a cryogenic closed circuit wind-tunnel

Over the past years, some very comprehensive models describing cryogenic wind tunnel performance have been developed for design and control purposes /2-4/. These models employed for process simulation embody complicating features and specialities, and consequently they suffer from elephantiasis. Their direct numerical realization is especially cumbersome because of the frequently arising instability in the solution of the model equations. Sometimes, it is difficult to find out whether these instabilities are caused by an unstable integration schema or the model equations themselves represent an unstable process.

Therefore, in real applications these models have to be considerably simplified; lumping /2/, linearization /4,5,14/, or other so-called "ad hoc" models based on the observations of physical and numerical experiments are used /6/.

In this paper the investigation focuses on the heat and mass transfer processes taking place in a closed circuit tunnel and many special features are neglected in order to get general information about the steady-state and transient performances. Corrections may result from adding to the problem such factors as variations in velocity, heat capacities, heat transfer coefficients, pressure drop, and radial and longitudinal mixing can be marginal.

MODELLING

The physical hypotheses employed to formulate the mathematical model are the following:

- there is no slip between the liquid droplets and the gas flow, liquid and gas phases have the same velocity;
- the temperature of the droplets is constant during their lifetime, and equal to the saturation temperature belonging to the circuit pressure;
- the droplets are supposed to have spherical form and their diameters are the same in a cross-section of the tunnel;
- the number of droplets is constant and they evaporate with the same rate in a cross-section;
- the droplet evaporation is completed during one turn-round of the gas flow, namely the droplet evaporation length is always smaller than the

length of the tunnel;

– volumetrical gas flow rate is considered to be constant along the length of the tunnel circuit, droplet evaporation does not cause significant change in gas mass or volume;

– the effect of the temperature change on gas properties, as density, specific heat, evaporation heat etc., is neglected;

– pressure drop is neglected, pressure is supposed to be constant and the same everywhere in the circuit;

– the cross section area of the tunnel does not vary;

– the wall temperature is constant and the same everywhere along the length of the tunnel;

– the heat transfer coefficient between gas and liquid phase is constant, it does not change with the droplet Reynolds number;

– the heat transfer coefficient between gas phase and tunnel wall is constant;

– in radial direction the flow is perfectly mixed, while in longitudinal direction there is no mixing at all.

Considering these assumptions the model equations can be developed on the basis of the mass and heat balances.

The mass balance for liquid phase results

$$A_c dx \frac{\partial c}{\partial t} = - \dot{V} \frac{\partial c}{\partial x} dx - N dA_e . \quad (1)$$

Heat transport from gas phase to the droplets provides heat for LN₂ evaporation at saturation temperature and for the warm-up to the bulk temperature of the gas flow, namely

$$\alpha_c (T - T_e) = N \left[r_e + c_{pG} (T - T_e) \right], \quad (2)$$

therefore the evaporation rate can be expressed as

$$N = \frac{\alpha_c (T - T_e)}{r_e + c_{pG} (T - T_e)} . \quad (3)$$

The injection rate of LN₂ can be expressed by the number of droplets entering into the tunnel through the nozzles during a time unit:

$$L_0 = \dot{n} \rho L \frac{d_0^3 \pi}{6} . \quad (4)$$

The LN_2 flow rate decreases in the direction of the flow because of the evaporation of the droplets. At a given cross-section this flow rate can be calculated as a function of the diameter of the droplets

$$L = \dot{V} c = \rho_L \dot{n} \frac{d^3 \pi}{6} . \quad (5)$$

Eliminating \dot{n} from Eqs (4) and (5), one may get for the diameter of the droplet at an arbitrarily chosen x coordinate of length

$$d = \left(\frac{\dot{V}}{L_0}\right)^{1/3} c^{1/3} d_0 , \quad (6)$$

where d_0 is the droplet diameter at $x = 0$, in the injection section. On the other hand, the liquid mass in a control volume $A_C dx$ is

$$c A_C dx = \frac{d^3 \pi}{6} \rho_L dn , \quad (7)$$

where dn is the number of droplets in the elementary control volume $A_C dx$.

The surface of the droplets in this volume can be expressed as

$$dA_e = d^2 \pi dn = \frac{6A_C}{\rho_L} \frac{c}{d} dx . \quad (8)$$

Employing Eq.(6), we obtain

$$dA_e = \frac{6A_C}{\rho_L d_0} \left(\frac{L_0}{\dot{V}}\right)^{1/3} c^{2/3} dx . \quad (9)$$

Now, the mass balance can be written in the following form

$$\frac{\partial c}{\partial t} + \frac{\dot{V}}{A_C} \frac{\partial c}{\partial x} + \frac{\alpha c (T - T_e)}{r_e + c_{pG} (T - T_e)} \frac{6}{d_0 \rho_L} \left(\frac{L_0}{\dot{V}}\right)^{1/3} c^{2/3} = 0 . \quad (10)$$

Let us introduce the following independent variables

$$\theta = \frac{t}{t_c} \quad \text{and} \quad \eta = \frac{x}{L_C} , \quad (11)$$

where t_c is the period time of the circuit flow

$$t_c = \frac{L_C}{w} \quad \text{and} \quad w = \frac{\dot{V}}{A_C} , \quad (12)$$

then the balance equation is

$$\frac{\partial c}{\partial \theta} + \frac{\partial c}{\partial \eta} + \frac{\alpha_c (T - T_e)}{r_e + c_{pG} (T - T_e)} \frac{6A_c L_c}{\rho_L d_o V^{4/3}} L_o^{1/3} c^{2/3} = 0 . \quad (13)$$

From a computational point of view, it is preferable to use the flow rate L , as independent variable instead of the liquid concentration c .

Considering, that

$$L = \dot{V} c , \quad (14)$$

the final form of the mass balance is

$$\frac{\partial L}{\partial \theta} + \frac{\partial L}{\partial \eta} + F(T, L) = 0 , \quad (15)$$

where

$$F(T, L) = \frac{\alpha_c (T - T_e)}{r_e + c_{pG} (T - T_e)} \frac{6t_c}{\rho_L d_o} L_o^{1/3} L^{2/3} . \quad (16)$$

The heat balance for the tunnel gas is

$$\begin{aligned} A_c dx \rho_G c_{pG} \frac{\partial T}{\partial t} = - \dot{V} \rho_G c_{pG} \frac{\partial T}{\partial x} dx + \alpha_w (T_w - T) D \pi dx - \\ - \alpha_c (T - T_e) dA_e + \frac{Q}{L_c} dx . \end{aligned} \quad (17)$$

Considering the expression of dA_e , eqs (9) and (14), we obtain

$$\begin{aligned} \frac{\partial T}{\partial t} + \frac{\dot{V}}{A_c} \frac{\partial T}{\partial x} + \frac{\alpha_c (T - T_e)}{\rho_G c_{pG}} \frac{6}{\rho_L d_o V} L_o^{1/3} L^{2/3} - \\ - \frac{\alpha_w D \pi}{\rho_G c_{pG} A_c} (T_w - T) - \frac{Q}{L_c A_c \rho_G c_{pG}} = 0 . \end{aligned} \quad (18)$$

Applying dimensionless variables

$$\frac{\partial T}{\partial \theta} + \frac{\partial T}{\partial \eta} + \frac{\alpha_c (T - T_e)}{\dot{V} \rho_G c_{pG}} \frac{6A_c L_c}{\rho_L d_o \dot{V}} L_o^{1/3} L^{2/3} -$$

$$- \frac{\alpha_w D \pi L_c}{\dot{V} \rho_G c_{pG}} (T_w - T) - \frac{Q}{\dot{V} \rho_G c_{pG}} = 0, \quad (19)$$

or

$$\frac{\partial T}{\partial \theta} + \frac{\partial T}{\partial \eta} + G(T, L) = 0, \quad (20)$$

where

$$G(T, L) = \frac{[r_e + c_{pG}(T - T_e)] F(T, L) - \alpha_w D \pi L_c (T_w - T) - Q}{\dot{V} \rho_G c_{pG}}. \quad (21)$$

The boundary conditions are

$$L(0, \theta) = L_o(\theta), \quad (22)$$

$$T(0, \theta) = T(1, \theta). \quad (23)$$

The heat transfer coefficients can be computed from the following formulas

- heat transfer between tunnel wall and gas flow /7/

$$Nu_w = 0.023 Re^{0.8} Pr^{0.4}, \quad (24)$$

where

$$Nu_w = \frac{\alpha_w D}{\lambda_G}, \quad Re = \frac{w D}{\nu_G}, \quad Pr = \frac{c_{pG} \mu_G}{\lambda_G}, \quad (25)$$

if $L_c < 50 D$, then

$$\alpha_w = \alpha_w \left[1 + \left(\frac{D}{L_c} \right)^{0.7} \right], \quad (26)$$

otherwise

$$\alpha_w = \alpha_w \quad (27)$$

CLOSED CIRCUIT CRYOGENIC WIND-TUNNEL

— heat transfer coefficient between gas phase and droplets /8/

$$Nu_d = 2 , \quad (28)$$

where

$$Nu_d = \frac{\alpha_c d_o}{2 \frac{\lambda}{g}} . \quad (29)$$

The dissipation heat of the fan power can be expressed in the following form

$$Q = K \rho_G W^3 A_C . \quad (30)$$

STEADY-STATE ANALYSIS

In this case the model can be reduced to the following ordinary differential equation system

$$\frac{dL}{d\eta} + F(T,L) = 0 , \quad (31)$$

$$\frac{dT}{d\eta} + G(T,L) = 0 . \quad (32)$$

The boundary conditions are

$$L(0) = L_0 , \quad (33)$$

$$T(0) = T(1) . \quad (34)$$

Concerning these conditions, there are two possibilities:

■ L_0 is prespecified, then $T(0)$ and therefore $T(1)$ is determined by the model equations,

■ $T(0)$ is given and L_0 is determined by the model.

One has to have in mind, that under normal operation conditions, the evaporation length is short, $\eta_{ev} \ll 1$, therefore the numerical inte-

gration of the coupled equations, (31), (32) must be carried out only up to $\eta = \eta_{ev}$, where η_{ev} can be calculated from $L(\eta_{ev}) = 0$, and in practice $L < 10^{-5} L_0$ is a suitable condition. Thus the $L = 0$ condition applies for $\eta \geq \eta_{ev}$, and the heat balance can be simplified

$$\dot{V} \rho_G c_{pG} \frac{dT}{d\eta} + \alpha_w D \pi L_C T = \alpha_w D \pi L_C T_w + Q, \quad (35)$$

which has the solution

$$T(\eta) = T(\eta_{ev}) - T_w^{\square} \exp[-(\eta - \eta_{ev})] + T_w^{\square} \quad (36)$$

for $\eta_{ev} \leq \eta \leq 1$

and where

$$T_w^{\square} = T_w + \frac{Q}{\alpha_w D \pi L_C} \quad (37)$$

Computations were carried out for three prespecified operational temperature, temperature in the injection cross-section, $T_0 = T(0) = 100, 150$ and 200 K at different wall temperatures. Data used for the calculations are shown in Table 1.

Table 1. Data used for steady-state analysis

T_0 (K)	c_{pG} (kJ/kg,K)	ρ_G (kg/m ³)	α_c (W/m ² ,K)	α_w (W/m ² ,K)	$T_w - T_0$ (K)
100	1.060	3.48	184.7	71.5	5
150	1.047	2.30	273.7	55.4	10
200	1.035	1.71	358.6	46.5	15

$T_e = 77$ K, $r_e = 193$ kJ/kg, $D = 3$. m, $L_C = 100$. m
 $V = 50$ m³/s, $d_0 = 10^{-4}$ m, $\rho_L = 809$ kg/m³, $K = 0$.

The numerical procedure was the following:

(a) guess $L_0 = L(0)$,

(b) integrate the system, Eqs (31), (32) with the initial conditions

L_0 and T_0 up to $\eta = \eta_{ev}$, using Runge-Kutta-Merson method with step size control,

CLOSED CIRCUIT CRYOGENIC WIND-TUNNEL

- (c) employing eq. (36) compute $T(1)$,
- (d) check the difference between T_0 and $T(1)$,
- (e) if the difference is not small enough, start again with a modified L_0 value.

For a numerical integration the use of a scheme with a changing step-size is advised because of the rapid change of $L(\eta)$.

Figures 2 and 3 show the gas temperature and liquid flow rate distributions along the length of the tunnel at two different operational temperatures, $T_0 = 100$ and 200 K, in case of different tunnel wall temperatures. These figures indicate that at lower operational temperature, the necessary injection rate is higher, the evaporation length is longer, the maximal temperature difference in gas phase is smaller at the same $T_w - T_0$ value. The increase of the value of $T_w - T_0$ has the same effect as the increase of the operational temperature T_0 , except that the droplet evaporation length does not change significantly. This fact is demonstrated clearly in Fig. 4.

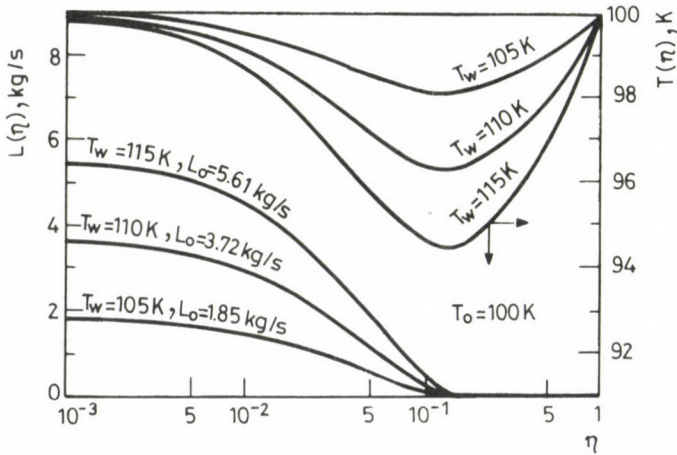


Fig. 2. Gas temperature and liquid flow rate distributions along the tunnel length at $T_0 = 100$ K operation temperature in case of different wall temperatures

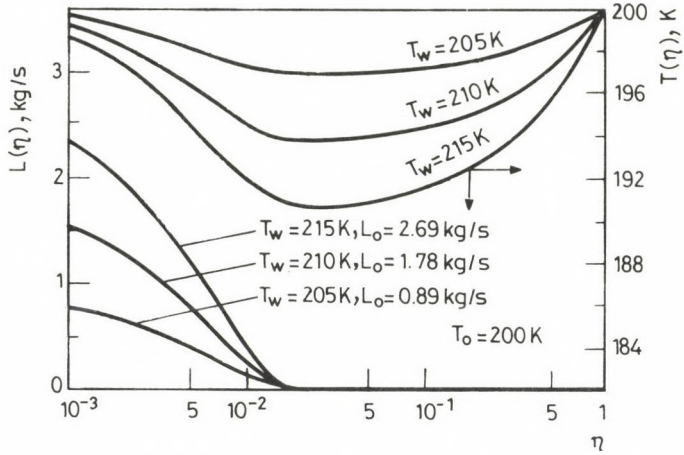


Fig. 3. Gas temperature and liquid flow rate distributions along the tunnel length at $T_0 = 200\text{ K}$ operation temperature in case of different wall temperatures

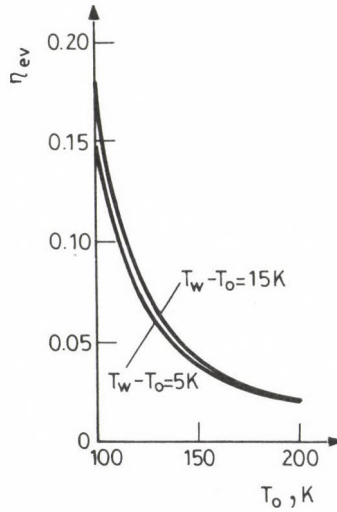


Fig. 4. Liquid droplets evaporation length as function of the operation temperature at different values of $T_w - T_0$

OPTIMAL WALL TEMPERATURE

The LN_2 injection rate and therefore the operation cost increases with increasing $T_w - T_o$, while the thickness of the insulation layer and thus the investment cost decreases. Assuming that the heat conduction coefficient of the insulation is constant and the ratio of the insulation thickness and the tunnel diameter small, the following heat balance can be written for the tunnel wall

$$\alpha_w D \pi \int_0^{L_c} (T_w - T(x)) dx = \frac{\lambda_i}{\delta_i} (T_a - T_w) D \pi L_c . \quad (38)$$

Here, it is also supposed, that the outside surface of the insulation is nearly at the ambient temperature, T_a . Eq. (38) can be written in dimensionless form:

$$Nu_i \int_0^1 (T_w - T(\eta)) d\eta = T_a - T_w , \quad (39)$$

or

$$Nu_i(T_w) = \frac{T_a - T_w}{T_w - \int_0^1 T(\eta) d\eta} , \quad (40)$$

where

$$Nu_i = \frac{\alpha_w \delta_i}{\lambda_i} . \quad (41)$$

In Fig. 5. we can see L_o versus T_w , and Nu_i versus T_w functions in case of $T_o = 100$ K operational temperature and at $T_a = 300$ K ambient temperature. Considering, that the total cost of the process is

$$K_t(T_w) = aL_o(T_w) + bNu_i(T_w) , \quad (42)$$

one may find an optimal wall temperature, at which K_t has its minimum.

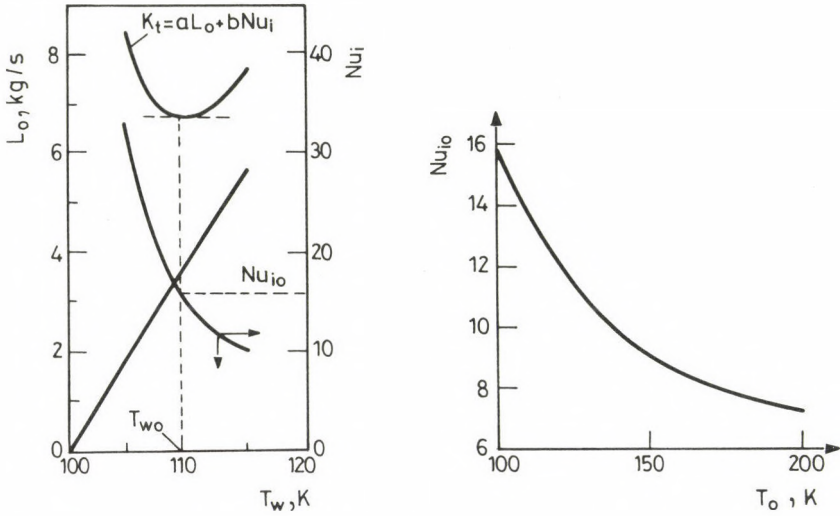


Fig. 5. Determination of the optimal wall temperature, T_{w0} and the optimal Nusselt number of the tunnel insulation, Nu_{i0}

Fig. 6. Optimal Nusselt number of the tunnel insulation versus operation temperature

Figure 6 shows how the optimal insulation Nusselt-number, Nu_{i0} depends on the operation temperature in case of $b/a = 0.2$ kg/s. This figure reveals the fact, that under $T_0 = 150$ K the cost of the process increases rapidly with decreasing T_0 . On the other hand, considerable Reynolds-number increase can be expected in this low temperature range only. The process, however is still cheaper than a conventional wind-tunnel yielding a similar Reynolds-number /13/.

TRANSIENT ANALYSIS

Sufficient tunnel operation can be carried out only under temperature control in the test section located far enough from the injection section to get uniform, one phase flow. Consequently, there is a significant time delay between LN_2 injection and its effect on the temperature in the test section depending on the gas velocity and the evaporation process. The other difficulty arises from the gas flow recycling because of the closed

CLOSED CIRCUIT CRYOGENIC WIND-TUNNEL

tunnel circuit. The recycled gas may cause positive feedback in the temperature, therefore initiate instability.

As a first approach, linear stability condition can be given by linearization of the balance equations and solving them analytically.

Let us introduce a new state variable

$$L' = L^{1/3} . \quad (43)$$

Then the balance equations have the form

$$\frac{\partial L'}{\partial \theta} + \frac{\partial L'}{\partial \eta} + F'(T, L_0) = 0 , \quad (44)$$

and

$$\frac{\partial T}{\partial \theta} + \frac{\partial T}{\partial \eta} + G'(T, L', L_0) = 0 , \quad (45)$$

where

$$F'(T, L_0) = \frac{\alpha_c (T - T_e)}{r_e + c_{pG} (T - T_e)} \frac{2A_c L_c}{\rho_L d_0 V} L_0^{1/3} , \quad (46)$$

$$G'(T, L', L_0) = \left\{ 3 \left[r_e + c_{pG} (T - T_e) \right] F' (L')^2 - \alpha_w D \pi L_c (T_w - T) - Q \right\} / \dot{V} c_{pG} \rho_G . \quad (47)$$

The linearized form of Eqs (44) and (45) around a steady-state solution is

$$\frac{\partial \tilde{L}}{\partial \theta} + \frac{\partial \tilde{L}}{\partial \eta} + F'_T \tilde{T} + F'_{L_0} \tilde{L}_0 = 0 , \quad (48)$$

$$\frac{\partial \tilde{T}}{\partial \theta} + \frac{\partial \tilde{T}}{\partial \eta} + G'_L \tilde{L} + G'_T \tilde{T} + G'_{L_0} \tilde{L}_0 = 0 , \quad (49)$$

where \tilde{L} and \tilde{T} stand for the deviation from the steady-state profile and the partial derivatives are evaluated along these steady-state solutions. That is why they depend on η , too.

Applying Laplace-transformation, we obtain

$$\frac{d}{d\eta} \begin{bmatrix} \hat{L}(s, \eta) \\ \hat{T}(s, \eta) \end{bmatrix} = - \begin{bmatrix} s & F'_T(\eta) \\ G'_L(\eta) & G'_T(\eta) + s \end{bmatrix} \begin{bmatrix} \hat{L}(s, \eta) \\ \hat{T}(s, \eta) \end{bmatrix} - \begin{bmatrix} F'_{L_0}(\eta) \\ G'_{L_0}(\eta) \end{bmatrix} \hat{L}_0(s). \quad (50)$$

The solution of the system is:

$$\begin{bmatrix} \hat{L}(s, \eta) \\ \hat{T}(s, \eta) \end{bmatrix} = \Omega \begin{bmatrix} \eta \\ 0 \end{bmatrix} \left\{ \begin{bmatrix} \hat{L}(s, 0) \\ \hat{T}(s, 0) \end{bmatrix} - \int_0^\eta (\Omega \begin{bmatrix} \xi \\ 0 \end{bmatrix})^{-1} \begin{bmatrix} F'_{L_0}(\xi) \\ G'_{L_0}(\xi) \end{bmatrix} \hat{L}_0(s) d\xi \right\} \quad (51)$$

which can be written in the form

$$Y(s, \eta) = \exp \left[- (M(\eta) + \eta sI) \right] Y(s, 0) - d(s, \eta) \hat{L}_0(s), \quad (52)$$

where

$$M(\eta) = \begin{bmatrix} 0 & \int_0^\eta F'_T(\xi) d\xi \\ \int_0^\eta G'_L(\xi) d\xi & \int_0^\eta G'_T(\xi) d\xi \end{bmatrix} \text{ and } I = \begin{bmatrix} 1 & 0 \\ 0 & 1 \end{bmatrix}. \quad (53)$$

Let us express

$$\exp \left[- M(\eta) \right] = \begin{bmatrix} \alpha_{11}(\eta) & \alpha_{12}(\eta) \\ \alpha_{21}(\eta) & \alpha_{22}(\eta) \end{bmatrix}. \quad (54)$$

Considering that

$$\exp \left[-s \eta I \right] = e^{-s\eta} I, \quad (55)$$

the resolvent matrix can be expressed as

$$\Omega \begin{pmatrix} \eta \\ 0 \end{pmatrix} = \exp \left[-M(\eta) + (\eta s I) \right] = e^{-s\eta} \begin{bmatrix} \alpha_{11}(\eta) & \alpha_{12}(\eta) \\ \alpha_{21}(\eta) & \alpha_{22}(\eta) \end{bmatrix} \quad (56)$$

where α_{ij} can be directly evaluated from the elements of $M(\eta)$.

Namely /10/

$$\exp \left[-M(\eta) \right] = e^{C_4/2} \frac{\text{sh} \Delta}{\Delta} \begin{bmatrix} \frac{\Delta}{\text{th} \Delta} - \frac{C_4}{2} & C_2 \\ C_3 & \frac{\Delta}{\text{th} \Delta} + \frac{C_4}{2} \end{bmatrix} \quad (57)$$

where

$$\Delta = \frac{1}{2} (C_4^2 + 4C_2C_3)^{1/2}, \quad C_2 = - \int_0^\eta F'_T(\xi) d\xi, \\ C_3 = - \int_0^\eta G'_L(\xi) d\xi, \quad C_4 = - \int_0^\eta G'_T(\xi) d\xi. \quad (58)$$

To find vector $d(s, \eta)$, let us express the inverse of the resolvent matrix as

$$\left(\Omega \begin{pmatrix} \xi \\ 0 \end{pmatrix} \right)^{-1} = e^{s\xi} \begin{bmatrix} \alpha_{11}(\xi) & \alpha_{12}(\xi) \\ \alpha_{21}(\xi) & \alpha_{22}(\xi) \end{bmatrix}^{-1} = e^{s\xi} \begin{bmatrix} \beta_{11}(\xi) & \beta_{12}(\xi) \\ \beta_{21}(\xi) & \beta_{22}(\xi) \end{bmatrix} \quad (59)$$

then

$$\int_0^\eta \left(\Omega \begin{pmatrix} \xi \\ 0 \end{pmatrix} \right)^{-1} \begin{bmatrix} F'_{L_0}(\xi) \\ G'_{L_0}(\xi) \end{bmatrix} d\xi = \begin{bmatrix} \int_0^\eta (\beta_{11}(\xi) F'_{L_0}(\xi) + \beta_{12}(\xi) G'_{L_0}(\xi)) e^{s\xi} d\xi \\ \int_0^\eta (\beta_{21}(\xi) F'_{L_0}(\xi) + \beta_{22}(\xi) G'_{L_0}(\xi)) e^{s\xi} d\xi \end{bmatrix} \quad (61)$$

Considering that, i.e.

$$\int_0^\eta \beta_{11}(\xi) F'_{L_0}(\xi) e^{s\xi} d\xi = \varepsilon_{11}(\eta) \left[1 + \sum_{m=1}^{\infty} s^m (\gamma_{11}(\eta))_m \right], \quad (61)$$

where

$$\varepsilon_{11}(\eta) = \int_0^\eta \beta_{11}(\xi) F_{L_0}'(\xi) d\xi \quad \text{and} \quad (\gamma_{11}(\eta))_m = \frac{\int_0^\eta \beta_{11}(\xi) F_{L_0}'(\xi) \xi^m d\xi}{m! \varepsilon_{11}(\eta)}, \quad (62)$$

the elements of vector d are

$$\begin{aligned} d_j(s, \eta) &= \sum_{i,k=1}^2 \alpha_{ji}(\eta) \varepsilon_{ik}(\eta) \left[1 + \sum_{m=1}^{\infty} s^m (\gamma_{ik}(\eta))_m \right] e^{-s\eta} = \\ &= d_j^*(s, \eta) e^{-s\eta}, \quad j = 1, 2 \end{aligned} \quad (63)$$

The solution for the temperature is

$$\hat{T}(s, \eta) = \alpha_{22}(\eta) \hat{T}(s, 0) e^{-s\eta} + \left[\alpha_{21}(\eta) + d_2^*(s, \eta) \right] \hat{T}_0(s) e^{-s\eta}. \quad (64)$$

The temperature in the injection section can be determined by the boundary condition

$$\hat{T}(s, 0) = \hat{T}(s, 1) = \hat{T}_0(s), \quad (65)$$

therefore

$$\hat{T}_0(s) = \frac{\alpha_{21}(1) + d_2^*(s, 1)}{1 - \alpha_{22}(1) e^{-s}} \hat{T}_0(s) e^{-s}. \quad (66)$$

Then the transfer function between temperature and LN_2 injection rate is

$$\begin{aligned} \mathcal{F}(s, \eta) &= \frac{\hat{T}(s, \eta)}{\hat{T}_0(s)} = \left[\alpha_{21}(\eta) + d_2^*(s, \eta) + \right. \\ &\quad \left. + \frac{\alpha_{21}(1) + d_2^*(s, 1)}{1 - \alpha_{22}(1) e^{-s}} \alpha_{22}(\eta) e^{-s} \right] e^{-s\eta} \end{aligned} \quad (67)$$

This transfer function can be calculated as a function of η numeri-

cally on the basis of the steady-state solution.

Keep in mind, that because

$$\lim_{\eta \rightarrow 0} \Omega \begin{vmatrix} \eta \\ 0 \end{vmatrix} = I \quad \text{and} \quad \lim_{\eta \rightarrow 0} \epsilon_{ik} = 0, \quad (68)$$

therefore

$$\lim_{\eta \rightarrow 0} \alpha_{21}(\eta) = 0; \quad \lim_{\eta \rightarrow 0} d_2^*(s, \eta) = 0$$

and

$$\lim_{\eta \rightarrow 0} \alpha_{22}(\eta) = 1.$$

(69)

In Eq. (67) the first term represents the direct effect of the liquid flow rate change and arises from the homogeneous solution. The second term arises from the inhomogeneous solution, and shows the effect of the injection rate change, involving cross-effects between temperature and liquid flow rate. The third term stands for the effect of the gas flow recycling, and the multiplier $e^{-s\eta}$ represents the time-lag between injection rate and the change in the gas temperature at the location η .

To give stability condition for the linearized system, let us consider eq. (66), in case no disturbances in the injection rate occur. Then

$$\hat{T}_0(s) \left[1 - \alpha_{22}(1)e^{-s} \right] = 0 \quad (70)$$

which means that

$$\tilde{T}_0(\theta) = \alpha_{22}(1) \tilde{T}_0(\theta - 1), \quad (71)$$

or let us consider $\theta - 1$ the time point, when the n -th lap of the gas flow circulation has been completed, then

$$\tilde{T}_0^{n+1} = \alpha_{22}(1) \tilde{T}_0^n. \quad (72)$$

If $|\alpha_{22}(1)| < 1$, the disturbance in temperature at $\eta = 0$, \tilde{T}_0 , decreases after every turn-round and consequently the process is stable.

If $|\alpha_{22}(1)| > 1$ the process is unstable, because the deviation from the

steady-state increases after every turn-round.

In our numerical example the system proved to be stable in every considered steady-state according to this condition, $0.5 < \alpha_{22}(1) < 0.7$. For lower operational temperature $\alpha_{22}(1)$ is bigger than for higher temperatures. Therefore at higher temperatures the convergency of the temperature to the steady-state after a perturbation is faster, which agrees with the experience obtained from experiments i.e. that the increase of heat insulation improves the controllability of the process /3/. In order to analyse the relation given by Eq. (67), let us find the temperature response for step-function input in the injection rate. If we consider the linear approximation of the exponential term in Eq. (61), $m=1$, we obtain for $d_2^*(s, \eta)$

$$d_2^*(s, \eta) = a_{20}(\eta) + sa_{21}(\eta), \quad (73)$$

where

$$a_{20}(\eta) = \sum_{i,k=1}^2 \alpha_{2i}(\eta) \varepsilon_{ik}(\eta), \quad (74)$$

$$a_{21}(\eta) = \sum_{i,k=1}^2 \alpha_{2i}(\eta) \varepsilon_{ik}(\eta) (\gamma_{ik}(\eta))_1. \quad (75)$$

Then, the temperature response is

$$\hat{T}(s, \eta) = \left[\alpha_{21}(\eta) + a_{20}(\eta) + sa_{21}(\eta) + \frac{\alpha_{21}(1) + a_{20}(1) + sa_{21}(1)}{1 - \alpha_{22}(1)e^{-s}} \alpha_{22}(\eta)e^{-s} \right] \frac{L_i}{s} e^{-s\eta}, \quad (76)$$

where L_i is the change in $L_0(\theta)$ at $\theta = 0$. It is useful to consider $\hat{T}(s, \eta)$ as a sum of four terms

$$\hat{T}/s, \eta) = \sum_{m=1}^4 \hat{T}_m(s, \eta), \quad (77)$$

where

$$\hat{T}_1(s, \eta) = \left[\alpha_{21}(\eta) + a_{20}(\eta) \right] \frac{L_i}{s} e^{-s\eta}, \quad (78)$$

$$\hat{T}_2(s, \eta) = a_{21}(\eta) L_i e^{-s\eta}, \quad (79)$$

$$\hat{T}_3(s, \eta) = \frac{\alpha_{21}(1) + a_{20}(1)}{s(e^s - \alpha_{22}(1))} \alpha_{22}(\eta) L_i e^{-s\eta}, \quad (80)$$

$$\hat{T}_4(s, \eta) = \frac{a_{21}(1) \alpha_{22}(\eta)}{e^s - \alpha_{22}(1)} L_i e^{-s\eta}. \quad (81)$$

Transforming back into the time domain, we obtain

$$\tilde{T}_1(\theta, \eta) = [\alpha_{21}(\eta) + a_{20}(\eta)] L_i 1(\theta - \eta), \quad (82)$$

$$\tilde{T}_2(\theta, \eta) = a_{21}(\eta) L_i \delta(\theta - \eta), \quad (83)$$

$$\tilde{T}_3(\theta, \eta) = [\alpha_{21}(\eta) + a_{20}(\eta)] \alpha_{22}(\eta) L_i \phi(\theta - \eta) \quad (84)$$

where

$$\phi(\theta - \eta) = \begin{cases} 0 & \text{if } 0 < \theta - \eta < 1 \\ \sum_{k=0}^{n-1} \alpha_{22}^k(1) & \text{if } n < \theta - \eta < n+1, n=1,2,\dots \end{cases} \quad (85)$$

Employing linear approximation for the exponential term in Eq. (81), one may get

$$\tilde{T}_4(\theta, \eta) = a_{21}(1) \alpha_{22}(\eta) L_i \exp [-(1 - \alpha_{22}(1))(\theta - \eta)]. \quad (86)$$

It can be seen, that after a finite step change in the injection rate, $\tilde{T}_0(\theta) = L_i 1(\theta)$, the temperature profile converges to a new steady-state distribution

$$T_s^{\text{new}}(\eta) = \lim_{\theta \rightarrow \infty} T(\theta, \eta) = T_s^{\text{old}}(\eta) + \lim_{\theta \rightarrow \infty} \tilde{T}(\theta, \eta) =$$

$$= T_s^{old}(\eta) + (\alpha_{21}(\eta) + a_{20}(\eta)) \left(1 + \frac{\alpha_{22}(\eta)}{1 - \alpha_{22}(1)}\right) L_i \cdot \quad (87)$$

The condition for the convergency of the temperature profile is also $\alpha_{22}(1) < 1$. The qualitative form of the temperature response is shown in Fig. 7 for the case if $\eta = \text{const}$.

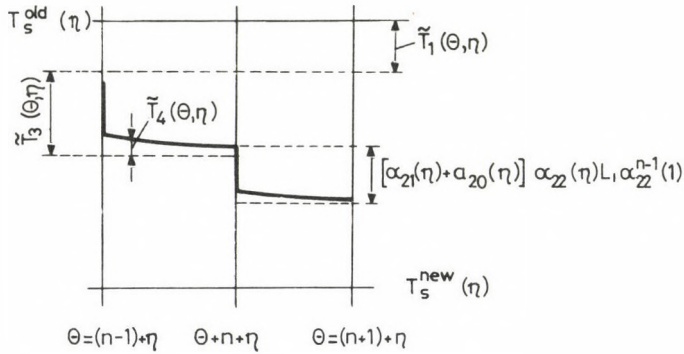


Fig. 7. Gas temperature response predicted by the linearized model in case of $L_i > 0$

NUMERICAL STUDY OF THE NON-LINEAR MODEL

The dynamical behavior of the non-linear system can be studied by numerical simulation. To solve the transient equations, eqs (15) and (20) the method of characteristics may be used (Fig. 8).

The characteristics are defined by

$$\frac{d\theta}{d\eta} = 1 \quad (88)$$

Along these characteristics the model equations are:

$$\left(\frac{dL}{d\eta}\right)_c = -F(T, L) \quad (89)$$

$$\left(\frac{dT}{d\eta}\right)_c = -G(T, L) \quad (90)$$

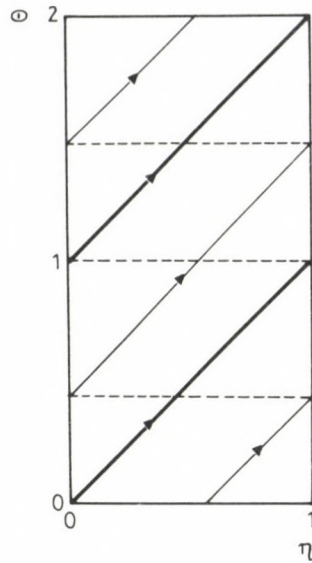


Fig. 8. The lines of characteristics

The boundary conditions are:

$$T(\theta, 0) = T(\theta, 1) , \quad (91)$$

$$L(\theta, 0) = L_i(\theta) . \quad (92)$$

The initial conditions are

$$T(0, \eta) = T_i(\eta) , \quad (93)$$

$$L(0, \eta) = L_i(\eta) . \quad (96)$$

Computations were carried out at $T_o = 100$ K operational temperature when $T_w - T_o = 5$ K.

Figure 9 shows how the gas temperature in the injection section $T_o(\theta)$ converges to the steady-state after a perturbation of 5 K, indicating that $\alpha_{22}(1) \cong 0.69 < 1$.

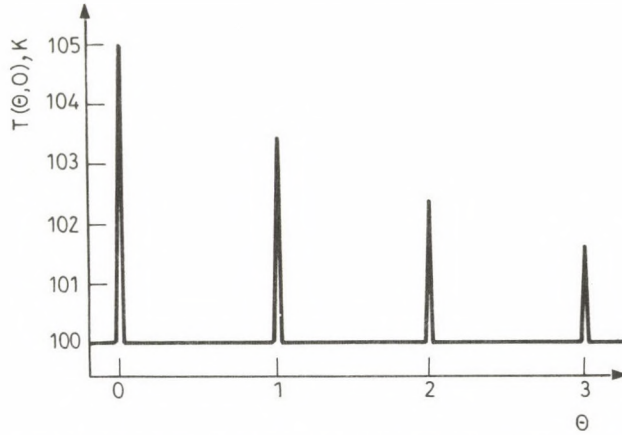


Fig. 9. Response of the non-linear model in case of disturbance in the gas temperature at the injection section

Figure 10 demonstrates the temperature transients in different cross-sections of the tunnel. The steady-state value of the injection rate was doubled at $\theta = 0$. It can be seen that these functions are very similar to that predicted by the linearized model.

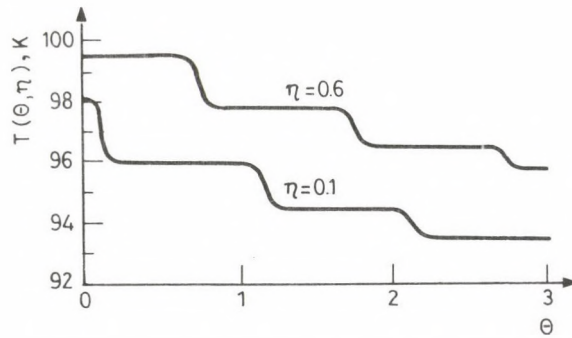


Fig. 10. Gas temperature response predicted by the non-linear model at different locations of the tunnel circuit in case of doubled injection rate

In Fig. 11 the temperature distributions along the tunnel length are shown at different time points. The temperature wave going around in the tunnel circuit is apparent.

CLOSED CIRCUIT CRYOGENIC WIND-TUNNEL

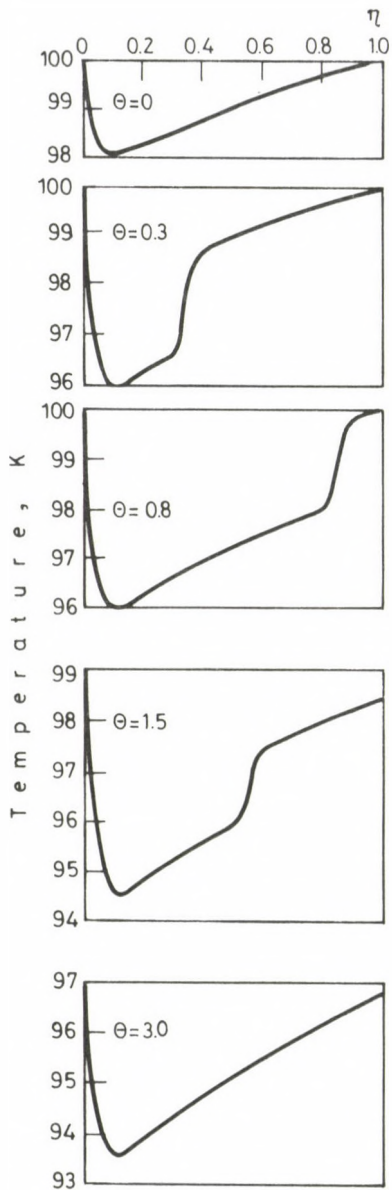


Fig. 11. Gas temperature distribution along the tunnel length at different time points in case of doubled injection rate

Figures 12-15 show the temperature as function of time at the injection section in the case of sinusoidal input in the injection rate. The sinusoidal temperature response reaches its steady state in different ways according to the relationship between the circuit frequency and the input signal (injection rate) frequency. When the period time of the input signal is not greater than that of the circuit, $t_c \geq t_{in}$, then two cases can be considered:

(a) $t_c \bmod t_{in} = 0$; the amplitude of the temperature response monotonously increases (Fig. 12).

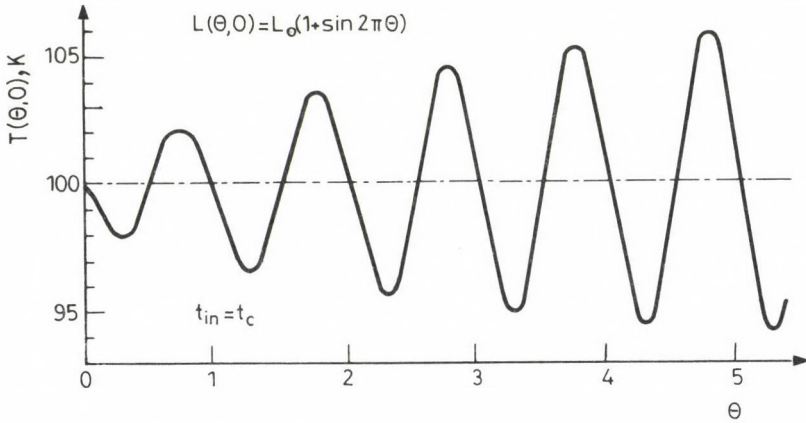


Fig. 12. Gas temperature response for sinusoidal injection rate input in case of $t_c \bmod t_{in} = 0$

(b) $t_c \bmod t_{in} \neq 0$; the amplitude of the temperature response decreases in an oscillatory way (Fig. 13)

If $t_{in} > t_c$, the possibilities are again

(c) $t_{in} \bmod t_c = 0$; the maximum as well as the minimum values of the temperature response increase, and the initially asymmetrical response function becomes symmetrical (Fig. 14)

(d) $t_{in} \bmod t_c \neq 0$; we get a similar response function to the one in the case of (b) (Fig. 15).

CLOSED CIRCUIT CRYOGENIC WIND-TUNNEL

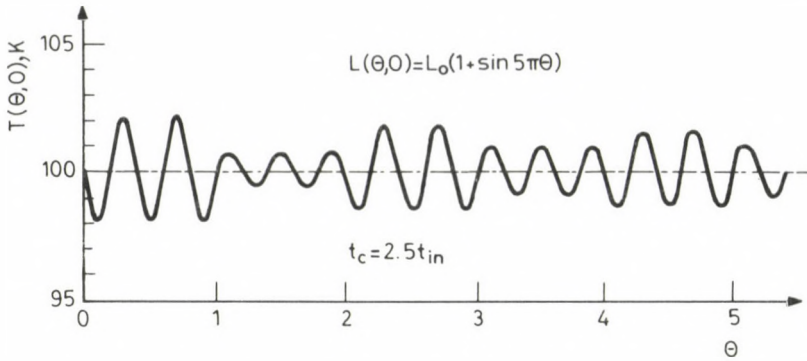


Fig. 13. Gas temperature response for sinusoidal injection rate input in case of $t_c \bmod t_{in} \neq 0$

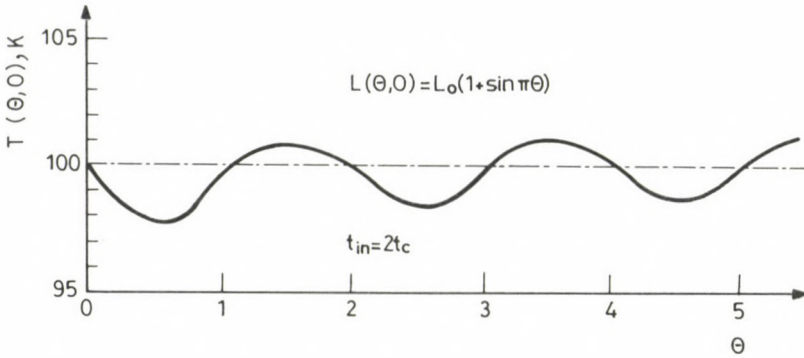


Fig. 14. Gas temperature response for sinusoidal injection rate input in case of $t_{in} \bmod t_c = 0$

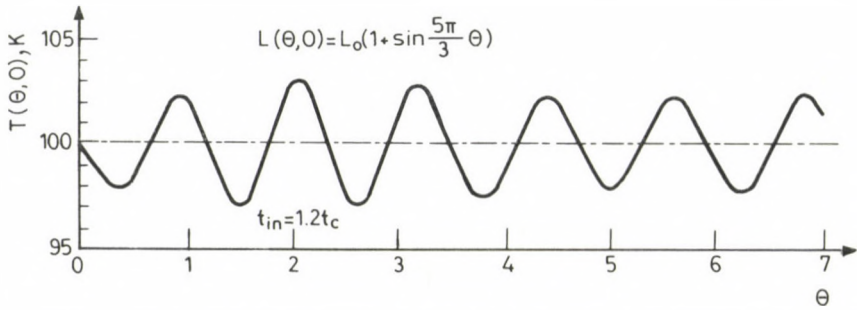


Fig. 15. Gas temperature response for sinusoidal injection rate input in case of $t_{in} \bmod t_c \neq 0$

CONCLUSION

Steady-state and transient analysis of a cryogenic closed circuit were presented. These analyses were based on a simplified mathematical model focusing on the heat and mass transfer processes taking place in the tunnel.

Steady-state analysis led to a trade-off between implementation cost (insulation thickness) and operation cost (LN_2 consumption). Numerical computations indicate, that stability condition evaluated from the linear transient analysis, provides reliable information for the non-linear system in the vicinity of a steady-state.

The model's validity can be extended to more general situations in many ways. For example, in setting-up of model equations, constant wall temperature was assumed, although one may consider a more general case, namely

$$\alpha_c(T_w - T) = k_{\text{eff}}(T_A - T) , \quad (97)$$

where k_{eff} is the overall heat transfer coefficient between the tunnel gas and the ambient.

One of the most important extensions can be to take the heat capacities of the tunnel wall and insulation into account. If the dynamical model is used for control design purposes around a steady-state, then these capacity terms can be neglected /3/. However, when the state of the tunnel gas is far from a steady-state, i.e. during cool-down operation, the heat capacities are important factors in the calculation of the cool-down time and the necessary LN_2 consumption. Then transient heat balance equations can be added to the model in order to calculate the transient wall temperature. Orthogonal collocation technique resulting ordinary differential equations is preferable /11/.

Although the physical model used for the analysis is very simple, it proved to be fairly adequate to describe the essentials of the heat and mass transfer in the circuit /12/. As illustration, in Table 2 one can find the experimental values of the gas temperature versus time measured in a pilot cryogenic low-speed TLT wind-tunnel during cool-down operation at the German Aerospace Centre (DFVLR), Köln-Porz. The predicted values provided by the model give good approximation.

CLOSED CIRCUIT CRYOGENIC WIND-TUNNEL

Table 2. Cool-down operation in a low-speed wind-tunnel /12/

Time (s)	Gas temperature at the test section (°C)	
	measured	predicted
0.0	22.0	22.0
194.0	10.0	11.6
271.0	6.0	7.8
376.0	2.0	3.1
541.0	-5.0	-3.6
661.0	-9.0	-7.9
842.0	-13.0	-13.7
975.0	-16.0	-17.5
1118.0	-20.0	-21.1
1275.0	-23.0	-24.6
1491.0	-26.0	-28.8
2247.0	-39.0	-39.0
2674.0	-43.0	-42.6

REFERENCES

1. Kilgore, R.A. and et. al.: "The Cryogenic Wind Tunnel Concept for High Reynolds-number Testing", NASA TN D-7762 (1974), Nov.
2. Balakrishna, S.: "Synthesis of a Control Model for a Liquid Nitrogen Cooled, Closed Circuit, Cryogenic Nitrogen Wind Tunnel and Its Validation". Progress Report, Old Dominion University, Norfolk, Virginia, (1979), Nov.
3. "Control System Study", SVERDRUP, ARO. Inc., Report 1980.
4. Paláncz, B. and Kronen R.: "Mathematische Modellierung, Simulation und Regelung Eines Kryogenen Wind-Kanals", DFVLR, WKT 21/82, Köln-Porz 1982
5. Kraft, D.: "Optimale Steuerung eines Tieftemperatur-Windkanals" 18. Regelungstechnisches Kolloquium, Boppard, West Germany, (1984), 17-18. Febr.
6. Stallings, R.L. and Lamb, M.: "A Simplified Method for Calculating Temperature-Time Histories in Cryogenic Wind Tunnels"., NASA Tech. Memo., NASA TM X-73949, Langley R. Cent., Virginia, (1976), Dec.
7. Ciborowski, J.: "The Bases of Unit Operations" in Ch.3., Heat Transfer and Convection, Wydawnictwa Naukowo-Techniczne, Warszawa 1969
8. Parti, M. and Paláncz, B.: "Mathematical Model for Spray Drying' Chem. Engng. Sci. 29, (1974), 355.

9. Paláncz, B.: "Analysis of the Performance of a Liquid Nitrogen-Cooled, Closed Circuit, Cryogenic Wind Tunnel and Its Application to the DFVLR's 3 m-Tunnel in Cologne, I., Steady-State Study" DFVLR WKT 8/80, Köln-Porz 1980
10. Bilous, O. and Amundson, N.R.: "Chemical Reactor Stability and Sensitivity, II., Effect of Parameters on Sensitivity of Empty Tubular Reactors", A.I.Ch. E. Journ. 1(1955), 513
11. Finlayson, B.A.: "Nonlinear Analysis in Chemical Engineering" McGraw-Hill, New York 1980
12. Paláncz, B., Distelrath, H.D. and Schneider, K.G.: "Determination of the Temperature Distribution in a Cryogenic Wind-Tunnel" (Theoretical and Experimental Investigations), DFVLR, WKT 16/81, Köln-Porz 1981
13. Viehweger, G.: "Kriogenisierung des Niedergeschwindigkeits-Windkanals" Köln-Porz,-Spezifikationsphase-, DFVLR, WKT 11/80, Köln-Porz 1980
14. Steinhäuser, R.: "Reglerentwurf für einem Tieftemperatur-Windkanal mittels Gütevektoroptimierung", Dissertation, TU Karlsruhe 1984

USE OF LOW-GRADE COAL AS FUEL OF POWER PLANTS

K. Reményi*

(Received 24 May 1985)

All over the world in power-station practice, low-grade fuels are being utilized. In Hungary our coals fuelled in power-station practice have large ash- and moisture-content, while with our lignites the xylitol of wooden structure is prevailing. On the basis of grinding and firing investigations a hammer/fan mill with excellent operational parameters and new types of burners providing sound combustion have been developed.

Industry and energy policy for the period till 2000 suggests that the national energy carrier resources be increasingly utilized.

The reducing availability of oil products for energetic uses can be compensated first of all by increasing use of coal and nuclear energy. Development already decided in the field of coal mining necessitates that, within the power plant capacity to be constructed in the 1990s, coal-fired power plants be constructed. In addition to Eocene mines, the utilization of strippable lignite resources permits additional coal-fired power plants to be developed, a realistic version being enlargement of the Gagarin Thermal Power Plant and construction of a new power plant in the area of Bükkábrány. Another way to reduce hydrocarbon consumption is to substitute coal for hydrocarbon in heat supply, first of all by coupled electricity generation and heat supply in back-pressure or pass-out condensation power plants.

The rise in prices of hydrocarbons resulted in changes also in the operation of the electric power system. The hydrocarbon fired power plants are operated to supply heat and to comply with the schedule while the utilization of existing coal fire power plants has been significantly increasing. The coal fired power plants with old equipment in majority need modernization and reconstruction to meet the increasing requirements.

The national energy development program is based in part on utilization of coal resources. Therefore, new high-capacity coal fired power plants are expected to enter the system although the time at which their capacity adds to the present capacity is unknown for the time being.

All the world over, low-grade fuels and/or the tailings of grading

*Dr.K.Reményi, H-1014 Budapest, Úri u. 38, Hungary

of high-grade fuels are used to fuel power plants. A fundamental condition for economic utilization are a plant design and operating process developed on the basis of highest theoretical knowledge in the field of fuel engineering. Recurrent and significant changes in the fuel quality make the control of the operating process of power plants especially difficult. Like all over the world, the ratio of hydrocarbons among the fuels for power plants was predominant also in Hungary before the early 1970s. After the rapid rise of oil prices, the reduction of the share of oil products in energetic development has become a fundamental point, a fact involving grave consequences with respect to both oil fired and coal fired power plants.

Table 1. Total heat demand (consumption) per fuel

	Coal		Oil		Hydrocarbon		Nuclear		TJ
1955									= 72.857
1965	127907	+	19728	+	8704				= 156.339
1975	152104	+	63885	+	52551				= 268.540
1983	159500	+	39239	+	108143	+	28715		335.597
			147382						
<hr/>									
			<u>1983:</u>	Coal			45.6 %		
				Hydrocarbon			44.3 %		
				Oil			9.5 %		
				Nuclear			8.1 %		

Table 1 shows the change of total heat demand of the power plants of MVMT (Trust of Hungarian Electricity Suppliers) as well as the distribution of heat consumption per fuel type in 1983. The ratio of coal based heat is highest in the Table 1.

Table 2 shows the distribution of basic energy carriers used for electricity generation per type. As shown in the Table, the ratio of coal has reduced slightly in the recent ten years, first of all due to reduction of use of brown coal for energetic purposes, but most significant is the reduction in the utilization of oil in this period while the ratio of natural gas has increased rapidly, a trend not welcome in the long run. Also nuclear energy, first of all to substitute for oil, entered the picture in 1983.

LOW-GRADE COAL AS FUEL

Table 2. Electricity production of MVMT power plants per type of basic energy carrier

	1973		1983	
	GWh	%	GWh	%
Brown coal for energetic uses	5.677	32.2	5.419	22.0
Lignite	4.352	24.7	3.779	15.4
Black coal semi-finished product	1.351	7.6	1.199	4.9
1 Total coal	11.380	64.5	10.397	42.3
2 Fuel oil	3.988	22.1	2.985	12.1
3 Natural gas	2.231	12.7	8.584	34.9
Total hydrocarbon	6.140	34.8	11.569	47.0
Water power	124	0.7	155	0.6
4 Nuclear energy	-	-	2.473	10.1
Total production:	17.644	100.0	24.594	100.0

Table 3 is a summary of the changes in distribution of coal used for electricity generation and heat supply per type. Lignite and brown coal are predominant while the ratio of black coal amounts almost invariably to 12.3 % within the total coal based heat for the year 1983.

In the recent years, the quality of coal for power plants has gone from bad to worse. This change in quality for the larger power plants in the country is illustrated in Table 4 while for electric power industry as a whole in Fig. 1. Responsibility for this degradation falls upon increasing ash content. Fuel for power plants consists of low-grade products and tailings which cannot be utilized for other purposes, containing, in addition two combustible components, large amounts of impurity and moisture.

From among the components of fuels used in power plants, the ash content is the most crucial problem. Ash of different kinds, with rather unfavourable consequences, is present in a high percentage in coal available in Hungary, the ash content of the different coal types varying in the range of 20 to 65 % depending on the conditions of mining and coal preparation process.

Table 3. Distribution of fuels within total electricity production and heat supply

	Year	10 ³ t	TJ
Lignite	1955	2.370	19.326
	1965	21871	22.038
	1975	6.230	41.758
	1983	7.533	50.344
Brown coal for energetic uses	1955	4.038	47.772
	1965	8.247	92.204
	1975	7.916	90.969
	1983	8.520	89.200
Black coal semi-finished product	1955	244	4.110
	1965	1.258	13.605
	1975	1.797	19.314
	1983	1.830	19.700
Total coal	1983	17.958	159.500
Oil	1955	42	1.649
	1965	491	19.590
	1975	1.579	63.859
	1983	971	39.240
Natural gas	1955	-	-
	1965	254	8.692
	1975	1.471	52.526
	1983	3.266	108.143*
Total hydrocarbon	1983		147.382
Nuclear	1983		27.300

*Of this high-inert gas: 315 million m³ (5260 TJ)

LOW-GRADE COAL AS FUEL

Table 4. Change of heat value in major coal fired power plants in the country

	Heat value, kJ/kg	
	1970	1983
<u>Lignite firing</u>		
Gagarin	6.553	6.662
November 7	9.761	9.535
<u>Brown coal firing</u>		
Ajka	11.006	10.847
Borsod	10.221	9.370
Oroszlány	11.198	10.674
Tatabánya	12.667	11.775
Tisza I	10.980	10.521
<u>Black coal firing</u>		
Pécs	10.487	10.563

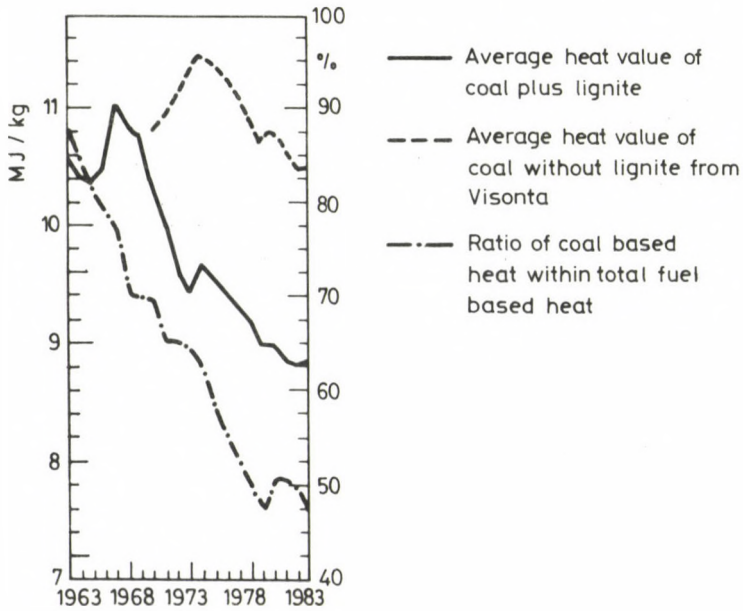
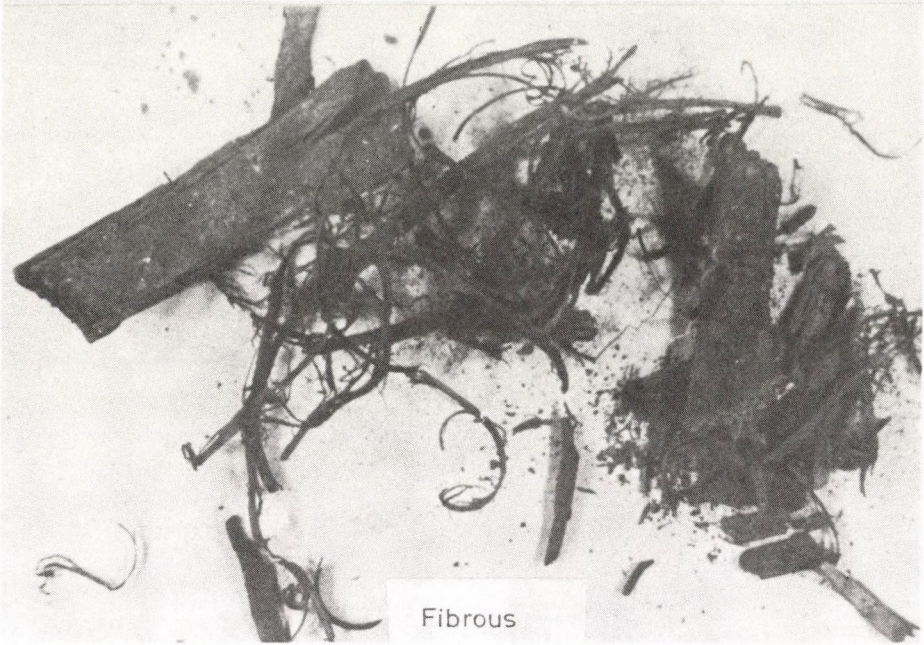


Fig. 1.



Fibrous

Fig. 2.



Good

Fig. 3.



Fig. 4.



Fig. 5.

The ash content of coal results in considerable troubles in both preparation and combustion of the fuel, as well as in the operation of the furnace. Serious difficulties arise also in transport, comminution, ignition of fuel, in control of the boiler, slagging, as well as in connection with abrasion of the pulverized coal pipes and different boiler elements, and in the system of slag removal. However, while facing all these difficulties, it is not only the unfavourable effects of ash content that have to be taken into consideration in evaluating the problems encountered in firing of the fuel but, instead, the equipment shall be developed so as to take combustibility, the effect of xylite in case of lignite, the properties of ash, and the harmful effect of moisture into account in combination to create favourable conditions for use of low-grade coal in the fuelling process.

Fine-ground impurities, entering the furnace, affect the conditions of ignition unfavourably, and result also in slag formation. At high temperatures prevailing especially in the vicinity of the burners, the fine fractions reach sticking temperature and adhere to the non-cooled surfaces of the wall.

Recently, less attention has been paid to problems resulting from the moisture content of fuel although the difficulties in the utilization of fuel arise as a combined effect of high ash content and moisture content. Moisture results in problems in transport and ignition. Residual moisture in pulverized coal entering the furnace contributes to abrasion in general, as well as to the corrosion of the afterheater surfaces. Xylite of different degree of decay in younger coals and in lignite, in addition to ash and moisture, results in troubles in both grinding and firing. On the basis of the macroscopic and microscopic character resulting from the degree of decay and/or carbonization, four typical xylite types can be distinguished, such as

- fibrous xylite (Fig. 2),
- "benignant" or bright xylite (Fig. 3),
- "intermediate" or dark xylite (Fig. 4),
- metaxylite (Fig. 5).

Apart from fibrous xylite occurring in reduced amounts, a common feature of the different types of xylite is the low cellulose and high lignite content, their properties indicating biological decay.

Although the tailings of the separation process contain still a

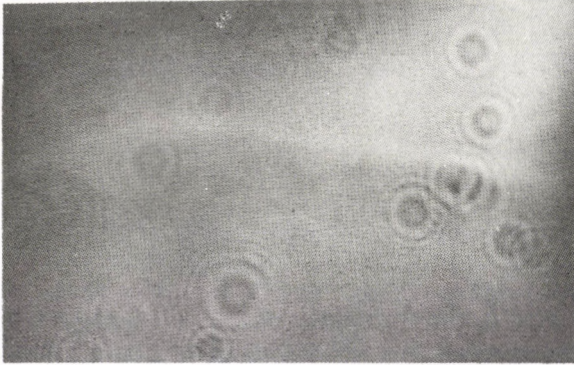
LOW-GRADE COAL AS FUEL

high percentage of components unfavourable in respect of firing after high-grade coal has been sorted out, this material is an important and valuable basic material for energetic uses. Thorough theoretical investigations and high-class constructional development help to overcome difficulties resulting from the increasingly inferior fuel quality. Research and development are necessary in both preparation of the fuel, and the firing process itself. Hungary, a country in rather unfavourable situation concerning availability of high-grade fuel, ranges among the top countries on a world scale in respect of research and development in this field. A plant ensuring coal preparation in accordance with the requirements of the firing process, or stable combustion in a possibly wide range of load, can be developed on the basis of thorough theoretical knowledge of diminution and combustion, respectively.

Both the preparation, and combustion itself, of coal are fundamentally determined by the behaviour of coal when burned. Accordingly, experiments are run on a wide scale, from laboratory size to industrial scale. Most up-to-date methods are used to study the combustion process. Pulsed holography permits information to be obtained during combustion of fuels on processes which have not been detectable earlier by the usual high-speed filming or Schlieren process etc. The studies included observation of phenomena taking place in the immediate vicinity of burning coal particles, and of changes in particle size. The holograms show sharp-cut interference rings around the burning particle, which lead to the conclusion that spherical wave phenomena may take place around the particle. Experiments to determine changes in the size of powderized coal particles revealed significant differences in the rate of dimensional changes depending on the degree of carbonization of the coal. Numerical relationships can be determined under given circumstances between grain size, oxygen concentration, and ambient temperature.

Hungarian coals of different degree of carbonization have been included in the experiments. The coal types tested were lignite, Eocene brown coal, and black coal, of an average particle diameter of 70 μm and 140 μm . The furnace temperature was adjusted at 850 $^{\circ}\text{C}$ and 1000 $^{\circ}\text{C}$, the oxygen content of gas to feed combustion was 5 % and 10 %, respectively. A giant pulse was used for holographic exposure. The image applied in the course of restoration permitted the size of all particles present in the space to be stud-

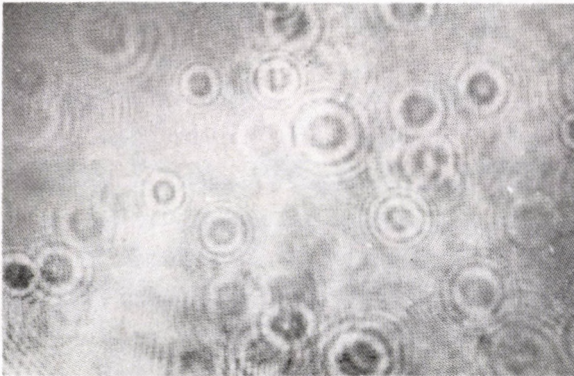
ied simultaneously. Presented in Fig. 6 are the holograms obtained for the combustion of 140 μm diameter black coal particles at 1000 $^{\circ}\text{C}$ and with O_2 of 5 % from among holograms of a large number produced in the course of the experiments.



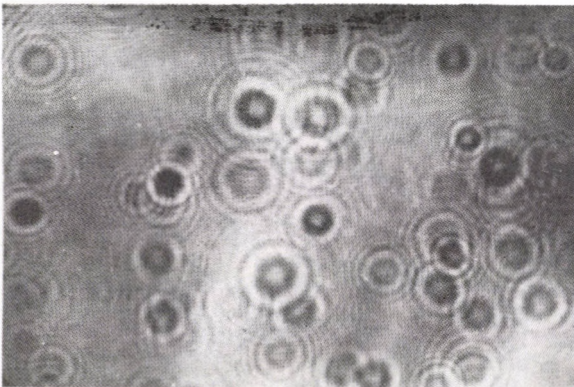
6th hole

Combustion in flue gas
at 10% O_2 concentration
and 1000 $^{\circ}\text{C}$

Initial particle diameter
125-160 μ



5th hole



Coal feeding from

3rd hole

Fig. 6.

LOW-GRADE COAL AS FUEL

As an example for numerical evaluation, the dimensional change of different coal particles with an oxygen concentration of 10 % and at a temperature of 1000 °C is diagrammatically illustrated as a function of the distance covered in Fig. 7.

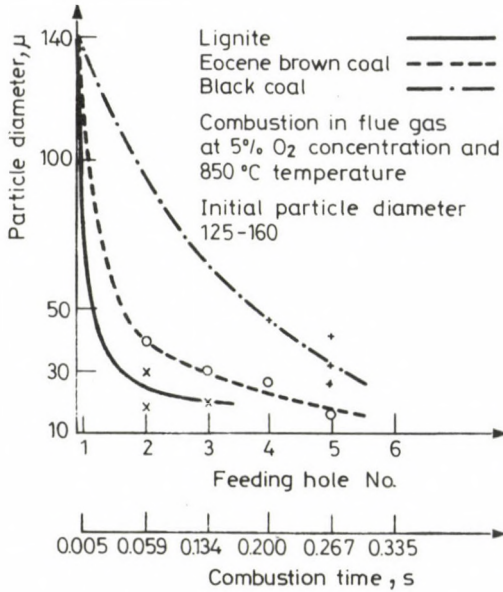


Fig. 7.

The coal preparation process, in particular the fineness of grinding in case of pulverized-coal firing, can be determined in the knowledge of the behaviour of coal in combustion. Preparation of coal for pulverized-coal fired boilers takes place at coal grinding plants.

The Hungarian power plants use ball mills, roller mills, hammer mills, and fan-type mills. Richest experience is available in operation of fan-type mills although the special local problems of any mill type are encountered. Fan-type mills are most widely used for grinding of the Hungarian brown coal and lignite.

The grinding mill is designed to grind, dry, and transport coal, the most complex process being required for grinding lignite of high ash, moisture, and xylite content.

For lignite from Gyöngyös, the incompatible grindability of both

components i.e. ash and lignite can be determined in addition to moisture in grinding under actual operating conditions. Ash of relatively high grindability becomes undesirably overground when ground together with tough, fibrous and woody xylite. With the ash content increasing, the drying gas demand of the mill decreases while the concentration of drying gas and pulverized coal increases, and as a result, the output of the mill reduces.

Favourable conditions for grinding coals mined in the country can be ensured only in a grinder specially developed for these purposes in the country. A combined hammer and beater mill of type NN6 developed in Hungary, of a grinding output of 32 t/h, has been successfully operating at the Bánhida Power Plant for years. Also, the prototype of a mill of similar design, of a capacity of 50 t/h, has been constructed first of all to meet the demand for the Bicske Power Plant but suited for grinding Hungarian brown coals of any type after minor modification. The layout, the rotor, and the air separator gates of the mill developed by VEIKI (Research Institute of Electric Power Industry) and constructed by the Disintegrating Mill Factory are shown in Figs 8, 9, 10, respectively. Patented units developed by VEIKI are the rough-grinding stages and the air separator of the mill, decisive units in respect of operation.

After the different factors affecting combustion of the fuel had been studied in detail, development of a burner for different applications under different conditions prevailing in the furnace in a wide load range was started at the Institute. As a result, a new pulverized coal burner called separator-type swirl burner was developed at VEIKI, for use as a starting burner for the startup of pulverized-coal fired boilers by pulverized coal, as a back-up burner in case of troubles in ignition or stability, and as a vapour burner in case of open-cycle firing. The speciality and versatility of the burner lies in that the limitations due to direct firing are partly offset by the firing system. The adjustable amount of highly inert gas transporting the pulverized coal, ground and dried in the grinding mill, to the burners can be separated from the pulverized coal in the burner; and primary air of almost arbitrary amount and temperature can be admixed to the fuel before being blown into the furnace. The burner prevents inert gases from entering the furnace or ignition zone, the combustion temperature being high and the ignition stable. In case of variable fuel quality, the optimum combustion temperature is adjustable. The firing system equipped

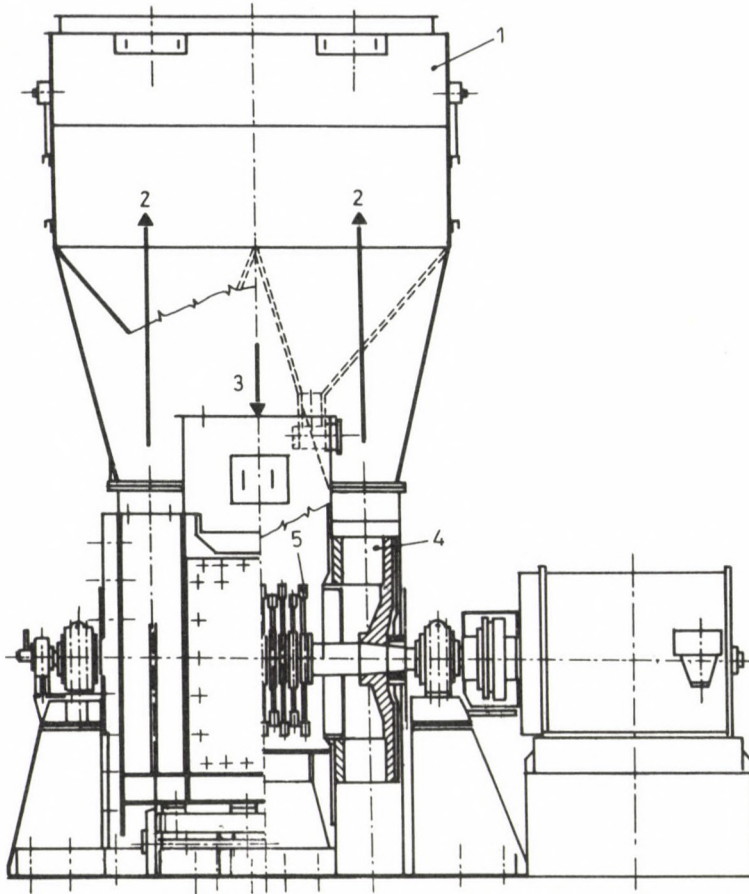


Fig. 8.

with the separator-type swirl burner is safe and simple. As is well known, the formation of a stable flame is significantly affected by the physical-chemical characteristics and reagency of the fuel, temperature, concentration of fuel and oxidizer in the combustible mixture, and by the mixing processes.

Coals of different type in general, and high-moisture lignites in particular, are blown directly into the furnace by means of the drying gas drawn from the furnace, to be burned there after having been ground and dried in the grinding mill. A considerable amount of inert gas enters the furnace, reducing there the oxygen concentration, pulverized coal concentra-

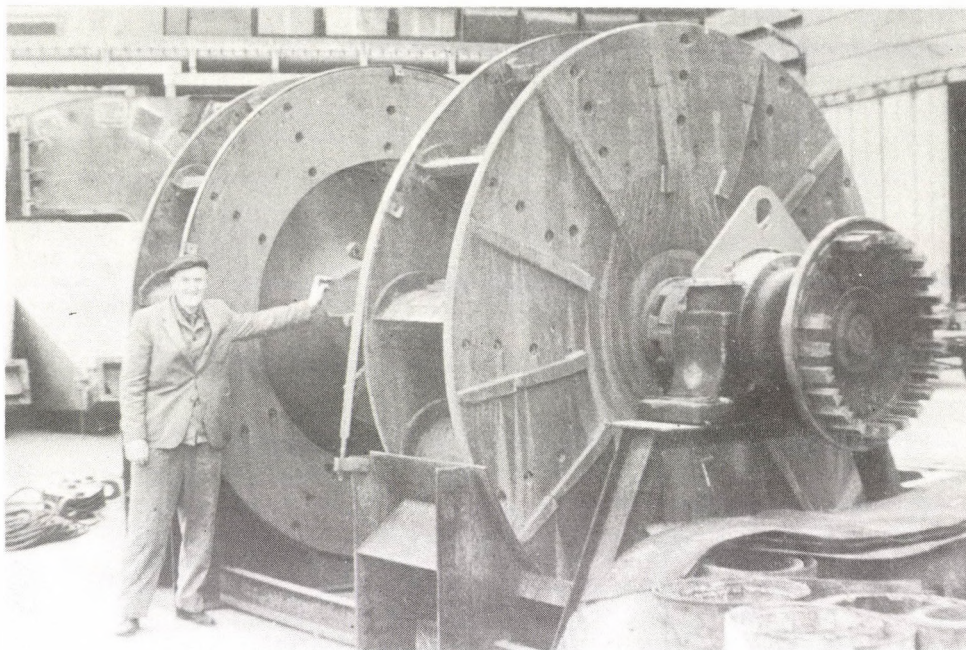


Fig. 9.

tion, and combustion temperature. Ignition can not even take place below an oxygen concentration depending on the fuel only. The effect of drying gas blown in is shown in Fig. 11. The curves in the Figure illustrate the change in adiabatic combustion temperature of lignites of different heat value for the combustion of raw coal in oxygen, ambient air, or by removal of 0 %, 50 %, or 100 % of the drying flue gas by some method. The average quality characteristics of given coal are, as follows:

Heat value	6.060 kJ/kg
Moisture	44 %
Ash	25 %

Removal of only 50 % of the drying gas results in a considerable temperature rise. This is especially important for the stability of firing when pulverized coal firing has to be brought about within a short time in a cold furnace in the phase of boiler startup. The significant difference between firing with combustion air and that with removal of 100 % of the drying gas is that while in the former case the combustion temperature is reduced by the moisture present in the coal, a considerable part of the moisture is removed together with the drying gas in the latter case.

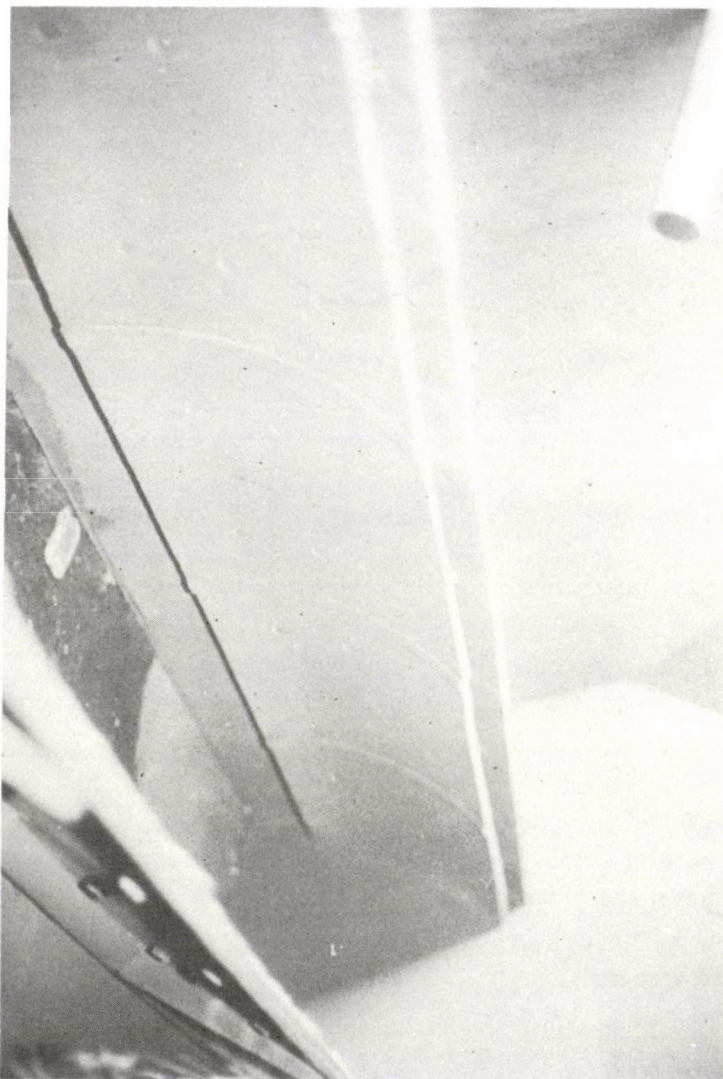


Fig. 10.

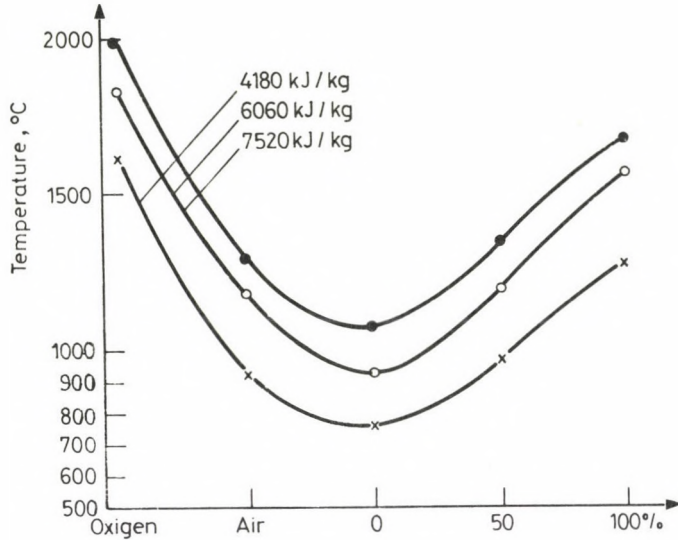


Fig. 11.

In the combustion process, an important parameter is the concentration of combustibles, which can be varied within wide limits by suitable separation of the drying gas or by admixture of primary air. The effect of concentration is evaluated on the basis of the rate of pressure changes in case the mixture of pulverized coal and air is burned in an 'explosion bomb'. The bomb is a sealed vessel of a volume of 70 dm^3 in which ignition takes place pyrotechnically. The value of pressure change, ΔP_{max} , and the average and maximum rate of pressure change, $\Delta P_{\text{max}} / \Delta t$ and $(dP/dt)_{\text{max}}$, respectively, are illustrated in Figs 12 and 13. It can be seen that, in the range of concentration studied, the rate of pressure changes that is the speed of combustion reduces considerably for low concentrations. E.g. in case of lignite from Bükkábrány, the speed of combustion is very low for a concentration of 300 g/m^3 that is the combustion is prolonged.

Based on the above considerations, a pulverized coal ignition system to start a lignite fired steam boiler of a steam output of 620 t/h has been designed, and built in. Pulverized coal comes from the grinder of another boiler operating next to that to be started so that no intermediate pulverized coal storage is necessary. The ignition system is schematically illustrated in Fig. 14.

LOW-GRADE COAL AS FUEL

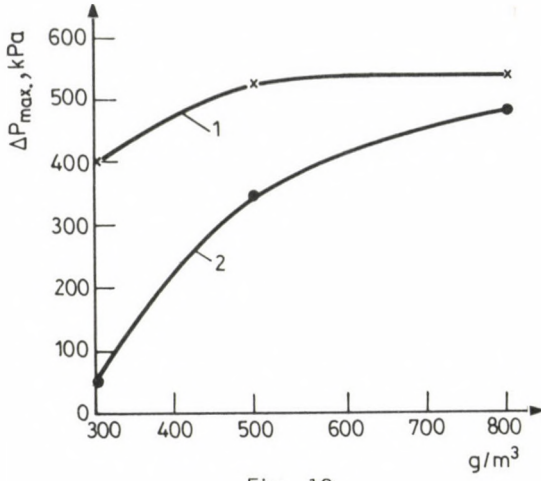


Fig. 12.

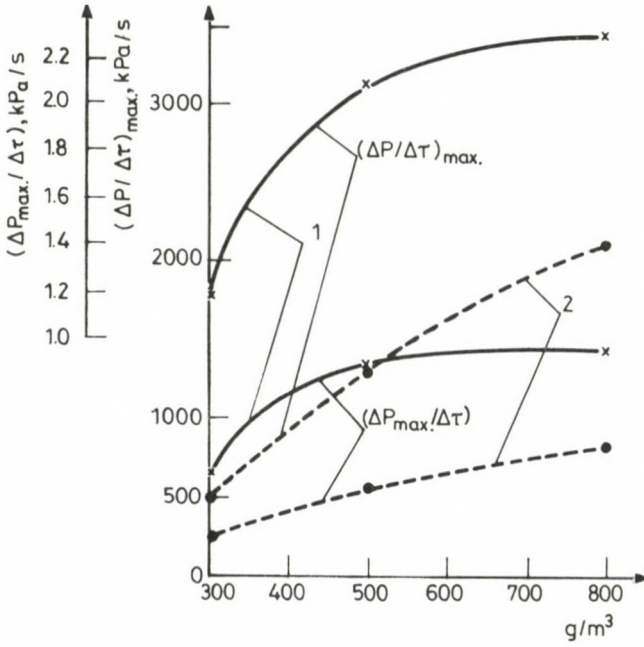


Fig. 13.

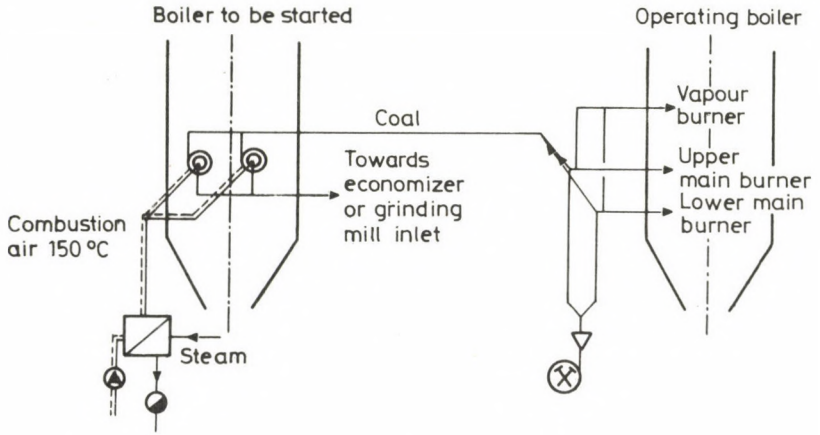


Fig. 14.

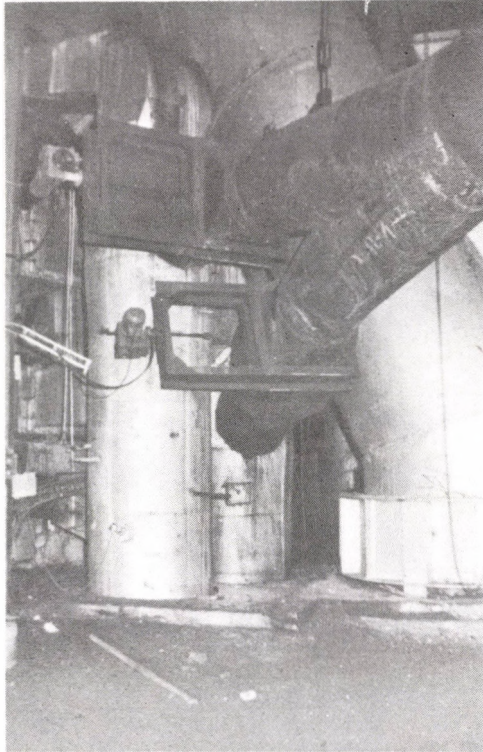


Fig. 15.

LOW-GRADE COAL AS FUEL

The photograph in Fig. 15 shows the different elements of the pulverized coal ignition system operated at the Gagarin Thermal Power Plant, and the pulverized coal outlets on the adjacent boiler serving as the source of pulverized coal. Fig. 16 shows the two 30 MW_t separator-type swirl burners.

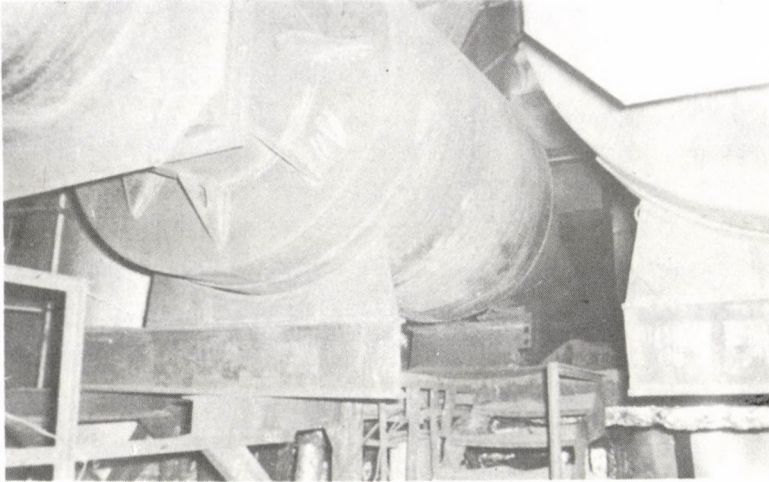


Fig. 16.

Tabulated in Table 5 are the most important characteristics of the system.

Table 5. Starting burner for 620 t/h boiler of Gagarin Thermal Power Plant

Specifications	
Boiler output	590 MW
Flow rate of gas transporting pulverized coal to burners	120.000 m ³ /h
Dust concentration	177 g/m ³
Heat value of coal	12.040 KJ/kg
Ultimate moisture in coal	12 %
Heat output per burner	30 MW
Primary air at starting burner	50 %
	of calculated combustion air demand
Primary air temperature	150 °C

In the development in the field of lignite firing, the next step was to raise the vapour burner, followed by realization of 'open-cycle' firing. Raise of the vapour burner resulted in removal of inert gas, separated by the vapour separator, from the active zone of the furnace only, while in open-cycle firing, the total amount of inert gas would by-pass the heating surfaces of the boiler to return at a point of suitable temperature after the air heater. Thus not only the conditions of ignition and combustion in the furnace are improved but also abrasion in flue II of the boiler reduces considerably due to the reduced rate of flow of flue gases.

A separator-type swirl burner has been designed for use as a vapour burner to separate, and feed with preheated air into the furnace, the pulverized coal that remained in the vapour line. The use of such a burner results in a system considerably simpler as compared with the usual practices.

The block diagram of the open cycle for a pulverized coal burner is shown in Fig. 17. Two separator-type swirl burners of a heat output of 2.5 MW each have been used as vapour burner.

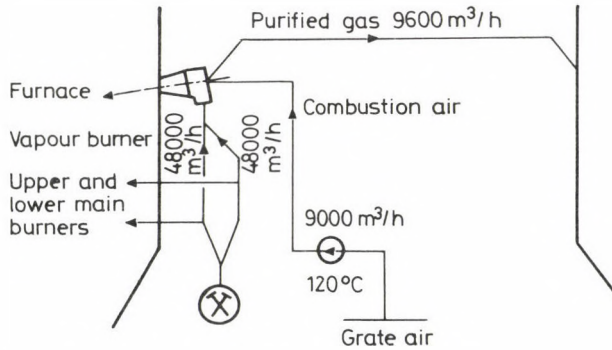


Fig. 17.

Taking into consideration a ventilation rate of $240 \cdot 10^3 \text{ m}^3/\text{h}$ and a maximum grinding output of 50 t/h for the grinding mill as well as a gas separation of 60/40 and a pulverized coal separation of 95/5, the specifications for the burner are as follows:

Heat output	2.5 MW
Gas flow rate	$48 \cdot 10^3 \text{ m}^3/\text{h}$
Combustion air flow rate	$4.5 \cdot 10^3 \text{ m}^3/\text{h}$ (120 °C)
($\underline{m} = 1.25$ air factor)	

LOW-GRADE COAL AS FUEL

An important advantage of the open cycle is that purified gas leaving the separator-type swirl burner bypasses flue II of the boiler and therefore the abrasion, first of all that of the economizer, reduces there considerably due to the reduced rate of flow. The abrasion reduces exponentially according to exponent 2.5 of the flow rate for identical material grade (flyash and material of economizer pipe).

Preliminary approximative calculations have been made for the extension of open cycle over the entire 320 t/h boiler (all the four pulverized coal burners operating in open-cycle system). The change in flue gas temperature is diagrammatically illustrated in Fig. 18.

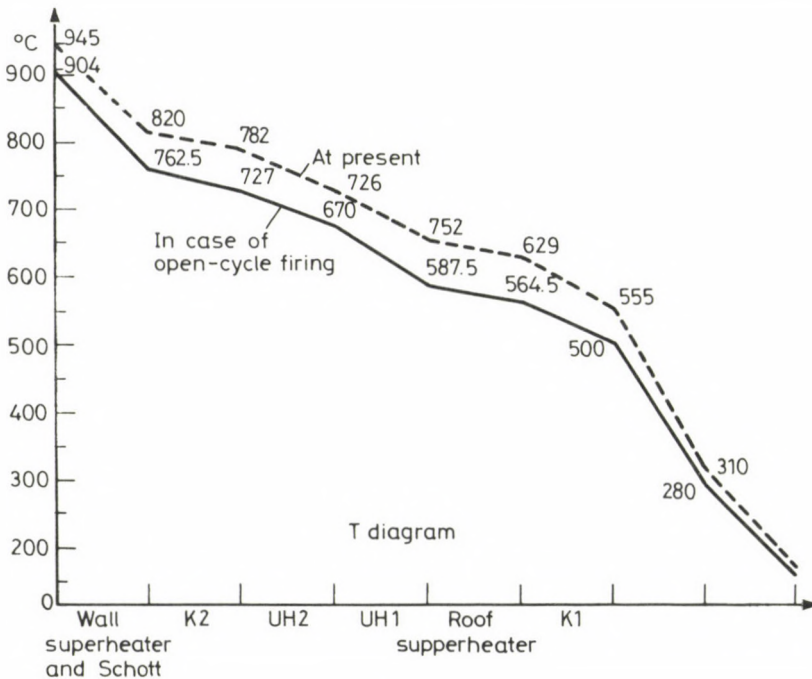


Fig. 18.

The use of low-grade coal and operation of the boilers at partial load result in instable fire. To operate the boilers without back-up firing that is without an increase in the use of hydrocarbons is an increasingly difficult job.

A firing system increasing the stability of firing without any sig-

nificant expenditure has been developed, and successfully used at Tatabánya I Thermal Power Plant, and Dorog Thermal Power Plant. No extinction of the flame is experienced in spite of the continuous decline in coal quality since the separator-type swirl burner developed by VEIKI has been built in, and the minimum load (without oil back-up) has reduced considerably. The modified firing system has fulfilled expectations also under operating conditions.

The heat flux of a burner may change in the range of 1.8 to 2.2 MW, depending on the output of the grinding mill, see photograph in Fig. 19.

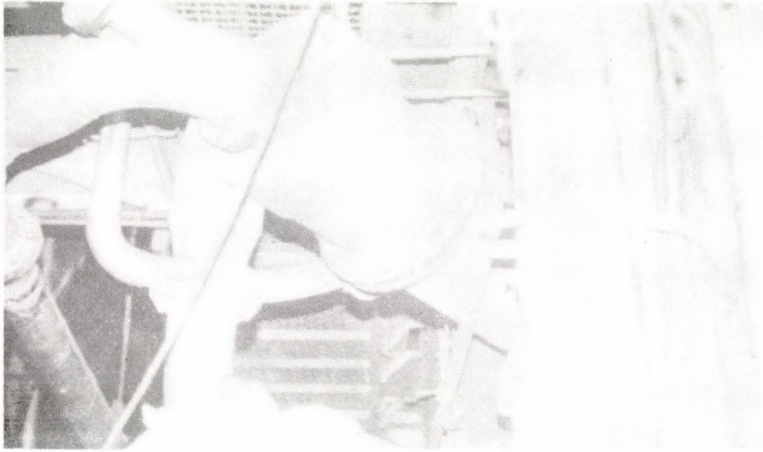


Fig. 19.

As compared with the earlier practice, the separator-type swirl burner offers the following advantages:

- Inert gases serving for drying (transport of pulverized coal) are separated and thus their unfavourable effect on the conditions of ignition and combustion can be avoided.
- The total amount of combustion air (if necessary) and the pulverized coal can be thoroughly mixed before entering the furnace.
- The temperature of combustion air can reach even the ignition point, bringing about favourable conditions for ignition.
- No hazards of coal dust explosion are impending under favourable conditions of ignition and combustion.
- The burner permits a simple firing system to be brought about.

BOOK REVIEWS

G. Franz (editor): Beton-Kalender 1986. Taschenbuch für Beton-, Stahlbeton- und Spannbetonbau, sowie die verwandten Fächer
Ernst und Sohn, Verlag für Architektur und technische Wissenschaften, Berlin 1986

The present volume 75 of the manual has been published in conformity with the old tradition in two parts, however, contrary to the previous volumes, in the format A5 instead of A6. This alteration permitted to use larger letter types and to present the figures and tables in a larger form.

The first part of the manual contains, in accordance with the long practice of many years, the fundamental knowledge necessary to the calculation of r.c. structures. It treats in detail of the material, properties and making of concrete (J. Bonzel), the kinds and products of steel (D. Bertram), the wood as building material and structural element (K. Möhler). A chapter elaborated in detail in a comprehensive framework deals with the calculation of the stresses induced in slabs of different forms, differently loaded and supported (K. Stiglat-H. Wippel). The paragraph treating of the dimensioning and checking the r.c. elements (E. Grasser), as well as designing calculation and the problems of buckling of slender r.c. elements (K. Kordina-U. Quast) call the reader's attention to the rich diagram material. In a special chapter are the problems of the stressed structures dealt with involving also those of the partially stressed constructions (H. Kupfer).

The second part of the manual admits plenty of space for publishing the norms in constructing r.c. structures (H. Goffin). A special chapter is devoted to the problems concerning the construction of the r.c. projects (G. Kühn), as well as the impermeable concrete structures (R. Linder); this latter treated in this form is published for the first time by the Beton-Kalender.

The chapter treating of the bridge building, disregarding the changes which took place in the meantime, has been dealt with also in earlier volumes (H. Bechert). In turn, a completely new and comprehensive chapter deals with the problems of the construction of reservoirs which involves all of the questions of reservoir construction and offers a particularly valuable information to the designer (E. Hampe); the publishing of

BOOK REVIEWS

this subject matter serves the public interest.

The authors of the different chapters of the Beton-Kalender are prominent persons of the respective profession who fulfilled their tasks with great care and an excellent pedagogic gift under the leading of the famous editor Prof. G. Franz. The rich subject matter of the manual is accompanied by numerous instructive figures and many tables which upgrade to a great extent the usefulness of the work.

After all, it can be laid down as a fact that the 75th volume of the Beton-Kalender truly mirrors the current situation of the science and practice on r.c.; it is an indispensable aid to the practitioners in r.c. construction which, owing to the richness of its content and up-to-dateness, might lay claim to a wide range interest not only in the own country of the editor but also in the international professional field.

Anton Joan: Cavitatia

Vol. II. Editura Academiei București 1985. 720 pages

After the publication of the first Volume, this voluminous second one followed with surprising promptness.

The contents of Volume II are: 1. Functioning of airfoil (either single or cascade) in the cavitation or supercavitation regime. 2. Cavitation of liquid flow past non airfoil obstacles. 3. Cavitation in pipes and flow measuring devices. 4. Cavitation in closing and control units and liquid distributors. 5. Cavitation in hydraulic turbines. 6. Cavitation in pumps. 7. Cavitation in reversible and radial-axial machines. 8. Cavitation on marine propellers. 9. Cavitation in bearings. 10. Cavitation in hydro-technical constructions. 11. Ultrasonic cavitation employed in various domains. 12. Cavitation in unconventional technological operation of material processing. 13. Cavitation in the blood circulatory system. 14. Contents in English and in Russian.

The extent of the different chapters are in good agreement with the importance of the subjects, e.g. the cavitation in hydraulic turbines and the cavitation in pumps are the longest chapters (202 and 148 pages, respectively). A good addendum to these chapters is the following one dealing with the cavitation in reversible and radial-axial machines. These chapters constitute excellent comprehensive treatment of the subjects.

BOOK REVIEWS

The good theoretical basis, the clear treatment of the problems, the numerous figures, diagrams and illustrations, the carefully selected plentiful bibliography are the good points of the book.

Further merit of the book is that the peripheral questions of the cavitation research, i.e. cavitation in chemistry and biology, cavitation in cryogenic liquids, abrasive cavitation processing, cavitation in the blood circulatory system etc. are methodically elaborated.

After close examination of the book it can be ascertained with pleasure that this large scale work of professor Anton is the first comprehensive treatise of cavitation research activity.

To promote the cavitation research activity, it is desirable to publish this excellent work in English, completed with author and subject indexes specifying the origin of the figures, diagrams and illustrations as well.

J.J. Varga

M. Herpy – J.C. Berka: Active RC Filter Design

Akadémiai Kiadó, Budapest 1986, 306 pages

The German edition of this book has already been reviewed in Acta Technica. The review is republished now because the English translation of the successful book has been issued together with Elsevier Science Publishers B.V.

Dr.-Ing. M. Herpy, author of the successful book "Analog Integrated Circuits" has undertaken to sum up the design of active filter networks with a co-author. Using their ten year industrial and educational experiences they had written a book that is useful for both the students in higher education and practical experts.

The book begins with a summary of network theory (1. Introduction, 2. Description of filter-networks). It is followed by a survey of the approximation of amplitude characteristics and group-delay characteristics (3. Approximation). The Active RC filter networks are discussed comprehensively in the 4th chapter (4. Synthesis of active RC filters). The 5th chapter discusses sensitivity and tolerances in detail. The most useful circuits of the vast family of biquadratic sections are evaluated on a common basis in the 6th chapter. A summary of the steps of the design procedure, with a view on the most important practical issues, such as dynamic range,

BOOK REVIEWS

measurements and tuning, follows. Actual filter design is demonstrated by 6 carefully worked out examples. Design formulas for 16 different second order sections and 2 different third order sections are discussed in a separate chapter. Diagrams and tables offer easy access to the most important catalogue data of filter design. The book ends with a rich bibliography and subject index.

The present edition is a revised version of a book originally published in Hungarian, in 1981. This explains some strong references to results obtained in Hungary.

In short, the book "Active RC Filter Design" discusses the cascade synthesis of RC filters in a remarkably concise and systematic way. It can warmly be recommended as a very good reference book to a wide circle of research, design and production specialists.

K. Géher

Wischers, B. (Editor): Betontechnische Berichte 1984/85.
Beton-Verlag GmbH, Düsseldorf 1986

The Betontechnische Berichte is a series of books, which contain papers published in the German periodical "beton" dealing with the actual problems and scientific results in the field of concrete techniques achieved in the Forschungsinstitut der Zementindustrie in Düsseldorf (Research Institute of the Cement-Industry in Düsseldorf) concerning the problems and professional work of the Verein Deutscher Zementwerke (VDZ) (Association of German Cement-Works). This volume contains the papers published in the years 1984 and 1985, and is the 24th book of the series. It contains six papers.

The general subject of this volume are the rheological properties of fresh concrete.

The first paper, written by J. Bonzel and J. Krell, discusses the assessment of the consistency in fresh concrete. Many different procedures have been developed to determine the consistency of fresh concrete, each procedure evaluating the various aspects of the workability in a different way. The paper deals with four kinds of procedures. Recommendations on the suitability and the potential application range of the various consistency test methods are given for construction practice.

The theme of the paper worked out by F.W. Locher, W. Rechenberg and

S. Sprung is concrete after a 20-year action of lime-dissolving carbonic acid. Water with a content of more than 60 mg CO_2/ℓ is very strongly aggressive according to DIN 4030, but for the determination of the limit values according to which the corrosive action is to be appreciated there were only a few older experiences available. Authors carried out a long-time test in which the test pieces were stored in a very strongly aggressive water. The conclusion of the research work was that dense concrete with an aggregate, which is insoluble in acids, may resist the attack of water with a content of up to 100 mg of lime-dissolving carbonic acid per liter without any protection.

Test-related influences on concrete flow determination is the theme of the paper of H. Grube and J. Krell. The spreading method of consistency tests is well suitable for the high-flow and wet concretes generally used on building sites. The research work carried out by authors evaluated the apparatus-dependent and test-dependent influence factors of the final test results. This led to recommendations for the avoidance of mistakes and the improvement of the uniformity of this consistency test method.

The paper of J. Bonzel and M. Schmidt treats the influence of distribution and orientation of steel fibres on the quality of steel fibre concrete. If steel fibres are not distributed proportionally in concrete and they are not orientated in all directions, the bearing behaviour of concrete will not be improved definitely. Authors made extensive investigations in which the effect of distribution, the orientation of fibres on properties of steel fibre concrete of different compositions have been studied. The test results showed that the steel fibres are mainly oriented vertically to the direction of concreting and that the properties of hardened concrete can only be improved essentially at this level by the addition of steel fibres.

The next paper is a report of the committee for fresh concrete of VDZ on the development of stiffening of concrete. This is an important problem, when placing of concrete happens after a longer period, using ready-mixed concrete. The paper informs on the investigation performed on the influence of cement on the rheological properties of cement paste. The investigation, and especially practice, have shown that composition and treatment of concrete as well as other factors have an influence on the development of stiffening of concrete with a given cement. The investigations

BOOK REVIEWS

achieved many results, but a systematic description of the problem is still lacking.

The sixth paper, written by J. Krell, discusses the influence of chemical and mineral reactions of cement on the development of cement paste and concrete stiffening. The subject of the paper is a part-problem of that of the previous one and handles the influencing of the consistency of the concrete mixture by chemical and mineral reactions of cement with the mixing water and by adding calcium sulphate as setting and hardening control agent. This paper also concludes that no exact statements can be deduced from the experiment.

Though each paper of this and the former volumes contain independent conclusions, the series of the volumes of *Betontechnische Berichte* also serves as a useful, general book of reference.

T. Gyengő

NOTICE TO CONTRIBUTORS

Papers in English* are accepted on condition that they have not been previously published or accepted for publication.

Manuscripts in two copies (the original type-written copy plus a clear duplicate one) complete with figures, tables, and references should be sent to

Acta Technica
Münnich F. u. 7. I. 111 A
Budapest, Hungary
H-1051

Although every effort will be made to guard against loss, it is advised that authors retain copies of all material which they submit. The editorial board reserves the right to make editorial changes.

Manuscripts should be typed double-spaced on one side of good quality paper with proper margins and bear the title of the paper and the name(s) of the author(s). The full postal address(es) of the author(s) should be given in a footnote on the first page. An abstract of 50 to 100 words should precede the text of the paper. The approximate locations of the tables and figures should be indicated on the margin. An additional copy of the abstract is needed. Russian words and names should be transliterated into English.

References. Only papers closely related to the author's work should be referred to. The citations should include the name of the author and/or the reference number in brackets. A list of numbered references should follow the end of the manuscript.

References to periodicals should mention: (1) name(s) and initials of the author(s); (2) title of the paper; (3) name of the periodical; (4) volume; (5) year of publication in parentheses; (6) numbers of the first and last pages. Thus: 5. Winokur, A., Gluck, J.: Ultimate strength analysis of coupled shear walls. *American Concrete Institute Journal* 65 (1968), 1029-1035.

References to books should include: (1) author(s) name; (2) title; (3) publisher; (4) place and year of publication. Thus: Timoshenko, S., Gere, J.: *Theory of Elastic Stability*. McGraw-Hill Company, New York, London 1961.

Illustrations should be selected carefully and only up to the necessary quantity. Black-and-white photographs should be in the form of glossy prints. The author's name and the title of the paper together with the serial number of the figure should be written on the back of each print. Legends should be brief and attached on a separate sheet. Tables, each bearing a title, should be self-explanatory and numbered consecutively.

Authors will receive proofs which must be sent back by return mail.

Authors will receive 50 reprints free of charge.

*Hungarian authors can submit their papers also in Hungarian.

Periodicals of the Hungarian Academy of Sciences are obtainable
at the following addresses:

AUSTRALIA

C.B.D. LIBRARY AND SUBSCRIPTION SERVICE
Box 4886, G.P.O., Sydney N.S.W. 2001
COSMOS BOOKSHOP, 145 Ackland Street
St. Kilda (Melbourne), Victoria 3182

AUSTRIA

GLOBUS, Höchstädtplatz 3, 1206 Wien XX

BELGIUM

OFFICE INTERNATIONAL DE LIBRAIRIE
30 A venue Marnix, 1050 Bruxelles
LIBRAIRIE DU MONDE ENTIER
162 rue du Mindi, 1000 Bruxelles

BULGARIA

HEMUS, Bulvar Ruszki 6, Sofia

CANADA

PANNONIA BOOKS, P.O. Box 1017
Postal Station "B", Toronto, Ontario M5T 2T8

CHINA

CNPICOR, Periodical Department, P.O. Box 50
Peking

CZECHOSLOVAKIA

MAD'ARSKÁ KULTURA, Národní třída 22
115. 66 Praha
PNS DOVOZ TISKU, Vinohradská 46, Praha 2
PNS DOVOZ TLACE, Bratislava 2

DENMARK

EJNAR MUNKSGAARD, Norregade 6
1165 Copenhagen K

FEDERAL REPUBLIC OF GERMANY

KUNST UND WISSEN ERICH BIEBER
Postfach 46, 7000 Stuttgart 1

FINLAND

AKATEEMINEN KIRJAKAUPPA, P.O. Box 128 SF-00101
Helsinki 10

FRANCE

DAWSON-FRANCE S. A., P. 40, 91121 Palaiseau
EUROPÉRIODIQUES S. A., 31 Avenue de Versailles, 78170 La Celle St. Cloud
OFFICE INTERNATIONAL DOCUMENTION ET
LIBRAIRIE, 48 rue Gay-Lussac
75240 Paris Cedex 05

GERMAN DEMOCRATIC REPUBLIC

HAUS DER UNGARISCHEN KULTUR
Karl Liebknecht-Straße 9, DDR-102 Berlin
DEUTSCHE POST ZEITUNGSVERTRIEBSAMT Straße der
Pariser Kommüne 3 4, DDR-104 Berlin

GREAT BRITAIN

BLACKWELL'S PERIODICALS DIVISION
Hythe Bridge Street, Oxford OX1 2ET
BUMPUS, HALDANE AND MAXWELL LTD.
Cowper Works, olney, Bucks MK46 4BN
COLLET'S HOLDINGS LTD., Denington Estate Wellingbo-
rough, Northants NN8 2QT
WM. DAWSON AND SONS LTD., Cannon House Folkstote,
Kent CT19 5EE
H. K. LEWIS AND CO., 136 Gower Street
London WC1E 6BS

GREECE

KOSTARAKIS BROTHERS INTERNATIONAL
BOOKSELLERS, 2 Hippokratous Street, Athens-143

HOLLAND

MEULENHOF-BRUNA B. V., Beulingstraat 2,
Amsterdam
MARTINUS NIJHOFF B.V.
Lange Voorhout 9 11, Den Haag

SWETS SUBSCRIPTION SERVICE

347b Heereweg, Lisse

INDIA

ALLIED PUBLISHING PRIVATE LTD., 13/14
Asaf Ali Road, New Delhi 110001
150 B-6 Monunt Road, Madras 600002
INTERNATIONAL BOOK HOUSE PVT. LTD.
Madame Cama Road, Bombay 400039
THE STATE TRADING CORPORATION OF INDIA LTD.,
Books Import Division, Chanralok 36 Janpath, New Delhi
110001

ITALY

INTERSCIENTIA, Via Mazzè 28, 10149 Torino
LIBRERIA COMMISSIONARIA SANSONI, Via Lamarmora 45,
50121 Firenze
SANTO VANASIA, Via M. Macchi 58
20124 Milano
D. E. A., Via Lima 28, 00198 Roma

JAPAN

KINOKUNIYA BOOK-STORE CO. LTD.
17-7 Shinjuku 3 chome, Shinjuku-ku, Tokyo 106-91
MARUZEN COMPANY LTD., Book Department, P.O. Box
5050 Tokyo International, Tokyo 100-31
NAKUA LTD. IMPORT DEPARTMENT
2-30-19 Minami Ikebukuro, Toshima-ku, Tokyo 171

KOREA

CHULPANMUL, Phenjan

NORWAY

TANUM-TIDSKRIFT-SENTRALEN A.S., Karl Johansgatan
41 43, 1000 Oslo

POLAND

WEGIERSKI INSTYTUT KULTURY, Marszałkowska 80,
00-517 warsawa
CKP-I W, ul. Towarowa 28, 00-958 Warszawa

ROUMANIA

D.E.P., Bucuresti
ILEXIM, Calea Grivitei 64-66, Bucuresti

SOVIET UNION

SOJUZPECHAT IMPORT, Moscow
and the post offices each town
MEZHDUNARODNAYA KNIGA, Moscow G-200

SPAIN

DIAZ DE SANTOS, Lagasca 95, Madrid 6

SWEDEN

GUMPERS UNIVERSITETSBOKHANDL AB
Box 346, 40125 Göteborg 1

SWITZERLAND

KARGER LIBRI AG, Petersgraben 31, 4011 Basel

USA

EBSCO SUBSCRIPTION SERVICES
P.O. Box 1943, Birmingham, Alabama 35201
F.W. FAXON COMPANY, INC.
15 Soutwest Park, Westwood Mass. 02090
READ-MORE PUBLICATIONS, INC.
140 Cedar Street, New York, N.Y. 10006

YUGOSLAVIA

JUGOSLOVENSKA KNJIGA, Terazije 27, Beograd
FORUM, Vojvode Mišića 1, 21000 Novi Sad

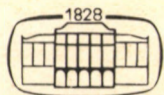
ACTA TECHNICA

ACADEMIAE SCIENTIARUM HUNGARICAE

EDITOR: P. MICHELBERGER

VOLUME 99

NUMBERS 3—4



AKADÉMIAI KIADÓ, BUDAPEST 1986

ACTA TECHN. HUNG.

ACTA TECHNICA

A JOURNAL OF THE HUNGARIAN ACADEMY OF SCIENCES

EDITORIAL BOARD

K. GÉHER, P. MICHELBERGER, J. PROHÁSZKA, T. VÁMOS

MANAGING EDITORS

P. CSONKA, GY. CZEGLÉDI

Acta Technica publishes original papers, preliminary reports and reviews in English, which contribute to the advancement of engineering sciences.

Acta Technica is published by

AKADÉMIAI KIADÓ

Publishing House of the Hungarian Academy of Sciences
H-1450 Budapest, Alkotmány u. 21.

Subscription information

Orders should be addressed to

KULTURA Foreign Trading Company
H-1389 Budapest P.O. Box 149

or to its representatives abroad

Acta Technica is abstracted/indexed in Applied Mechanics Reviews, Current Contents-Engineering, Technology and Applied Sciences, GeoRef Information System, Science Abstracts.

© Akadémiai Kiadó, Budapest

CONTENTS

<u>Chhangani, O.P.-Lenkei, P.:</u> Graphical presentation of compressive membrane action in one-way slabs	221
<u>Chhangani, O.P.-Lenkei, P.:</u> Short-time deflections of two-way slabs .	233
<u>van Dac, Iran:</u> On the dynamics of a man-machine system	249
<u>Ecsedi, I.:</u> Bounds of the numerical value of rotational flexibility .	273
<u>Füzy, J.:</u> Simulation of the timber lattice shell without "in-plane" shear capacity by double-layer cosserat surface	287
<u>Kalishky, S.-Knébel, I.:</u> Optimum design of plastic bar structures for shakedown and dynamic loading	297
<u>Kämpfe, B.-Michel, B.:</u> A new approach to X-ray diffraction analysis of stress states in surface layers	313
<u>Kollár, L.P.:</u> Buckling analysis of coupled shear walls by the multi-layer sandwich model	317
<u>Risteski, Ice B.:</u> Mathematical method for determination of thermal contact resistance between solidifying metal and mold	333
<u>Szidarovszky, J.:</u> The analysis of single-cell box beams by the hinged model	349
<u>Szidarovszky, J.:</u> Cross sectional characteristics of single-cell box beams with a cross section of rectangular elements	383
<u>Szidarovszky, J.:</u> Relationship between Saint-Venant's principle and Bernoulli-Navier's theorem as well as Bredt's formulae and warping	397
<u>Vásárhelyi, A.-Lógó, J.:</u> Design of steel frames by multicriterion optimization	413
BOOK REVIEWS	
<u>Horváth, K.Z.:</u> The selection of load-bearing structures for buildings	419
<u>Márkus, Gy.:</u> Kreis- und Kreisringplatten unter periodischer Belastung	420

<u>Reinelt, G.:</u> 'The Linear Ordering Problem: Algorithms and Applications'	421
<u>Vértes, Gy.:</u> Structural Dynamics	422

GRAPHICAL PRESENTATION OF COMPRESSIVE MEMBRANE ACTION IN ONE-WAY SLABS

Chhangani, O.P.* and Lenkei, P.**

(Received: 25 April 1986)

A graphical procedure is presented for the rigid plastic slab with linear elastic horizontal restraint. The flow theory approach was used to develop an equation to determine the compressive membrane force for small deflections. Thus the effect of linear elastic horizontal boundary restraint upon the load carrying capacity of the one-way slab has been demonstrated. The equation developed shows that the parameters affecting the membrane action are those affecting the yield criterion and boundary restraint. The graphical presentation shows the load-enhancement to be expected from the compressive membrane action for one-way slab in the range of small deflections.

1. INTRODUCTION

It is a well known fact that the load carrying capacity of reinforced concrete slab with a horizontal restraint at the boundaries may be greater than the capacity of a similar unrestrained slab.

This behaviour can be attributed to the fact that in pure bending of reinforced concrete, with small steel proportions, the neutral axes at failure are very close to the surface and bending is accompanied by lateral displacement at either of the supports. If these deformations are incompatible with the support conditions, no bending collapse will occur. As the slab deflects, changes of the geometry cause the slab edges to tend to move outward and to react against the boundary elements. This action will induce compressive membrane forces in the range of small deflections which will enhance the flexural strength of the slab sections. This will cause the ultimate load of the slab to be greater than the ultimate load calculated using Johansen's yield line theory.

* Chhangani, O.P., Research scholar on leave from India

** Prof. Dr. P. Lenkei, Division Director, Hungarian Institute for Building Science, Budapest, Hungary

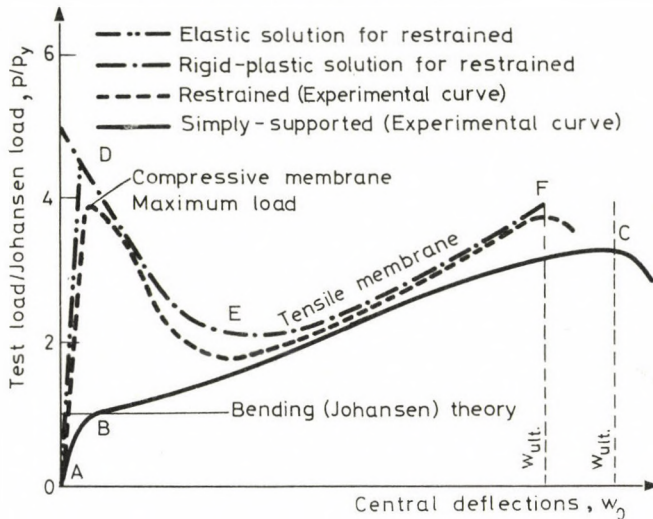


Fig. 1. Typical load deflection diagram

Figure 1 shows a typical load parameter p against a typical deflection parameter, w_0 . At the maximum load, crushing of the concrete in compression zone will occur and immediately the load carried by the slab decreases rapidly. This is sometimes referred to as the "snap through" phase. At the failure as the slab snaps through, the load drops as the neutral axis moves toward the surfaces and the compressive membrane force decreases. At this stage of minimum load the slab may be cracked right through its thickness in the middle and tensile membrane forces start to form in the central region. In case the reinforcement is sufficiently ductile, the load may then again start rising. The maximum load is precisely due to compressive membrane action. This behaviour or phenomenon is termed sometimes as "arching action" or "dome effect".

Recently two very interesting literature reviews have been published by Desayi and Kulkarni /2/ and another historical review by Braestrup /1/. In his historical review, he has classified the entire work under two categories:

- (i) deformation theory and
- (ii) flow theory.

The difference in these theories lies in the definition of strains.

MEMBRANE ACTION IN ONE-WAY SLABS

In the deformation theory, the total strains in the material are used whereas in the flow theory, the strain increments are considered.

The concept is here further generalized on the basis of flow theory considerations. Further, the axial stiffness of slab and its boundary restraints have been modelled by horizontal elastic springs. The complete behaviour of a rigid-perfectly-plastic one-way spanning partially restrained slab is analyzed by flow theory.

Recently Eyre and Kemp /3/ have presented a graphical solution for predicting membrane action for one-way spanning restrained slab.

DESCRIPTIVE MODEL

A uniformly loaded one-way spanning continuous slab and its ends modelled by horizontal linear elastic springs are shown in Fig. 2.

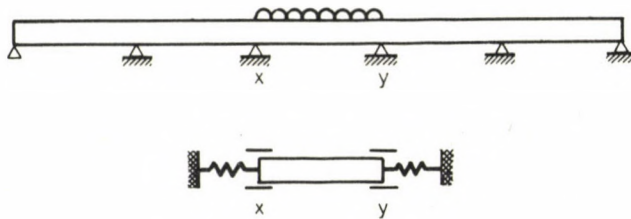


Fig. 2. Continuous slab and a model of a continuous one-way spanning slab

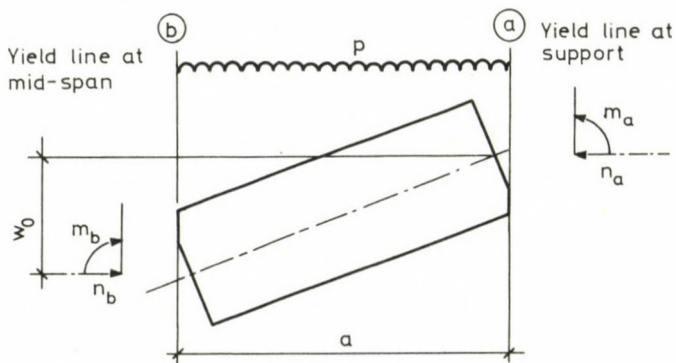


Fig. 3. Deformation of half strip

To be more general, we consider that the reinforcements at the mid-span and at the supports are different. Figure 3 shows the failure mode of the slab if it failed when flexural plastic hinges would form at the mid-span and supports, and the collapse load would be equal to Johansen load, i.e., yield line theory value p_y .

The effect of the partial restraint at the supports will delay the increase in the collapse load until the slabs starts jamming against the surroundings. Then the load will increase to some value p which will be higher than the Johanson load p_y .

3. YIELD CRITERION OF ONE-WAY SPANNING SLAB

The yield criterion, assuming the reinforcement and concrete both as rigid-perfectly-plastic, for a single reinforced concrete section was first given by Wood /5/ in the non dimensional parabolic form

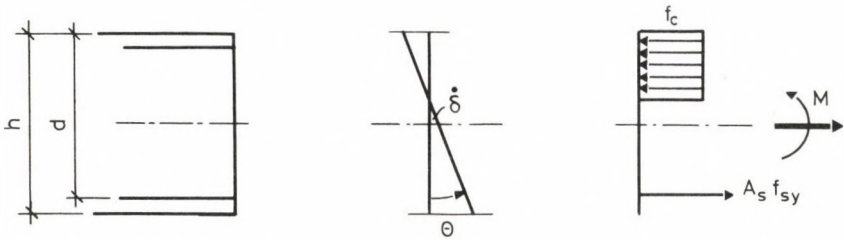


Fig. 4. Stress-strain diagram of the section

$$\text{for } \dot{\theta} < 0; \quad f(m,n) = -\frac{m_a}{m_u} - 1 - \alpha_2 \left(\frac{n_a}{n_0}\right) + \beta_2 \left(\frac{n_a}{n_0}\right)^2 \leq 0 \quad (1)$$

$$\dot{\theta} > 0; \quad f(m,n) = +\frac{m_b}{m_u} - 1 - \alpha_1 \left(\frac{n_b}{n_0}\right) + \beta_1 \left(\frac{n_b}{n_0}\right)^2 \leq 0 \quad (2)$$

where

$$\alpha = \frac{\frac{h}{2} - h_0}{z_0} = \frac{\frac{h}{2d} - 2 \frac{1 \cdot 1 f_{sy} \epsilon}{f_{cu}}}{1 - \frac{1 \cdot 1 f_{sy} \epsilon}{f_{cu}}} \quad (3)$$

MEMBRANE ACTION IN ONE-WAY SLABS

and

$$\beta = \frac{h_o}{2z_o} = \frac{\frac{1 \cdot l f_{sy} \rho}{f_{cu}}}{1 - \frac{1 \cdot l f_{sy} \rho}{f_{cu}}} \quad (4)$$

α and β can be calculated for the different percentage of steel at support and mid-span using Eqs /3/ and /4/.

The yield force of tension steel \bar{n}_o at support and n_o at mid-span can be calculated from the following equations if the effective cover and yield stress of the steel is same at both of these places:

$$\bar{n}_o = \rho_a d f_{sy} , \quad (5a)$$

and

$$n_o = \rho_b d f_{sy} . \quad (5b)$$

It must be kept in mind that this type of yield criterion is valid for moments and axial forces acting in any direction relative to the reinforcement directions and is independent of the moments and axial forces acting transversely to the slab section; in other words this criterion is of square yield type.

4. KINEMATICAL EQUATION

If the elastic deformations had to be taken into consideration, then the physical gap at the boundaries or possible elastic deformations must be overcome before the slab reaches the unrestrained collapse load. This means that the membrane action will start at some nonzero initial deflection of the slab. This can be achieved by replacing the lateral support by a boundary linear elastic spring, the flexibility of which includes the contribution by the in-plane flexibility of the slab. However, lumping of boundary flexibilities into a single parameter of linear elastic spring stiffness is a crude approximation of the real behaviour. Furthermore, this theory is being developed on yield line collapse mechanism and will not be suitable for the slab that assumes totally different deflected shape in the elastic range.

Figure 5 shows half of the slab strip of length a failing plastically under a load p with central deflection w_o , the geometrical equation of

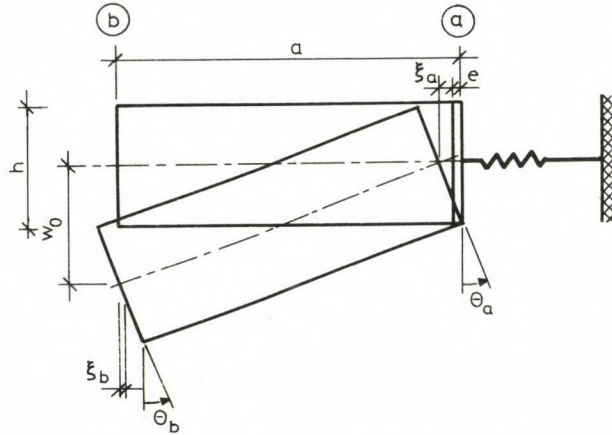


Fig. 5. Modelled half strip

this pattern of deflection being:

$$(a + \xi_a + \xi_b + e)^2 = a^2 + w_0^2, \quad (6)$$

neglecting higher order terms, this will reduce to

$$\xi_a + \xi_b + e = \frac{w_0^2}{2a}. \quad (7)$$

For flow theory approach, the compressive strain remains compressive as long as the compressive strain is increasing in magnitude.

This means that we are looking for the axis of instantaneous rotation of the section. To obtain this, we differentiate the geometrical equation /7/ with respect to time:

$$\dot{\xi}_a + \dot{\xi}_b + \dot{e} = \frac{w_0 \dot{w}_0}{a}, \quad (8)$$

other kinematic equations are

$$\dot{\theta}_a = -\frac{\dot{w}_0}{a}; \quad \dot{\theta}_b = \frac{\dot{w}_0}{a} \quad (9)$$

where $\dot{\theta}_a$ and $\dot{\theta}_b$ are rigid-plastic rotations.

5. GENERAL EQUATION FOR MEMBRANE ACTION

If the yield criterion is

$$f(m, n) = 0, \quad (10)$$

then the plastic flow of the section will start. The flow rule (the normality law) applied to the yield condition gives:

$$\dot{\kappa} = \dot{\theta} = \frac{\lambda \partial f(m, n)}{\partial m} = \text{curvature strain}, \quad (11)$$

$$\dot{\epsilon} = \dot{\xi} = \frac{\lambda \partial f(m, n)}{\partial n} = \text{extension strain} \quad (12)$$

where λ is an arbitrary non-negative scalar factor.

Using yield conditions defined in Eqs (11) and (12) we obtain

$$\dot{\theta}_a = \lambda \left(\frac{\partial f}{\partial m_a} \right) = - \lambda \left(\frac{1}{\bar{m}_u} \right), \quad (13)$$

$$\dot{\xi}_a = \lambda \left(\frac{\partial f}{\partial n_a} \right) = \lambda \left[- \frac{\alpha 2}{\bar{n}_0} + 2 \beta_2 \frac{n_a}{\bar{n}_0^2} \right]. \quad (14)$$

Combining these two equations, we get

$$\dot{\xi}_a = - \bar{m}_u \dot{\theta}_a \left[- \frac{\alpha 2}{\bar{n}_0} + 2 \beta_2 \frac{n_a}{\bar{n}_0^2} \right]. \quad (15)$$

Similarly we obtain this relationship for mid-span

$$\dot{\xi}_b = \bar{m}_u \dot{\theta}_b \left[- \frac{\alpha 1}{\bar{n}_0} + 2 \beta_1 \frac{n_b}{\bar{n}_0^2} \right] \quad (16)$$

Here we introduce the constitutive equation for the linear spring and further modify it to obtain instantaneous elongation,

$$e = \frac{n_a}{S}, \quad \text{or} \quad \dot{e} = \frac{\dot{n}_a}{S} \quad (17)$$

Finally, two static equations are developed for horizontal force and moment equilibrium respectively. For horizontal force equilibrium we obtain

$$n_a = n_b, \quad (18)$$

For moment at the support, we obtain another moment equilibrium equation:

$$\frac{p \cdot a^2}{2} = -m_a + m_b - n_b w_0. \quad (19)$$

With Eqs (1), (2), (8) and (13) through (19), the whole problem can be described. For the solution of these equations, Eqs (15) to (18) are substituted into Eq. (8). Applying Eqs (9) and (18), this results in a first order differential equation for the membrane action:

$$\frac{\bar{m}_u \dot{w}}{a} \left[-\frac{\alpha 2}{\bar{n}_0} + 2\beta \frac{n_a}{\bar{n}_0 2} \right] + \frac{m_u \dot{w}_0}{a} \left[-\frac{\alpha 1}{n_0} + 2\beta \frac{n_b}{n_0 2} \right] + \frac{n_a}{S} = \frac{w_0 \dot{w}_0}{a}. \quad (20)$$

Applying Eq. (18) we obtain:

$$\left(\frac{m_u \beta 2}{\bar{n}_0} + \frac{m_u \beta 1}{n_0} \right) 2 n_a - \left(\frac{\alpha 2 \bar{m}_u}{\bar{n}_0} + \frac{\alpha 1 m_u}{n_0} \right) + \frac{a \dot{n}_a}{S w_0} = w_0. \quad (21)$$

Using $a/s = \phi$; and replacing derivation with respect to time by derivation with respect to the deflection as done by Janas (4), we get:

$$2 B n_a - A + \phi \frac{d n_a}{d w_0} = w_0 \quad (22)$$

where

$$B = \frac{\bar{m}_u \beta 2}{\bar{n}_0 2} + \frac{m_u \beta 1}{n_0 2}, \quad (23)$$

$$A = \frac{\alpha 2 \bar{m}_u}{\bar{n}_0} + \frac{\alpha 1 m_u}{n_0}, \quad (24)$$

$$\phi \frac{d n_a}{d w_0} = w_0 + A - 2 B n_a. \quad (25)$$

MEMBRANE ACTION IN ONE-WAY SLABS

Replacing $w_0 + A - 2B n_a = t$ and differentiating this with respect to t we obtain:

$$1 - 2B \frac{d n_a}{d w_0} = \frac{d t}{d w_0} , \quad (26 a)$$

or

$$1 - \frac{2B t}{\phi} = \frac{d t}{d w_0} . \quad (26 b)$$

As a result of integrating after rearrangement of terms, we get an equation for n_a as shown below:

$$n_a = C \exp \left(-\frac{2Bw_0}{\phi} \right) - \frac{\phi}{4B^2} + \frac{w_0}{2B} + \frac{A}{2B} . \quad (27)$$

Applying the boundary condition $w_0 = 0$; $n_a = 0$ we obtain,

$$C = -\frac{A}{2B} + \frac{\phi}{4B^2} . \quad (28)$$

Eq. (27) can be rewritten as

$$n_a = C \left[\exp \left(-\frac{2B w_0}{\phi} \right) - 1 \right] - \frac{w_0}{2B} . \quad (29)$$

Once the values of normal forces n_a and n_b are known, we can calculate the moments m_a and m_b from yield condition Eqs (1) and (2) respectively. If these values are substituted again in the equilibrium equation, we will get the relationship between load p and deflection w_0 .

GRAPHICAL SOLUTION

We use the same slab example as used by Eyre and Kemp /3/. This unit width of a one-way spanning slab, partially built in at the ends, is required to carry a total distributed load of 10.6 kN/m^2 on the slab over a span of 4 m. The following data are taken from the same example:

$$f_{cu} = 35 \text{ N/mm}^2, \quad f_{sy} = 250 \text{ N/mm}^2, \quad \rho = 0.004,$$

$$h = 150 \text{ mm and } d = 120 \text{ mm}.$$

For the sake of simplicity, assume that the reinforcement and the effective concrete cover are the same at the centre and at the supports.

For positive bending, the yield criterion of Eq. (2) can be written in the following form:

$$\frac{m}{m_u} = 1 + \alpha \left(\frac{n}{n_0}\right) - \beta \left(\frac{n}{n_0}\right)^2, \quad (30)$$

and the normal force is calculated from Eq. (29).

In the case of the former example slab we get from Eqs (23) and (24),

$$B = \frac{2m_u \beta}{n_0}, \quad (31)$$

$$A = \frac{2m_u \alpha}{n_0}. \quad (32)$$

Furthermore, assume that the value of the spring stiffness is:

$$S = 5 \cdot 10^5 \text{ kN/m}.$$

If the slab is designed in accordance with the yield line theory,

$$\frac{p_y a^2}{2} = 2 m_u \quad (33)$$

From all these parameters, we can calculate normal force n for the different values of w_0 .

The equilibrium equation for this half strip can be written as follows:

$$\frac{p a^2}{2} = 2m - n w_0 \quad (34)$$

and, from Eqs (33) and (34),

$$\frac{p}{p_y} = \frac{m}{m_u} - \frac{n w_0}{2 m_u} \quad (35)$$

MEMBRANE ACTION IN ONE-WAY SLABS

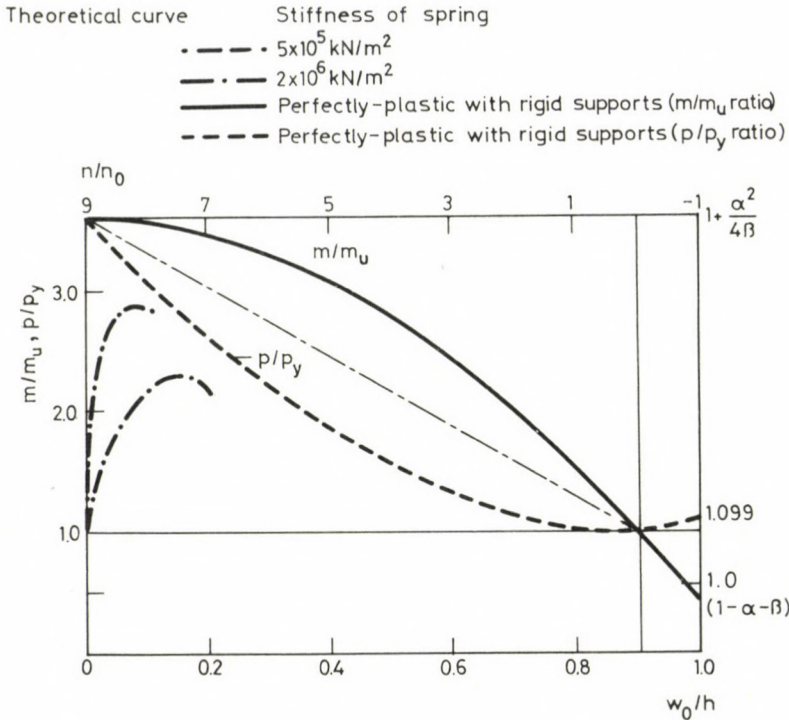


Fig. 6. Graphical plotting of the solution

The load-enhancement-deflection curve (or interaction diagram between p/p_y and w_0/h) can be plotted by means of Eqs (29), (30) and (35).

The results are illustrated in Fig. 6.

REFERENCES

1. Braestrup, M.W.: Dome effect in r.c. slabs; rigid plastic analysis, Proceedings of the ASCE, 106, No. ST 6, June (1980), 1255-1262.
2. Desayi, P.—Kulkarni, A.B.: Membrane action, deflection and cracking of two-way reinforced concrete slabs. Matériaux et constructions, 10, No. 59 (1977), 303-312.
3. Eyre, J.R. — Kemp, K.O.: A graphical solution for predicting the increase in strength of concrete slabs due to membrane action, Magazine of Concrete Research, London, England, 35, No. 124, Sept. (1983), 151-156.
4. Janas, M.: Arching action in elastic — plastic plates. J. Struct. Mechanics, 1/3/ (1973), 277-293.

CHHANGANI, O.P.—LENKEI, P.

5. Wood, R.H.: Plastic and elastic design of slabs and plates. Thames and Hudson, London 1961, 344.

SHORT-TIME DEFLECTIONS OF TWO-WAY SLABS

Chhangani, O.P.* and Lenkei, P.**

(Received: 3 November 1986)

A method to calculate short-time deflection of two-way slabs of different boundary conditions is presented. The effective moment of inertia function developed by Branson is examined and a modification of the equation proposed in ACI approach is suggested. The method presented herein considers the influence of reinforcement, material properties of both concrete and steel, and physical dimensions of the slab. Thus the deflections corresponding to cracking and service loads can easily be calculated following the equations developed for the slabs of different boundary conditions. Comparison of the method is made with the experimental studies of Hung and Nawy and the results are found to agree satisfactorily with the experimental values.

NOTATION

C_1, C_2	constants
E_c	modulus of elasticity of concrete
I_{cr}	moment of inertia of cracked section
I_g	gross moment of inertia
I_g^{meff}	modified effective moment of inertia (function)
L_x, L_y	length of slab specimen in x and y directions
M_{cr}	cracking moment
M	bending moment
X	dimensionless parameter
a, b, c, d	power coefficients
f_y	yield stress of steel
f_c	cylindrical strength of concrete
h	thickness of slab
m	power coefficient in Branson's equations
q	intensity of loading
q_{cr}	intensity of cracking load
q_j	Johansen's load
q_w	serviceability load or working load
δ	deflection of slab
$\delta_{exp}, \delta_{cal}$	experimental deflection and theoretical deflection
ζ	coefficient used as a multiplier in elastic theory to calculate deflections
$\lambda, \bar{\lambda}$	factors
ρ_x, ρ_y	percentage of reinforcement in x and y directions

* Chhangani, O.P., Research scholar on leave from India

** Prof. Dr. P. Lenkei, Division Director, Hungarian Institute for Building Science, Budapest, Hungary

INTRODUCTION

Ultimate strength is usually taken as a basis for the design of up-to-date concrete structures. The application of this procedure along with the higher strength of the construction materials permits more slender structures to be used. If a slab is designed on the basis of the strength criterion alone, the degree of safety against collapse may be adequate but at the same time the performance of the structure at the service load unsatisfactory. For this reason, the excessive deflection of structural members and systems must be included in the compliance criteria, the most important ones being strength at ultimate loads, deflection at service loads, and crack widths at service loads. Since the strength consideration alone generally results in selection of a slab depth, this leads to in-service problems, in particular, to excessive deflections in slabs.

There are some works based on empirical or semiempirical approach. Empirical approach was used by Shukla and Mittal /12/ whereas Rangan, and McMuller /11/, and Gilbert /8/ developed suitable span-depth ration formulae. The semiempirical approach presented by Desayi and Kulkarni /4, 5/ predict the load-deflection curve in the form of piecewise straight lines upto Johansen's load for restrained and simply supported slabs.

Desayi and Muthu /6, 7/ presented a method for determining load deflection curves for simply supported and restrained slabs using a decreasing moment of inertia function. Deflection is calculated in two steps. First, in the range of zero to cracking load, elastic plate theory is used while in the second step the effect of cracking is modelled by selecting a decreasing moment of inertia function.

In this work Branson's method /2, 3/ for calculating deflections has been examined and a procedure is suggested to calculate the load-deflection behaviour of two-way slabs beyond cracking.

1. DEVELOPMENT OF BRANSON'S EQUATION

In this proposed method we calculated deflections in two steps. In the first step, deflection is calculated from zero load to cracking load. In the second step, an effective moment of inertia concept is used to model the reduction in flexural rigidity of the slab along with a factor λ , to calculate deflection of the slab beyond cracking.

DEFLECTIONS OF TWO-WAY SLABS

In the first step, in the range of zero to cracking load, deflection is determined on the basis of the elastic plate theory /13/ and formulae are determined for different boundary conditions of slabs as:

$$\delta = \frac{\zeta q L_x^4}{E_c I_g} \quad (1)$$

where $q \leq q_{cr}$.

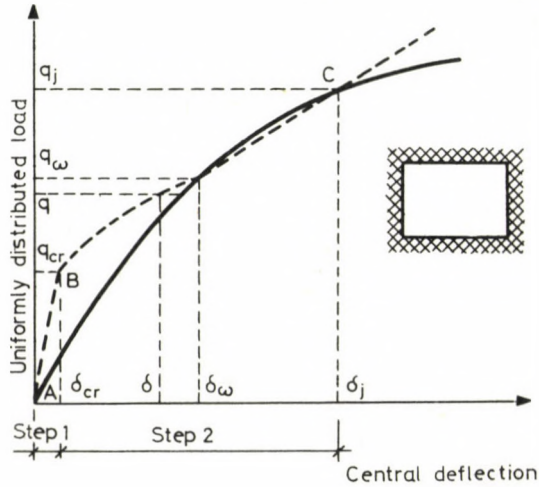


Fig. 1. Load deflection curve of two-way slabs

After the onset of cracking, the flexure rigidity decreases. To model this behaviour, the effective moment of inertia of the slab section as recommended by Branson is used in a modified form. Hence the formula for deflection for $q_j > q > q_{cr}$ will be

$$\delta = \frac{\zeta q L_x^4}{\lambda E_c I_{meff}} \quad (2)$$

where

$$I_{meff} = \left(\frac{q_{cr}}{q} \right)^m (I_g - I_{cr}) + I_{cr} \quad (3)$$

The difference between this equation and that of Branson's as recom-

mended by ACI 318 /1/ lies in the use of power coefficient m. It was found that the recommended power coefficient, 3, was not suited for use in slabs due to the higher ratio of q_{CR}/q . Furthermore, the difference between I_g and I_{CR} for slabs is considerably larger than for beams and if the stiffness is not modelled properly this may result in highly underestimated deflections.

To verify these observations, deflections for the three sets of different boundary conditions of Hung and Nawy /10/ slabs were calculated. The power coefficient of Branson's equation was varied from 1.0 to 4.0 with an increment of 0.1 and deflections were calculated at working load and at Johansen's load. The calculated deflections were compared with the experimental deflections taken from the experimental curves of Hung and Nawy. It was found that the experimental values were always higher than the computed ones even for a power coefficient by 4 in Branson's formula. As has been pointed out by Branson /3/ and observed during these calculations, Eq. (3) is not very sensitive to its power coefficient. Hence it was decided to use a power coefficient 4 in further calculations.

In addition to this a factor λ was introduced in the denominator of deflection formula as done in Eq. (2). The value of λ was determined using the experimental value of deflection at working load. The values of λ obtained for different slabs of different boundary conditions are shown in Tables 1, 2 and 3. This non-dimensional parameter was further related to the sectional and strength properties of the slab as follows:

$$\lambda = C1 \cdot X + C2 \tag{4}$$

where

$$X = (\varrho_x + \varrho_y)^a \left(\frac{f_y}{f_c} \right)^b \left(\frac{L_x}{L_y} \right)^c \left(\frac{L_x}{h} \right)^d \tag{5}$$

The power coefficients in this equation are worked out by an iterative procedure suggested by Holman /9/. During the computations, the best possible power coefficients were selected which at the same time resulted in a higher coefficient of correlation with equation (4). The procedure of calculations outlined above is shown in the flow chart in Fig. 2.

Now formulae for three different sets of slabs of different boundary conditions are developed. Their results are compared with the experimental values. The theoretical curves obtained are superimposed on the experimental curves for comparison.

DEFLECTIONS OF TWO-WAY SLABS

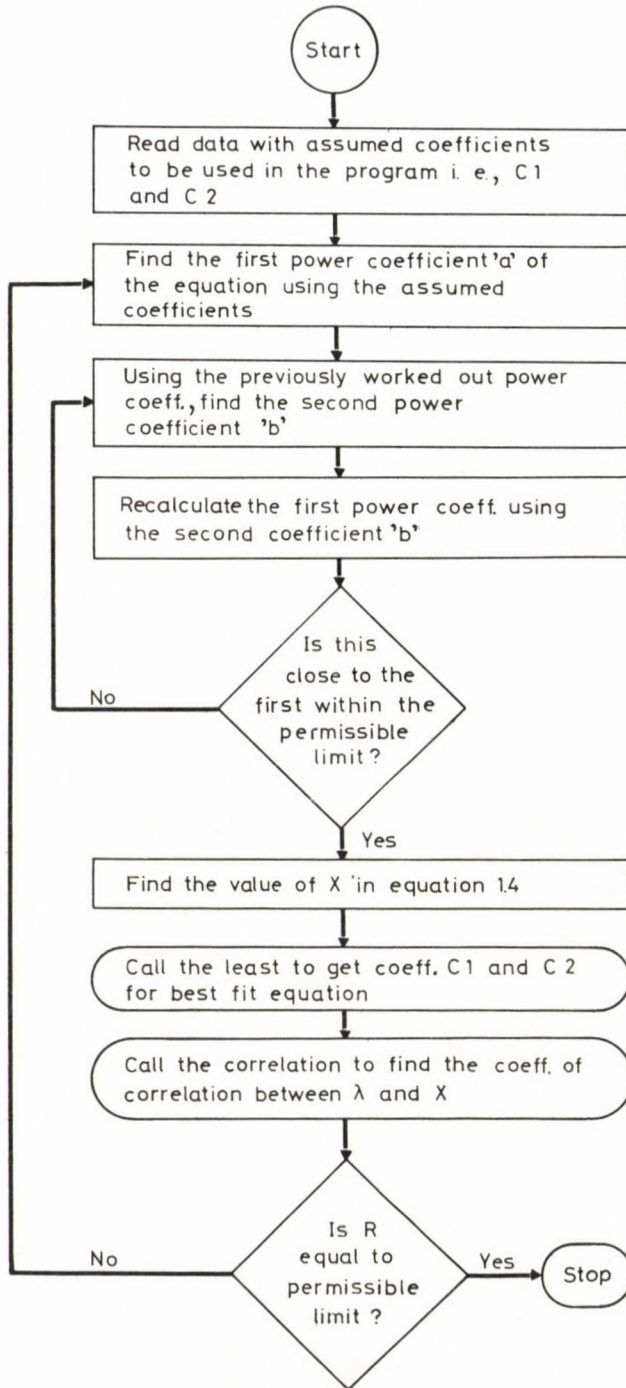


Fig. 2. Flow chart

2. EXAMPLE: SLABS, WITH ALL THE FOUR SUPPORTS BUILT IN

For C1 and C4 of series of slabs of Hung and Nawy, /10/ the following equations were obtained after analysis of their data on the basis of the principle explained in the preceding part:

$$\lambda = 1.2031 \cdot 10^{-3} X + 0.0997 , \quad (6)$$

or approximately

$$\lambda = 1.2 \cdot 10^{-3} X + 0.1 \quad (6 a)$$

where

$$X = (\varphi_x + \varphi_y)^{0.20} \left(\frac{f_{sy}}{f'_c} \right)^{0.0279} \left(\frac{L_x}{L_y} \right) \left(\frac{L_x}{h} \right)^2 , \quad (7)$$

or approximately

$$X = (\varphi_x + \varphi_y)^{0.2} \left(\frac{f_{sy}}{f'_c} \right)^{0.028} \left(\frac{L_x}{L_y} \right) \left(\frac{L_x}{h} \right)^2 . \quad (7 a)$$

Figure 3 shows the variation of λ with X , the coefficient of correlation of Eq. (6) being 0.84.

Using equations (2), (3), (6) and (7), the deflection at an intensity of $q_j > q > q_{Cr}$ can be calculated. The deflection at $q = q_{Cr}$ was also calculated using factor λ .

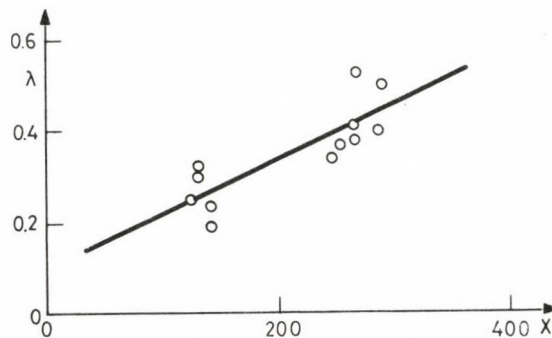


Fig. 3. Variation of λ with x

DEFLECTIONS OF TWO-WAY SLABS

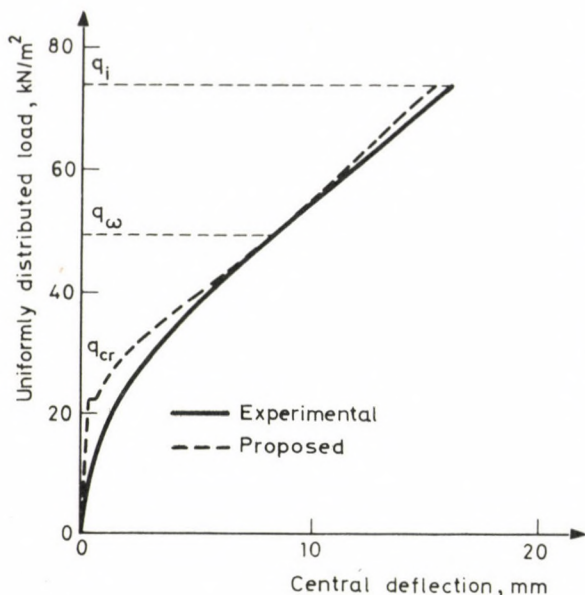


Fig. 4. Load deflection curve of slab C1-2

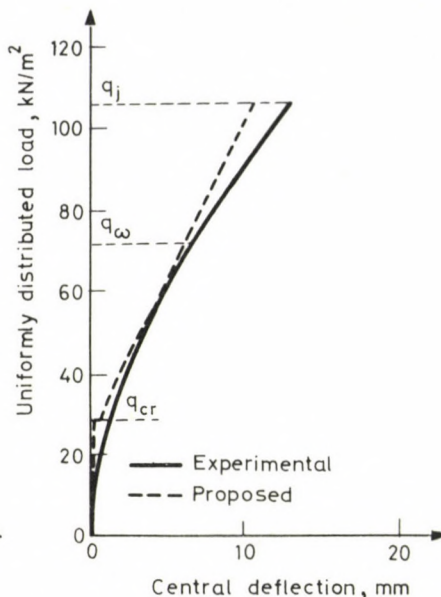


Fig. 5. Load deflection curve of slab C4-1

The calculated deflections have been compared with the experimental values and the results are tabulated in Table 1 as the ratio of experimental values to the computed values. The mean value and the coefficient of variation at working load are 1.026 and 16.5 % respectively. At Johansen's load, these values are 1.193 and 25.77 % respectively. It can be seen that the proposed method gives good results at working load but the coefficient of variation is somewhat higher at Johansen's load.

It was observed during the calculation that near Johansen's load, the effective moment of inertia was almost equal to the cracked moment of inertia due to the very small ratio of q_{cr}/q in Eq. (3). However, if we want to improve the results at this stage, we can formulate another factor $\bar{\lambda}$ and the value of this can be calculated using the experimental value of deflection at Johansen's load. The proposed equations (4) and (5) can be developed for deflection at load intensity $q_j > q > q_w$. However, in practice, the situation at working load is more important than at Johansen's load. Hence it was decided to use the proposed formulae only.

Figures 4 and 5 show the comparison of curves developed on the basis of the proposed method and experimentally. The proposed curve is shown in

Table 1. Comparison of deflections for the sets C1 and C4 of slabs

Slab	Properties	λ	X	Ratio of experiment to computed deflection	
				At working load	At Johansen's load
C1-1	Square (Isotropic)	0.504	291.22	0.910	1.80
C1-2		0.413	264.72	1.011	1.020
C1-3		0.372	252.76	1.082	1.091
C1-4		0.345	244.10	1.153	1.033
C1-5		0.387	265.56	1.086	1.025
C1-6		0.524	268.38	0.807	1.176
C1-7		0.404	287.02	1.101	1.753
C4-1	Rectangular (Isotropic)	0.234	141.31	1.137	1.353
C4-2		0.253	123.22	0.979	0.292
C4-3		0.192	142.52	1.414	1.4076
C4-4		0.320	130.10	0.799	0.841
C4-5		0.308	130.07	0.832	0.888
			Mean	1.026	1.193
Coefficient of variation				16.5 %	25.77 %

the modified form at cracking load where the influence of factor λ is also considered.

3. EXAMPLE: SLABS WITH THE ADJACENT SUPPORTS BUILT-IN,
AND TWO SUPPORTS SIMPLY SUPPORTED

The slabs of series C3 and C6 of Hung and Nawy /10/ were used to develop the formula as explained earlier. The following equations were obtained:

$$\lambda = 3.39274 \cdot 10^{-7} \cdot X + 0.3705, \quad (8)$$

or approximately

$$\lambda = 3.39 \cdot 10^{-7} \cdot X + 0,37 \quad (8 a)$$

where

DEFLECTIONS OF TWO-WAY SLABS

$$X = (\varphi_x + \varphi_y)^{-1.8147} \left(\frac{f_{sy}}{f'_c} \right)^{-0.28253} \left(\frac{L_x}{L_y} \right) \left(\frac{L_x}{h} \right)^2, \quad (9)$$

or approximately

$$X = (\varphi_x + \varphi_y)^{-1.8} \left(\frac{f_{sy}}{f'_c} \right)^{-0.28} \left(\frac{L_x}{L_y} \right) \left(\frac{L_x}{h} \right)^2. \quad (9 a)$$

The variation of λ with X is shown in Fig. 6, the coefficient of correlation of Eq. (8) being 0.886.

Following Eqs (2), (3), (8) and (9), the deflection at an intensity of $q_j > q > q_{CR}$ can be calculated. Deflection at $q = q_{CR}$ was also modified using factor λ . Comparison of the computed and experimental values is shown in Table 2. The mean value and the coefficient of variation at working load are 1.012 and 8.64 %, respectively. At Johansen's load, these values are 1.294 and 11.67 % respectively.

Table 2. Comparison of deflections for series C3 and C4 of slabs

Slab	Properties	λ	X	Ratio of experiment to computed deflection	
				At working load	At Johansen's load
C3-1	Square (Isotropic)	0.464	2.7693×10^5	1.000	1.375
C3-2		0.381	2.4073×10^5	1.183	1.475
C3-3		0.645	9.6526×10^5	1.073	1.233
C3-4		0.682	5.5154×10^5	0.957	1.201
C3-5		0.629	5.9594×10^5	0.913	1.465
C6-1	Rectangular (Isotropic)	0.529	3.1418×10^5	0.906	1.191
C6-2		0.410	1.9858×10^5	1.073	1.398
C6-3		0.437	1.8746×10^5	0.994	1.011
			Mean	1.012	1.294
Coefficient of variation				8.64 %	11.67 %

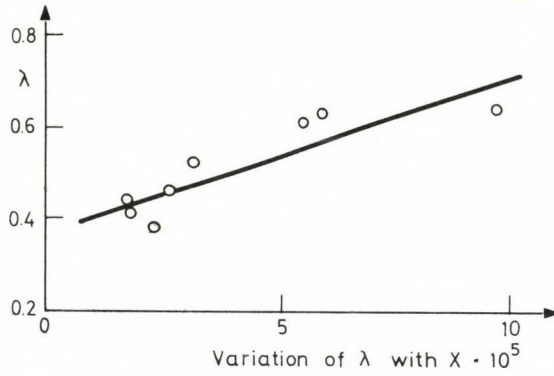


Fig. 6. Variation of λ with x

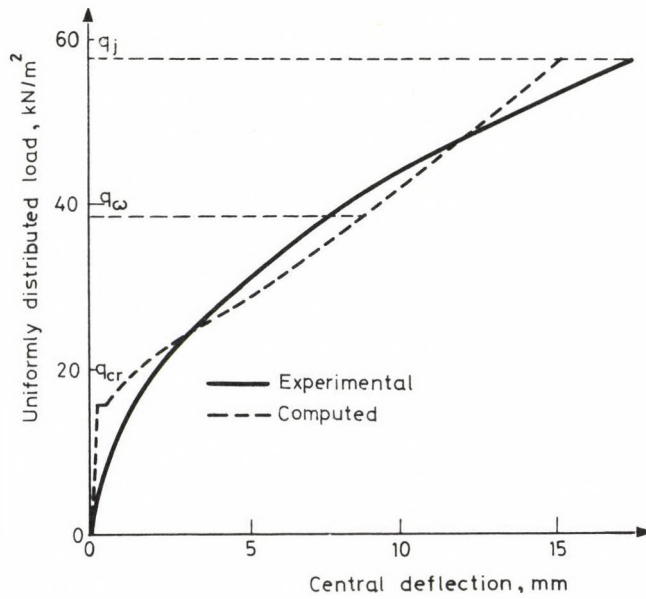


Fig. 7. Load deflection curve of slab C3-4

DEFLECTIONS OF TWO-WAY SLABS

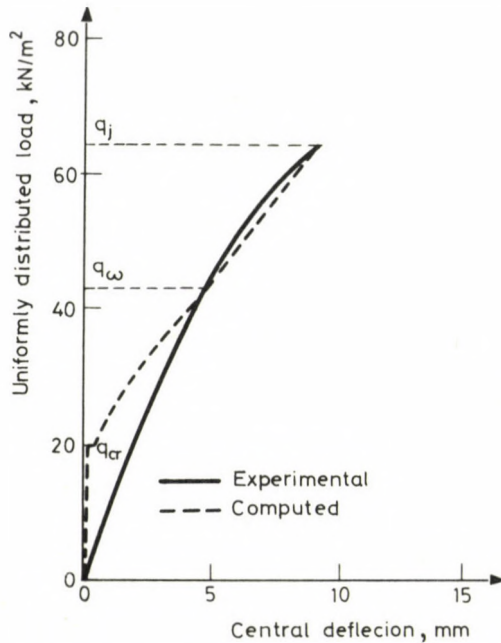


Fig. 8. Load deflection curve of slab C6-3

Figures 7 and 8 show the comparison of curves developed on the basis of the proposed method and experimentally. The proposed curve is shown in modified form at cracking load where the influence of factor λ is also considered. It can be seen that the proposed method is in close agreement with the experimental results.

4. EXAMPLE: SLABS WITH THREE SUPPORTS BUILT IN AND ONE SUPPORT SIMPLY SUPPORTED

According to the principle as explained earlier, the 9 slabs of series C2 and C5 of Hung and Nawy's /10/ experiments were examined. The following equations were found to best comply with equation (10), the coefficient of correlation being 0.76:

$$\lambda = 2.1495 \cdot 10^{-8} \cdot X + 0.2957, \quad (10)$$

or approximately,

$$\lambda = 2.15 \cdot 10^{-8} X + 0.30 \quad (10 a)$$

where

$$X = (q_x + q_y)^{-2.304} \left(\frac{f_{sy}}{f'_c} \right)^{-0.31} \left(\frac{L_x}{L_y} \right) \left(\frac{L_x}{h} \right)^2 \quad (12)$$

Figure 9 shows the variation of λ with X .

With the use of Eqs (2), (3), (10) and (12), the deflection at an intensity of $q_j > q > q_{cr}$ can be calculated. A comparison of the computed and experimental values is shown in Table 3 as the ratio of experimental values to computed values. The mean value and the coefficient of variation at working load are 1.018 and 13.16 % respectively. At Johansen's load, these values are 1.123 and 14.02 % respectively.

Table 3. Comparison of deflections for slabs sets C2 and C5

Slab	Properties	λ	X	Ratio of experiment to computed deflection	
				At working load	At Johansen's load
C2-1		0.376	1.54437x10 ⁶	0.892	1.131
C2-2		0.379	8.27125x10 ⁶	1.241	1.045
C2-3	Square	0.565	8.12909x10 ⁶	0.832	1.023
C2-4	(Isotropic)	0.364	4.18912x10 ⁶	1.051	0.994
C2-5		0.313	1.80907x10 ⁶	1.069	1.192
C5-1	Rectangular	0.360	1.42088x10 ⁶	0.913	1.072
C5-2	(Isotropic)	0.371	2.54250x10 ⁶	0.944	0.929
C5-3		0.252	5.10050x10 ⁵	1.221	1.488
C5-4		0.305	5.95167x10 ⁵	1.003	1.233
Mean				1.018	1.123
Coefficient of variation				13.16 %	14.02 %

Figures 10 and 11 show the comparison of the theoretical curves developed on the basis of the proposed method, superimposed on the experimental curves. The proposed curves are modified at cracking load where the influence of factor λ is also taken into account.

DEFLECTIONS OF TWO-WAY SLABS

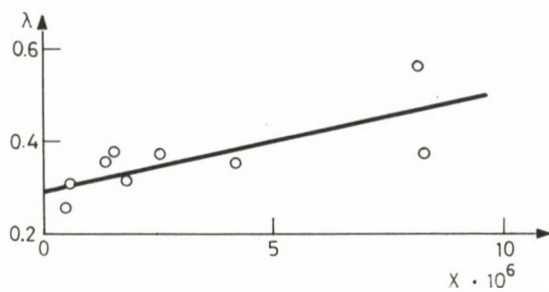


Fig. 9. Variation of λ with x

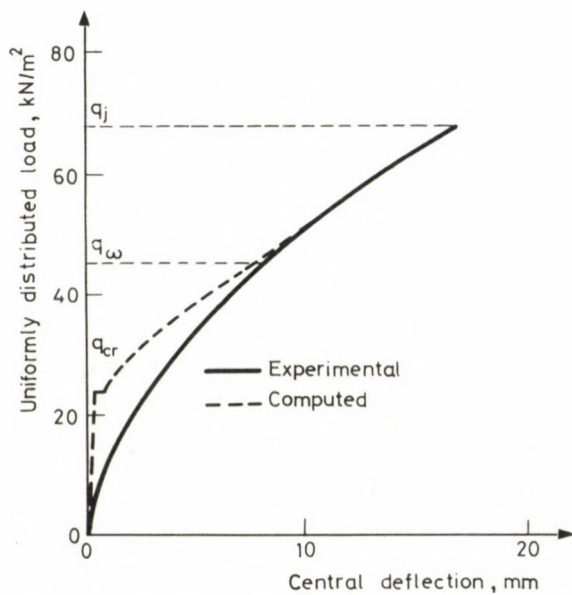


Fig. 10. Load deflection curve of slab C2-4

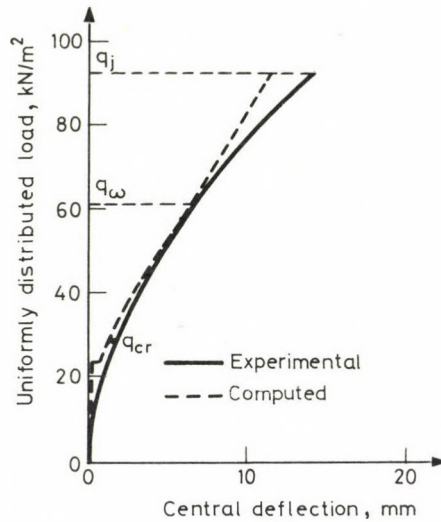


Fig. 11. Load deflection curve of slab C5-4

CONCLUSION

A method using Branson's equation to calculate deflections in two-way slabs is presented. Three different sets of formulae applicable to the slabs of varying boundary conditions are developed. The deflection computed using this procedure at working load is compared with the experimental results of Hung and Nawy's /10/ tests;

a/ For slabs with all the four supports built-in, the average value of the $\delta_{\text{exp}}/\delta_{\text{cal}}$ ratio is 1.026 and the coefficient of variations 16.5 %.

b/ For slabs with two adjacent supports built-in and two other supports simply supported, the average value of the $\delta_{\text{exp}}/\delta_{\text{cal}}$ ratio is 1.012, and the coefficient of variations 8.64 %.

c/ For slabs with three supports built in and one simply supported, the average value of $\delta_{\text{exp}}/\delta_{\text{cal}}$ is 1.018, and the coefficient of variations 13.16 %.

DEFLECTIONS OF TWO-WAY SLABS

It can be seen that the suggested method predicts satisfactorily the deflections for these three type of slabs. If more data will be available, the empirical coefficients of the equations can certainly be improved.

REFERENCES

1. ACI Committee 318; Building code requirements for reinforced concrete (ACI-318-83), American Concrete Institute, Detroit 1983, pp. 111.
2. Branson, D.E.: Design procedures for computing deflections. *Journal of ACI*, 65, No. 9., Sept. (1968), 730-742.
3. Branson, D.E.: Deformation of concrete structures, McGraw-Hill, Inc., 1977, 546.
4. Desayi, P. and Kulkarni, A.B.: Load deflection behaviour of restrained reinforced concrete slabs. *Journal of the Structural Division, ASCE*, 103, No. ST2, Feb. (1977), 405-419.
5. Desayi, P. and Kulkarni, A.B.: Load deflection behaviour of simply supported rectangular reinforced concrete slabs, IABSE Proceedings, P-11, (1978), 1-16.
6. Desayi, P. and Muthu, K.U.: Short-term deflections of rectangular, restrained reinforced concrete slabs. *Proc. Inst. Civil Engrs.*, Part 2, 67, June (1979), 529-536.
7. Desayi, P. and Muthu, K.U.: Short-time deflections of rectangular simply supported R.C. slabs. *Advances in Concrete Technology*, Pergamon, Oxford 1980, 118-128.
8. Gilbert, R.J.: Deflection control of reinforced concrete slabs. *The Institution of Engineers, Australia, Civil Engineering Transactions* (1983), 274-279.
9. Holman, J.P.: Heat transfer, fourth ed., McGraw-Hill, New York 1976, 530.
10. Hung, T.Y. and Nawy, E.G.: Limit strength and serviceability factors in uniformly loaded isotropically reinforced two-way slabs. *American Concrete Institute, Special Publication SP-30*, 1971, 301-324.
11. Rangan, B.V. and Mc Muller, A.E.: A rational approach to control of slab deflections. *ACI Journal, Proc.* 75, June (1978), 256-262.
12. Shukla, S.N. and Mittal, M.K.: Short-term deflections in two-way reinforced concrete slabs after cracking. *Journal of ACI Proc.* 73, July (1976), 416-419.
13. Timoshenko, S.P. and Krieger, W.: *Theory of plates and shells*, 2nd Ed., McGraw-Hill, Kogakusha 1959.

ON THE DYNAMICS OF A MAN-MACHINE SYSTEM

Tran van Dac*

(Received: 14 January 1986)

In this work, the dynamics of a man-machine system is dealt with, where the mechanical part consists of a hydraulic servomechanism and a load acting as inertia. On the basis of the results, the stability of special cases, and the possibility of a limit cycle are analyzed, where also the hysteretic backlash is taken into consideration.

INTRODUCTION

Man-machine systems where the mechanical part consists of a controlled process and a servomechanism controlled by an operator are often encountered in the different fields of engineering. From the point of view of control engineering, this part of the system can be modelled as a control system of negative feedback. A more interesting, rather sophisticated, problem is to model the operator in respect of control engineering. Several authors have considered the operator to be a proportional phase lead-lag element with time delay /2/ while others recommend a model with compensated integral transfer function of phase-lead character /3/, or a sampled-data model. No doubt, an element with time delay is found in every model. The theory of retarded differential difference equation shall be applied to find an asymptotic solution to the suitably selected state variable.

For given model, necessary and sufficient conditions have been proven for the stability of such a system /1/ to derive the stability maps in planes of different coefficient and technical parameters. Also, by means of a simple method /5/, we get to know transient characteristics of quite a number, and a special, asymptotic, Nyquist plot has been obtained (a case like this has never been encountered in the literature so far). Here the question arises as how to apply the Nyquist stability criterion to determination of the system stability? Will a limit cycle occur in the system if there exists a hysteretic backlash between the servomechanism and the controlled process (e.g. in case of vehicles with power-assisted steering unit)

*Dr. Prof. Tran van Dac, Truong DHBK Hanoi (Hanoi Institute of Technology), Department of Precision Mechanics and Applied Optics Technical University of Budapest

and if so, limit cycle/s/ of what features, and how many, will occur?

Investigated below are these questions, and some simple illustrative examples are given. For the sake of a better understanding, first the history of the method is dealt with and then the different questions will be discussed in detail.

1. STRUCTURE, STABILITY CRITERIA AND STABILITY MAPS OF THE SYSTEM

1.1 Structure

Using a human operator model /2/

$$H(s) = K_e(1 + T_e s)e^{-T_H s} ,$$

a servomechanism with transfer function

$$Y_1(s) = K_1 / s(T_1 s + 1)$$

and a controlled process with transfer function

$$Y_2(s) = 1/Js^2 ,$$

where K_e - human operator's gain
 T_e - human operator's time constant
 T_H - human time delay (or dead time)
 K_1 - servomechanism gain
 T_1 - servomechanism time constant
 J - load or inertia
 s - Laplace transform variable
 x^a - input signal and
 x^s - output signal as well as
 x_e - error signal of the complex system,

the block diagram shown in Fig. 1 can be plotted.

For sake of simplicity, $x = x_e$ will be used.

Now the complex system can be described by retarded differential difference equation (RDDE)

$$\dot{\underline{x}} + \underline{A}\underline{x} + \underline{B}\underline{x}(t-1) = \underline{0} \quad (1.1)$$

where

$$\underline{x} = [x_1, x_2, x_3, x_4]^T \quad \text{and} \quad \underline{0} = [0, 0, 0, 0]^T$$

are the column vectors,

ON A MAN-MACHINE SYSTEM

$$\underline{A} = \begin{bmatrix} 0 & -1 & 0 & 0 \\ 0 & 0 & -1 & 0 \\ 0 & 0 & 0 & -1 \\ 0 & 0 & a_0 & a_1 \end{bmatrix}$$

and

$$\underline{B} = \begin{bmatrix} 0 & 0 & 0 & 0 \\ 0 & 0 & 0 & 0 \\ 0 & 0 & 0 & 0 \\ b_0 & b_1 & 0 & 0 \end{bmatrix}$$

constant matrices, while

$$a_1 = 2 \zeta_0 \frac{T_H}{T_0} ;$$

$$a_0 = \left(\frac{T_H}{T_0} \right)^2$$

$$b_1 = \frac{K_e T_H^3 T_e}{J T_0^2} ;$$

$$b_0 = \frac{K_e T_H^4}{T_0^2}$$

$$T_0 = \sqrt{T_1 / K_1} ;$$

$$\zeta_0 = \frac{1}{2 \sqrt{T_1 K_1}} .$$

1.2 Stability criteria

For the system with the transfer function given in Fig. 1, the stability criteria can be derived from the following theorem /1/:

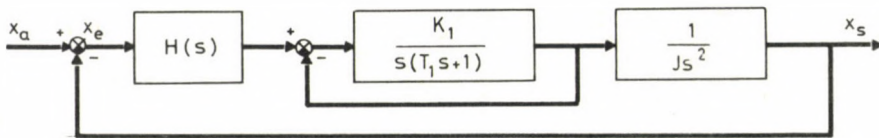


Fig. 1.

Theorem: For characteristic equation

$$D(iy) = M(y) + iS(y) = 0$$

of RDDE (1.1), where

$$M(y) = \operatorname{Re}D(iy) = y^4 - a_0 y^2 + b_1 y \sin y + b_0 \cos y,$$

$$S(y) = \operatorname{Im}D(iy) = -a_1 y^3 + b_1 \cos y + b \sin y,$$

and if y_k , the zeros of $M(y)$, $y \in \mathbb{R}^+$ are arranged so as to result in $y_k > y_{k+1}$, ($k=1,2,3,\dots,m$; briefly: $k=\overline{1,m}$), then the system will be stable provided

$$\text{i) } S(y_k) \neq 0 \quad (1.2a)$$

and

$$\text{ii) } \sum_{k=1}^m (-1)^{k+1} \operatorname{sign} S(y_k) = -2 \quad (1.2b)$$

Here the proof of the theorem is disregarded because you may read it in detail in /1/. After all, the relationships given in (1.2) are the stability conditions for the complex system in question.

1.3 Stability maps

Now the stability conditions set out in (1.2) are given a positive form. For the stability maps plotted in the planes of parameters a_1 , a_0 , b_1 and b_0 , the following equations are available as equations of the boundary lines of the stability regions:

$$-a_1 y_j^{*3} + b_1 y_j^* \cos y_j^* - b_0 \sin y_j^* = 0 \quad (1.3a)$$

$$y_j^{*4} - a_0 y_j^{*2} + b_1 y_j^* \sin y_j^* + b_0 \cos y_j^* = 0 \quad (1.3b)$$

where y_j^* ($j = \overline{1, \infty}$) zeros of function $S(y)$, $y \in \mathbb{R}^+$.

On the basis of the general stability criterion and arrangement of zeros y_j^* , the location of the stability range that is whether it lies to the right or to the left from the boundary lines can be determined. The results are shown in Figs 2 and 3.

Apparently, the use of the stability maps would be more convenient if they were plotted in the planes of the technical parameters, e.g. in planes (T_H, T_e) , (ζ_0, J) , or (T_H, T_e) . Then, for plane (T_H, T_e) ,

ON A MAN-MACHINE SYSTEM

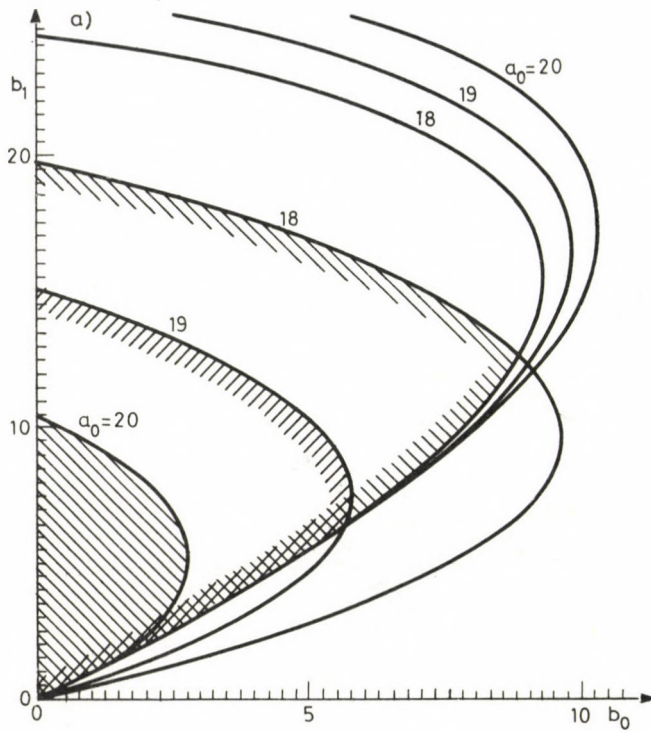


Fig. 2a ($a_1 = 0$)

$$T_H^4 - \frac{y^2 \cos y}{P} T_H^2 + \frac{A_1 y^3 \sin y}{PA_0} T_H + \frac{y^4 \cos y}{PA_0} = 0 \quad (1.4a)$$

$$T_e = \frac{A_1 y^2}{PA_0 T_H^2 \cos y} + T_H \frac{\tan y}{y} \quad (1.4b)$$

is obtained, where

$$A_1 = \frac{2 \zeta_0}{T_0}$$

$$A_0 = \frac{1}{T_0^2}$$

$$P = \frac{K_e}{J} ,$$

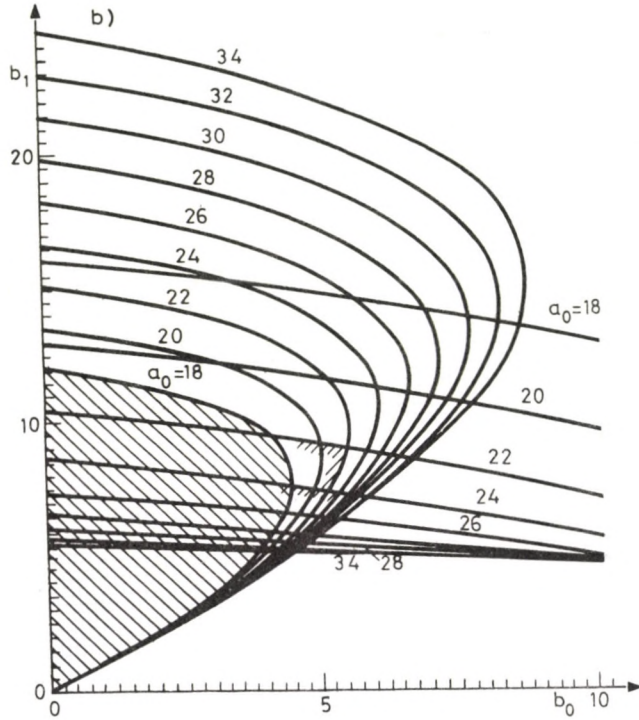


Fig. 2b ($a_1 = 0.3$)

the stability map being shown in Fig. 4.

Similarly, in plane (T_0, J) , equations

$$aT_0^2 + bT_0 + c = 0 \tag{1.5a}$$

$$J = \frac{(T_e - T_H \tan y/y) K_e T_H^2 \cos y}{2 \zeta_0 T_0} , \quad y \in \mathbb{R}^+ \tag{1.5b}$$

give the boundary lines for the stability region where

$$a = (T_e - T_H \tan y/y) y^2 \cos^2 y$$

$$b = 2 \zeta_0 \left[T_H^2 + (T_e - T_H \tan y/y) T_H \sin y \cos y \right] \tag{1.5c}$$

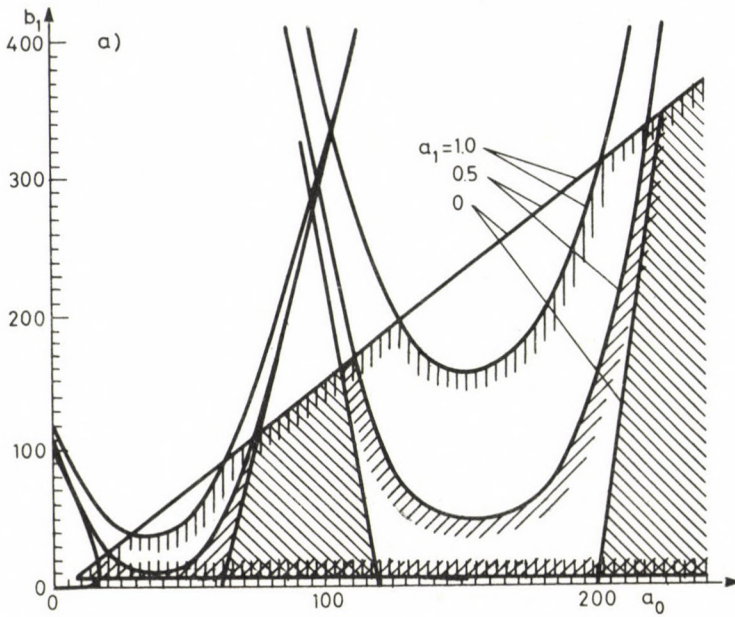


Fig. 3a ($b_0 = 5$)

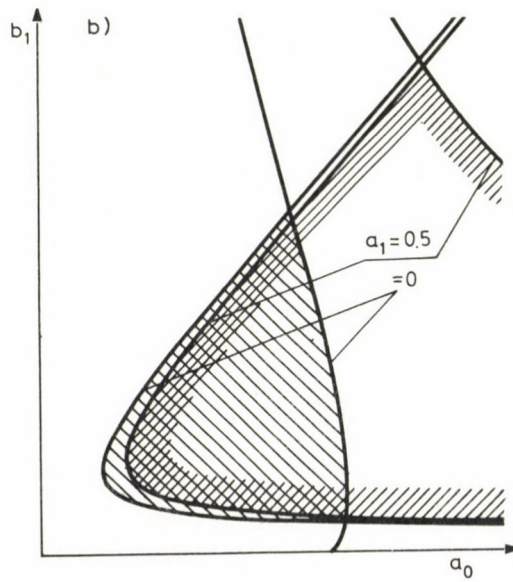


Fig 3b ($b_0 = 5, a_1 = 0.5, 0.0$)

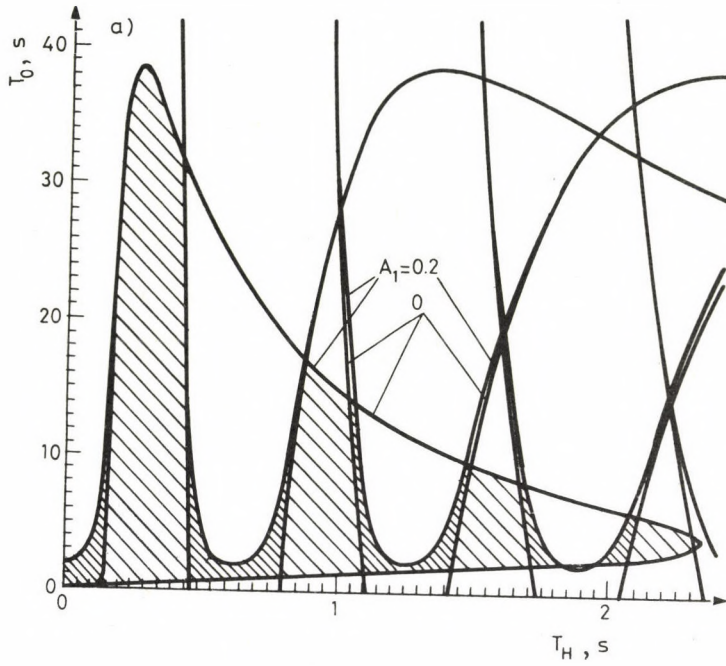


Fig. 4a ($A_0 = 100, P = 0.1$)

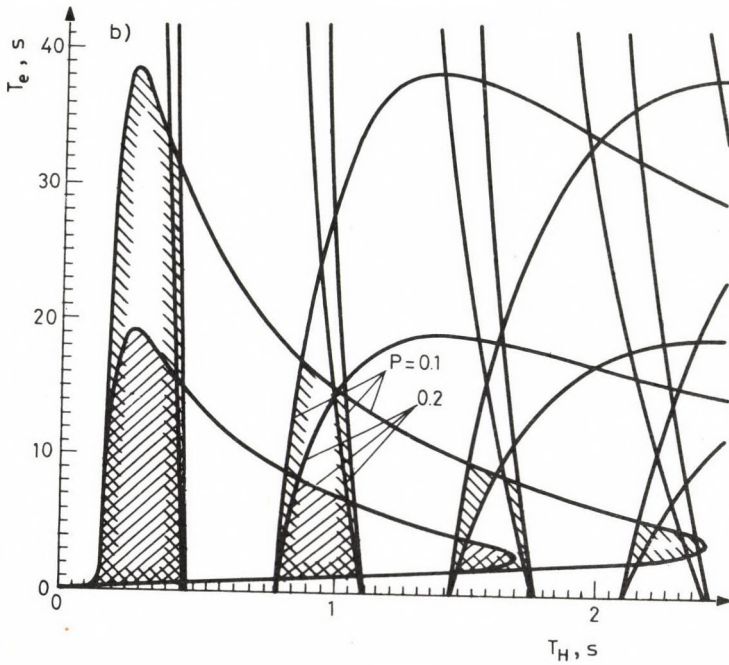


Fig. 4b ($A_0 = 100$)

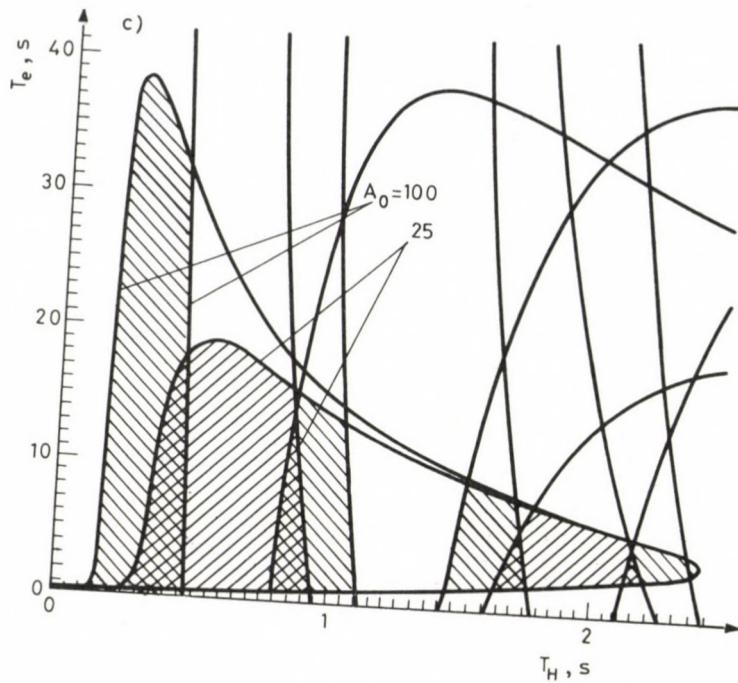


Fig. 4c ($P = 0.1$)

$$c = (T_e - T_H \tan y/y) T_H^2 \cos y$$

(see Fig. 5).

Finally, in plane (T_0, ζ_0) , equations of the boundary lines of the stability range are

$$T_0 = \frac{T_H \left[y^2 - PT_e T_H y \sin y - PT_H^2 \cos y \right]^{1/2}}{y^2} \quad (1.6a)$$

$$\zeta_0 = \frac{PT_e T_H^3 y \cos y - PT_H^4 \sin y}{2T_0} \quad (1.6b)$$

(see Fig. 6).

The above results can be used (in the form of different stability maps) to investigate the system that is for analysis or, in a sense, for

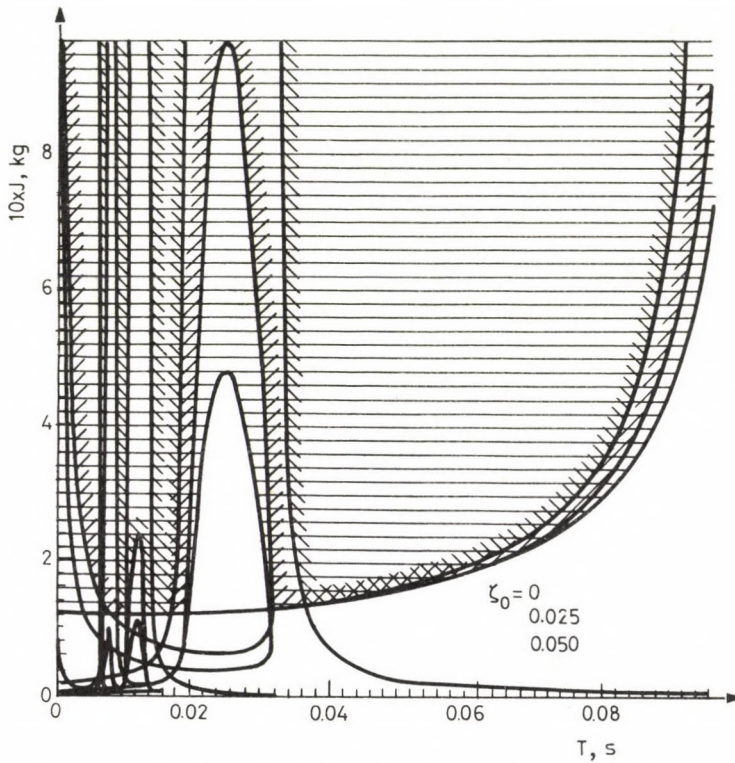


Fig. 5 ($T_e = 2$ [sec], $T_H = 0.15$ [sec], $K_e = 0.6$)

synthesis of the system (concerning, as a matter of fact, the structure shown in Fig. 1).

The examples given later in this work show demonstratively how to use the stability maps.

2. THE LIMIT CYCLE PROBLEM

If, as shown in Fig. 7, there exists a hysteretic backlash between the servomechanism and the controlled object at the different connections of the mechanical transmission line, a limit cycle may take place in the complex system. A block diagram equivalent to the appropriate block diagram algebra can be obtained in this case (Fig. 8).

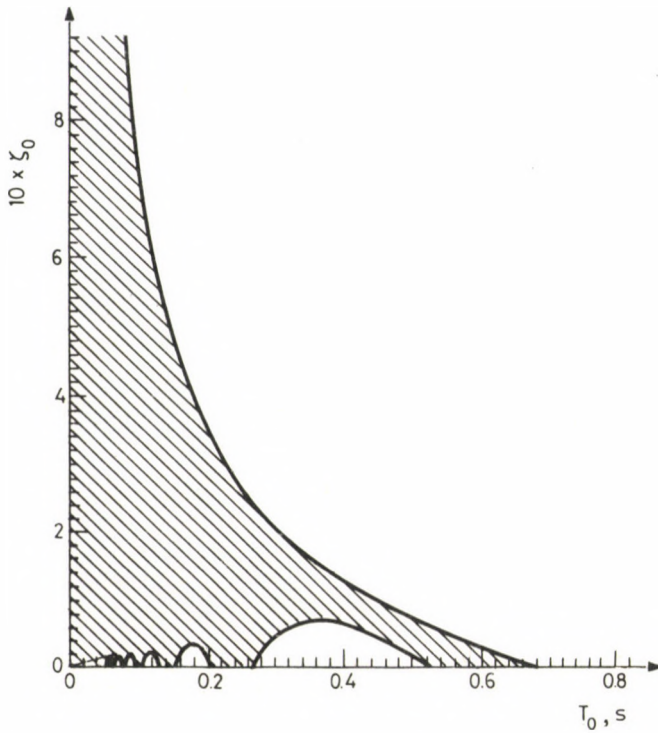


Fig. 6 ($P = 0.1, T_H = 2.2$ [sec] , $T_e = 4$ [sec])

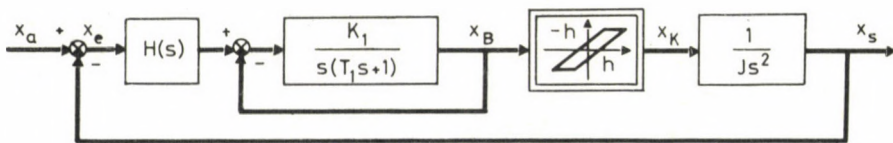


Fig. 7

Actually, the complex system has become nonlinear as a result of hysteretic backlash, and there exists a closed loop containing a nonlinear feedforward element and a variable (or non-rigid) feedback element.

As there is only one nonlinearity in the system, the describing function method is used to detect the limit cycle taking place in the complex system. Therefore, a limit cycle will occur if, and only if, equation

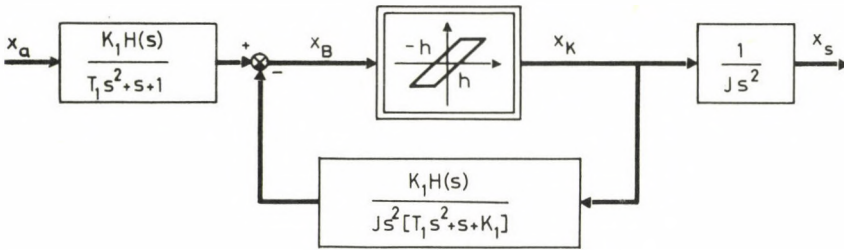


Fig. 8

$$1 + N(B) \frac{K_1 H(i \omega)}{J(i \omega)^2 [T_1 (i \omega)^2 + i \omega + K_1]} = 0 \quad (2.1a)$$

or

$$\frac{-1}{N(B)} = \frac{K_e (1 + i \omega T_e) e^{-i \omega T_H}}{J(i \omega)^2 [T_0^2 (i \omega)^2 + 2 \zeta_0 T_0 (i \omega) + 1]} \quad (2.1b)$$

where B – amplitude of the sinusoidal input signal of nonlinearity N ,
 $N(B)$ – describing function of hysteretic backlash
 is satisfied /6/.

It is easy to see that the right-hand side of (2.1b) fully agrees with the transfer function of the linear open-loop system if $s = i \omega$. This fact suggests that the loop transfer function of the system free of feedback is directly applicable independently of the location of the nonlinearity that is of whether it is found in the feedforward line or in the feedback line. Actually, the physical implication of how a limit cycle is taking place in the complex system can be better understood on the basis of Fig. 8.

Figure 11 shows that more limit cycles may take place in the man-machine system, both convergent and divergent ones.

By means of a suitable computer program, the parameters of the limit cycle that is the amplitude and frequency of the input signal of the nonlinearity (see Figs 7 and 8) can be obtained. At the same time, also the type of the limit cycle can be determined on the basis of the type of inter-section.

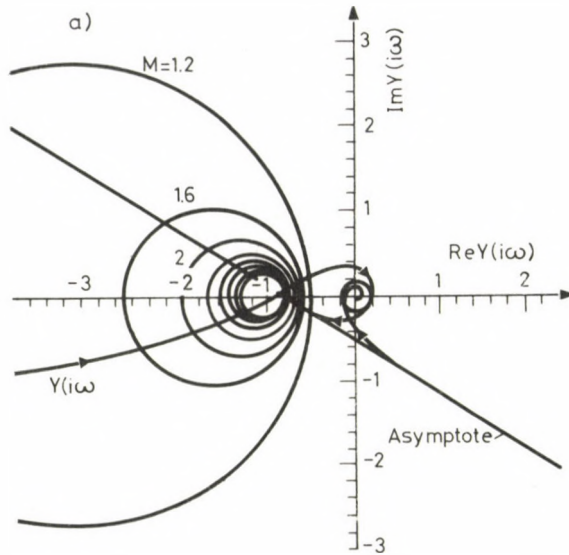


Fig. 9a

$J = 6$ [kg], $\zeta_0 = 0$, $T_0 = 0.15$ [sec];
 $T_e = 4$ [sec], $T_H = 2.2$ [sec], $K_e = 0.6$
 (Nyquist chart having asymptote for stability case)

3. SOME COMMENTS ON THE USE OF THE NYQUIST CRITERION

The system can be still stable even if the damping ratio of the man-machine system in question is zero (or negative). However, in this case, the shape of the Nyquist plot differs from the shape usually obtained. Namely, the curve has an asymptote in this case so that difficulties are encountered in application of the Nyquist criterion. The problem lies in that whether or not point $-1 + i0$ of extended complex plane $Y(i\omega)$ is enclosed by the closed curve containing the infinitely distant point. Our earlier investigations justified and generalized the applicability of the Nyquist criterion /1/. Namely, in the direction of frequency increase, near the origin, the curve continues running clockwise. Therefore, the conditions under which the system is stable can be determined. Accordingly, the following practical rule applies:

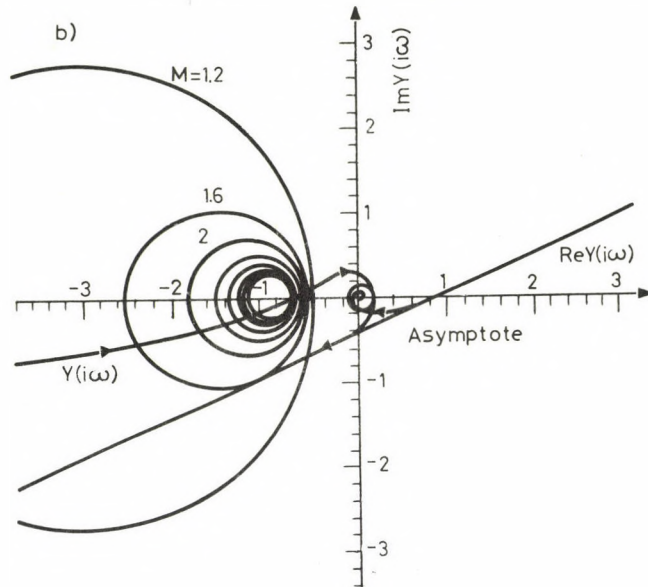


Fig. 9b

$J = 6$ [kg] , $\zeta_0 = 0$, $T_0 = 0.1$ [sec] ;
 $T_e = 3.5$ [sec] , $T_H = 2.05$ [sec] , $K_e = 0.6$
 (Nyquist chart having asymptote for instability case)

If there exists an asymptote for the Nyquist curve, this will bifurcate extended complex plane $Y(i\omega)$, and the system will be stable if, and only if, point $-1 + i0$ and the origin lie in the opposite semi-plane (Fig.9), moreover, also the Nyquist plot do not encircle the critical point $-1 + i0$.

Essentially, this rule allows of a generalization of the Nyquist criterion in engineering practice.

4. EXAMPLES

Given below are some simple examples to illustrate the above results.

Reader can follow these examples without any difficulty. Note that any detail can be found earlier and later in this work so that no detailed explanations are given here.

Three typical cases are presented first: the stable case, the unstable case, and the critical case (where point $-1 + i0$ is intersected by the Nyquist curve). Then, the problem of the limit cycle will be discussed on

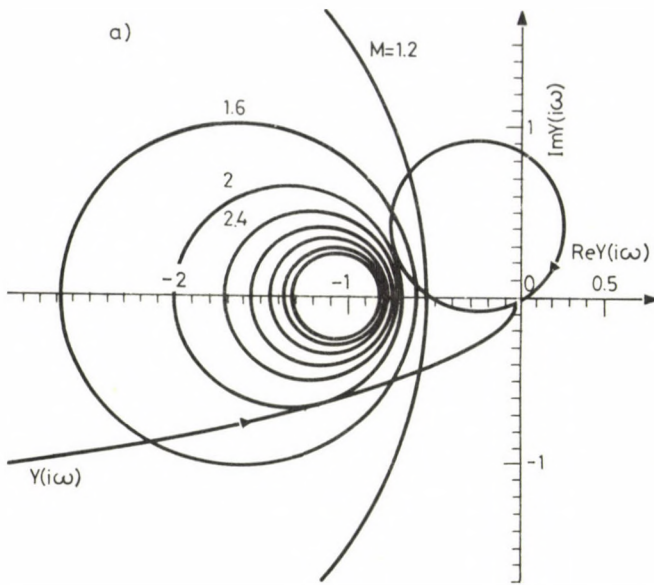


Fig. 10a

$$\begin{aligned}
 J &= 6 \text{ [kg]} , T_0 = 0.1 \text{ [sec]} , \zeta_0 = 0.01; \\
 T_H &= 0.1 \text{ [sec]} , T_e = 2 \text{ [sec]} , K_e = 0.6 \\
 &\text{(stable case; overshooting with } M \approx 2)
 \end{aligned}$$

the basis of the describing function method, using it as a function of dimensionless variable h/B . The last point to be discussed is applicability of the Nyquist criterion, especially for two cases where there exist an asymptote for the curve, one being stable while the other unstable.

Note that the necessary informations are given in each Figure. Therefore, any misunderstanding can be avoided, and the correctness and accuracy of the different stability maps and the validity of what has been said above can be checked on the basis of the Figures (Figs 10 through 12).

5. CONCLUSIONS, ANALYSIS

As has been seen, mathematical tools not very complicated indeed can be used to answer questions arising in relation with stability and transient phenomena of a rather complicated system like that discussed here, although

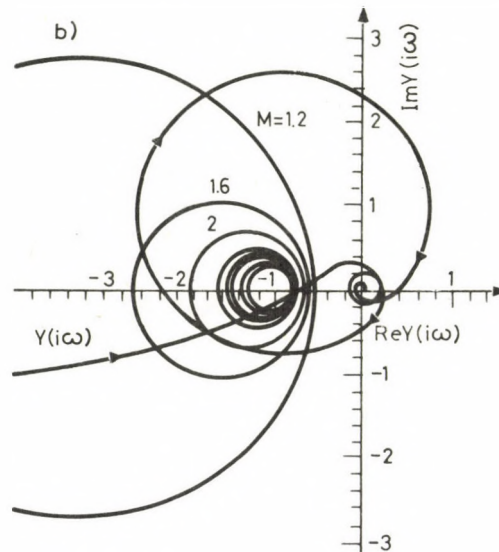


Fig. 10b

$$J = 6 \text{ [kg]} , T_0 = 0.15 \text{ [sec]} , \zeta_0 = 0.01;$$

$$T_H = 2 \text{ [sec]} , T_e = 4 \text{ [sec]} , K_e = 0.6$$

(case of instability)

no time function has been given for the system response. However, no difficulties are encountered theoretically because if the input signal of the system is a Dirac (delta) function, then the output signal of the system can be determined by means of formula

$$x_s(t) = \frac{2}{\pi} \int_0^{\infty} \text{Re } W(i\omega) \cos \omega t d\omega$$

/6/ where $W(s)$ is the transfer function of the closed system. Integration can be simply carried out by means of a computer, and then also error signal $x_e(t)$ can be determined. In practice, if the complex system is stable, the integrand function will be very small in case of high frequencies. Thus integration can be stopped at a certain frequency value.

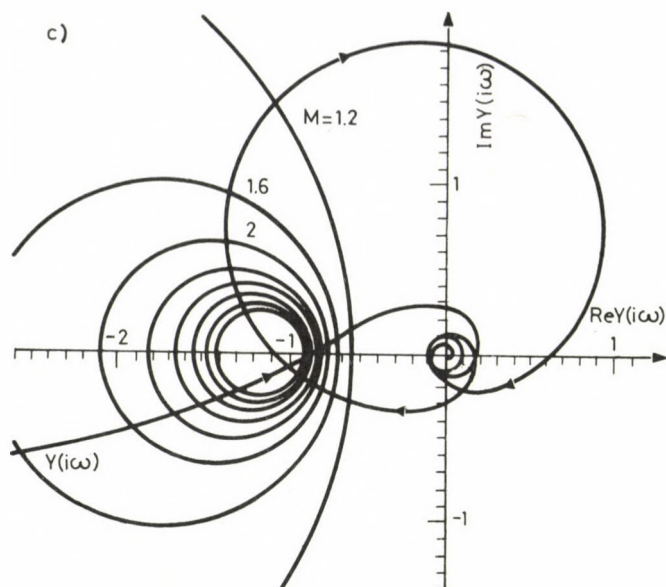


Fig. 10c

$$J = 6 \text{ [kg]}, T_0 = 0.1 \text{ [sec]}, \zeta_0 = 0.01;$$

$$T_H = 2.02 \text{ [sec]}, T_e = 3.75 \text{ [sec]}, K_e = 0.6$$

(critical case; sinusoidal oscillation occurs in the system)

The stability maps consist of more disjunct parts of finite or infinite number in the planes of different parameters because a perfect correspondence is not always existing between the planes. However, the number of the stability domains in these parameter planes reduces as damping increases until, finally, they run into each other.

The human influence (as a compensating element) makes the technical part stable when damping is zero. In other words, without human influence, the system would certainly be unstable if there were no energy dissipation in the technical part in a dynamic state.

5.2 Stability maps

5.2/a Stability maps in the planes of coefficients

If there is no damping ($a_1 = 0$), then, below a certain limit a_0 in coefficient plane (b_0, b_1), the stability region will be extended by the

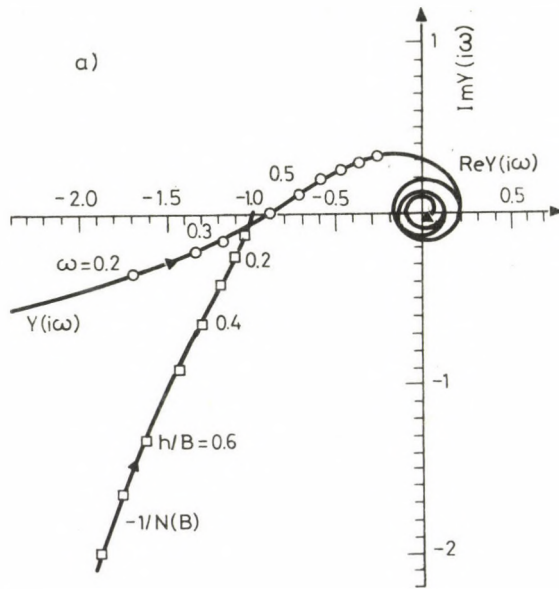


Fig. 11a

$$J = 6 \text{ [kg]} , T_0 = 0.1 \text{ [sec]} , \zeta_0 = 0.1;$$

$$T_H = 2.2 \text{ [sec]} , T_e = 4 \text{ [sec]} , K_e = 0.6$$

(convergent limit cycle occurs in the system with $h/B = 0.05$ and

$$\omega \approx 0.35/\text{sec})$$

(The backlash free system is table)

higher value of a_0 . However, above this limit, the situation is reversed, moreover, this stability region may even vanish.

It can be seen in plane (a_0, b_1) that the stability range consists of disjunct domains (Fig. 3).

In case $a_1 \neq 0$, the effect of damping is unfavourable for lower values of a_0 and b_1 as several parts of the stability region reduce (Fig. 3b). However, the same parts of the stability region will increase as the values of a_0 and b_1 increase and finally, beyond a certain limit, the system becomes stable provided

$$M(y_1^*) < 0 , \quad y_1^* \in (0, \pi/2)$$

as a single condition.

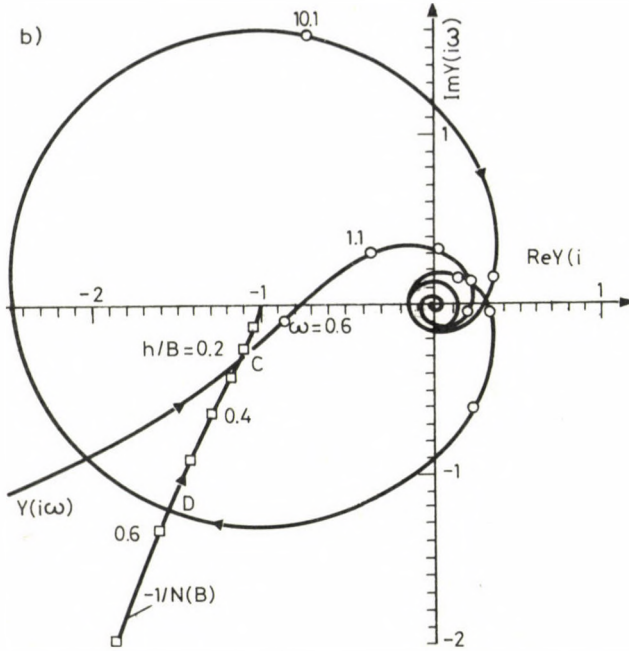


Fig. 11b

$$J = 6 \text{ [kg]} , \quad \zeta_0 = 0.01, \quad T_0 = 0.1 \text{ [sec]} ;$$

$$T_e = 5 \text{ [sec]} , \quad T_H = 1.9 \text{ [sec]} , \quad K_e = 0.6$$

(Case of the unstable backlash free system; C denotes a convergent limit cycle and D denotes a divergent limit cycle. The nonlinear system may be stable with the convergent limit cycle beside a frequency $\omega \approx 0.6/\text{sec}$ backlash-amplitude ratio $h/B \approx 0.25$)

5.2/b Stability maps in the planes of technical parameters

In plane (T_H, T_e) , the stability region consists similarly of more disjunct parts in case of a negligible damping ratio, with, however, the number of these parts not being infinite. The number of these parts and the parts themselves increase as P and T_0 reduce but, in this case, in accordance with a different law (Fig. 4). If damping is prevailing in the system, the parts of the stability range will increase and, beyond a certain limit of damping, they run into each other. It can be seen in the map that there exists an extremum for both T_H and T_e , a fact suggesting that there exist

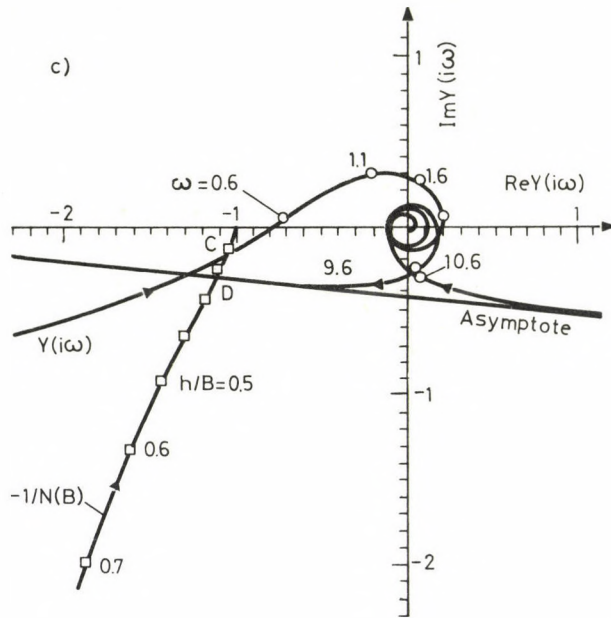


Fig. 11c

$$J = 6 \text{ [kg]} , T_0 = 0.1 \text{ [sec]} , \zeta_0 = 0;$$

$$T_H = 2.05 \text{ [sec]} , T_e = 4 \text{ [sec]} , K_e = 0.6$$

(Case of Nyquist chart having unstable asymptote. Point C denotes the convergent limit cycle and point D denotes the divergent case. Parameters of point C: $h/B \approx 0.13$, $\omega \approx 0.45 \text{ sec}$)

optimum states in a sense. For instance, the optimum value of T_e can be found by the operator only after a long practice, and a prompt response of the operator is required to reach the optimum state where T_e is maximum. Interestingly enough, if the operator's reflex is 'too good' ($T_H \rightarrow 0$), instability may take place again as a result of 'human fluster'. In case of $T_e \approx T_{e \text{ opt}}$, the response of a well experienced operator may be slow and T_H may assume quite a high value. Thus, there exists a hyperbolic relationship between the operator's experience and attention. On the other hand, we might be right in saying that instability results from excessively long dead time. Accordingly, the critical values must be greater than the average human lag phase.

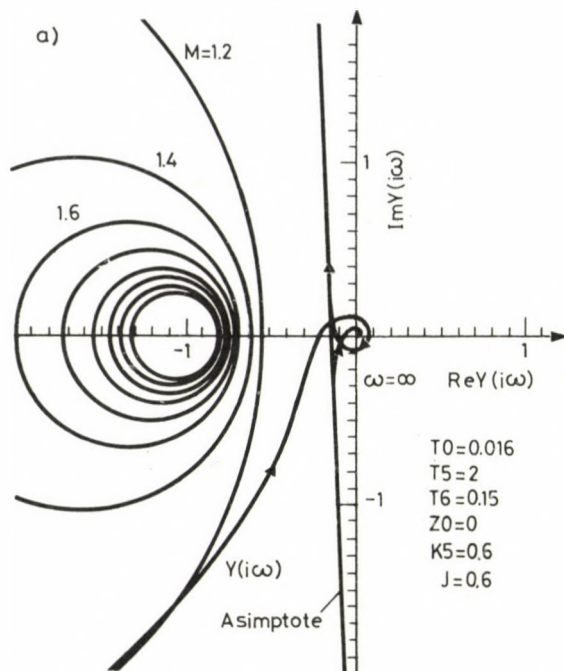


Fig. 12a

$J = 6$ [kg], $T_0 = 0.016$ [sec], $\zeta_0 = 0$;
 $T_H = 0.15$ [sec], $T_e = 2$ [sec], $K_e = 0.6$
 (Stability case)

Curve $J(T_0)$ permits the effect of the technical parameters to be investigated. It is a matter of fact that the inertia affects the system stability favourably (Fig. 5). Considering time constant T_0 , an optimum interval can be determined on the basis of the asymptotic lines even in case of slight damping.

Sometimes parameters T_0 and ζ_0 are of interest as parameters characteristic of oscillation and transients of the mechanical part of the system. As shown also in Fig. 6, there are notches of an infinitely large number in the stability region, reducing and becoming more and more densely arranged as they approach the origin. At the same time, a hyperbolic relationship can be detected also between these two quantities. It can be shown that lower values of T_H and P increase the stability region, and for given values of

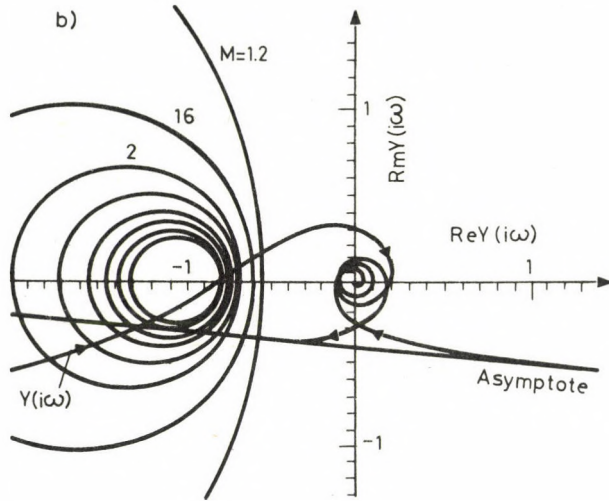


Fig. 12b

$$J = 6 \text{ [kg]} , \quad \zeta_0 = 0, \quad T_0 = 0.1 \text{ [sec]} ;$$

$$T_e = 4 \text{ [sec]} , \quad T_H = 2.05 \text{ [sec]} , \quad K_e = 0.6$$

(The Nyquist chart having an asymptote for the instability case)

T_H, T_0 , there is an interval of ζ_0 which ensures stability for the complex system. Values falling outside of this interval make the system unstable (Fig. 6), and, finally, this interval increases with reducing P and T_0 in full agreement with the fact that the system's aptitude to instability increases as a result of a higher loop gain.

5.2/c Features of the limit cycle

In a man-machine system of a structure described, hysteretic backlash always results in one or more limit cycle(s). Considering the nature of these limit cycles, there exists a convergent limit cycle in a relatively low frequency range in case the system, free of backlash, is stable (as can be stated on the basis of intersection of the Nyquist curve and the curve of negative reciprocal describing function $-1/N(B)$) while both convergent and divergent limit cycles may take place if the system is unstable, the convergent limit cycle being of lower frequency.

Surprisingly enough, this fact suggests that an a priori unstable system may become stable (but never asymptotically!) in a state correspond-

ON A MAN-MACHINE SYSTEM

ing to the convergent limit cycle if we, in one way or other, could operate the system in this state. Therefore, nonlinearity affects the system favourably in respect of operability in this case.

5.2/d Again a comment on use of the Nyquist criterion:

In the man-machine system, the non-regular case where there exists an asymptote for the Nyquist plot may be encountered. In this case, the Nyquist criterion applies invariably, and the system will be stable if, and only if, point $-1+i0$ and the origin of the extended complex plane, $Y(i\omega)$, are separated by the asymptote, moreover, also the Nyquist plot do not encircle the critical point $-1+i0$. However, efforts are usually made in practice to avoid such situations if possible, and simpler system structures controllable by simpler system structure and tools are preferred.

ACKNOWLEDGEMENT

The author wishes to express his thanks to Professor Oliver Petrik, Head of Department of Precision Mechanics and Applied Optics, BME, for the careful review of this paper and his help in submitting it for publication.

Acknowledgement is made to Professor Mátyás Horváth, Head of Department of Production Engineering, BME, for the possibility of using the Computer Unit of his Department by author.

BOUNDS OF THE NUMERICAL VALUE OF ROTATIONAL FLEXIBILITY

I. Ecsedi*

(Received: 5 September 1986)

The proof of lower and upper bounds of rotational flexibility of a homogeneous, isotropic, rotationally symmetric disk of variable thickness, made of linearly elastic material, is based fundamentally on two minimum theorems of the elasticity theory.

NOTATION

r, ϕ	polar co-ordinates
ρ	density
ω	angular velocity
a	radial co-ordinate of 'inner' mantle surface of the disk
b	radial co-ordinate of 'outer' mantle surface of the disk
E	Young modulus
ν	Poisson number
u	radial displacement
σ_r, σ_ϕ	normal stresses
$\epsilon_r, \epsilon_\phi$	specific elongation
N_r, N_ϕ	stress resultants (N/m)
U_r, U_ϕ	strain energy
H	rotational flexibility
V	volume
J	moment of second order
$n_r, n_\phi, \alpha_r, \alpha_\phi, t$	} auxiliary values
α	natural angular frequency
R	ring centre radius
v	ring width,

the other quantities and variables being defined in the text.

1. INTRODUCTION

Figure 1 illustrates a homogeneous, isotropic, rotationally symmetric disk of variable thickness, made of linearly elastic material.

The state of stress, strain, displacement of the disk rotating at constant angular velocity ω can be brought about by solution of the boundary value problem described by the following equations:

*Dr. I. Ecsedi, H-3524, Miskolc, Klapka Gy. u. 36. IX/2., Hungary

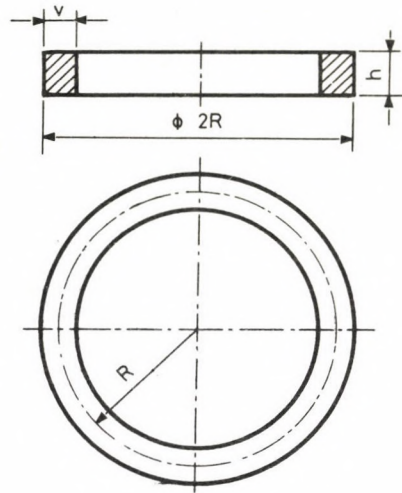
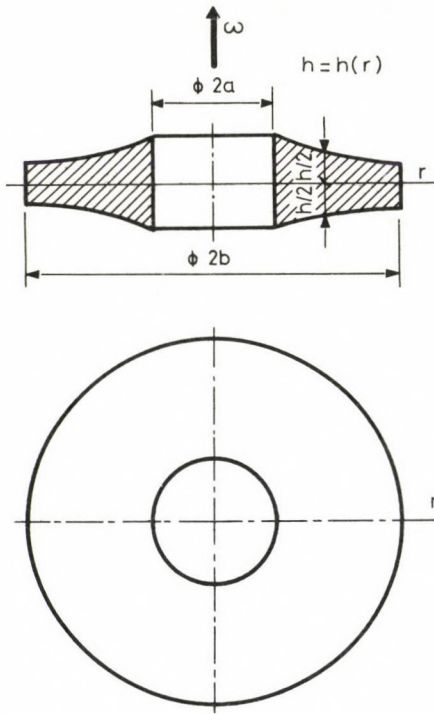


Fig. 1. Rotationally symmetric disk of variable thickness

Fig. 2. Thin ring

$$\frac{dN_r}{dr} + \frac{N_r - N_\phi}{r} + \rho h r \omega^2 = 0, \quad (1.1)_1$$

$$N_r(a) = 0, \quad N_r(b) = 0, \quad (1.1)_{2,3}$$

$$N_r = \frac{E h}{1 - \nu^2} (\epsilon_r + \nu \epsilon_\phi) \quad (1.2)_1$$

$$N_\phi = \frac{E h}{1 - \nu^2} (\nu \epsilon_r + \epsilon_\phi) \quad (1.2)_2$$

$$\epsilon_r = \frac{du}{dr}, \quad \epsilon_\phi = \frac{u}{r}, \quad (1.3)_{1,2}$$

where $h = h(r)$ thickness of the disk

$N_r = h \sigma_r$, $N_\phi = h \sigma_\phi$ stress resultants.

BOUNDS OF ROTATIONAL FLEXIBILITY

Equilibrium equations (1.1)_{1,2,3} show that a rotating disk is investigated where no load is acting upon the inner and outer mantle surface, the disk being loaded only by the force system distributed over the volume of density

$$q_r = \rho r \omega^2 . \quad (1.4)$$

Strain energy U of the disk can be determined by means of formula

$$U = \frac{\pi}{E} \int_a^b \frac{1}{h} \left[N_r^2 + N_\phi^2 - 2 \nu N_r N_\phi \right] r dr . \quad (1.5)$$

The quantity defined as

$$H = \frac{U}{\omega^4} \quad (1.6)$$

is called rotational flexibility of the disk.

Rotational flexibility H is a function of the shape of the disk, material constants E , ν , and density ρ . It can be seen that this statement is correct in the following way:

Consider new variables $n_r, n_\phi, \alpha_r, \alpha_\phi, t$ defined by rule

$$N_r = \omega^2 n_r, \quad N_\phi = \omega^2 n_\phi, \quad (1.7)_{1,2}$$

$$\epsilon_r = \omega^2 \alpha_r, \quad \epsilon_\phi = \omega^2 \alpha_\phi, \quad (1.8)_{1,2}$$

$$u = \omega^2 t . \quad (1.9)$$

A combination of equations (1.1), (1.2), (1.3), (1.7), (1.8), (1.9) shows that $n_r, n_\phi, \alpha_r, \alpha_\phi, t$ are a solution to the boundary value problem described by the following equations:

$$\frac{dn_r}{dr} + \frac{n_r - n_\phi}{r} + \rho h r = 0, \quad (1.10)_1$$

$$n_r(a) = 0, \quad n_r(b) = 0, \quad (1.10)_{2,3}$$

$$n_r = \frac{Eh}{1 - \nu^2} (\alpha_r + \nu \alpha_\phi), \quad (1.11)_1$$

$$n_{\phi} = \frac{Eh}{1 - \nu} \frac{1}{2} (\alpha_r + \alpha_{\phi}) \quad (1.11)_2$$

$$\alpha_r = \frac{dt}{dr}, \quad \alpha_{\phi} = \frac{t}{r} \quad (1.12)_{1,2}$$

It can be seen on the basis of the above formulae that functions $n_r = n_r(r)$, $n_{\phi} = n_{\phi}(r)$ are determined by constants a, b, function $h = h(r)$, density ρ , and material constants E, ν .

A combination of formulae (1.5), (1.6), (1.7) give

$$H = \frac{\pi}{E_a} \int_a^b \frac{1}{h} (n_r^2 + n_{\phi}^2 - 2\nu n_r n_{\phi}) r dr \quad (1.13)$$

It comes from the comment on equations (1.10), (1.11), (1.12) as well as from formula (1.13) that the statement to be proved is correct. Also, it follows from the definition of H that it is positive in any case.

Using the relationships found on pages 96 – 97 of /1/, it is easy to show that, in case $h = \text{constant}$, the value of H can be determined on the basis of the following formula:

$$H = \frac{\pi}{96} \rho^2 \frac{h}{E} \left[(b^6 - a^6)(7 - 6\nu - \nu^2) + (b^4 a^2 - b^2 a^4)(27 + 18\nu + 32\nu^2) \right] \quad (1.14)$$

Figure 2 illustrates a ring of thickness h and width v. Using the usual approximations, one can write that

$$\sigma_r = 0, \quad \sigma_{\phi} = \rho \omega^2 R^2 \quad (1.15)_{1,2}$$

Formulae (1.5)_{1,2} and relationship

$$U = \frac{1}{2E} \int_v \sigma_{\phi}^2 dV = \frac{1}{2} \sigma_{\phi}^2 V = \frac{\pi}{E} R^5 v h \rho^2 \omega^4 \quad (1.16)$$

suggest that the value of rotational flexibility of a thin ring, H, is given by formula

$$H = \frac{\pi}{E} R^5 v h \rho^2 \quad (1.17)$$

BOUNDS OF ROTATIONAL FLEXIBILITY

The accurate value of the rotational flexibility of a rotationally symmetric disk of variable thickness can be determined only in some special cases, like in case $h = h(r)$ is a function of the following shape /1,2/:

$$h(r) = h_0 \left(\frac{r}{a}\right)^n, \quad (1.18)$$

$n = \text{constant}$.

In the general case, no accurate (strict) solution to the boundary value problem described by equations (1.10), (1.11), (1.12) is known and thus production of the accurate (strict) value of rotational flexibility H is not possible either. In cases like this, efforts are made to set limits to the value of H . This paper has been intended first of all to derive inequality relations by means of which lower and upper bounds can be set to the accurate (strict) value of rotational flexibility without the knowledge of the accurate (strict) solution to the boundary value problem described by equations (1.11), (1.12), (1.10).

2. LOWER BOUND

2.1 Theorem

There exists inequality relation

$$H \geq 2\pi \int_a^b h \rho r^2 f dr - \frac{\pi E}{1-\nu^2} \int_a^b h \left[\left(\frac{df}{dr}\right)^2 + \left(\frac{f}{r}\right)^2 + 2\nu \frac{df}{dr} \frac{f}{r} \right] r dr \quad (2.1)$$

where $f = f(r)$ denotes a univariable function, continuous over closed interval $a \leq r \leq b$ and continuously differentiable at least twice per section, otherwise arbitrary.

Proof:

The proof of relation (2.1) can be directly obtained from the minimum theorem for potential energy functional applied to the kinematically possible displacement field written in the following form:

$$\tilde{u} = f(r) \omega^2. \quad (2.2)$$

2.2 Theorem

There exists inequality relation

$$H \geq \pi \frac{1 - \nu^2}{E} \rho^2 \frac{\left(\int_a^b h r^2 F dr \right)^2}{\int_a^b \left[r \left(\frac{dF}{dr} \right)^2 + \frac{F^2}{r} + 2 \nu F \frac{dF}{dr} \right] dr} \quad (2.3)$$

where $F = F(r)$ is a not equally zero function over closed interval $a \leq r \leq b$, the continuity properties of which complying with those of function $f = f(r)$ given in theorem 2.1.

Proof:

Let relation (2.1) be applied to function

$$f(r) = \lambda F(r) \quad (2.4)$$

being an arbitrary real constant. From relationship

$$H \geq 2 \pi \lambda \int_a^b h \rho r^2 F dr - \frac{\pi E}{1 - \nu^2} \lambda^2 \int_a^b h \left[\left(\frac{dF}{dr} \right)^2 + \left(\frac{F}{r} \right)^2 + 2 \nu \frac{dF}{dr} \frac{F}{r} \right] r dr \quad (2.5)$$

so obtained, existing for any possible value $-\infty < \lambda < \infty$ of variable λ , relation (2.3) can be obtained by a simple extremum calculation provided the coefficient of λ^2 is non-zero that is

$$F(r) \neq 0, \quad a \leq r \leq b. \quad (2.6)$$

3. UPPER BOUND

3.1 Theorem

There exists inequality relation

$$H \leq \frac{\pi}{E} \int_a^b \left\{ \frac{1}{h} \left[\frac{c^2}{r} + r \left(\frac{dc}{dr} \right)^2 - 2 \nu c \frac{dc}{dr} \right] - (6 + 2 \nu) \rho r^2 c \right\} dr + \frac{\pi}{E} \int_a^b h \rho^2 r^5 dr \quad (3.1)_1$$

BOUNDS OF ROTATIONAL FLEXIBILITY

where $c = c(r)$ denotes a univariable function, continuous over closed interval $a \leq r \leq b$ and continuously differentiable at least once per section, otherwise arbitrary, which satisfies the homogeneous boundary conditions given below:

$$c(a) = 0, \quad c(b) = 0. \quad (3.1)_{2,3}$$

Proof:

The proof of the inequality relation (3.1) is based on the minimum theorem for complementary energy from which it can be obtained by application of the statically possible stress field of the following form:

$$\tilde{N}_r = \frac{c}{r} \omega^2, \quad (3.2)_1$$

$$\tilde{N}_\phi = \frac{dc}{dr} \omega^2 + \rho r^2 h \omega^2. \quad (3.2)_2$$

3.2 Theorem

Assume $C = C(r)$ to be a univariable function continuous over closed interval $a \leq r \leq b$ and at least once continuously differentiable, which is non-equally zero in closed interval $a \leq r \leq b$. Assume furthermore that function $C = C(r)$ satisfies boundary conditions

$$C(a) = 0, \quad C(b) = 0. \quad (3.3)_{1,2}$$

There exists inequality relation

$$H \leq \frac{\pi}{E} \rho^2 \left(C_0 - \frac{C_1^2}{C_2} \right) \quad (3.4)$$

where

$$C_0 = \int_a^b h r^5 dr, \quad (3.5)_1$$

$$C_1 = \int_a^b (3 + \nu) r^2 C dr, \quad (3.5)_2$$

$$C_2 = \int_a^b \frac{1}{h} \left[\frac{C^2}{r} + r \left(\frac{dC}{dr} \right)^2 - 2 \nu C \frac{dC}{dr} \right] dr. \quad (3.5)_3$$

Proof:

Let the inequality relation (3.1) be applied to function

$$c(r) = \lambda C(r), \quad (3.6)$$

where λ arbitrary real constant. From relationship

$$H \leq \frac{\pi}{E} \rho^2 (\lambda^2 C_2 - 2\lambda C_1 + C_0) \quad (3.7)$$

so obtained, relation (3.4) can be calculated by means of simple extremum calculations.

4. COMMENTS ON UPPER AND LOWER BOUNDS

4.1 Relation

The brief discussion in connection with relation (2.1) suggests that a sign of equality in relation (2.1) will apply only if

$$f(r) = t(r) \quad a \leq r \leq b. \quad (4.1)$$

By means of another brief discussion concerning relation (2.3), it is possible to show that a sign of equality in relation (2.3) will apply only if

$$F(r) = k t(r) \quad a \leq r \leq b, \quad (4.2)$$

where k is a non-zero, otherwise arbitrary, real constant.

4.2 Relation

The discussions associated with relations (3.1), (3.4) suggest that a sign of equality in relation (3.1) will apply only if

$$c(r) = \frac{Eh}{1-\nu^2} \left(r \frac{dt}{dr} + \nu t \right), \quad (4.3)$$

while in relation (3.4) only if

$$C(r) = k \frac{Eh}{1 - \nu^2} \left(r \frac{dt}{dr} + \nu t \right), \quad (4.4)$$

where k is a non-zero, otherwise arbitrary, real constant.

5. AN INEQUALITY RELATION

5.1 Theorem

Let the least natural angular frequency associated with the rotationally symmetric radial free vibration of a rotationally symmetric disk of variable thickness and of density ρ on the inner and outer mantle surface be denoted with α , the momentum of second order of the rotationally symmetric disk of variable thickness and of density ρ , calculated for the axis of rotation, with J while the rotational flexibility of the disk in question with H .

There exists inequality relation

$$2 H \alpha^2 \leq J. \quad (5.1)$$

Proof:

It is well known that α^2 can be obtained as a solution to the minimum problem given below:

$$\alpha^2 = \min_{p=p(r)} \frac{\frac{E}{1 - \nu^2} \int_a^b r h \left[\left(\frac{dp}{dr} \right)^2 + \frac{p^2}{r^2} + 2 \nu \frac{dp}{dr} \frac{p}{r} \right] dr}{\rho \int_a^b r H p^2 dr} \quad (5.2)$$

Function $p = p(r)$ in formula (5.2) in closed interval $a \leq r \leq b$ is a non-equally zero function which is continuous over closed interval $a \leq r \leq b$ and at least twice continuously differentiable per section in this interval.

Assume that $p(r) = t(r)$ (5.3)
in relation (5.2).

It follows from equations (4.2), (4.3) that

$$\alpha^2 \leq \frac{\frac{E}{1-\nu^2} \int_a^b r h \left[\left(\frac{dt}{dr} \right)^2 + \left(\frac{t}{r} \right)^2 + 2\nu \frac{dt}{dr} \frac{t}{r} \right] dr}{\rho \int_a^b r h t^2 dr} \quad (5.4)$$

On the basis of the Schwarz inequality, it can be written that

$$\left(\int_a^b \rho r h t r dr \right)^2 \leq \int_a^b \rho r h t^2 dr \int_a^b \rho r h r^2 dr. \quad (5.5)$$

The inequality relation (5.1) to be verified is directly obtained by combining relationships (2.3), (2.4), (5.4), (5.5) and formula

$$J = 2 \pi \rho \int_a^b r^3 h dr \quad (5.6)$$

5.2 Relation

It is quite easy to show that the sign of equality in relation (5.1) applies in case of a ring of width ν and thickness h as illustrated in Fig. 2. Natural angular frequency α of the radial rotationally symmetric free vibration of the ring can be determined on the basis of formula

$$\alpha^2 = \frac{U}{L}, \quad (5.7)$$

where

$$\begin{aligned} U &= \frac{1}{2E} \int_V \sigma_\phi^2 dV = \frac{\sigma_\phi^2}{2E} V = \frac{1}{2} E \left(\frac{e}{R} \right)^2 2 \pi R \nu h = \\ &= e^2 \frac{E}{R} \nu h \pi, \end{aligned} \quad (5.8)$$

$$L = \frac{1}{2} \int_V \rho e^2 dV = \frac{1}{2} \rho e^2 V = \frac{1}{2} \rho e^2 2 R \pi \nu H = e^2 \rho R \nu H \pi \quad (5.9)$$

BOUNDS OF ROTATIONAL FLEXIBILITY

In writing relationship (5.8),

$$\sigma_{\phi} = E \frac{e}{R} \quad (5.10)$$

has been utilized, where e is the amplitude of radial displacement. It follows from the above formulae that

$$\alpha^2 = \frac{E}{\rho R^2} \quad (5.11)$$

On the other hand,

$$J = 2 \pi R^3 \rho h v \quad (5.12)$$

in the present case.

By the use of formulae (1.17), (5.11), (5.12), it is possible to show that what we have said, namely that the sign of equality in relation (5.1) applies in case of a thin ring, a statement to be proved, is correct.

6. EXAMPLE FOR BRINGING ABOUT BOUNDS

6.1 Relation

On the basis of formula (2.3),

$$F = 1, \quad a \leq r \leq b \quad (6.1)$$

shall be selected to arrive at lower bound

$$H \geq \pi \frac{1 - \nu^2}{E} \rho^2 \frac{\left(\int_a^b h r^2 dr \right)^2}{\int_a^b \frac{h}{r} dr} \quad (6.2)$$

6.2 Relation

From relation (3.1), the upper bound given below,

$$H \leq \frac{\pi}{E} \rho^2 \int_a^b h r^5 dr, \quad (6.3)$$

can be obtained via substitution

$$c(r) = 0 \quad a \leq r \leq b \quad (6.4)$$

6.3 Relation

Assume that $c(r) = m(r)$ (6.5)
 in relation (3.1), where

$$m(r) = \frac{Eh}{1 - \nu} \frac{1}{2} \left(r \frac{dt}{dr} + \nu t \right). \quad (6.6)$$

In this case, the sign of equality applies in relation (3.1) that is

$$H = \frac{\pi}{E} \int_a^b \frac{1}{h} \left[\left(\frac{m^2}{r} + r \left(\frac{dm}{dr} \right)^2 - 2 \nu m \frac{dm}{dr} \right) - 2(3 + \nu) \rho r^2 m \right] dr + \frac{\pi}{E} \int_a^b h \rho^2 r^5 dr. \quad (6.7)$$

It is easy to accept that

$$H \geq \frac{\pi}{E} \left(\nu \int_a^b m^2 \frac{d}{dr} \left(\frac{1}{h} \right) dr - 2(3 + \nu) \int_a^b \rho r^2 m dr + \int_a^b h \rho^2 r^5 dr \right). \quad (6.8)$$

In relation (6.8), we have written that

$$\begin{aligned} -2 \int_a^b \frac{1}{h} \frac{dm}{dr} m dr &= - \int_a^b \frac{d}{dr} \left(\frac{m^2}{h} \right) dr + \int_a^b m^2 \frac{d}{dr} \left(\frac{1}{h} \right) dr = \\ &= - \left[\frac{m^2}{h} \right]_a^b + \int_a^b m^2 \frac{d}{dr} \left(\frac{1}{h} \right) dr = \int_a^b m^2 \frac{d}{dr} \left(\frac{1}{h} \right) dr, \end{aligned} \quad (6.9)_1$$

since

$$m(a) = 0, \quad m(b) = 0. \quad (6.9)_{2,3}$$

Now the investigation is limited to the case where

$$\frac{dh}{dr} < 0, \quad a \leq r \leq b. \quad (6.10)$$

It can be shown by elementary calculation that in this case

BOUNDS OF ROTATIONAL FLEXIBILITY

$$\min_{k(r)} \left\{ \nu \int_a^b k^2 \frac{d}{dr} \left(\frac{1}{h} \right) dr - 2(3 + \nu) \int_a^b \rho k r^2 dr \right\} =$$

$$= \frac{(3 + \nu)^2}{\nu} \rho^2 \int_a^b \frac{r^4}{\frac{d}{dr} \left(\frac{1}{h} \right)} dr . \quad (6.11)$$

With relationships (6.8) and (6.11) combined, the following theorem is obtained:

6.4 Theorem

Assume that

$$\frac{dh}{dr} < 0 , \quad a \leq r \leq b . \quad (6.12)$$

Inequality relation

$$H \geq \frac{\pi}{E} \rho^2 \left[\int_a^b h r^5 dr - \frac{(3 + \nu)^2}{\nu} \int_a^b \frac{r^4}{\frac{d}{dr} \left(\frac{1}{h} \right)} dr \right] \quad (6.13)$$

exists in this case.

6.5 Relation

Assume that

$$h(r) = A r^{-n} , \quad n > 0 . \quad (6.14)$$

Using inequality relations (6.4) and (6.13), the following bounds can be brought about in this case:

$$H \leq \frac{\pi}{E} \rho^2 A \frac{a^{6-n} - b^{6-n}}{n-6} , \quad (6.15)$$

$$H \geq \frac{\pi}{E} \rho^2 A \frac{a^{6-n} - b^{6-n}}{n-6} \delta(n) , \quad (6.16)$$

where

$$\delta(n) = 1 - \frac{(\nu + 3)^2}{n\nu} , \quad (n \neq 6) . \quad (6.17)$$

ECSEDI, I.

For the case $n = 6$, we obtain by use of the Bernoulli - L'Hospital rule that

$$\frac{\pi}{E} \rho^2 A \ln \left(\frac{b}{a} \right) \geq H \geq \frac{\pi}{E} \rho^2 A \ln \left(\frac{b}{a} \right) \delta \quad (6.18)$$

REFERENCES

1. S.P. Timoshenko-J.N. Goodier: Teoria uprugosti. Izd. Nauka. Glav. red. Fiz-Mat. lit. Moskva. 1975. pp. 96-99.
2. Chi-Teh Wang: Applied Elasticity. McGraw-Hill Publishing Company Ltd. New York - London - Toronto. 1953. pp. 63-70.

SIMULATION OF THE TIMBER LATTICE SHELL WITHOUT "IN-PLANE" SHEAR CAPACITY
BY DOUBLE-LAYER COSSERAT SURFACE

J. Füzy*

(Received: 5 September 1986)

Lattice shell as a term is used to describe doubly curved surface formed from a lattice of timber laths bolted together at uniform spacing. The laths are able to rotate around the bolts freely so a substituting surface have been found in the field of Cosserat theory.

NOTATION

Tensor notation is used, the Einstein summation convention is regarded as valid, Greek indices can take the values 1 and 2 only.

$N_{\alpha\beta}$	membrane forces in the lattice shell
$M_{\alpha\beta}$	"out-of-plane" moments in the laths
Q_{α}	shear forces corresponding to $M_{\alpha\beta}$
$M_{\alpha 3}$	"in-plane" moments in the laths
$n_{\alpha\beta}, m_{\alpha\beta}$	corresponding stresses, moments and forces in the substituting continuum shell
$q_{\alpha}, m_{\alpha 3}$	
u_{α}, u_3	displacement vector of the continuum shell
$d_{\alpha\beta}, d_{3\alpha}$	deformation tensor of the continuum shell
$d_{\alpha 3}$	
$f_{\alpha}, f_3^{(1)}$	rotation vector of the laths (double-layer Cosserat-surface)
$f_3^{(2)}$	
$b_{\alpha\beta}$	curvature tensor
$\epsilon_{\alpha\beta 3}, e_{\alpha\beta 3}$	
$\square \parallel_{\alpha} \square \parallel^{\alpha}$	covariant and contravariant derivations
\square_{α}	partial derivations
E, G	elastic moduli of the timber
I_{op}, I_{ip}, I_t	
$b_1=b_2=b$	spacing of the lattice
$\mathcal{L} \square$	differential operator (Pucher)

INTRODUCTION

Lattice shells consisting of timber laths running in two direction, such as timber lattice roof of the "Mannheim Bundesgartenschau" (1) can be

*J. Füzy, Hungarian Institute for Building Science (ÉTI) 1113 Budapest, Dávid F. u. 6., Hungary

used advantageously to cover large areas. The term lattice shell is used in this paper to describe a doubly curved surface formed from a lattice of timber laths bolted together at uniform spacing in two directions. When flat, the lattice is a mechanism with one degree of freedom. After erection, an element of a lattice shell consists of a parallelogram of four laths.

The method of erection was developed by Professor Otto. The first structure of this type was erected for the German Building Exhibition, Essen, 1962, (2). In 1965, in collaboration with Professor Rolf Gutbord of Stuttgart, he won the design competition of the German Federal Pavilion for Montreal Expo' 67 (4). The main structure was a large continuous cable net roof, within the roof there was a timber lattice dom covering an auditorium.

BASIC RELATIONS

General Statements

Due to the method of erection (1), the lattice shell can be considered sufficiently shallow for all the approximations used in the shallow-shell theory to be accepted. The laths are set closely enough to substitute the structure by a surface. The conditions of such an approximation were clarified in (3).

There occur several problems in the course of the computations so we attempt to set up differential equations suitable for calculating the internal forces and deformations of lattice shells of such kind by using a continuous surface. The special structure considered here cannot take membrane shear forces in the classical sense, but the shear forces acting on the laths can be connected with the couple-stresses of the micro-polar surface which, in that case, correspond to the "in-plane" moments rising in the laths. The rotation $f_3^{(1)}$ and $f_3^{(2)}$ of the laths about the intersection point are independent. (See Fig. 1.)

The corresponding forces and stresses acting on the lattice and the surface shell element are shown on Fig. 2.

The general equations of a Cosserat-surface can be written as follows (5):

TIMBER LATTICE SHELL

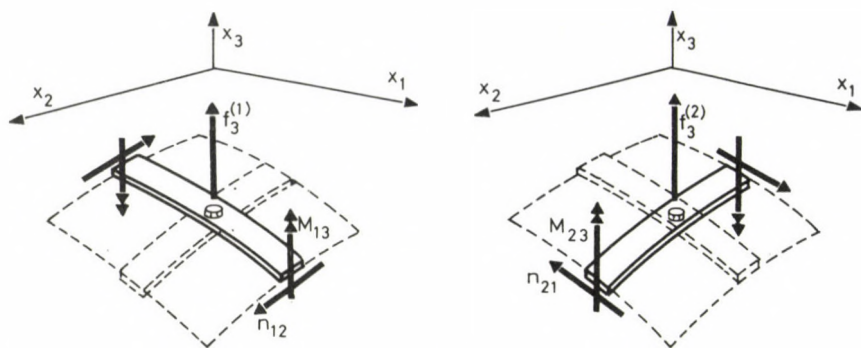


Fig. 1. Notation

$$\left. \begin{aligned} d_{\alpha\beta} &= u_{\alpha} \parallel_{\beta} - u_3 b_{\alpha\beta} - \epsilon_{\alpha\beta 3} f^3 \\ d_{3\beta} &= u_{3, \beta} - u_{\gamma} b^{\gamma\beta} - \epsilon_{3\beta\gamma} f^{\gamma} \\ d_{\beta 3} &= -u_{\gamma} b^{\gamma\beta} - \epsilon_{\beta 3\gamma} f^{\gamma} \end{aligned} \right\} \text{geometrical relations}$$

$$\left. \begin{aligned} n^{\alpha\beta} \parallel_{\alpha} + q^{\alpha} b^{\beta}_{\alpha} &= 0 \\ n^{\alpha\beta} b_{\beta\alpha} + q^{\alpha} \parallel_{\alpha} &= p_3 \end{aligned} \right\} \text{stress equilibrium (1)}$$

$$\left. \begin{aligned} m^{\alpha\beta} \parallel_{\alpha} - m^{\alpha 3} b^{\beta}_{\alpha} - q^{\beta} &= 0 \\ m^{\alpha 3} \parallel_{\alpha} - m^{\alpha\beta} b_{\alpha\beta} - n^{\alpha\beta} \epsilon_{\alpha\beta} &= 0 \end{aligned} \right\} \text{couple-stress equilibrium}$$

Because in our case we assumed the shell to be shallow and the coordinate system to be rectangular, the difference between the covariant and contravariant derivatives vanishes and only partial derivatives exist, the equilibrium equations take the form as follows:

$$\left. \begin{aligned} n_{11,1} + n_{21,2} + q_1 b_{11} + q_2 b_{12} &= 0 \\ n_{12,1} + n_{22,2} + q_1 b_{21} + q_2 b_{22} &= 0 \end{aligned} \right\} \quad (2)$$

$$n_{11} b_{11} + n_{12} b_{21} + n_{21} b_{12} + n_{22} b_{22} + q_{1,1} + q_{2,2} = p_3 \quad (3)$$

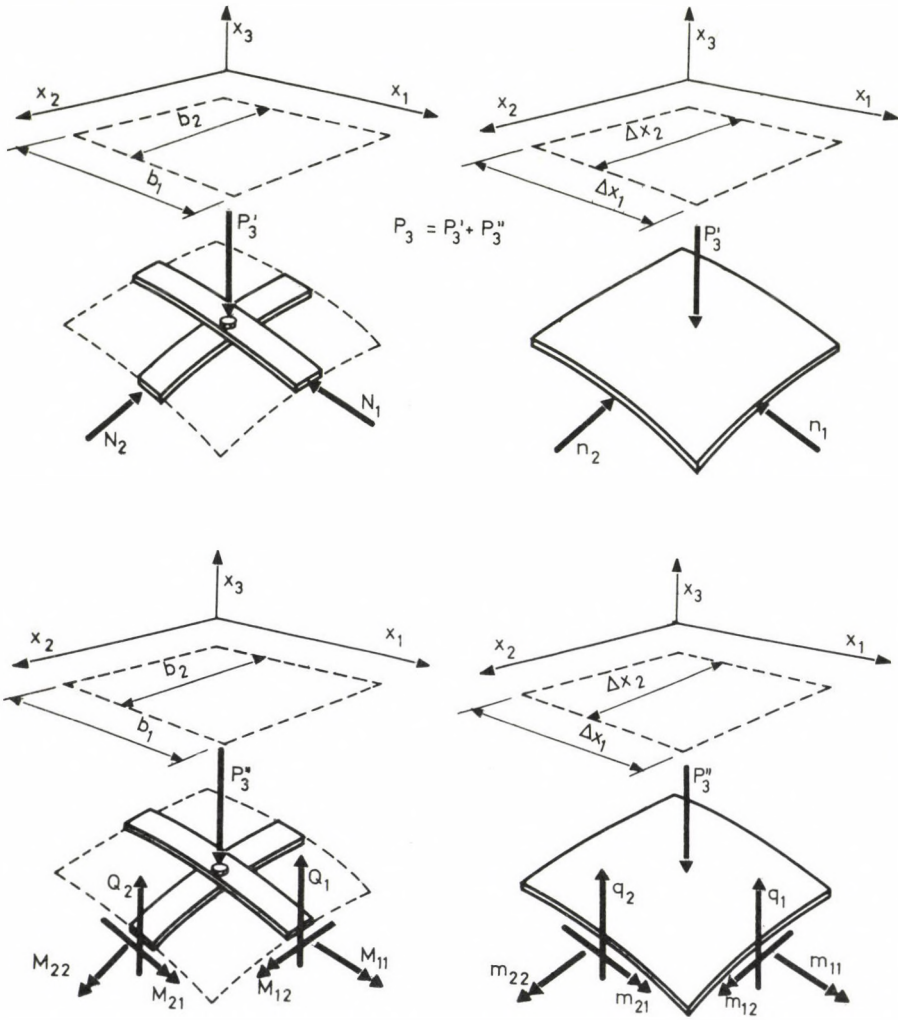


Fig. 2. Corresponding forces and stresses

$$\left. \begin{aligned} m_{11,1} + m_{21,2} - m_{13}b_{11} - m_{23}b_{12} - q_1 &= 0 \\ m_{12,1} + m_{22,2} - m_{13}b_{21} - m_{23}b_{22} - q_2 &= 0 \end{aligned} \right\} \quad (4)$$

$$\left. \begin{aligned} m_{13,1} - m_{11}b_{11} - m_{12}b_{12} - n_{12}e_{12} &= 0 \\ m_{23,2} - m_{22}b_{22} - m_{21}b_{21} - n_{21}e_{21} &= 0 \end{aligned} \right\} \quad (5)$$

TIMBER LATTICE SHELL

It is worth mentioning that in this theory $m_{11} = -m_{22}$ are the torsion moments and m_{12} and m_{21} are the bending moments. Taking into account that the value of the permutation tensor is $e_{12} = -e_{21} = 1$, the final form of eqs (5) will be:

$$\left. \begin{aligned} m_{13,1} - m_{11}b_{11} - m_{12}b_{12} &= n_{12} \\ m_{23,2} - m_{22}b_{22} - m_{21}b_{21} &= n_{21} \end{aligned} \right\} \quad (5)$$

According to this shell theory the bending moments will be obtained from the derivative of the independent variable, rotation function f_α , i.e. from the relative rotation.

Constitutive equations

The theory discussed above differs from the normal bending theory of shells in that the couple-stresses m_{13} and m_{23} exist, so it is justified to formulate the rotation vector based on the following assumption:

$$f_\alpha = \frac{1}{2}u_{3,\gamma} e_{3\gamma\alpha} \quad \text{and} \quad f_3 \equiv f_3^{(1)}, f_3^{(2)} \quad (6)$$

which means that the rotation vector of the surface point is defined by the kinematic constraint above and only $f_3^{(1)}$ and $f_3^{(2)}$ components are independent variables. In components:

$$\begin{aligned} f_1 &= u_{3,2} \\ f_2 &= -u_{3,1} \\ f_3^{(1)}, f_3^{(2)} \end{aligned} \quad (7)$$

Based on that assumption the following simplified constitutive equations are proposed:

$$m_{12} = k_1 u_{3,11} \quad \text{where} \quad k_1 = EI_{op}/b$$

$$m_{21} = k_1 u_{3,22}$$

$$m_{11} = -m_{22} = k_2 u_{3,12} \text{ where } k_2 = (GI_t)/b \quad (8)$$

$$q_1 = k_1 u_{3,1}$$

$$q_2 = k_2 u_{3,2}$$

and

$$\left. \begin{aligned} m_{13} &= k_3 f_{3,1}^{(1)} \\ m_{23} &= k_3 f_{3,2}^{(2)} \end{aligned} \right\} \text{ where } k_3 = EI_{ip} / b \quad (9)$$

$$\left. \begin{aligned} n_{12} &= k_4 d_{12} = k_4 f_3^{(1)} \\ n_{21} &= k_4 f_3^{(2)} \end{aligned} \right\} \text{ where } k_4 = \frac{12EI_{ip}}{b^3}$$

As $f_3^{(1)}$ and $f_3^{(2)}$ represent the rigid rotation of surface point connected with one of the laths, the relation between d_{12} and n_{12} can be deduced in the following way (see Fig. 3):

$$f_3^{(1)} = n_{12} \frac{d^3}{12 EI_{ip}}$$

$$f_3^{(2)} = n_{21} \frac{b^3}{12 EI_{ip}}$$

By setting up these simplified constitutive equations further assumptions were adopted, namely:

- the lattice structure has no contraction, so the corresponding surface must have zero Poisson ratio,
- in the deformation relations in eqs (1) the members multiplied with several components of tensor $b_{\alpha\beta}$ are neglected reasonable the shell is assumed to be shallow,
- the dimension of the laths are supposed to be similar in the two directions.

Governing equations of the problem

Substituting the constitutive equations defined above in the equilibrium equations (2), (3), (4) and (5) and substituting q_α from (4) into

TIMBER LATTICE SHELL

eqs (3) and taking into account that $b_{12} = b_{21}$ we obtain the following set of equations:

$$\left. \begin{aligned} n_{11,1} + n_{21,2} & & q_1 b_{11} + q_2 b_{12} &= 0 \\ n_{12,1} + n_{22,2} & & q_1 b_{21} + q_2 b_{22} &= 0 \end{aligned} \right\} \quad (10.a)$$

$$\left. \begin{aligned} n_{11} b_{11} + n_{22} b_{22} + \mathcal{L} u_3 & & -(m_{13} b_{11} - m_{23} b_{12}), 1^- \\ & & -(m_{13} b_{21} - m_{23} b_{12}), 2^+ \\ & & + b_{12} (n_{12} + n_{21}) &= & p \end{aligned} \right\} \quad (10.b)$$

$$\left. \begin{aligned} k_3 f_{3,11}^{(1)} & & -m_{11} b_{11} - m_{12} b_{12} &= & = 2k_4 f_3^{(1)} \\ k_3 f_{3,22}^{(2)} & & -m_{22} b_{22} - m_{21} b_{21} &= & = 2k_4 f_3^{(2)} \end{aligned} \right\} \quad (11)$$

where the differential operator is:

$$\mathcal{L} \square \equiv k_1 \square_{,1111} + k_2 \square_{,1122} + k_1 \square_{,2222} \quad (12)$$

Comparing these equations with the results of Kollar's (9) article we have found that if we neglect the members multiplied by several components of the curvature tensor $b_{\alpha\beta}$ (middle column), based on the assumption that the shell is shallow, the eqs (10) are essentially the same, but eqs (11) is new in this form. The original form of (5) can be found in (9) also.

In this paper we supposed the laths have the same dimensions and spacing, but in the same way it is possible to derive more general equations for different laths.

If we accept the same approximations as in (9), the middle column can be neglected in (10) and (11) and we obtain:

$$\left. \begin{aligned} n_{11,1} + n_{21,2} &= 0 \\ n_{12,1} + n_{22,2} &= 0 \end{aligned} \right\} \quad (13)$$

$$\eta_{11}b_{11} + \eta_{22}b_{22} + \mathcal{L} u_3 = p_3 \quad (14)$$

$$\left. \begin{aligned} k_3 f_{3,11}^{(1)} &= k_4 f_3^{(1)} \\ k_4 f_{3,22}^{(2)} &= k_4 f_3^{(2)} \end{aligned} \right\} \quad (15)$$

We can eliminate η_{21} and η_{12} in eqs (13) by using eqs (9). Eqs (11) can be written in a simpler form if we eliminate the common members in k_3 and k_4 in eqs (15). Finally, we get the following set of equations:

$$\eta_{11,1} = -k_4 f_{3,2}^{(1)} \quad (16)$$

$$\eta_{22,2} = k_4 f_{3,1}^{(2)} \quad (17)$$

$$\eta_{11}b_{11} + \eta_{22}b_{22} + \mathcal{L} u_3 = p_3 \quad (18)$$

$$\frac{b^2}{24} f_{3,11}^{(1)} = f_3^{(1)} \quad (19)$$

$$\frac{b^2}{24} f_{3,22}^{(2)} = f_3^{(2)} \quad (20)$$

We have five equations containing five unknown functions η_{11} , η_{22} , u_3 , $f_3^{(1)}$ and $f_3^{(2)}$.

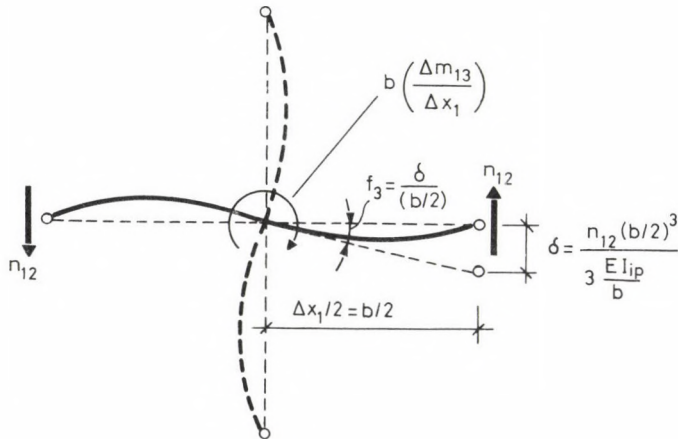


Fig. 3. Constitutive relation between rotation and shear force

TIMBER LATTICE SHELL

CONCLUSION

Timber lattice shells such as the "Bundesgartenschau" in Mannheim have been discussed in the paper. The timber laths running in two directions were positioned originally in plane, the planned shell surface has been realized by the lifting method while the laths at the edge of the shell structure still remain in plane. Applying this lifting method the structure would be charged with "eigenstresses" as bending moment in plane, the shear forces corresponding to these moments and, when the forces of lifting act no longer and the laths are fixed along the edges, normal (arch) forces in the laths also. In this paper we do not intend to deal with the lifting method and the eigenstresses caused by it.

This paper is focused mainly on the computing method of the forces due to the outer load. The results should be superposed on the eigenstresses, to be defined by another computing method.

A substituting continuum is proposed which must fulfil the governing equations (16), (17), (18), (19) and (20). Examining eqs (19) and (20) it can be stated that the rotation $f_3^{(1)}$ and $f_3^{(2)}$ which are characteristic of the "in-plane" bending moments, depends only on the boundary conditions, in the main field of the surface they vanish, eqs (19) and (20) being a damped wave equations. The width of the boundary layer where $f_3^{(1)}$ and $f_3^{(2)}$ exist depends on the lattice spacing.

From eqs (16) and (17) it is plausible that the normal (arch) forces in the laths depend on one variable only (because the shell cannot take shear stresses) and so the outer load p_3 can be balanced by them only in part, a further part of the load must be balanced by the "out-of-plane" moments and shear stresses according to eqs (18).

It is worth mentioning that the boundary layer where $f_3^{(1)}$ and $f_3^{(2)}$ differ from zero must not necessarily connected with the edge of the shell.

REFERENCES

1. Happold, E., Liddell, W.: Timber Lattice Roof for the Mannheim Bundesgartenschau, Structural Eng. 53: 1975, 99-135.
2. Roland C.: The Work of Frei Otto; Longman, 1970.
3. Hegedüs I.: Computation of the Stretched Network Shape of Timber Lattice Shells, Acta Techn. Hung. 1985 (in print)
4. Report on the German Pavilion for the Montreal Expo' 1967, Institute für Leichte Flächentragwerke (unpublished)

FÜZY, J.

5. Füzy J.: Civil Engineering Applications of Microelastic Continua, Hungarian Institute for Building Science Scientific Reports Series 1985.
6. Flügge W.: Tensor Analysis and Continuum Mechanics, Springer Verlag, New York – Heidelberg – Berlin, 1982.
7. Flügge W.: Statik und Dynamik der Schalen, Springer Verlag, Berlin – Göttingen – Heidelberg, 1962.
8. Flügge W.: Stresses in Shells, Springer Verlag, Berlin – Heidelberg – New York 1973.
9. Kollár L.: Continuum Equations of Timber Lattice Shells, Acta Techn. Hung. 94 (1982), 133–141.

OPTIMUM DESIGN OF PLASTIC BAR STRUCTURES FOR SHAKEDOWN
AND DYNAMIC LOADING

S. Kaliszky* and I. Knébel**

(Received: 28 January 1986)

In this paper, two different problems of optimum design are presented. The first problem is the optimum design of elastic-perfectly plastic bar structures (frames and trusses) under variable (shakedown) loading while the second one is the optimum design of rigid-perfectly plastic bar structures under dynamic pressure with specified displacement constraints. In both cases, nonlinear objective functions are used. The proposed two methods can be formulated as a nonlinear programming problem and their solutions are based on the same iterative procedure. The applications are illustrated by numerical examples.

INTRODUCTION

The optimum design of elasto-plastic frames under variable repeated (shakedown) loading with linear objective function was studied among others by Heyman /14/, Cohn and Parimi /15/. This can be formulated as a linear programming problem. A few other papers deal with the optimum design of rigid-plastic structures under short-time dynamic pressure or impulsive loading (e.g. /11, 12, 16/). In this case, the problem is more complicated and leads to nonlinear programming.

The first part of this paper deals with the generalization of the optimum design methods described in /14/ and /15/ using nonlinear objective functions and extending the solution to any kind of bar structures (frames, trusses etc.). In the second part, the general approximate method given in /11, 12/ will be applied to bar structures under dynamic pressure using again non-linear objective function. The solution of both problems is based on the same iterative procedure which was already successfully applied to the optimum design of elastic structures with displacement constraints and/or specified internal forces /6, 7, 10/.

* Prof. S. Kaliszky, Technical University, H-1111 Budapest, Műgyetem rkp. 3., Hungary

** I. Knébel, Research Fellow, Technical University, H-1111 Budapest, Műgyetem rkp. 3., Hungary

2. GEOMETRICAL RELATIONSHIPS

In the fundamental equations of bar structures, among others three geometrical variables play important role: area A , moment of inertia I and plastic bearing capacity Q_p (plastic moment M_p or yield force N_p) of the cross-sections. Assume that the relationships between these variables can be expressed by formulae

$$Q_p = B_0 A^{1/\alpha} \quad \text{or} \quad A = B Q_p^\alpha, \quad (1)$$

$$I = C_0 A^{1/\beta} \quad \text{or} \quad A = C I^\beta. \quad (2)$$

For example in case of frames with rectangular cross-sections and with given ratio $b = 2a$, one can obtain (Fig. 1/a):

$$M_p = \frac{\sigma_y}{2\sqrt{2}} A^{3/2}, \quad \text{or} \quad A = \left(\frac{2\sqrt{2}}{\sigma_y} \right)^{2/3} M_p^{2/3}, \quad (3)$$

$$I = \frac{1}{6} A^2, \quad \text{or} \quad A = \sqrt{6} I^{1/2}. \quad (4)$$

Here σ_y is the yield stress of the material.

In case of I beams with fixed height b and web thickness v , formulae (1) and (2) can be approximated by linear relationships (Fig. 1/b):

$$M_p \approx \frac{\sigma_y b}{2} A, \quad \text{or} \quad A \approx \frac{2}{\sigma_y b} M_p, \quad (5)$$

$$I \approx \frac{b^2}{4} A, \quad \text{or} \quad A \approx \frac{4}{b^2} I. \quad (6)$$

For trusses the relationships are also linear

$$N_p = \sigma_y A, \quad \text{or} \quad A = \frac{1}{\sigma_y} N_p. \quad (7)$$

3. OPTIMUM DESIGN OF STRUCTURES SUBJECT TO SHAKEDOWN

Consider a linear elastic-perfectly plastic statically r times indeterminate bar structure with given geometry and constructed of $i = 1, 2, \dots, n$ prismatic members with cross-sectional areas A_i , moments of

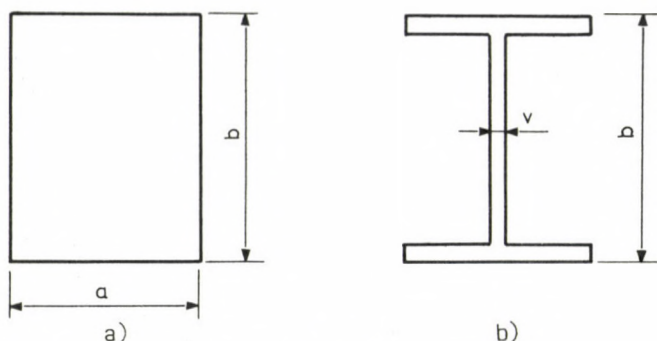


Fig. 1.

inertia I_i , plastic bearing capacities Q_{pi} and given lengths λ_i . The structure is subjected to variable repeated (shakedown) loading. Let us denote the extremal values of the internal forces calculated from all the possible combinations of the variable loads and arising in critical cross-sections $j = 1, 2, \dots, m$ with Q_{jmax} and Q_{jmin} , respectively. Besides, Q_{Rj} denote the unknown self-equilibrating residual internal forces of the critical cross-sections. Then, the shakedown of the structure can be expressed in the following manner [13]:

$$Q_{jmax} + Q_{Rj} \leq Q_{pi}, \quad (j = 1, 2, \dots, m) \quad (8)$$

$$Q_{jmin} + Q_{Rj} \geq -Q_{pi}.$$

The criterion of optimality (minimum volume) is of the form:

$$V = \sum \lambda_i A_i = \min! \quad (i = 1, 2, \dots, n) \quad (9)$$

Besides, the minimum values of the cross-sectional areas or that of the bearing capacities might be specified

$$A_i \geq A_0, \quad \text{or} \quad Q_{pi} \geq Q_{p0} \quad (10)$$

where A_0 and Q_{p0} are given constants.

Q_{jmax} and Q_{jmin} appearing in the inequalities (8) are in nonlinear relationship with A_i and I_i and with Q_{pi} , respectively:

$$Q_{j\max} = Q_{j\max}(A_i, I_i) = Q_{j\max}(Q_{pi}), \quad (11)$$

$$Q_{j\min} = Q_{j\min}(A_i, I_i) = Q_{j\min}(Q_{pi})$$

while Q_{Rj} can be expressed in linear form in terms of unknown statically indeterminate forces X_k ($k = 1, 2, \dots, r$):

$$Q_{Rj} = \sum_{k=1}^r a_{kj} X_k. \quad (12)$$

Here a_{kj} denote constants.

Substituting formulae (1), (2), (11) and (12) in Eqs (8) – (10), our optimum design problem can be formulated as follows:

minimize

$$V = \sum_{i=1}^n \ell_i B_i Q_{pi}^\alpha, \quad (13)$$

subject to

$$Q_{j\max}(Q_{pi}) + \sum_{k=1}^r a_{kj} X_k \leq Q_{pi}, \quad (i = 1, 2, \dots, m) \quad (14)$$

$$Q_{j\min}(Q_{pi}) + \sum_{k=1}^r a_{kj} X_k \geq -Q_{pi},$$

$$Q_{pi} \geq Q_{po}.$$

This is a nonlinear mathematical programming problem, from which statically indeterminate forces X_k , ($k = 1, 2, \dots, r$) and design variables Q_{pi} , ($i = 1, 2, \dots, n$) can be determined. The direct solution of this problem is, however, fairly complicated and therefore generalizing the idea of /10, 13/, an iterative solution described below might be applied.

In the first step, let us choose proper initial values for the cross-sectional areas and denote them with A_i^0 . Using Eqs (1) and (2), I_i^0 and Q_{pi}^0 can be calculated and from these the first values of $Q_{j\max}$ and $Q_{j\min}$ (denoted with $Q_{j\max}^1$ and $Q_{j\min}^1$) respectively, can also be determined by the elastic solution of the structure. Substituting these values in Eqs (13) and (14), we obtain the problem:

OPTIMUM DESIGN OF BAR STRUCTURES

$$\text{minimize}_n \quad V^{(1)} = \sum_{i=1}^n \ell_i B_i \left[Q_{pi}^{(1)} \right]^\alpha, \quad (15)$$

subject to

$$Q_{jmax}^{(1)} + \sum_{k=1}^r a_{kj} X_k^{(1)} \leq Q_{pi}^{(1)},$$

$$Q_{jmin}^{(1)} + \sum_{k=1}^r a_{kj} X_k^{(1)} \geq -Q_{pi}^{(1)}, \quad (16)$$

$$Q_{pi}^{(1)} \geq Q_{po}.$$

This mathematical programming problem is much simpler than the former one defined by Eqs (13) and (14), since now $Q_{jmax}^{(1)}$ and $Q_{jmin}^{(1)}$ denote constants and therefore the inequalities (16) are linear and only the objective function (15) is nonlinear. The solution of this problem provides $X_k^{(1)}$, $Q_{pi}^{(1)}$ and $A_i^{(1)}$, $I_i^{(1)}$ respectively. Then the corrected values of Q_{jmax} and Q_{jmin} can be calculated and the procedure described above should be repeated until the differences between the results of two subsequent steps are sufficiently small.

The mathematical programming problem with nonlinear objective function and linear constraints can be solved by the use of the reduced gradient method elaborated by Wolfe /9/. For the solution, computer programs are available /8/. According to experience with the solution of different numerical examples, the convergency of the iteration is good and after a few steps, sufficiently correct results can be obtained.

4. OPTIMUM DESIGN OF STRUCTURES SUBJECTED TO DYNAMIC PRESSURE

Consider a rigid-perfectly plastic bar structure (frame or truss) with given geometry constructed of $i = 1, 2, \dots, n$ prismatic members with cross-sectional areas A_i , plastic bearing capacities Q_{pi} and given lengths ℓ_i . The structure is subjected to high-intensity, short-time dynamic pressure which is normal to the axis of the structure and is expressed in the form

$$T(s,t) = p(t) T_0(s), \quad (17)$$

Here $T_0(s)$ defines the distribution of the loads along axis s of the structure and loading parameter function $p(t)$ describes the time variation of the pressure.

First let us consider the equivalent quasi-static problem. To calculate a kinematically admissible load multiplier p_c for quasi-static load $T_0(s)$, we have to consider a yield mechanism which is defined by displacement function $w(s)$ and deformations q_j of plastic parts $j = 1, 2, \dots, m$ (hinges or bars) of the structure. Then, according to the kinematical theorem of limit analysis /13/, p_c can be obtained from formula

$$p_c = \frac{\sum_{j=1}^m Q_{pj} q_j}{\int_0^L T_0(s)w(s)ds} \quad , \quad (18)$$

where

$$L = \sum_{i=1}^n \ell_i \quad .$$

In case of dynamic pressure, the positions of the plastic parts (hinges or bars) are generally not fixed during the action because of the inertia forces i.e. the structure undergoes unstationary motion described by a function $w(s,t)$. After time t_f , the structure stops moving and permanent displacements $w_f = w(s,t_f)$ remain in the structure. The goal of the dynamic analysis is to calculate the permanent displacements which should not exceed given allowable values.

The analysis of the unstationary motion even in case of simple structures is fairly complicated. Therefore, to simplify the solution, we might apply a kinematical approximation /11, 12/. According to this method, a kinematically admissible displacement field has to be superimposed on the structure and then its motion can be described by a function in a separated-variable form

$$w(s,t) = W(t)w_0(s) \quad . \quad (19)$$

Here $w_0(s)$ is any postulated kinematically admissible displacement field (yield mechanism) and $W(t)$ an unknown displacement parameter function. Using this approximation, the problem is reduced to the investigation of an equivalent one-degree-of-freedom system the solution of which can be expressed in close form. Assuming e.g. a square loading parameter function shown in Fig. 2, the maximum value of $W(t)$ can be obtained as follows /11, 12/:

OPTIMUM DESIGN OF BAR STRUCTURES

$$W_f = \frac{1}{2} K p_0 t_0^2 \left(\frac{p_0}{p_c} - 1 \right) . \quad (20)$$

Having W_f , the permanent displacements of the structure can be approximated by function

$$w_f = W_f w_0(s) . \quad (21)$$

In Eq. (20), p_c is the kinematically admissible load multiplier for load $T_0(s)$ and associated with assumed displacement field $w_0(s)$, and K is a constant:

$$K = \frac{\int_0^L T_0(s) w_0(s) ds}{\rho \sum_{i=1}^n A_i \int_0^l w_0^2(s) ds} \quad (22)$$

Here ρ is the density of the material of the structure. The reliability of the approximation might be improved by using more kinematically admissible displacement functions $w_{oh}(s)$, $h = 1, 2, \dots, r$ and calculating the corresponding permanent displacements $w_{fh} = W_{fh} w_{of}(s)$. Then, their maximum values are competent in the design.

Having the results given above and using the square loading parameter function of Fig. 2, the optimum design problem can be formulated as below:

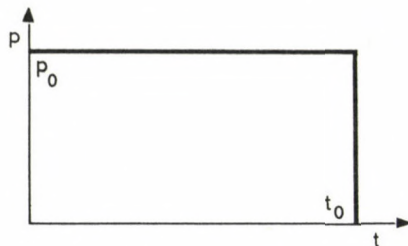


Fig. 2.

minimize

$$V = \sum_{i=1}^n A_i l_i , \quad (23)$$

subject to

$$W_{fh} = \frac{1}{2} K_h p_o t_o^2 \left(\frac{p_o}{p_{oh}} - 1 \right) \leq W_{oh}, \quad (24)$$

$$A_i \geq A_o.$$

Here

$$p_{ch} = \frac{\sum_{j=1}^m Q_{pjh} q_{jh}}{\int_0^L T_o(s) w_{oh}(s) ds} = \frac{1}{C_h} \sum_{j=1}^m q_{jh} Q_{pjh}, \quad (25)$$

$$K_h = \frac{\int_0^L T_o(s) w_{oh}(s) ds}{\rho \sum_{i=1}^n A_i \int_0^{\ell_i} w_{oh}^2(s) ds} = \frac{C_h}{\rho \sum_{i=1}^n D_{ih} A_i}, \quad (26)$$

W_{oh} denotes the specified permissible values of displacement parameter functions $W_h(t)$ and

$$C_h = \int_0^L T_o(s) w_{oh}(s) ds, \quad D_{ih} = \int_0^{\ell_i} w_{oh}^2(s) ds \quad (27)$$

are constants.

With (1), (25) and (26) substituted into Eqs (23) and (24) we can write:

minimize

$$V = \sum_{i=1}^n \ell_i B_i Q_{pi}^\alpha; \quad (i = 1, 2, \dots, n), \quad (28)$$

subject to

$$\frac{1}{\rho_0 C_h} \sum_{j=1}^m q_{jh} Q_{pjh} \geq \frac{K_h}{K_h + 2 \frac{w_{oh}}{\rho_0 t_0^2}} = \frac{\frac{C_h}{\sum_{i=1}^n D_{ih} B_{oi} Q_{pi}^\alpha}}{\frac{C_h}{\sum_{i=1}^n D_{ih} B_{oi} Q_{pi}} + 2 \frac{w_{oh}}{\rho_0 t_0^2}}, \quad (29)$$

$$(j = 1, 2, \dots, m; h = 1, 2, \dots, r),$$

$$Q_{pi} \geq Q_{po}.$$

As it is seen, both the objective function and the design constraints are nonlinear functions of design parameters Q_{pi} . To solve the problem, one can use the same iterative procedure that was described in Section 3. First we assume proper initial values for Q_{pi} (say $Q_{pi}^{(0)}$), calculate the right side of Eqs (29), and solve the mathematical programming problem with linear constraints and nonlinear objective function. Obtaining design variables $Q_{pi}^{(1)}$, we repeat this procedure until the differences between the results of two subsequent steps are sufficiently small.

5. EXAMPLES

The application of the methods described above will be illustrated for the structure shown in Fig. 3. The cross-section of the frame is rectangular with ratio $b = 2a$ (see Fig. 1/a). Cross-sectional areas A_i or plastic moments $M_{pi} = B_0 A_i^{3/2}$ of the three bars ($i = 1, 2, 3$) are the design variables. The critical cross-sections are at the corners and at the points of application of loads ($j = 1, 2, \dots, m = 6$). Using Eq. (13), the optimality condition is, as follows:

$$V = 6M_{p1}^{2/3} + 10M_{p2}^{2/3} + 6M_{p3}^{2/3} = \min! \quad (30)$$

a) First suppose that the elasto-plastic structure is subjected to static variable forces $0 \leq F_1 \leq 5$ kN and $0 \leq F_2 \leq 15$ kN which can

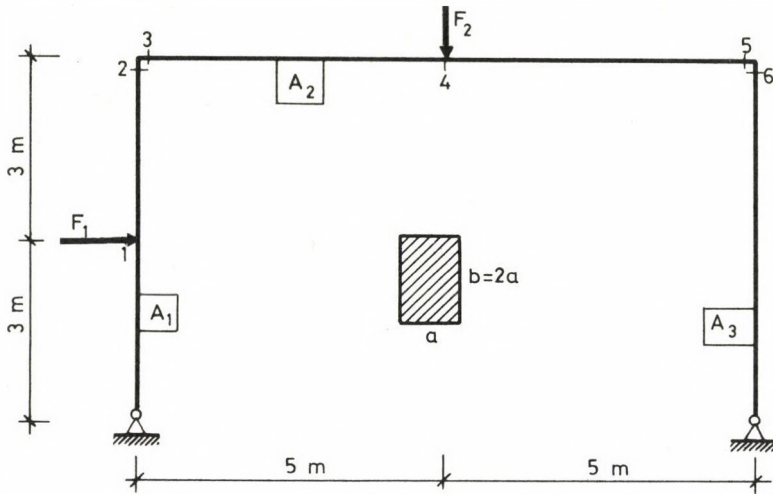


Fig. 3.

act separately or in combination, and consider the problem of optimum design subject to shakedown.

Statically indeterminate forces X_1 and X_2 of the elastic structure calculated from $F_1 = 5$ kN and $F_2 = 15$ kN, respectively are

$$X_1 = \frac{112.5/I_1 + 1350/I_2 + 360/I_3}{72/I_1 + 360/I_2 + 72/I_3} \quad \text{and} \quad (31)$$

$$X_2 = \frac{-1125/I_2}{72/I_1 + 360/I_2 + 72/I_3}$$

The corresponding bending moments, M_{j1} and M_{j2} of the critical cross-sections and residual bending moments M_{Rj} calculated from unknown force X_R are shown in Table 1. Following Eqs (8), the condition of shakedown has the form

$$M_{j\max} + M_{Rj} \leq M_{pi} \quad , \quad (32)$$

$$M_{j\min} + M_{Rj} \geq -M_{pi} \quad .$$

OPTIMUM DESIGN OF BAR STRUCTURES

For the minimum values of the areas and plastic moments no restrictions are specified, i.e. $A_0 = M_{p0} = 0$.

Table 1

j	M_{j1}	M_{j2}	M_{Rj}
1	$2X_1$	$3X_2$	$3X_R$
2	$-15+6X_1$	$6X_2$	$6X_R$
3	$-15+6X_1$	$6X_2$	$6X_R$
4	$-22.5+6X_1$	$37.5+6X_2$	$6X_R$
5	$-30+6X_1$	$6X_2$	$6X_R$
6	$-30+6X_1$	$6X_2$	$6X_R$

First let us assume that $I_i = I^{(0)} = \text{const}$ and $M_{pi} = M_p^{(0)} = \text{const}$ and solve this simple problem. Using Eqs (31) and Table 1, $M_{j\text{max}}^{(0)}$ and $M_{j\text{min}}^{(0)}$ can be obtained and the condition (30) can be replaced by $M_p^0 = \min!$ This together with Eqs (32) is equivalent to the usual shakedown problem where, however, instead of the common shakedown parameter of the loads, it is constant plastic moment $M_p^{(0)}$ that has to be determined. The solution is shown in the first row of Table 2.

Assuming now that $I_i = I^{(0)} = \text{const}$ but $M_{pi} = M_{pi}^{(1)}$ ($i = 1,2,3$) are unknown, let us solve the problem again. The solution of the linear inequalities (32) with the nonlinear optimality condition yields the results shown in the second row of Table 2.

Using Eqs (3) and (4), from these plastic moments the new values of moments of inertia $I_i^{(1)}$ can be obtained and then $M_{j\text{max}}^{(1)}$ and $M_{j\text{min}}^{(1)}$ can also be determined. This makes possible the solution of the next mathematical programming problem which yields plastic moments $M_{pi}^{(2)}$.

Repeating the procedure, after a few steps sufficiently good results can be obtained.

As seen in Table 2, the optimum plastic moments deviate significantly from the solution of the frame with constant plastic moment and savings of 15 % in volume of the frame are obtained. Note that steps 1-5 yield less

Table 2

steps	M_{p1}	M_{p2}	M_{p3}	V
0	25.8	25.8	25.8	192.0
1	11.7	25.8	20.0	162.4
2	9.89	27.6	20.3	163.7
3	9.21	28.3	20.6	164.2
4	8.91	22.6	20.7	164.5
5	8.78	28.7	20.8	164.6
6	8.72	28.8	20.8	164.7
7	8.69	28.8	20.8	164.7
8	8.67	28.8	20.8	164.7

volume than the last two ones but the corresponding plastic moments and moments of inertia are not compatible since they do not fulfil the inequalities (32).

b) Consider now the dynamic problem when dynamic forces $F_1 = p_0 \cdot 5$ kN and $F_2 = p_0 \cdot 15$ kN are acting simultaneously and are characterized by the square loading parameter function of Fig. 2 with values $p_0 = 1$ and $t_0 = 0.05$ s. The density of the material is $\rho = 8000$ kg/m³ and the permissible permanent displacements in vertical and in horizontal directions are $W_0^V = 0.25$ m and $W_0^H = 0.30$ m respectively. The minimum value of the applicable plastic moment is $M_{p0} = 5$ kNm.

The possible yield mechanisms of the structure are shown in Table 3. These 4 mechanisms, however, depending on whether the plastic hinges are at the right or the left hand side of the corners, lead to 12 different load multipliers ($h = 1, 2, \dots, r = 12$). Using Eqs (18) and (22), the corresponding values of K_h and p_{ch} are given in Table 3. Then, considering Eqs (29), inequalities

$$\frac{p_{ch}}{p_0} \geq \frac{K_h}{K_h + 2 w_{oh} / p_0 t_0^2} \quad (h = 1, 2, \dots, r = 12) \quad (33)$$

can be constructed which together with the objective function (30) and with restriction

Table 3.

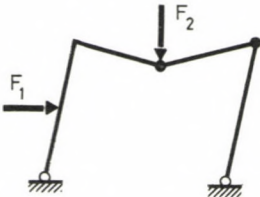
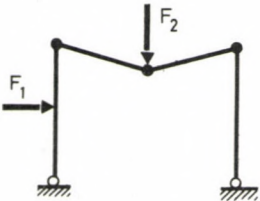
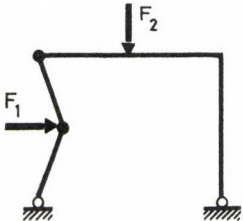
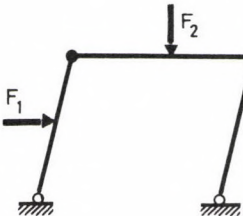
yield mechanisms	K_h	P_{ch}
	$K_1 = K_2 = \frac{(5 \cdot 3 + 15 \cdot 5) \cdot 10^3}{8 \cdot 10^3 \left(\frac{6^3}{3} A_1 + 2 \cdot \frac{5^3}{3} A_2 + 6^2 \cdot 10 A_2 + \frac{6^3}{3} A_3 \right)}$	$P_{c1} = \frac{4M_{p2}}{5 \cdot 3 + 15 \cdot 5}$ $P_{c2} = \frac{2M_{p2} + 2M_{p3}}{5 \cdot 3 + 15 \cdot 5}$
	$K_3 = K_4 = -K_5 = K_6 = \frac{15 \cdot 5 \cdot 10^3}{8 \cdot 10^3 \left(2 \cdot \frac{5^3}{3} A_2 \right)}$	$P_{c3} = \frac{M_{p1} + 2M_{p2} + M_{p3}}{75}$ $P_{c4} = \frac{3M_{p2} + M_{p3}}{75}$ $P_{c5} = \frac{M_{p1} + 3M_{p2}}{75}$ $P_{c6} = \frac{4M_{p2}}{75}$

Table 3. (cont.)

yield mechanisms	K_h	P_{ch}
	$K_7 = K_8 = \frac{5 \cdot 3 \cdot 10^3}{8 \cdot 10^3 \left(\frac{3^3}{3} A_1 \right)}$	$P_{c7} = \frac{2M_{p1} + M_{p2}}{15}$ $P_{c8} = \frac{3M_{p1}}{15}$
	$K_9 = K_{10} = K_{11} = K_{12} =$ $= \frac{5 \cdot 3 \cdot 10^3}{8 \cdot 10^3 \left(\frac{6^3}{3} A_1 + 6^2 \cdot 10 A_2 + \frac{6^3}{3} A_3 \right)}$	$P_{c9} = \frac{M_{p1} + M_{p2}}{15}$ $P_{c10} = \frac{M_{p1} + M_{p3}}{15}$ $P_{c11} = \frac{M_{p2} + M_{p3}}{15}$ $P_{c12} = \frac{2M_{p2}}{15}$

$$M_{pi} \geq M_{po} = 5 \text{ kNm} \quad (34)$$

define the mathematical programming problem.

Since the left sides of Eqs (33) are linear functions of design variables M_{pi} , the same iterative procedure can be used as in the former example. First, we assume $A_i = A_i^{(0)}$ = constant and we solve the linear inequalities (33) with the nonlinear objective function for $M_{pi}^{(1)}$.

Then, using values $M_{p1}^{(1)}$, we repeat this procedure. The results of iteration are shown in Table 4.

Table 4

steps	M_{p1}	M_{p2}	M_{p3}	V
0	19.1	19.1	19.1	157.2
1	5.0	26.3	11.8	137.2
2	5.0	24.0	15.3	137.7
3	5.0	24.5	14.7	137.9
4	5.0	24.4	14.8	137.8
5	5.0	24.4	14.8	137.8

Using different values for the duration of pressure denoted with t_o , one can obtain different optimum solutions. These are given in Table 5. It can be seen that with the duration of pressure increased, the solution tends to the results of the optimum design of the corresponding quasistatic problem.

Table 5

t_o (s)	M_{p1}	M_{p2}	M_{p3}	V
0.05	5.0	24.4	14.8	137.8
0.2	4.99	25.0	19.6	146.6
1	5.0	25.0	20.1	147.3
	5.0	25.0	20.0	147.3

REFERENCES

1. Gallagher, R.H., Zienkiewicz, O.C.: Optimum Structural Design. John Wiley. New York 1973.
2. Brandt, A.M.: Kryteria i metody optymalizacji Konstrukcji. Państwowe Wyd. Naukowe. Warszawa 1977.
3. Fox, R.L.: Optimization methods for engineering design. Addison-Wesley Reading — London 1971.
4. Rozvany, G.I.N.: Optimal design of flexural systems. Beams, grillages, slabs, plates and shells. Pergamon Press. Oxford, New York 1976.
5. Farkas, J.: Optimum design of metal structures. Akadémiai Kiadó, Budapest 1984.
6. Khot, N.S., Berke, L., Venkayya, V.B.: Minimum weight design of structures by the optimality criterion and projection method. Proc. Structures and Structural Dynamics Conference. St. Louis, 1979.
7. Khot, N.S., Berke, L., Venkayya, V.B.: Comparison of optimality criteria algorithms for minimum weight. Design of Structures, AIAA Journal, Vol. 17, Number 2, February 1979, p. 182–190.
8. Best, M.J.: FCDPAK, A Fortran-IV subroutine to solve differentiable mathematical programmes. Department of Combinatorics and Optimization, Research Report, University of Waterloo, Canada 1973.
9. Künzi, H.P., Krelle, N., Randow, R.: Nichtlineare Programmierung. Springer-Verlag, Berlin 1979.
10. Berke, L., Kaliszky, S., Knébel, I.: Optimal design of elastic bar structures subject to displacement constraints and prescribed internal and reaction forces (to be published).
11. Kaliszky, S.: Kinematical method for the analysis of inelastic structures under dynamic loading. Advances in Mechanics, Vol. 4. No.1. (1981), 29–47.
12. Heirloo, M., Kaliszky, S.: Optimal Design of Dynamically Loaded Rigid-Plastic Structures. Application: Thick-Walled Concrete Tube. J. Struct. Mech. 9/3/, (1981), 235–251.
13. Kaliszky, S.: Plastizitätslehre. VDI-Verlag, Düsseldorf 1984.
14. Heyman, J.: Minimum design of frames under shakedown loading. J. Eng. Mech.Div.Proc. ASCE EM4. 1958. Paper 1790.
15. Cohn, M.Z., Parimi, S.R.: Optimal design of plastic structures for fixed and shakedown loading. J. Applied Mechanics. June (1973), 595–599.
16. Lepik, Ü., Mróz, Z.: Optimal design of plastic structures under impulsive and dynamic pressure loading. Int.J.Solids Struct. 13/7. (1977), 657–674.

A NEW APPROACH TO X-RAY DIFFRACTION ANALYSIS OF STRESS STATES
IN SURFACE LAYERS

B. Kämpfe and B. Michel*

(Received: 24 June 1986)

Presented in this work are the possible applications of X-ray stress analysis. Problems arise for difficult stress states with gradients of residual stresses arising deep in the sample, gradients of solid solution, strong textures and shear components of stress parallel to the surface. For the latter problem a relatively simple method of investigation is presented which eliminates the other influencing factors almost completely.

X-ray stress analysis has found increasing use in the recent ten years /1/, /2/ in connection with the possibility of nondestructive determination of residual stresses in surface layers of materials. Today X-ray stress analysis is considered an independent field of X-ray diffraction analysis. The improvement of measuring techniques resulted in a reduced use of the $\sin^2\psi$ -method /3/ which had been the most widely used method in X-ray stress investigations earlier. Gradients of residual stresses and solid solution concentration deep in the sample, shear stresses parallel to the surface and textures are the "distortion parameters". On the other hand, these difficulties led to a continuous methodical improvement of X-ray stress investigations. In the following, a new method of X-ray stress analysis is presented. The basis for all diffraction techniques is the measurement of residual strains, using the lattice spacing of selected hkl planes as internal strain gauges and determining the strains in particular directions in the sample. In X-ray measurements, a direction is defined by two angles, φ and ψ , φ defining the orientation of the scattering plane relative to two directions in the sample surface while ψ the tilt of the chosen direction in the scattering plane relative to the normal of the surface (see Fig. 1). If the strain in the specimen coordinates is ε_{ij} , strain $\varepsilon_{\varphi\psi}$ measured in the direction defined by ψ and ρ will be given by a simple tensor rotation, where x_3 is in the direction of the surface normal.

*Dr.sc.techn. Bernd Kämpfe—Prof. Dr.sc. nat Bernd Michel, Institut für Mechanik der Akademie der Wissenschaften der DDR, 9010 Karl-Marx-Stadt, PSF 408, DDR

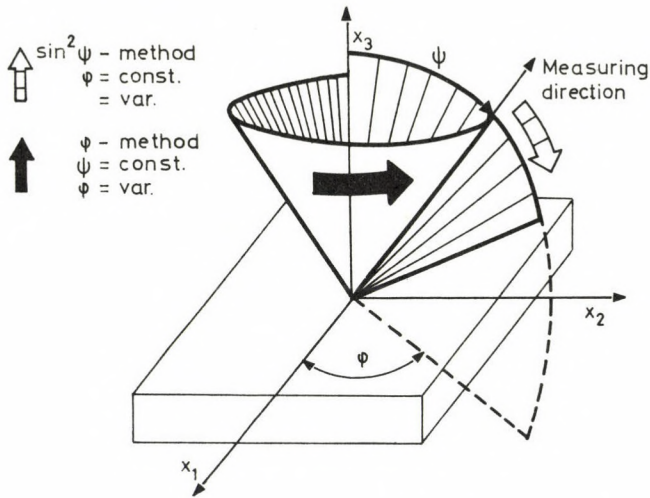


Fig. 1. Distinction between $\sin^2\psi$ -method and φ -method

$$\epsilon_{\varphi,\psi} = [\epsilon_{11} \cos^2\varphi + \epsilon_{12} \sin 2\varphi + \epsilon_{22} \sin^2\varphi - \epsilon_{33}] \sin^2\psi + \epsilon_{33} [\epsilon_{13} \cos\varphi + \epsilon_{23} \sin\varphi] \sin 2\psi \quad (1)$$

The traditional X-ray technique is to choose a specific (hkl) diffraction line and to determine its shift ($\Delta\vartheta$) as a function of $\sin^2\psi$ for constant ρ

$$\epsilon_{\psi,\varphi=\text{const}} = -\cot\vartheta \Delta\vartheta$$

where ϑ is the bragg-angle. The $\epsilon_{\varphi,\psi}$ vs $\sin^2\psi$ plots give simple linear expressions and good results provided the components of stress normal to the free surface σ_{13} , σ_{23} and σ_{33} in the specimen domain (near the surface) investigated are nearly zero. Difficulties will arise if this assumption fails as the investigation is often made after wear, grinding and other mechanical loads /4/. The problem of analysis lies then in that for different angles ψ , also the diffraction lines are generated in different depths of material below the free surface /5/. Thus the result is based on points of measurement of different stress states as these must be other than zero at depths below the free surface. A measurement of the diffraction peaks as a function of φ for constant ψ solves the problem (Fig. 1) because the penetration depth of X-rays is independent of φ /6/. ψ can be varied by rotating the specimen around its surface normal. This

X-RAY DIFFRACTION ANALYSIS

is easy with most X-ray diffractometer types, and leads only to minor systematical errors in the measurement. Another remarkable advantage of these investigation techniques is that the symmetry of residual stress state is directly reflected in the $\varepsilon \varphi \psi$ vs. φ plots /7/. In this way, the directions of main stresses and maximum shear stresses as related to the surface can be easily determined /8/. The investigations, including a large number of different materials and stress states /9/, showed that both ψ and ω diffractometers could be successfully used for the φ -method. In application with ω -diffractometers, the φ -method yielded better results than the $\sin^2 \psi$ method, especially with the use of a focussing slit. The stresses and stress states obtained in this way showed a good agreement with the expected values, especially for shear stresses and position of principal stress axis.

REFERENCES

1. E. Macherauch: Stand und Perspektiven der röntgenographischen Spannungsmessung. Metall 34 (1980), 443, 1087.
2. B. Kämpfe: Röntgenographische Spannungsmessung. FMC-Series des Instituts für Mechanik der DDR 1 (1982), No. 3,8.
3. E. Macherauch and P. Müller: Das $\sin^2 \psi$ -Verfahren der röntgenographischen Spannungsmessung. Zeitschrift angew. Physik 13 (1961), 305.
4. B. Kämpfe and P. Zimmermann: Röntgenographische Spannungsmessung an spannend bearbeiteten Stahloberflächen. FMC-Series 3 (1984), No. 8.11.
5. B. Kämpfe: Dissertationsschrift zur Promotion B, TH Karl-Marx-Stadt, (1983).
6. B. Kämpfe and B. Michel: Neue Wege in der röntgenographischen Spannungsmessung. FMC-Series 4, No. 14.48.
7. W. Lode and A. Peiter: Prinzip-Analyse von zwei Röntgenverformungsmessverfahren. Arch. Eisenhüttenwesen 53 (1982), 77.
8. B. Kämpfe et al. WP G01 N / 268 031 1.
9. B. Kämpfe and E. Auerswald: Röntgenographische Spannungsmessung mit dem ρ -Umlauf-Verfahren. FMC-Series 5 (1986), in print.

BUCKLING ANALYSIS OF COUPLED SHEAR WALLS BY THE MULTI-LAYER SANDWICH MODEL

László P. Kollár*

(Received: 11 March 1986)

It is well known that the continuum model of a shear wall is a sandwich beam which consists of 'stiff' and 'soft' layers. The paper presents the differential equation system of the multi-layer sandwich beam, and gives a method and closed formulas to determine the critical load in case of a concentrated force acting on the top of the beam. The paper also shows that the critical load of a multi-layer sandwich cantilever is - to a close approximation - equal to the critical load of a triple-layer sandwich beam, i.e. a sandwich with thick faces.

1. INTRODUCTION

Shear walls are often analysed with the aid of the continuum method /5,7,8,9/. The replacement continuum of a shear wall is a sandwich construction consisting of 'stiff' and 'soft' layers.

In this paper we deal with sandwich constructions having $n+1$ stiff layers which are separated by n soft layers. We suppose that both the soft and the stiff layers are incompressible in transverse direction. The soft layers have only shearing rigidities, they are soft (i.e. they exhibit no resistance at all) in bending and in compression in the vertical direction. The shear rigidities of the stiff layers are infinite, their bending and vertical tensile stiffnesses are finite. We assume that the distance between the axes of two consecutive stiff layers is equal to the width of the soft layer. In case of $n=1$ (when only one soft layer separates the two stiff layers), the structure is identical with the 'sandwich with thick faces' /1/. The sandwich with thick faces has three different rigidities (Fig. 1): the global bending rigidity (B_0) which comes from the tensile stiffnesses of the faces, the shear rigidity (S) of the core, and the local bending rigidity (B_g) of the stiff faces with respect to their own centroidal axes.

Pomázi has dealt with the stability analysis of multi-layer sandwich plates in /4/, taking the transverse compressibility of the soft layers into account, so his model is more general than ours. In the case of Navier-type boundary conditions, he presented analytical solutions.

*László P. Kollár, H-1122 Budapest, Karap u. 9, Hungary.

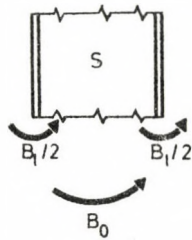


Fig. 1.

Our sandwich model (which is equal to the model of shear walls developed by Rosman /5/) is suited, because of its simplicity, not only to obtain numerical results but also to draw qualitative conclusions.

The basic idea of approximately replacing a multi-layer sandwich beam with a sandwich with thick faces has been suggested by István Hegedűs.

The paper presents the differential equation system of a multi-layer sandwich construction under arbitrary distribution of the normal load along the beam axis, and gives an exact solution for the case of a concentrated force acting on top of the sandwich cantilever. It is also shown that the replacement sandwich with thick faces gives in fact a very good approximation for calculating the critical load of the multi-layer sandwich column.

2. THE BUCKLING DIFFERENTIAL EQUATION SYSTEM OF THE MULTI-LAYER SANDWICH BEAM

The sandwich construction in Fig. 2 consists of $n+1$ stiff and n soft layers. Let the overall height of the beam be H . The local bending rigidities of the stiff layers are $EI_0, \dots, EI_1, \dots, EI_n$.

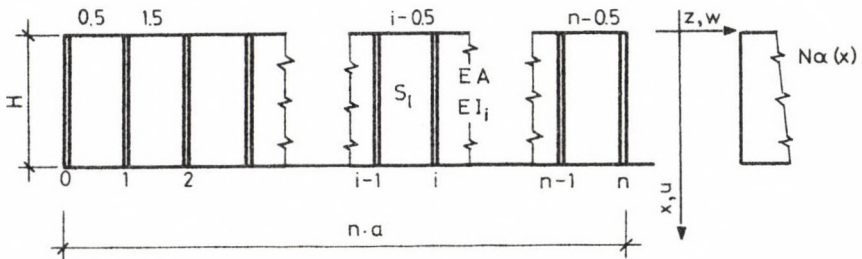


Fig. 2.

BUCKLING ANALYSIS OF SHEAR WALLS

We shall denote the stiff layers with 'integer' indices, and the soft layers with 'half' indices (Fig. 2). In order to obtain qualitative conclusions we will show the derivation for a regular sandwich construction, where the distances of the centroidal axes of the adjoining stiff layers are equal to each other, and are denoted with a ; the shear rigidities of the soft layers are equal to each other (denoted with S_ρ), and the tensile stiffnesses of the stiff layers are also equal (denoted with EA).

Further notations are: E is the modulus of elasticity, I_i is the moment of inertia of the i -th stiff layer, A is the cross-sectional area of one stiff layer. The shear rigidity S_ρ of one soft layer is defined by (13).

Let the vertical loads act on every stiff layer with the same distribution $p(x)$ along the x axis. This causes normal forces $N(x) = N \alpha(x)$, where N is the parameter and $\alpha(x)$ defines the distribution of the normal force.

Since every layer is incompressible in transverse direction, the horizontal displacements of the stiff layers are equal to each other. Let us denote the horizontal displacement function with $w(x)$, and the vertical displacement function with $u(x, z)$. The shearing strain of the $(i+0.5)$ -th soft layer is

$$\gamma_{i+0.5}(x) = w'(x) + \frac{\partial u(x, z)}{\partial z} .$$

We denote with dash the derivative with respect to x . Assume that due to the negligible bending rigidities of the cores, the shearing strain is invariable along the horizontal direction between two consecutive stiff layers.

Let us denote the vertical displacement function of the i -th stiff layer with u_i , and let us introduce a function

$$\phi_{i+0.5}(x) = - \frac{u_{i+1}(x) - u_i(x)}{a} . \quad (1)$$

We can write the previous expression for $\gamma_{i+0.5}(x)$ with the aid of (1) in the following way, well known in sandwich theory (Fig. 3):

$$w'(x) = \phi_{i+0.5}(x) + \gamma_{i+0.5}(x) \quad (i=1, 2, \dots, n) . \quad (2)$$

Let us write the equation for equilibrium of the moments at a height x , with respect to the geometrical center line of the cross-section of the

beam. The moment of the external forces is

$$M_E(x) = \sum_{i=0}^n \int_0^x P_i(\xi) [w(x) - w(\xi)] d\xi .$$

We also need its derivative:

$$M_E'(x) = \sum_{i=0}^n w'(x) \int_0^x P_i(\xi) d\xi = (n+1) N \alpha(x) w'(x) . \quad (3)$$

The moment of the external forces has to be equal to the moment of internal forces, which consists of two parts:

$$M_I(x) = M_\lambda(x) + M_0(x) . \quad (4)$$

$M_\lambda(x)$ is due to the bending of the stiff layers, $M_0(x)$ is due to their compression. From the bending-curvature relationship we obtain:

$$M_\lambda(x) = -B_\lambda w''(x) , \quad (5)$$

where

$$B_\lambda = \sum_{i=0}^n EI_i .$$

Let us determine the value of M_0 from the deformations. With u_0 and $\phi_{i-0.5}$ ($i=1,2,\dots,n$) we can determine u_i :

$$u_i(x) = u_0(x) - a \sum_{j=1}^i \phi_{j-0.5}(x) . \quad (6)$$

The vertical force in the i -th layer is

$$F_i(x) = u_i'(x) EA , \quad (7)$$

and the equation of the vertical equilibrium becomes

$$\sum_{i=0}^n F_i(x) = (n+1)N \alpha(x) . \quad (8)$$

Let us denote with $\bar{u}(x)$ the common vertical displacement of the layers prior to buckling. We thus have $\bar{u}'(x) = N \alpha(x)/(EA)$. Using expressions (6-8) we obtain

$$u_0'(x) = \bar{u}'(x) + \frac{a}{n+1} \sum_{i=1}^n (n-i+1) \phi_{i-0.5}'(x) .$$

The expression for global bending moment – at height x, with respect to the geometrical center line of the cross-section – can be written as

$$M_0(x) = - EA a^2 \frac{1}{2} \sum_{i=1}^n \phi_{i-0.5}(x)(n+1-i)i . \quad (9)$$

This expression becomes much simpler in case of $\phi(x) = \phi_{0.5}(x) = \dots = \phi_{n-0.5}(x)$. Denoting with

$$I_0 = A a^2 \frac{1}{2} \sum_{i=1}^n (n+1-i)i = A a^2 \frac{1}{12} n (n+1)(n+2)$$

the moment of inertia of the stiff layers without their own local moments of inertia, and using notation

$$B_0 = EI_0 = EA a^2 \frac{1}{12} n (n+1)(n+2) , \quad (10)$$

we obtain expression

$$M_0 = - B_0 \phi'(x) ,$$

which is analogous to the well-known moment-curvature relationship of bent bars.

Let us differentiate with respect to x the expressions of (5) and (9), and introduce them into equations $M_E' = M_I'$. Using equations (3,4,5,9), we obtain

$$(n+1)N \alpha(x)w'(x) = - B_0 w''(x) - EA \frac{1}{2} a^2 \sum_{i=1}^n \phi_{i-0.5}''(x)(n+1-i)i$$

Now we have to derive the relationship between ϕ and γ . Let us consider the i-th stiff layer, and cut vertically the connecting soft layers along their middle line. The distributed forces (t and τ) are illustrated in Fig. 4 with positive sign. Between forces τ and displacement u'' the following relation holds:

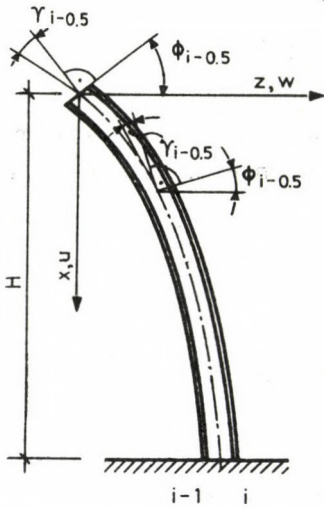


Fig. 3.

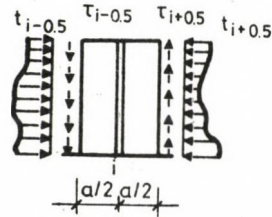


Fig. 4.

$$u_i''(x) = \frac{\tau_{i-0.5}(x) - \tau_{i+0.5}(x)}{EA} + \bar{u}''(x) \quad (12)$$

and according to the definition of S_ℓ ,

$$\tau_{i+0.5}(x) = \frac{S_\ell}{a} \gamma_{i+0.5}(x) \quad (13)$$

With (12) and (13) we eliminate $u_i(x)$ from (1) and obtain

$$\phi_{i-0.5}''(x) = -\frac{S_\ell}{a^2 EA} (-\gamma_{i-1.5}(x) + 2\gamma_{i-0.5}(x) - \gamma_{i+0.5}(x)) \quad (i=1,2,\dots,n) \quad (14)$$

where — because of (13) —

$$\gamma_{-0.5}(x) = \gamma_{n+0.5}(x) = \emptyset \quad (15)$$

Introducing the following notations:

BUCKLING ANALYSIS OF SHEAR WALLS

$$\underline{C} = \begin{bmatrix} 2 & -1 & & & \\ -1 & 2 & -1 & & \\ & & \cdot & \cdot & \cdot \\ & & & -1 & 2 \end{bmatrix}, \quad \underline{\phi} = \begin{bmatrix} \phi_{0.5}(x) \\ \phi_{1.5}(x) \\ \dots\dots \\ \phi_{n-0.5}(x) \end{bmatrix}, \quad \underline{\gamma} = \begin{bmatrix} \gamma_{0.5}(x) \\ \gamma_{1.5}(x) \\ \dots\dots \\ \gamma_{n-0.5}(x) \end{bmatrix} \quad (16)$$

we can write

$$\underline{\phi}''(x) = -\frac{S_\ell}{a^2 EA} \underline{C} \underline{\gamma}(x) .$$

In this equation \underline{C} is a tridiagonal matrix, whose inverse is the following one-pair matrix /6/ (i and j are the indices of the rows and columns respectively):

$$\underline{C}^{-1} = \begin{cases} \frac{i(n+1-j)}{n+1}, & \text{if } i \leq j \\ \frac{j(n+1-i)}{n+1}, & \text{if } i \geq j . \end{cases} \quad (17)$$

Hence we obtain

$$\underline{\gamma}(x) = -\frac{a^2 EA}{S_\ell} \underline{C}^{-1} \underline{\phi}''(x) . \quad (18)$$

Let us express $w'(x)$ with the aid of (2) and (18):

$$\begin{bmatrix} 1 \\ 1 \\ \dots \\ 1 \end{bmatrix} w'(x) = \underline{\phi}(x) - \frac{a^2 EA}{S_\ell} \underline{C}^{-1} \underline{\phi}''(x) . \quad (19)$$

(11) and (19) constitute the differential equation system of our problem. With the aid of (19) we can express the function w in (11) by ϕ , so we obtain a differential equation system of the fourth order

$$(n+1)N \alpha(x) \left(\underline{\phi} - \frac{a^2 EA}{S_\ell} \underline{C}^{-1} \underline{\phi}'' \right) = -B_\lambda \left(\underline{\phi}'' - \frac{a^2 EA}{S_\ell} \underline{C}^{-1} \underline{\phi}'''' \right) - a^2 EA \underline{A} \underline{\phi}'' \quad (20)$$

where \underline{A} is an (nxn) matrix (a dyad):

$$\underline{A} = \begin{bmatrix} 1 \\ 1 \\ \dots \\ 1 \end{bmatrix} \underline{a}^* ; \quad \underline{a}^* = \frac{1}{2} (n+1-j)j . \quad (21)$$

In case of $n=1$ (i.e. for a sandwich beam with thick faces) we have

$$\underline{C}^{-1} = [0.5] \quad \text{and} \quad \underline{A} = [0.5] \quad , \quad (22)$$

so that the equation system (20) degenerates into equation (7) of /2/.

In case of a cantilever built-in at the bottom and free at the top, the boundary conditions of the differential equation system (20) are the following: At the bottom ($x=H$) because of the built-in end $u_1=0$, and from (1):

$$\underline{\phi}(H) = \underline{0} \quad . \quad (23.a)$$

The rotations of the stiff layers are equal to zero ($w' = 0$), so using also (23.a):

$$\underline{\phi}''(H) = \underline{0} \quad . \quad (23.b)$$

The conditions at the top ($x=0$) are: Integrating (12) we obtain $u_1'(0) = \bar{u}'(0)$, so that

$$\underline{\phi}'(0) = \underline{0} \quad , \quad (23.c)$$

(and also $M_0=0$); furthermore there is no bending at the top ($M_x=0$), so that from $w''=0$:

$$\underline{\phi}'''(0) = \underline{0} \quad . \quad (23.d)$$

3. SANDWICH CANTILEVER UNDER A CONCENTRATED FORCE ACTING ON THE TOP

In case of $\alpha(x)=1$, i.e. if there are only concentrated forces acting on the top of the stiff layers, we can easily solve the differential equation system (20). The solution which also meets the boundary conditions (23) is:

$$\underline{\phi}^k(x) = \underline{\phi}^k \cos \frac{(2k-1)\pi}{2H} x \quad , \quad (k=1,2,\dots) \quad .$$

Let us substitute this into (20), and divide it by $\cos(2k-1) \pi x/(2H)$. The lowest eigenvalue belongs to $k=1$, so we obtain

$$P\left(\underline{E} + \frac{\pi^2}{4H^2} \frac{a^2 EA}{S_\ell} \underline{C}^{-1}\right) \underline{\phi} = \left[\frac{B_\ell \pi^2}{4H^2} \left(\underline{E} + \frac{\pi^2}{4H^2} \frac{a^2 EA}{S_\ell} \underline{C}^{-1}\right) + \frac{EAa^2 \pi^2}{4H^2} \underline{A} \right] \underline{\phi} \quad (24)$$

BUCKLING ANALYSIS OF SHEAR WALLS

where \underline{E} is the unit matrix, and the elements of $\underline{\phi}$ do not depend on x ; furthermore

$$P = (n+1) N$$

is the parameter of the load, of which the critical value is P_{cr} .

(24) is a homogeneous linear equation system of $\underline{\phi}$, which has a nontrivial solution only if the determinant of the matrix of the equation system (24) is equal to zero. Using notations

$$P_{\ell} = \frac{\pi^2 B_{\ell}}{4H^2}$$

and

$$D = \frac{\pi^2 a^2 EA}{4H^2}$$

this condition assumes the following form:

$$\det \left[(P_{cr} - P_{\ell}) (\underline{E} + \frac{D}{S_{\ell}} \underline{C}^{-1}) - D \underline{A} \right] = 0 . \quad (25)$$

(25) is an equation of the n -th degree for P_{cr} . $P_{cr} = P_{\ell}$ is the root of (25) with multiplicity $(n-1)$, \underline{A} being a dyad. Consequently, with the $(n-1)$ root factors of equation (25) dropped out we obtain a linear equation for the n -th root.

Let us first examine root $P_{cr} = P_{\ell}$. In this special case, equation (25) does not contain equation (11). In fact if we take into consideration that the horizontal displacements of the stiff layers are equal to each other, i.e.

$$w_0 = w_1 = \dots = w_n , \quad (26)$$

we obtain trivial solution $\underline{\phi} = \underline{0}$. Therefore P_{ℓ} is not a critical load of the structure.

3.1 Critical loads in case of $n=1, 2$ and 3

In case of $n=1$, i.e. if one soft layer separates the two stiff layers, we will obtain from equation (10):

$$B_0 = \frac{a^2 EA}{2} . \quad (27)$$

Let us denote the critical load of a cantilever with rigidity B_0 by

$$P_0 = \frac{\pi^2 B_0}{4H^2} = \frac{D}{2} . \quad (28)$$

Considering (22), we obtain the same critical load as in /1,2/:

$$P_{cr} = \left[P_0^{-1} + S^{-1} \right]^{-1} + P_\ell \quad (29)$$

where $S = S_\ell$.

In case of $n=2$, we obtain from equations (17) and (21):

$$\underline{C}^{-1} = \frac{1}{3} \begin{bmatrix} 2 & 1 \\ 1 & 2 \end{bmatrix}, \quad \underline{A} = \begin{bmatrix} 1 & 1 \\ 1 & 1 \end{bmatrix} .$$

The value of determinant (25) is

$$(P_{cr} - P_\ell)^2 \left[\left(1 + \frac{2}{3} \frac{D}{S_\ell}\right)^2 - \frac{1}{9} \frac{D^2}{S_\ell^2} \right] + (P_{cr} - P_\ell) \left[-\left(1 + \frac{2}{3} \frac{D}{S_\ell}\right) 2D + \frac{2}{3} \frac{D^2}{S_\ell} \right] = 0 .$$

Using the following notations

$$S = 2 S_\ell$$

and from (10):

$$B_0 = 2 a^2 EA \quad (30)$$

and

$$P_0 = \frac{\pi^2 B_0}{4H^2} = 2 D ,$$

we obtain expression (29) for calculating the critical load of the structure.

The elements of $\underline{\phi}$ are $\phi_{0.5} = \phi_{1.5}$.

We thus have the result that the critical load of a three-stiff-layer cantilever is equal to the critical load of a cantilever with thick faces (two-stiff-layer sandwich), where the local bending rigidity is equal to the sum of bending rigidities of the stiff layers the shear rigidity to the sum of rigidities of the soft layers while the global rigidity is defined by (30).

In case of $n=3$ we obtain from equation (17) and (21)

BUCKLING ANALYSIS OF SHEAR WALLS

$$\underline{C}^{-1} = \frac{1}{4} \begin{bmatrix} 3 & 2 & 1 \\ 2 & 4 & 2 \\ 1 & 2 & 3 \end{bmatrix}, \quad \underline{A} = \frac{1}{2} \begin{bmatrix} 3 & 4 & 3 \\ 3 & 4 & 3 \\ 3 & 4 & 3 \end{bmatrix},$$

From equation (25) we can derive the expression for P_{cr} :

$$P_{cr} = P_{\ell} + \frac{5 D \left(1 + \frac{3}{10} \frac{D}{S_{\ell}}\right)}{\left[1 + \left(1 + \frac{\sqrt{2}}{2}\right) \frac{D}{S_{\ell}}\right] \left[1 + \left(1 - \frac{\sqrt{2}}{2}\right) \frac{D}{S_{\ell}}\right]} \quad (31)$$

The elements of ϕ are (Fig. 5a):

$$\phi_{0.5} = 1.707 \quad \phi_{1.5} = \phi_{2.5}$$

The exact value (31) of the critical load is closely approximated by the following approximate formula:

$$\begin{aligned} \bar{P}_{cr} &= P_{\ell} + \frac{5 D \left[1 + \left(1 - \frac{\sqrt{2}}{2}\right) \frac{D}{S_{\ell}}\right]}{\left[1 + \frac{5}{3} \frac{D}{S_{\ell}}\right] \left[1 + \left(1 - \frac{\sqrt{2}}{2}\right) \frac{D}{S_{\ell}}\right]} = \\ &= P_{\ell} + \left[P_0^{-1} + S^{-1} \right]^{-1} \end{aligned} \quad (32)$$

where

$$P_0 = \frac{\pi^2 B_0}{4H^2} = 5 D, \quad S = 3 S_{\ell}$$

and from (10)

$$B_0 = 5 a^2 EA \quad (33)$$

It can be shown by simple algebraic transformations that (32) always yields a greater value for the critical load than (31). The difference becomes maximum if $B_{\ell} = 0$, and $D/S_{\ell} = \sqrt{2}$. In this case:

$$\frac{\bar{P}_{cr}}{P_{cr}} = \frac{\sqrt{2} + 1}{\frac{59}{60} \sqrt{2} + 1} = 1.009859,$$

so that the error is always less than 1 %.

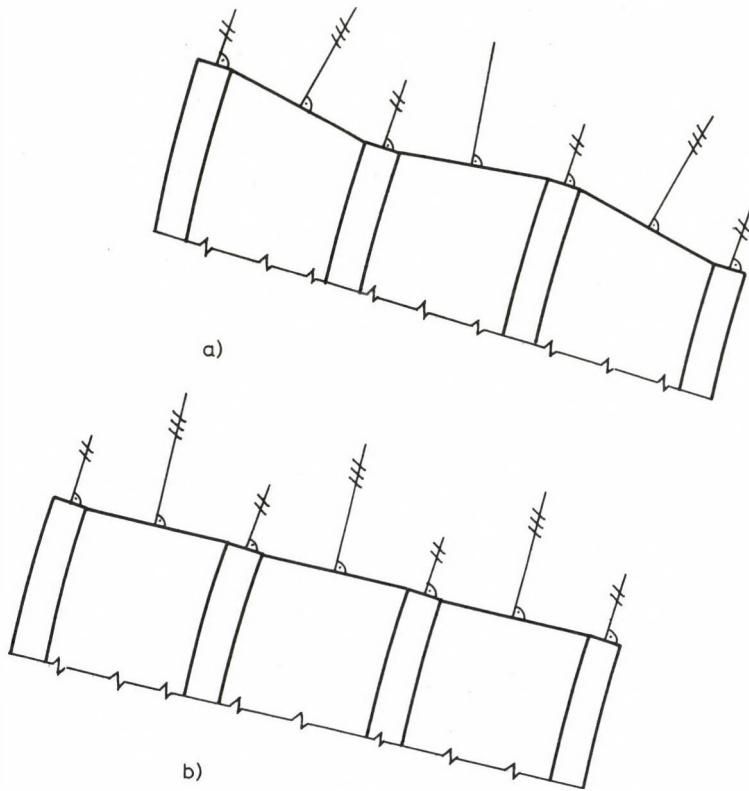


Fig. 5.

We could also obtain the same approximate value \bar{P}_{cr} for P_{cr} assuming that (Fig. 5b):

$$\phi_{0.5} = \phi_{1.5} = \phi_{2.5} \cdot$$

In this case, the differential equation system becomes a single equation of which the eigenvalue is \bar{P}_{cr} . With this assumption we rendered our model somewhat more rigid than the real one; on the other hand, instead of a sandwich beam with four stiff layers we can examine a replacement sandwich with only two stiff layers.

Note that the previous assumption is only valid for the vertical displacements (u_1) of the stiff layers: the points at the same height on the axis of the stiff layers remain on one straight line after deformation. The

BUCKLING ANALYSIS OF SHEAR WALLS

rotations of the layers may be different. The approximation is rather poor in describing local behaviour ($\phi_{0.5} \neq 1.707 \phi_{1.5}$), but very good for the global behaviour (stability, horizontal displacements) of the beam.

3.2 Critical load in case of an arbitrary n

Let us multiply equation (24) from the left by \underline{C} . After rearranging, and introducing notation

$$\lambda = \frac{P - P_\ell}{D} \quad , \quad (34)$$

we obtain

$$\left(\underline{C} + \frac{D}{S_\ell} \underline{E} \right) = \begin{bmatrix} (\underline{a}^* \underline{\phi}) / \lambda \\ 0 \\ 0 \\ \dots \\ 0 \\ (\underline{a}^* \underline{\phi}) / \lambda \end{bmatrix} \quad , \quad (35)$$

where \underline{a}^* is a row of matrix \underline{A} (21). The coefficient matrix of equation (35) is tridiagonal. Let us introduce a new variable θ defined by equation

$$2 + \frac{D}{S_\ell} = 2 \operatorname{ch} \theta \quad . \quad (36)$$

The inverse of (35) becomes a one-pair matrix /6/ as follows:

$$\left(\underline{C} + \frac{D}{S_\ell} \underline{E} \right)^{-1} = \begin{cases} \frac{\sinh i \theta}{\sinh \theta} \frac{\sinh(n+1-j) \theta}{\sinh(n+1) \theta} \quad , \text{ if } i \leq j \\ \frac{\sinh j \theta}{\sinh \theta} \frac{\sinh(n+1-i) \theta}{\sinh(n+1) \theta} \quad , \text{ if } i \geq j \end{cases} \quad (37)$$

On the right side of equation (35), only the first and the last terms are different from zero, so that

$$\phi_{i-0.5} = \frac{\underline{a}^* \underline{\phi}}{\lambda} \frac{1}{\sinh(n+1) \theta} [\sinh(n+1-i) \theta + \sinh i \theta] \quad . \quad (38)$$

Multiplying equation (38) by $(\underline{a}^* \lambda)$, we obtain

$$\lambda = \sum_{i=1}^n \frac{(n+1-i) i}{2} \frac{1}{\sinh(n+1) \theta} [\sinh(n+1-i) \theta + \sinh i \theta] \quad . \quad (39)$$

The critical load is

$$P_{cr} = \lambda D + P_{\ell} .$$

We will obtain the approximate value of the critical load if we replace the multi-layer sandwich construction with a simple sandwich with thick faces, whose replacement rigidities are the following:

$$B_{\ell} = \sum_{i=0}^n EI_i ; \quad S = nS_{\ell} , \quad B_0 = \frac{EAa^2 n(n+1)(n+2)}{12} . \quad (41)$$

In the next table we calculated the maximum values of ratio \bar{P}_{cr}/P_{cr} for various n values as a function of D/S_{ℓ} .

n	D/S_{ℓ}	\bar{P}_{cr}/P_{cr}
1	arbitrary	1.0000
2	arbitrary	1.0000
3	1.414	1.0099
4	1.000	1.0204
5	0.750	1.0299
6	0.585	1.0381
7	0.469	1.0451
8	0.387	1.0512
9	0.324	1.0564
10	0.276	1.0610
11	0.237	1.0650
12	0.206	1.0685
20	0.089	1.0866
30	0.043	1.0974

The results show that the approximation is good enough also in case of great n values. (We could obtain the critical values (39) also by means of the method of finite difference equations. For example, Pomázi /4/ used this method to calculate the critical loads of sandwich-plates with regular built-up of the layers.)

4. CONCLUSIONS. THE REPLACEMENT SANDWICH BEAM

It was shown in Section 3 that the critical load of a multi-layer sandwich beam under concentrated forces acting on the top was always very close to the critical load of an appropriately chosen sandwich beam with thick faces. So the latter can serve as the replacement model of the previous one.

BUCKLING ANALYSIS OF SHEAR WALLS

We may also use the method of replacement in more general cases. In calculating for critical load (also for loading cases other than concentrated forces) we can replace the multi-layer sandwich beam with a sandwich with thick faces (consisting of two stiff layers and one soft layer). The rigidities of the replacement sandwich beam are the following: the shear rigidity is equal to the sum of the rigidities of the soft layers; the local bending rigidity is equal to the sum of the bending rigidities of the stiff layers, and the global bending rigidity consists of the 'Steiner terms' of the stiff layers:

$$B_0 = \sum_{i=0}^n EA_i s_i^2,$$

where the number of the stiff layers is $n+1$, A_i is the area of the cross-section of the i -th stiff layer, and s_i is its distance from the centroid of the entire cross-section. This approximation is equivalent to the assumption: $\phi_{0.5} = \phi_{1.5} = \dots = \phi_{n-0.5}$. This assumption is very far from reality, because the values of ϕ are different in general cases, nevertheless, the overall behaviour of the beam is not significantly affected by it, and the approximation based on this simplification yields really good results.

Based on these principles, we can also substitute a sandwich cantilever with thick faces for a multiply coupled shear wall, and we can calculate its critical load also in case of arbitrary load distributions.

REFERENCES

1. Allen, H.G.: Analysis and Design of Structural Sandwich Panels. Pergamon Press, Oxford, 1969.
2. Hegedűs, I. – Kollár, L.P.: Buckling of sandwich columns with thick faces subjected to axial loads of arbitrary distribution. Acta Techn. Acad. Sci. Hung. 97. (1984) 123–131.
3. Hegedűs, I. – Kollár, L.P.: On generalized bar-models and their physical interpretations. Acta Techn. Acad. Sci. Hung. (At press.)
4. Pomázi, L.: A réteges lemezek stabilitásának vizsgálatáról (On the stability analysis of multi-layer sandwich plates. In Hungarian), Építés, Kutatás, Fejlesztés, Budapest, 1974. 45–51.
5. Rosman, R.: Die statische Berechnung von Hochhauswänden mit Öffnungsreihen. Bauingenieur-Praxis, Heft 65. W. Ernst und Sohn, Berlin-München, 1965.
6. Rózsa, P.: Lineáris algebra és alkalmazásai. (Linear algebra and its applications. In Hungarian), Műszaki Könyvkiadó, Budapest, 1974.

7. Szerémi, L.: Magasházak merevítőrendszerének számítása kontinuum modell alkalmazásával. (Calculation of shear-wall systems of tall buildings by the continuum model. In Hungarian), BME (Technical University of Budapest), Építőmérnöki Kar, Építőanyagok Tanszék, Tudományos Közlemények 21. Beton és Vasbeton, 1975. 123–140.
8. Szmodits, K.: Útmutató panelépületek statikai tervezéséhez (Manual for designing panel constructions. In Hungarian), Építéstudományi Intézet, Budapest, 1975.
9. Zalka, K.: Nyílássorokkal áttört falak stabilitásvizsgálata folytonos modellel. (Stability analysis of coupled shear-walls by the continuum method. In Hungarian), Építés-Építészettudomány, 1982. 143–154.

MATHEMATICAL METHOD FOR DETERMINATION OF THERMAL CONTACT RESISTANCE
BETWEEN SOLIDIFYING METAL AND MOLD

Ice B. Risteski*

(Received: 7 January 1986)

In the classical solution to one dimensional solidifications Schwarz showed that in case of perfect thermal contact the interface temperature between the mold and solidifying material was constant. Adams hypothesized that in actual casting problems with imperfect thermal contact, one could still use the interface temperature computed by Schwarz's solution but now acting through a film resistance upon mold and another film resistance upon solidifying metal. The problem of solidifying a metal by a constant-temperature source acting through a film resistance is solved using the method of successive approximations. Taking experimental data for depth solidified vs time, the first problem is solved inversely to determine the film resistance between the constant-temperature source and the solidifying metal. Using experimental curves for temperature vs depth at various times, the second problem is also solved inversely in order to determine the film resistance between the mold and the constant-temperature source. The overall film resistance between the mold and solidifying metal is the sum of the two resistances. Experiments indicate that the two resistances cannot be assumed equal.

NOTATION

Dimensional Quantities

c - specific heat
 h - film conductance
 k - conductivity
 L - latent heat of fusion
 e - arbitrary reference length
 t - time
 T - temperature
 T_f - fusion temperature
 x_f - position
 z - position of freezing front
 $K=k/\rho c$ - diffusivity
 ρ - density

Nondimensional Quantities

H - film conductance
 L' - latent heat of fusion
 T' - temperature
 X - position
 Y - position of freezing front
 τ - time

*Smederevo Iron and Steel Works, 11300 Smederevo, Yugoslavia

1. INTRODUCTION

The most general mathematical solution available for a liquid freezing on a mold is the one-dimensional solution according to Schwarz /1/. The Schwarz solution is for the case of a semi-infinite liquid at a uniform temperature coming into perfect thermal contact (no interfacial resistance) with a semiinfinite chill at a uniform temperature below the fusion temperature of the liquid. One of the important results of the Schwarz solution is that it predicts an interface temperature that is constant. In the real world perfect thermal contact is not attainable for different reasons; surface contamination, bridging of surface roughness by the liquid causing voids, shrinkage of the casting, and so forth.

One way to model this resistance to heat flow at the interface is to assume that there is a film between the mold and the casting that has no heat capacity but has resistance to the flow of heat and therefore a finite conductance. In general one would expect the value of the film resistance to be temperature dependent and possibly dependent on the rate of heat flux. Practically speaking, the quantification of this film resistance through experimentation is very difficult. It is difficult because the precise measurement of temperature in the melt and locating the freezing front at various times are very difficult to do. Also, the correct method of interpreting experimental results is not always clear. Instrumentation of large castings is difficult enough; for thin films instrumentation is virtually impossible. For certain experiments it is possible to analytically determine the interface resistance if the resistance is assumed constant.

Adams /2/ has hypothesized that in case of real casting problems the interface temperature predicted by the Schwarz solution could be used but now would be acting through a film resistance upon the mold and another film resistance upon the casting. Figure 1 shows the model of a mold and casting system with interfacial conductance h . What Adams /2/ proposed is shown in Fig. 2, where T_1 is the interface temperature predicted by the Schwarz solution. Mathematically, this has broken the problem into two separate parts; a mold heated by a temperature source T_1 acting through a film of conductance h_1 , and a casting cooled by a temperature sink T_1 acting through a film of conductance h_2 .

Adams took h_1 and h_2 to be different. Results presented later in this paper indicate that in general they are different. An exact solution

THERMAL CONTACT RESISTANCE

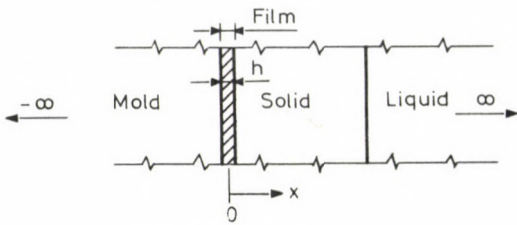


Fig. 1. Idealized mold-casting system

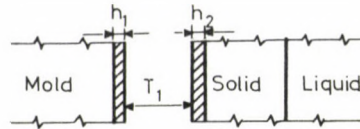


Fig. 2. The mold-casting system decomposed into two separate problems

for a semiinfinite body, initially at some uniform temperature and heated or cooled by a constant temperature source acting through a film of constant conductance is available [1]. The problem of a solidifying liquid chilled by a constant temperature sink acting through a film of constant conductance cannot be solved exactly. However, for the case when the liquid is at the saturation temperature, an analytical solution may be formulated by the method of successive approximations. This method has been applied by Savino and Siegel [3] to the problem of a warm moving liquid solidifying on an isothermal wall. In their problem there was perfect thermal contact between the liquid and the wall but there was convective heat transfer from the liquid to the solid-liquid interface.

In this paper the method of successive approximations is applied to the previously described problem. The solution is finally expressed in such a way that knowing the thickness solidified vs time, film conductance h_2 between T_1 and the casting can be found by finding the first zero of a transcendental function. A similar procedure is used to determine film conductance h_1 between T_1 and the mold. The technique is applied to some experimental results.

2. FORMULATION OF THE PROBLEM

For the case when the liquid metal is at the fusion temperature, the problem is governed by the following equations.

In the solidified portion

$$k \frac{\partial^2 T}{\partial x^2} = \frac{\partial T}{\partial t}, \quad 0 \leq x \leq z.$$

The boundary conditions

$$-k \frac{\partial T}{\partial x} = h(T_1 - T) \quad x = 0$$

and

$$\left. \begin{aligned} k \frac{\partial T}{\partial x} &= \frac{\rho L dz}{dt} \\ T &= T_f \end{aligned} \right\} x = z .$$

The initial condition in the liquid is

$$T = T_f , \quad t = 0 .$$

Define the following nondimensional parameters

$$T' = \frac{T - T_f}{T_f - T_1} ,$$

$$X = x/e ,$$

$$Y = z/e ,$$

where e is an arbitrary reference length.

$$\tau = kl/e^2 ,$$

$$H = lh/k ,$$

$$L' = \frac{L}{c(T_f - T_1)} .$$

The governing equations for the problem then become

$$\frac{\partial^2 T'}{\partial X^2} = \frac{\partial T'}{\partial \tau} , \quad 0 \leq X \leq Y \quad (1)$$

and

$$\frac{\partial T'}{\partial X} = H(1 + T') , \quad X = 0 \quad (2)$$

THERMAL CONTACT RESISTANCE

$$\left. \begin{aligned} \frac{\partial T'}{\partial X} &= L' \frac{dY}{d\tau} \\ T' &= 0 \end{aligned} \right\} X = Y \quad (3)$$

Initially

$$T' = 0, \quad \tau = 0 \quad (4)$$

First Eq.(1) is integrated from an arbitrary position in solid X to solid-liquid interface Y to obtain

$$\frac{\partial T'}{\partial X} = \frac{\partial T'}{\partial \xi} \Bigg|_{\xi=Y} - \int_X^Y \frac{\partial T'}{\partial \tau} (\xi, \tau) d\xi \quad (5)$$

The first interface condition (3) is now used to find

$$\frac{\partial T'}{\partial X} = L' \frac{dY}{d\tau} - \int_X^Y \frac{\partial T'}{\partial \tau} (\xi, \tau) d\xi \quad (6)$$

This result is now integrated from surface X = 0 to an arbitrary point X:

$$T'(X, \tau) - T'(0, \tau) = L' X \frac{dY}{d\tau} - \int_0^X \left[\int_{\eta}^Y \frac{\partial T'}{\partial \tau} (\xi, \tau) d\xi \right] d\eta \quad (7)$$

Using the boundary condition (2) and Eq. (6) evaluated at X = 0 gives

$$\begin{aligned} T'(0, \tau) &= \frac{1}{H} \frac{\partial T'}{\partial X} \Bigg|_{X=0} - 1 = \\ &= \frac{L}{H} \frac{dY}{d\tau} - \frac{1}{H} \int_0^Y \frac{\partial T'}{\partial \tau} d\xi - 1 \end{aligned} \quad (8)$$

Substitution of (8) into (7) gives

$$\begin{aligned} T'(X, \tau) &= L' \left(X + \frac{1}{H} \right) \frac{dY}{d\tau} - 1 - \frac{1}{H} \int_0^Y \frac{\partial T'}{\partial \tau} d\xi - \\ &- \int_0^X \int_{\eta}^Y \frac{\partial T'}{\partial \tau} d\xi d\eta \end{aligned} \quad (9)$$

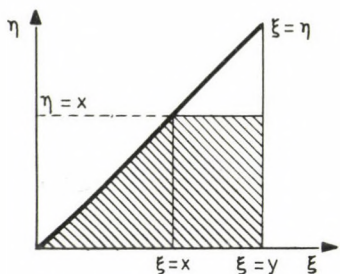


Fig. 3. Region of integration of Eq. (9)

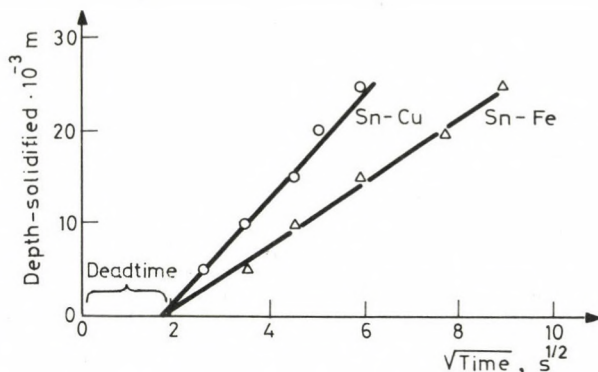


Fig. 4. Experimental data for depth solidified vs $(\text{time})^{1/2}$

With reference to Fig. 3, the order of intergration is now changed according to the following procedure. The slashed region is the domain of intergration, thus

$$\int_0^X \int_{\eta}^Y F(\xi) d\xi d\eta = \int_0^X \int_0^{\xi} F(\eta) d\eta d\xi + \int_X^Y \int_X^X F(\eta) d\eta d\xi$$

Applying this procedure to Eq. (9) gives

$$T'(X, \tau) = -1 + L'(X + \frac{1}{H}) \frac{dY}{d\tau} - \frac{1}{H} \int_0^Y \frac{\partial T'}{\partial \tau} d\xi - \int_0^X \xi \frac{\partial T'}{\partial \tau} d\xi - X \int_X^Y \frac{\partial T'}{\partial \tau} d\xi \quad (10)$$

The order of differentiation and integration is now changed to find

$$T'(X, \tau) = -1 + L'(X + \frac{1}{H}) \frac{dY}{d\tau} - \frac{\partial}{\partial \tau} \left[\frac{1}{H} \int_0^Y T'(\xi, \tau) d\xi + \int_0^X \xi T'(\xi, \tau) d\xi + X \int_X^Y T'(\xi, \tau) d\xi \right] \quad (11)$$

THERMAL CONTACT RESISTANCE

Since it is the time to solidify a given thickness that is of interest, write

$$Y = F(\tau) .$$

It is now helpful to transform variables. Although the solution is unknown at this juncture, if it is unique then there will be an inverse to the above relation such that

$$\tau = \tilde{F}(Y) .$$

Noting that

$$\frac{\partial}{\partial \tau} = \frac{dY}{d\tau} \frac{\partial}{\partial Y} ,$$

Eq. (11) may now be written in terms of X and Y:

$$T'(X,Y) = -1 + L'(X + \frac{1}{H}) \frac{dY}{d\tau} - \frac{dY}{d\tau} - \frac{\partial I(X,Y)}{\partial Y} \quad (12)$$

where

$$I(X,Y) = \frac{1}{H} \int_0^Y T'(\xi, Y) d\xi + \int_0^X \xi T'(\xi, Y) d\xi + X \int_X^Y T'(\xi, Y) d\xi . \quad (13)$$

In order to prove the validity of changing the order of integration and differentiation to obtain expression (11) from (10) it is only necessary to form $\partial I(X,Y)/\partial \tau$ and apply Leibnitz's rule in differentiation of integrals with variable limits. Then use the fact that $T'(Y,Y)=0$ and invert the transformation from Y to τ .

Rewriting Eq. (12)

$$\frac{dY}{d\tau} = \frac{T'(X,Y) + 1}{L'(X + \frac{1}{H}) - \frac{\partial I(X,Y)}{\partial Y}} \quad (14)$$

At $X = Y$, $T' = 0$ so that

$$\frac{dY}{d\tau} = \frac{1}{L'(Y + \frac{1}{H}) - \frac{\partial I(X,Y)}{\partial Y} \Big|_{X=Y}} \quad (15)$$

Define

$$G(Y) = I(Y, Y) = \int_0^Y \left(\frac{1}{H} + \xi \right) T'(\xi, Y) d\xi \quad . \quad (16)$$

It can be demonstrated that

$$\frac{dG(Y)}{dY} = \frac{\partial I(X, Y)}{\partial Y} \Bigg|_{X=Y} \quad . \quad (17)$$

Equation (15) thus becomes

$$\frac{dY}{d\tau} = \frac{1}{L'(Y + \frac{1}{H}) - \frac{dG}{dY}} \quad (18)$$

which can be integrated to give

$$\tau = L' \left(\frac{Y^2}{2} + \frac{Y}{H} \right) - G(Y) \quad . \quad (19)$$

Substituting Eq. (18) into Eq. (12) gives

$$T'(X, Y) = -1 + \frac{L'(X + \frac{1}{H}) - \frac{\partial I}{\partial Y}}{L'(Y + \frac{1}{H}) - \frac{dG}{dY}} \quad (20)$$

Up to this point no approximations have been made. The differential equation has been integrated as far as possible, making use of the boundary conditions in order to obtain a form to which the method of successive approximations can be applied.

3. SOLUTION

1st Approximation

The first approximation is found by taking $G=0$ and $I=0$ in Eqs (19) and (20) to obtain

$$\tau_1 = L' \left(\frac{Y^2}{2} + \frac{Y}{H} \right) \quad (21)$$

and

$$T'_1 = -1 + \frac{(X + \frac{1}{H})}{(Y + \frac{1}{H})} \quad . \quad (22)$$

THERMAL CONTACT RESISTANCE

The first approximation is physically meaningful. It is none other than the London-Seban solution /4/ for the solidification of a liquid at the fusion temperature, cooled by a temperature sink acting through a film conductance H and where the heat capacity effects of the solidified portion have been ignored. This means that the temperature varies linearly in the solid as can be seen in Eq. (22).

2nd Approximation

The second approximation is determined by using τ_1 and T_1' to determine values for G and I from Eqs (13) and (16). Thus

$$G_2(Y) = \int_0^Y \left(\frac{1}{H} + \xi\right) T_1'(\xi, Y) dY$$

and

$$I_2(X, Y) = \frac{1}{H} \int_0^Y T_1'(\xi, Y) d\xi + \int_0^X \xi T_1'(\xi, Y) d\xi + X \int_X^Y T_1'(\xi, Y) d\xi .$$

Performing these intergrations yields

$$G_2 = -\frac{1}{6} \left(\frac{1}{H} + Y\right)^2 + \frac{1}{2H^2} - \frac{1}{3H^3 \left(Y + \frac{1}{H}\right)} ,$$

$$I_2 = \frac{1}{2} \left(X + \frac{1}{H}\right) \left(\frac{1}{H} - Y\right) + \frac{X^2}{2} - \frac{1}{3H^3 \left(Y + \frac{1}{H}\right)} - \frac{1}{6} \frac{\left(X + \frac{1}{H}\right)^3}{\left(Y + \frac{1}{H}\right)} .$$

The following derivatives are then found

$$\frac{dG_2}{dY} = -\frac{1}{3} \left(Y + \frac{1}{H}\right) + \frac{1}{3H^3 \left(Y + \frac{1}{H}\right)^2} \tag{23}$$

and

$$\frac{dI_2}{dY} = -\frac{1}{2} \left(X + \frac{1}{H}\right) + \left[\frac{1}{3H^3} + \frac{\left(X + \frac{1}{H}\right)^3}{6} \right] / \left(Y + \frac{1}{H}\right)^2 \quad (24)$$

Equations (23) and (24) are now substituted into Eqs (19) and (20) to find the second approximation

$$\tau_2 = \tau_1 + \frac{1}{6} \left(Y + \frac{1}{H}\right)^2 - \frac{1}{2H^2} + \frac{1}{3H^3 \left(Y + \frac{1}{H}\right)} \quad (25)$$

$$T'_2 = -1 + A/B, \quad (26)$$

where

$$A = L' \left(X + \frac{1}{H}\right) + \frac{1}{2} \left(X + \frac{1}{H}\right) - \frac{\frac{1}{3H^3} + \frac{1}{6} \left(X + \frac{1}{H}\right)^3}{\left(Y + \frac{1}{H}\right)^2},$$

$$B = L' \left(Y + \frac{1}{H}\right) + \frac{1}{3} \left(Y + \frac{1}{H}\right) - \frac{1}{3H^3 \left(Y + \frac{1}{H}\right)^2}.$$

3rd Approximation

The third and last approximation is determined in the same fashion that the second approximation was determined. Since only the approximation for time vs depth is required it will only be necessary to determine G_3 . Substituting Eq. (26) into Eq. (16) yields upon intergration

$$G_3 = -(1/2 + 1/6DH^3)(Y + 1/H)^2 + 1/3D(L' + 2/5)(Y + 1/H)^5 + \\ + 1/2H^2 - 1/3DH^3(L' + 1/2)(Y + 1/H)^2 + 1/5DH^5 \quad (27)$$

where

$$D = (Y + 1/H)^3(L' + 1/3) - 1/3H^3. \quad (28)$$

The third approximation for the time vs depth is

$$\tau_3 = \tau_1 - G_3. \quad (29)$$

In order to check this solution a comparison was made with Neumann's solution /1/ for the case of infinite surface conductance (zero surface resistance). Neumann's solution is an exact solution for the case of a semiin-

THERMAL CONTACT RESISTANCE

finite saturated liquid whose surface temperature is held fixed at some temperature below the fusion temperature. It is, thus, a special case of the Schwarz solution. The third approximation and Neumann's solution agreed exactly, for all intents and purposes, for a variety of problems. The following example shows that when there is a finite film conductance between the temperature sink and the solidifying liquid there is a significant difference between Neumann's solution and the solution developed here as would be expected.

Example

As an example, consider the problem of liquid tin chilled by a 96°C sink acting through a film of conductance $h=6.02 \text{ kW/m}^2 \text{ }^{\circ}\text{C}$. Table I gives the pertinent physical properties.

Table I Properties of Tin

k	ρ	c	L	T_f
60.2 W/M ⁰ C	7300 Kg/m ³	0.26 KJ/Kg ⁰ C	58.3 KJ/Kg	232 ⁰ C

Table II shows the time to solidify various depths as predicted by the Neumann solution and the three approximate solutions τ_1 , τ_2 , τ_3 .

Table II Depth solidified vs time by the Neumann and approximate solutions when there is a finite film conductance
 $h = 6.02 \text{ KW/m}^2 \text{ }^{\circ}\text{C}$

$z \cdot 10^{-2} \text{ m}$	$t_{\text{neu}} \text{ s}$	$t_1 \text{ s}$	$t_2 \text{ s}$	$t_3 \text{ s}$	t fin dif
0.2	0.121	1.15	1.21	1.21	1.21
0.4	0.491	2.52	2.74	2.74	2.74
0.6	1.104	4.15	4.58	4.55	4.55
0.8	1.971	5.97	6.66	6.61	6.61
1.0	3.090	7.90	9.08	8.99	8.99
1.2	4.360	10.20	11.50	11.40	11.40
1.4	6.400	12.60	14.50	14.30	14.30
1.6	7.886	15.60	17.80	17.60	17.60
1.8	9.980	18.40	21.20	20.70	20.70
2.0	12.340	21.30	24.70	24.50	-

Recall that τ_1 corresponds to the London-Seban solution. The results are presented in dimensional form.

Notice that the Neumann solution predicts a much shorter time to solidify a given depth than any of the approximations. This is because there is no resistance to heat flow on the surface in the Neumann solution. Also notice the first approximation t_1 , which is the London-Seban solution, which predicts a shorter time to solidify a given depth than the other two approximations. This is because in the London-Seban solution the solidified part cannot store heat but acts merely like a resistance. As can be seen, the approximate analytical solution agrees well with the finite difference solution. It was found that the approximate solution was very sensitive to roundoff error in the computation process and that it was necessary to use double precision in performing the calculations on an IBM 1130.

4. DETERMINATION OF h FROM EXPERIMENTAL DATA

Experimentally measured values of depth vs time can be used to determine the interfacial film conductance between the mold and casting using the previously described solution provided that the mold and casting behave as if they were semiinfinite for the range of measurements to be analyzed and provided that the melt was initially at or near the saturation temperature while the mold was initially at some uniform temperature. The procedure is as follows: First, knowing the initial temperature of the mold and the thermal properties of the mold and casting, the interface temperature that would be expected in the case of perfect thermal contact is computed from the Schwarz solution /1/ which is

$$T_1 = \left[T_f + \frac{k_1}{k_2} \left(\frac{K_2}{K_1} \right)^{1/2} T_m \operatorname{erf}(\lambda) \right] / \left[1 + \frac{k_1}{k_2} \left(\frac{K_2}{K_1} \right)^{1/2} \cdot \operatorname{erf}(\lambda) \right], \quad (30)$$

where

- K_1, K_2 — thermal diffusivities of the mold and casting,
- T_1 — initial mold temperature at $t=0$,
- T_m — fusion temperature,
- k_1, k_2 — thermal conductivities of the mold and casting,
- erf — error function, and
- λ — root of transcendental equation

$$\lambda e^{\lambda^2} \left[\frac{k_2}{k_1} \left(\frac{K_1}{K_2} \right)^{1/2} + \operatorname{erf}(\lambda) \right] - \frac{C_2 T_f}{\pi^{1/2} L_f} = 0 \quad (31)$$

with C_2 being the specific heat of the casting.

THERMAL CONTACT RESISTANCE

Knowing T_1 from the above equations and the depth solidified in a given time from experimental data, the value of h_2 necessary for Eq. (29) to be satisfied can be found as follows. Equation (29) is rewritten as

$$f(h) = \tau_3 - \tau_1 + G_3 \quad (32)$$

The correct value of h_2 is the first root of $f(h)$ that is, the value of h that causes $f(h)$ to vanish. This can be accomplished by well known techniques /5/.

The value of h_1 between T_1 and the mold is similarly determined. Knowing T_1 and the temperature at a point in the mold as a function of time the solution for a semiinfinite body heated by convection can be solved inversely to find h_1 . The solution of this problem is /1/

$$T_1(x, t) = T_1 \left\{ \operatorname{erfc} \left[\frac{x}{2(K_1 t)^{1/2}} \right] - \exp \left[\frac{h_1}{k_1} \left(x - \frac{h_1 t}{\rho_1 c_1} \right) \right] \cdot \operatorname{erfc} \left[\frac{x}{2(K_1 t)^{1/2}} + \frac{h_1}{k_1} (K_1 t)^{1/2} \right] \right\} \quad (33)$$

Thus, the value of h_1 can be determined by finding the value of h that satisfies Eq. (33) for given values of T_1 , x , and t .

The total film conductance is then found from

$$h = \left(\frac{1}{h_1} + \frac{1}{h_2} \right)^{-1} \quad (34)$$

5. APPLICATION TO RESULTS OF AN EXPERIMENT

Molten tin was solidified on both a copper chill and a steel chill. The apparatus and the differential thermometry technique used to determine depth solidified at various times is described in an article by Prates et al /6/. The temperature of the molten tin was kept as close to the fusion temperature as possible in order to eliminate the effect of superheat. The ambient temperature was 21°C. One problem that could not be eliminated was stirring of the liquid during the pouring operation. Stirring revealed itself as erratic output on the recorder similar to that reported by Prates et al /6/. This tended to retard the onset of solidification.

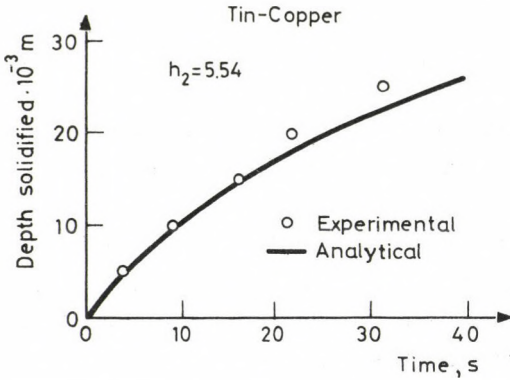


Fig. 5. Comparison of analytical with experimental results of depth solidified time for tin on a copper chill

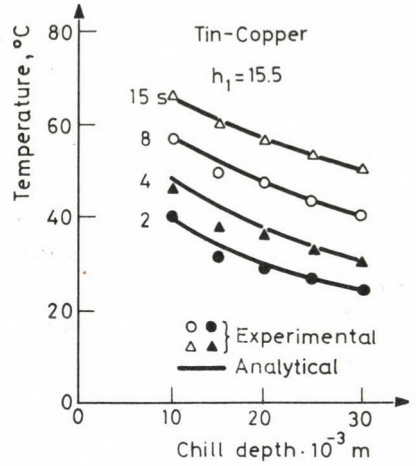


Fig. 6. Comparison of analytical with experimental results of temperature position in the chill for various times for tin on a copper chill

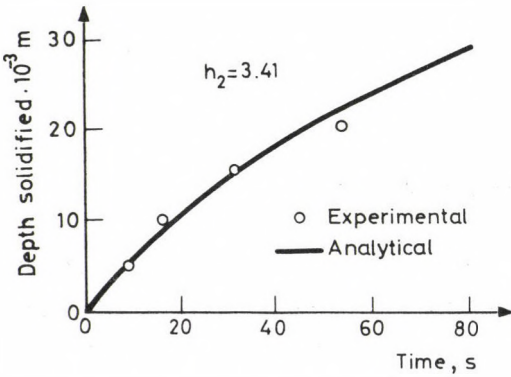


Fig. 7. Comparison of analytical with experimental results of depth solidified time for tin on a cold rolled steel chill

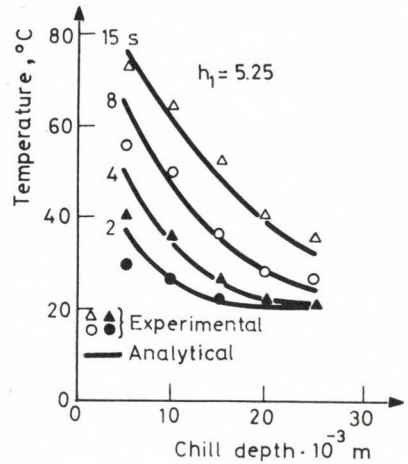


Fig. 8. Comparison of analytical with experimental results of temperature position in the chill for various times for tin on a cold rolled steel chill

THERMAL CONTACT RESISTANCE

Figure 4 shows the data for the two experiments for depth solidified vs the square root of time, presented in this way because of perfect thermal contact depth solidified is proportional to the square root of time. Passing straight lines through the data shows that they intersect the $t^{1/2}$ axis at $t=3.05$ s. This value is used as an estimate of the deadtime prior to the onset of solidification. Table III details the data pertinent to the experiment and the data.

Table III Thermal Properties

	$k, W/M^{\circ}C$	$\rho, Kg/m^3$	$c, KJ/Kg^{\circ}C$	$L_f, KJ/Kg$	$T_f, ^{\circ}C$	$T_o, ^{\circ}C$
Tin	60.2	7300	0.26	58.3	232	234.0
Copper	394.0	7960	0.386			21
C.R.S	67.1	7860	0.628			21

In using Eq. (32) to determine h_2 , the deadtime of 3.05 s is subtracted from the time for a given depth to solidify. In determining the values of h_1 for the chill blocks, no deadtime is used since they commence warming up immediately. The computed results are given in Table IV.

Table IV Results of Analysis

	$T_p, ^{\circ}C$	h_1	h_2	$h=(1/h_1+1/h_2)(KW/M^2 ^{\circ}C)$
Sn-Cu	96.5	15.5	5.54	4.08
Sn-Fe	140.7	5.25	3.41	2.075

Note that h_1 and h_2 are unequal in both cases. Figure 5 shows a plot of the depth solidified vs time as predicted by Eq. (29) compared with the experimental data where the deadtime has been subtracted for the use of tin solidifying on a copper chill. Figure 8 shows plots of temperature vs depth into the chill for various times as computed by Eq. (33) compared with experimental data. Figure 7 and 8 show the same type of results for tin on the cold rolled steel chill.

6. DISCUSSION

The method of successive approximations used here provides an analytical solution for the solidification of a semiinfinite saturated liquid whose surface is cooled by a temperature sink acting through a film resistance. The method is accurate and was easily programmed along with the Schwartz solution to determine the film conductance between a mold and a casting from the results of an experiment. It has several advantages over the finite difference technique for these problems where it applies. In order to determine a film conductance from an experiment using a finite difference technique, a trial and error procedure that is slow and costly is required whereas the analytical approach can be used with a root finding procedure, as outlined in the text, to determine the film conductance automatically and very rapidly.

REFERENCES

1. H.S. Carslaw and J.C. Jaeger: *Conduction of Heat in Solids*, Oxford University Press, Oxford 1959.
2. C.M. Adams: *Liquid Metals and Solidification*. Amer. Soc. for Metals, Cleveland, 1958.
3. J.M. Savino and R. Siegel: *Int. J. Heat Mass Trans.*, 1969, vol. 12, pp. 803-809.
4. A.L. London and R.A. Seban: *Trans. ASME*, 1943, vol. 65, pp. 771-778.
5. G. Milovanović: *Numerical Analysis*, (in Serbian), Naučna knjiga, Beograd, 1985.
6. M. Prates, J. Fissolo, and H. Biloni: *Met. Trans.*, 1972, vol. 3, pp. 1419-1425.

THE ANALYSIS OF SINGLE-CELL BOX BEAMS BY THE HINGED MODEL

J. Szidarovszky*

(Received: 25 June 1985)

By resolving the eccentric load of a single-cell box beam into a symmetric and an antisymmetric part, we arrive at the solution by superimposition. The symmetric problem can be easily solved by the wellknown formulas of the elementary theory of structures. The anti-symmetric problem, however, is quite complicated and the aim of this paper is to present a procedure for this problem. The single-cell box beam consists of perpendicular walls which are connected by rigid joints. We assume the beam is intersected at the joints and there hinges are built-in. This "hinged beam" is braced by densely placed "supporting frames". The procedure presented applies the equations of elementary theory of strength of materials to the physical model of this hinged beam and the supporting frames. The beam is divided into sections and the stresses are determined with the help of matrix equations.

NOTATION

A_0, A_n	spring constant at a support,
A_0^i	frame-rigidity (the lateral stiffness of the supporting frame),
a_i	length of section i ,
E^i	modulus of elasticity,
F	cross sectional area,
h	distance between the stress axes of the two horizontal walls (flange plates),
$h_1 = h_f$	perpendicular distance between the upper stress axis and the neutral axis,
$h_2 = h_a$	perpendicular distance between the lower stress axis and the neutral axis,
I	moment of inertia (second moment of area of the cross sectional area) about the axis perpendicular to the plane of bending,
i	nodal point, boundary of a section or reference to a section,
I_b	substitute moment of inertia of the vertical wall with the two horizontal walls,
I_f	substitute moment of inertia of the upper horizontal flange plate,
I_a	substitute moment of inertia of the lower horizontal flange plate,
$I_b^a = I_b/2$	horizontal component of the frame reactive force,
Q	distance between the stress-axes of the vertical walls (webs),
k	length of the beam,
ℓ	external vertical concentrated force,
P	resultant/shearing force,
R	shearing force,
t	vertical co-ordinate perpendicular to the axis of the beam,
x	horizontal co-ordinate perpendicular to the axis of the beam,
y	

*Dr. J. Szidarovszky, H-1089 Budapest, Bíró Lajos u. 42., Hungary

SZIDAROVSKY, J.

z	co-ordinate along the axis of the beam,
α	angular displacement,
β_t	change in angle of the supporting frame,
η	displacement,
κ	built in change in angular displacement
σ	normal stress,
τ	shearing stress,
ξ	abscissa.
<u>E</u>	unit matrix.

Subscripts

o	refers to place $z=0$ or $n=0$,
z	refers to place z ,
l	refers to place $z=l$
i	refers to a section or to the boundary of a section,
n	refers to the last section or to the end of the beam or to the boundary of the last section,
κ	refers to the cause of the built in angular displacement,
σ	refers to normal stress,
τ	refers to shearing stress,
v	refers to vertical direction, force or wall,
a	refers to lower horizontal wall (flange plate),
f	refers to upper horizontal wall (flange plate),
h	refers to horizontal-direction, -force or -wall,
p	refers to external vertical force,
q	refers to frame-reaction

1. INTRODUCTION

Demand for constructing bridges and other types of construction emerged early in the history of mankind. Materials and structural size were decided on good or bad experiences at that time. It was only later on, when economic structural arrangements and calculation methods were developed. A good example for this is the box-beam bridge. The simplest and widely used version of box-beam bridges is the single-cell box-beam bridge, shown in Fig.1.

The aim of this paper is to analyze the single-cell box-beam bridge of right angled cross section, subjected to static, vertical, antisymmetric load with the aid of the theory of strength of materials. We present a unified method which makes it possible to determine the normal and shearing stresses of the beam of deformable cross section as accurately as with the beams subjected to a symmetric load. The effect of the diaphragms and their stresses are also examined.

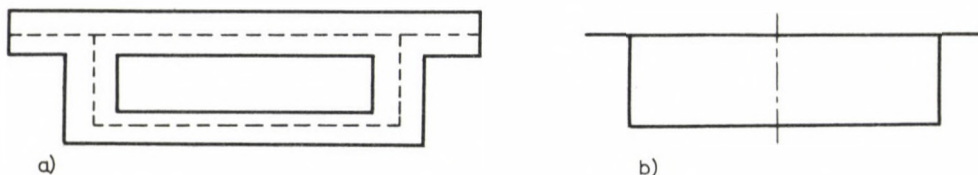


Fig. 1.

This paper establishes the mathematical and physical models and works out the mathematical procedures. Practical application /6/, the effect of warping and restrained warping /7/ and certain generalizations as well as the demonstration of the validity of our assumptions /8/ are given in following papers.

We do not intend to analyze non-elastic behaviour, dynamic response, the effect of the degree of non-linearity in elasticity, the effect of temperature, creep and shrinkage, local stresses, buckling and the phenomenon of shear-lag.

1.1 Single-cell box beam

When examining the behaviour of the single-cell box beam subjected to vertical, eccentric load, we resolve the external load p^x into a symmetric and an antisymmetric part in the planes of the vertical walls of the box beam. The symmetric part consists of forces $p^x/2$ acting downwards in the planes of the vertical walls and the antisymmetric part is made up from forces $p/2$: one acting downwards in the wall and the other acting upwards in the other wall. The relation between p and p^x assumes the form as seen in Figure 2

$$p = p^x \frac{s_2 - s_1}{s_2 + s_1} \quad (1.1.1)$$

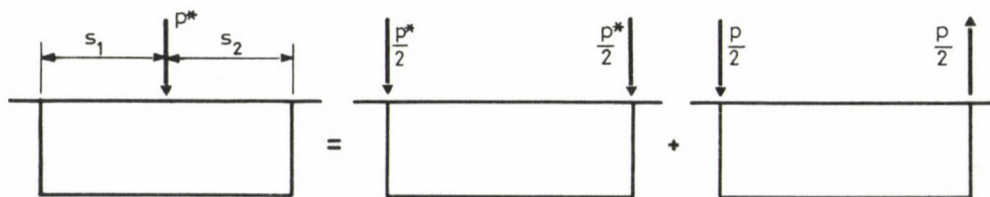


Fig. 2.

In the case of the above resolution, neither the torque nor the bending moment change and the resolution yields exact cross sectional stress components in the hinged beam. However, because of the partially built-in points, the resolution cannot be considered exact for the actual beam.

The symmetric stress components resulting from the symmetric load can be determined accurately enough for civil engineering calculations with the equations of the theory of strength of materials, only the effect of shear-lag modifying the normal stresses should be taken into account in certain cases.

The analysis of the antisymmetric problem, however, is somewhat more difficult. Due to the antisymmetric vertical load, the vertical walls of the box beam develop bending moments and one part of torsion resulting from the antisymmetric load is accounted for by bending of the vertical walls and the other part is taken by torsion of the box beam as a whole. It follows therefore that

1. Due to the vertical antisymmetrical load, both the horizontal and the vertical walls are in bending in their planes, i.e.
 - a) normal stresses and consequently bending deformations develop in the walls,
 - b) shearing forces causing shearing deformations also develop in the walls.
2. The torsion of the whole cross section results in shearing forces and shearing deformations in both the vertical and the horizontal walls.
3. The shearing deformation causes incompatible deformations in certain cross sections which develop redundants, i.e. warping developed from shearing caused by torsion is restricted.

1.2 The analysis of simply supported beam by the matrix method

Let us divide the simply supported beam of length l shown in Fig. 3 into n sections. Section i subjected to force P_i at point i , lies between nodal points $(i-1)$ and i . The equation

$$M_i = M_{i-1} + R_i a_i \quad (1.2.1)$$

holds, where M_i is the bending moment at nodal point i and R_i is the shearing force along the section i and a_i denotes the length of section i . With P_{i-1} acting at nodal point $i-1$, we have

ANALYSIS OF SINGLE-CELL BOX BEAMS

where we have

$$\frac{R}{(n)} \begin{bmatrix} R_1 \\ \cdot \\ \cdot \\ \cdot \\ R_i \\ \cdot \\ \cdot \\ \cdot \\ R_n \end{bmatrix} \quad (1.2.10a)$$

$$\underset{(n) \times (n-1)}{K_2} = \begin{bmatrix} \frac{1}{a_1} & \cdot & \cdot & \cdot & \cdot & \cdot & \cdot & \cdot & \cdot & \cdot \\ \frac{1}{a_2} & \frac{1}{a_2} & \cdot & \cdot & \cdot & \cdot & \cdot & \cdot & \cdot & \cdot \\ \cdot & \cdot & \cdot & \cdot & \cdot & \cdot & \cdot & \cdot & \cdot & \cdot \\ \cdot & \cdot & \cdot & -\frac{1}{a_i} & \frac{1}{a_i} & \cdot & \cdot & \cdot & \cdot & \cdot \\ \cdot & \cdot & \cdot & \cdot & \cdot & \cdot & \cdot & \cdot & \cdot & \cdot \\ \cdot & \cdot & \cdot & \cdot & \cdot & \cdot & -\frac{1}{a_{n-1}} & \frac{1}{a_{n-1}} & \cdot & \cdot \\ \cdot & \cdot & \cdot & \cdot & \cdot & \cdot & \cdot & \cdot & -\frac{1}{a_n} & \cdot \end{bmatrix} \quad (1.2.11)$$

and

$$\underset{nx(n-1)}{K_3} = \underset{(n) \times (n-1)}{K_2} \underset{(n-1) \times (n-1)}{C}^{-1} \underset{(n-1) \times (n-1)}{K_1} \quad (1.2.12)$$

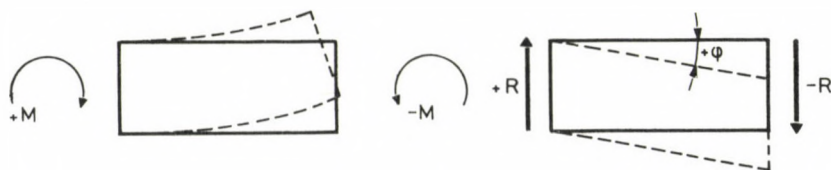


Fig. 4.

On the basis of Figures 4 and 5 we can establish the displacement equations

$$\eta_{i-1} = \eta_i - a_i \alpha_i - \frac{a_i^2}{6EJ_i} (M_{i-1} + 2M_i) - \frac{a_i}{6F_i} R_i, \quad (1.2.13)$$

and

$$\eta_{i+1} = \eta_i + a_i \alpha_i - \frac{a_{i+1}^2}{6EJ_{i+1}} (M_{i+1} + 2M_i) + \frac{a_{i+1}}{6F_{i+1}} R_{i+1}, \quad (1.2.14)$$

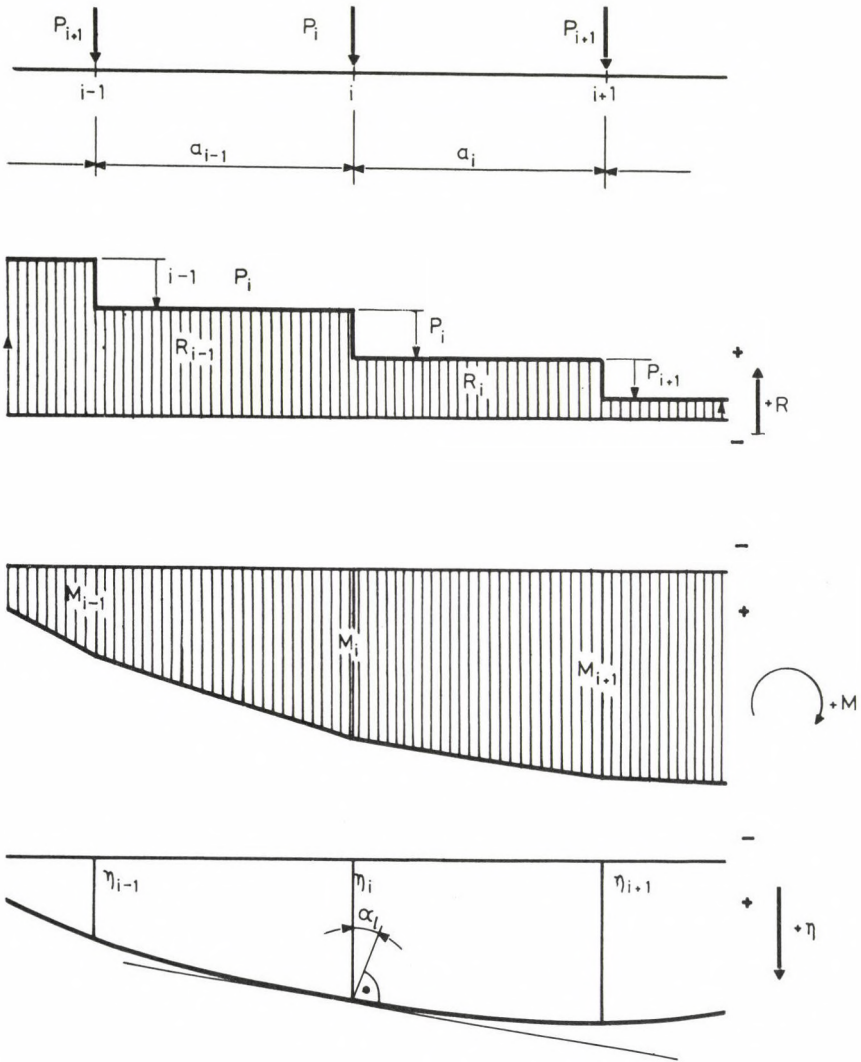


Fig. 5.

and

$$\begin{matrix}
 & \phi_1^{a_2} & -\phi_2^{a_1} & & \cdot & & & & \\
 & \cdot & \phi_2^{a_3} & & -\phi_3^{a_2} & & \cdot & & \\
 \underline{K}_5 = & & & & & & & & \\
 (n-1) \times n & & & & \phi_{n-2}^{a_{n-1}} & -\phi_{n-1}^{a_{n-2}} & & & \\
 & & & & & & \phi_{n-1}^{a_n} & -\phi_n^{a_{n-1}} &
 \end{matrix} \quad (1.2.22)$$

Substituting Eq. (1.2.8) into Eq. (1.2.18), we obtain

$$\underline{\eta} = \underline{C}^{-1} \underline{K}_4 \underline{M} + \underline{C}^{-1} \underline{K}_6 \underline{M} = \underline{K}_7 \underline{P} + \underline{K}_8 \underline{P} \quad , \quad (1.2.23)$$

where

$$\underline{K}_7 = \underline{C}^{-1} \underline{K}_4 \underline{C}^{-1} \underline{K}_1 \quad , \quad (1.2.24)$$

(n-1) x (n-1)

and

$$\underline{K}_8 = \underline{C}^{-1} \underline{K}_6 \underline{C}^{-1} \underline{K}_1 \quad . \quad (1.2.25)$$

(n-1) x (n-1)

If the frame-rigidity of the diaphragms at the supports of the box beam is of finite magnitude, the upper wall as a beam is on elastic supports. Only the reactive forces of the diaphragms act at the supports so they are the reactions of the beam. In the case of elastic supports, with spring constants A_0 and A_n , the displacement of section i is obtained from

$$\eta_i = \eta_0 + (\eta_n - \eta_0) \frac{\ell_i}{\ell} \quad , \quad (1.2.26)$$

where

$$\ell_i = \sum_{j=1}^i a_j \quad , \quad (1.2.27)$$

or, with the help of the shearing forces

$$\eta_i = \frac{(\ell - \ell_i) R_1}{\ell A_0} - \frac{\ell_i R_n}{\ell A_n} \quad , \quad (1.2.28)$$

which assumes the matrix form

$$\underline{\eta} = \underline{K}_9 \underline{R} = \underline{K}_{10} \underline{P} \quad , \quad (1.2.29)$$

$$K_{\cong 2} = \frac{1}{a} \quad (n \times (n-1)) \quad \left[\begin{array}{cccc} 1 & & & \\ -1 & 1 & & \\ & -1 & 1 & \\ & & \dots & \dots \\ & & & -1 & 1 \\ & & & & -1 \end{array} \right] = \frac{1}{a} \bar{K}_{\cong 2} \quad (1.2.11/a)$$

$$K_{\cong 3} = \frac{1}{a} \bar{K}_{\cong 2} \frac{1}{a} \bar{C}^{-1} a^2 \underline{\underline{E}} = \bar{K}_{\cong 2} \bar{C}^{-1}, \quad (n \times (n-1)) \quad (1.2.12/a)$$

$$K_{\cong 4} = \frac{a^3}{6EJ} \quad ((n-1) \times (n-1)) \quad \left[\begin{array}{cccc} 4 & 1 & & \\ 1 & 4 & 1 & \\ & & \dots & \dots \\ & & & 1 & 4 & 1 \\ & & & & & & 1 & 4 & 1 \\ & & & & & & & & & 1 & 4 \end{array} \right] = \frac{a^3}{6EJ} \bar{K}_{\cong 4}, \quad (1.2.21/a)$$

$$K_{\cong 5} = \frac{a^2}{GF} \quad ((n-1) \times n) \quad \left[\begin{array}{cccc} 1 & -1 & & \\ & 1 & -1 & \\ & & \dots & \dots \\ & & & 1 & -1 & \\ & & & & & & 1 & -1 \end{array} \right] = \frac{a^2}{GF} \bar{K}_{\cong 5}, \quad (1.2.22/a)$$

$$K_{\cong 6} = \frac{a^2}{GF} \bar{K}_{\cong 5} \frac{1}{a} \bar{K}_{\cong 2} = \frac{a}{GF} \bar{K}_{\cong 5} \bar{K}_{\cong 2}, \quad ((n-1) \times (n-1)) \quad (1.2.20/a)$$

$$K_{\cong 7} = \frac{1}{a} \bar{C}^{-1} \frac{a^3}{6EJ} \bar{K}_{\cong 4} \frac{1}{a} \bar{C}^{-1} a^2 \underline{\underline{E}} = \frac{a^3}{6EJ} \bar{C}^{-1} \bar{K}_{\cong 4} \bar{C}^{-1}, \quad ((n-1) \times (n-1)) \quad (1.2.24/a)$$

$$K_{\cong 8} = \frac{1}{a} \bar{C}^{-1} \frac{a}{GF} \bar{K}_{\cong 5} \bar{K}_{\cong 2} \frac{1}{a} \bar{C}^{-1} a^2 \underline{\underline{E}} = \frac{a}{GF} \bar{C}^{-1} \bar{K}_{\cong 5} \bar{K}_{\cong 2} \bar{C}^{-1} = \frac{a}{GF} \bar{C}^{-1}, \quad ((n-1) \times (n-1)) \quad (1.2.25/a)$$

If

$$A_0 = A_n$$

$$\begin{matrix}
 \underline{K}_{\underline{9}} = \frac{a}{A_0 \ell} \\
 (n-1) \times n
 \end{matrix}
 \begin{bmatrix}
 n-1 & \cdot & & 1 \\
 n-2 & \cdot & & 2 \\
 \cdot & \cdot & \cdot & \cdot \\
 n-i & \cdot & & i \\
 \cdot & \cdot & \cdot & \cdot \\
 1 & \cdot & \cdot & n-1
 \end{bmatrix}
 \cdot
 = \frac{1}{nA_0} \underline{K}_{\underline{9}} \quad , \quad (1.2.31/a)$$

$$\begin{matrix}
 \underline{K}_{\underline{10}} \\
 (n-1) \times (n-1)
 \end{matrix}
 = \frac{1}{nA_0} \underline{K}_{\underline{9}} \underline{K}_{\underline{2}} \underline{C}^{-1} \quad , \quad (1.2.30/a)$$

$$\begin{matrix}
 \underline{K}_{\underline{11}} \\
 (n-1) \times (n-1)
 \end{matrix}
 = \frac{a}{GF} \underline{C}^{-1} + \frac{1}{nA_0} \underline{K}_{\underline{9}} \underline{K}_{\underline{2}} \underline{C}^{-1} \quad . \quad (1.2.33/a)$$

Let us now introduce relative angular displacements denoted by κ_j ($j=1, \dots, n-1$) at the nodal points. According to Fig. 6, we have

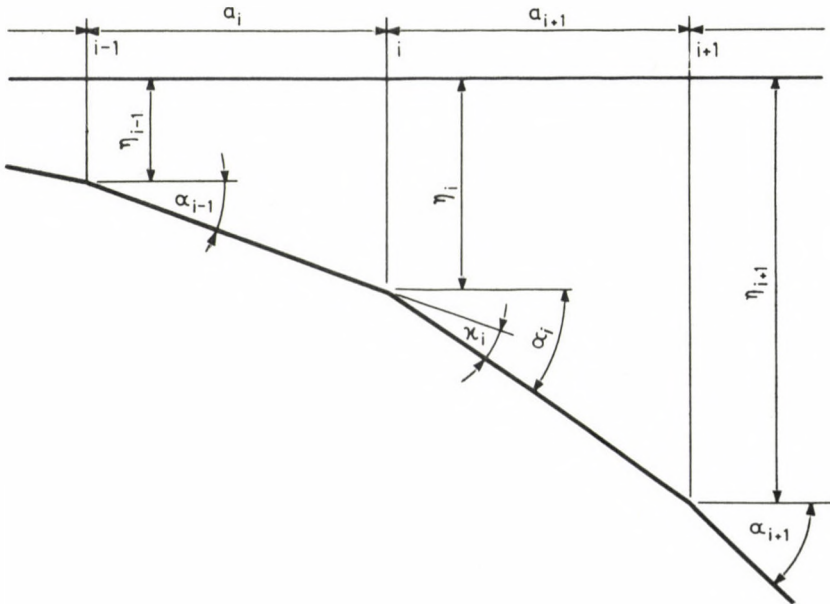


Fig. 6.

$$\alpha_{i+1} = \alpha_i + \kappa_i, \tag{1.2.34}$$

and

$$\eta_i = \eta_{i-1} + a_i \alpha_{i-1} \tag{1.2.35}$$

where α_i denotes the angular displacement along the length of section i . A derivation, similar to the one which resulted in Eq. (1.2.3), now yields

$$-a_i \eta_{i+1} + (a_i + a_{i+1}) \eta_i - a_{i+1} \eta_{i-1} = -a_i a_{i+1} \kappa_i, \tag{1.2.36}$$

from which, in a similar way as in the case of Eq. (1.2.8), we obtain the matrix equation

$$\underline{\eta} = -\underline{C}^{-1} \underline{K} \underline{\kappa}, \tag{1.2.37}$$

where

$$\underline{\kappa}_{(n-1)} = \begin{bmatrix} \kappa_1 \\ \cdot \\ \kappa_i \\ \cdot \\ \kappa_{n-1} \end{bmatrix} \tag{1.2.38}$$

1.3 Basic assumptions

In this paper we use the following assumptions.

1. The box beam is a simply supported beam (Fig. 7).
2. The longitudinal axis of the box beam is perpendicular to the axes of the two supports (Fig. 7).

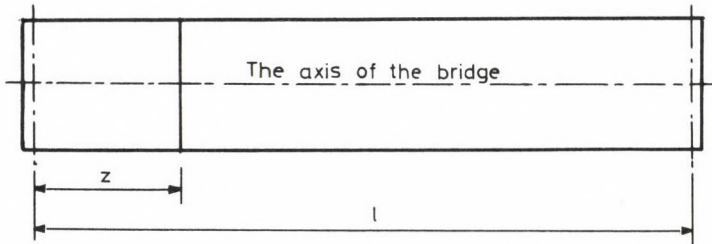


Fig. 7.

ANALYSIS OF SINGLE-CELL BOX BEAMS

3. The box beam has a single-cell cross section (Fig. 8).

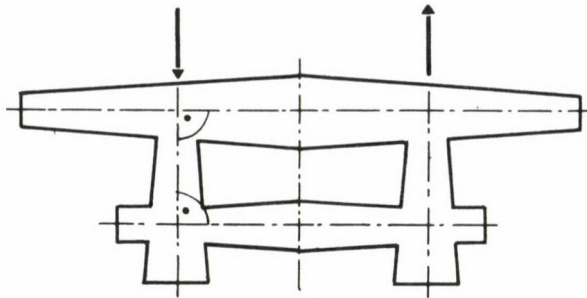


Fig. 8.

4. The cross section has a vertical symmetry axis (Fig. 8).

5. The walls meet at rigid joints.

6. The antisymmetric vertical forces of static nature act along the stress axes of the vertical walls (Fig. 8). (The notion of the stress axis is defined in /6/)

7. The stress axes of the walls in the cross section are perpendicular to each other (Fig. 8).

8. The analysis is carried out according to the first order theory of the strength of materials and the material of the beam is linearly elastic, homogeneous and isotropic. Only Bernoulli-Navier's assumption is replaced by formula (2.3.1).

9. The torsional rigidity of the individual walls is negligible.

Of the above assumptions, No 1 to No 8 are generally accepted assumptions frequently used in papers /1/, /2/, /3/, /4/, /5/, but there are also some alterations:

1. In the ninth assumption we do not assume, as it is normally assumed, that the walls are thinwalled members, we only assume that the torsional rigidity of the individual walls is negligible.

2. We do not stipulate that the cross section of the beam is constant.

3. We do not stipulate that the end-diaphragms are infinitely rigid.

4. We do not stipulate that the rigidities of the diaphragms are the same.

The cases when the cross section is a symmetrical trapezoid or the beam is subjected to horizontal forces or to couples are analysed in another paper /8/.

2. THE ANALYSIS OF THE HINGED BEAM

2.1 The model for the analysis

The model of the box beam bridge subjected to antisymmetric load (Fig. 8) is considered to be a compound structure building of individual planar walls. We cut the box beam into these individual walls (Fig. 9/b) and replace the internal forces along the joints by external forces resulting in 3 forces and 3 couples (Fig. 10).

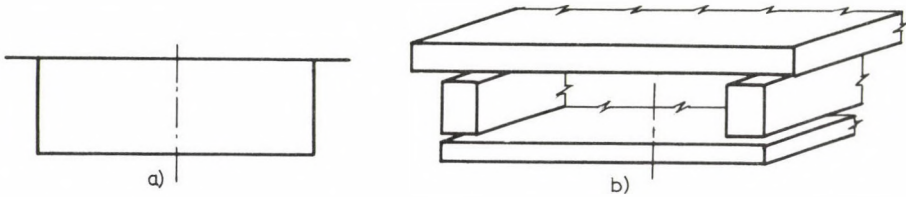


Fig. 9.

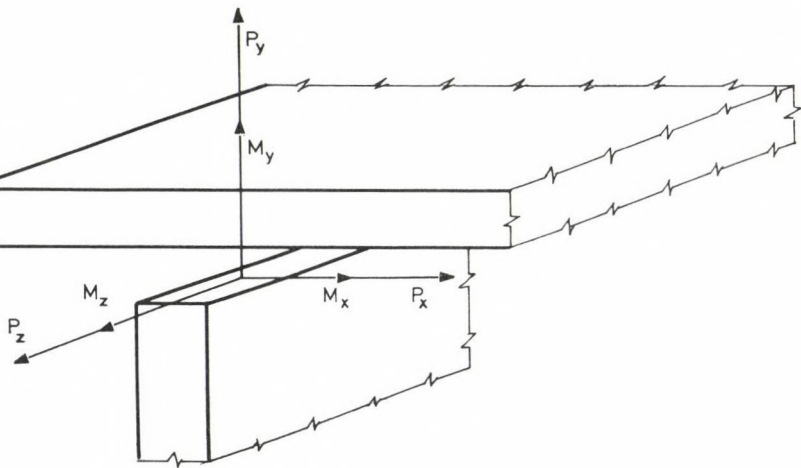


Fig. 10.

ANALYSIS OF SINGLE-CELL BOX BEAMS

By connecting the walls by hinged joints along the stress axes we arrive at the hinged beam (Fig. 11). We assume that the torsional rigidities of the individual walls are negligible so that the hinged beam cannot resist either moments M_z or forces P_x . These moments and forces, however, have to be accounted for, so that we introduce the supporting frames by building the hinged beam into closed, rigid, densely placed frameworks whose rigidity equals the rigidity per unit length of the box beam (Fig.12).

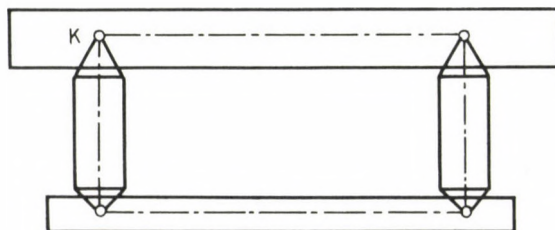


Fig. 11.

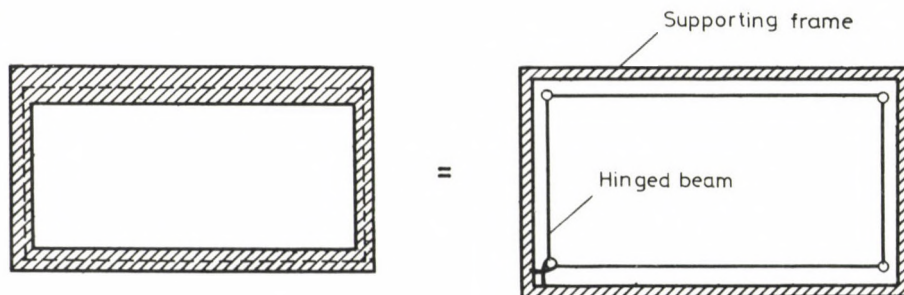


Fig. 12.

2.2 The basic system

In response to the external load, the angles between the straight lines connecting the joints of the hinged beam undergo alteration (Fig. 13/a). The hinges of the hinged beam and the corner points of the supporting frame translate together so that the supporting frame undergoes deformation. The deformation of the supporting frame is caused by the vertical and horizontal forces ($-Q_v$ and $-Q$) which are transmitted from the hinged

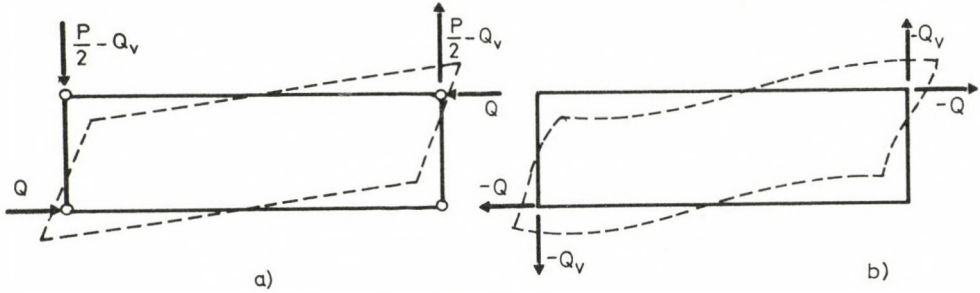


Fig. 13.

beam to the supporting frame (13/b). Forces $-Q_v$ and $-Q$ develop M_z internal bending moment at the corners of the supporting frame. It follows from the equilibrium of the frame that forces $-Q_v$ and $-Q$ are equivalent to the force Q_c . Q_c and $-Q_c$ act at the opposite corners of the frame and they have a common action line, the diagonal of the frame (Fig. 14), so they constitute a couple of zero value.

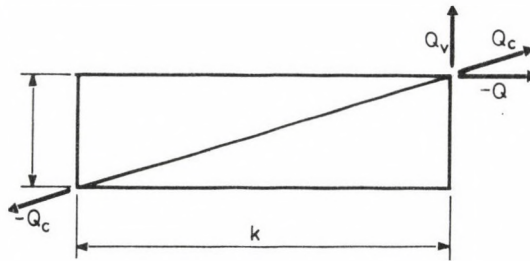


Fig. 14.

The formula

$$Q_v = \frac{h}{k} Q \quad (2.2.1)$$

follows from the principle of similar triangles and shows that the external forces acting on the frame can be characterized by one unknown vector, vector Q . It follows from Newton's third law that the supporting frame also transmits forces Q_v and Q to the hinged beam (Fig. 13/a). The deformation of the hinged beam is caused by the vertical external forces $P/2$ and the vertical and horizontal reactive forces Q_v and Q .

ANALYSIS OF SINGLE-CELL BOX BEAMS

We choose the system consisting of the hinged beam and the supporting frames as the basic system of the statically indeterminate box beam. We shall determine the unknown reaction Q on the condition that the hinged beam and the supporting frames develop the same deformation.

2.3 Stresses in the box beam subjected to antisymmetric load

2.3.1 Stresses in the box beam of thin-walled cross section, subjected to antisymmetric load

If the box beam of thin-walled cross section is subjected to vertical or horizontal antisymmetric load, the distribution of the stresses in the walls, according to Bernoulli-Navier's theorem, is linear. If the beam has a vertical axis of symmetry and the planes of the walls are perpendicular to each other, the normal stresses are expressed by the formula

$$\sigma = \theta \times y \quad (2.3.1)$$

as shown in Fig. 15 where the origin of the co-ordinate system is the zero point of the stresses.

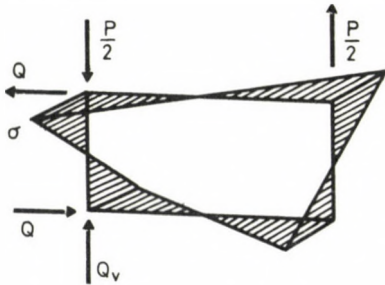


Fig. 15.

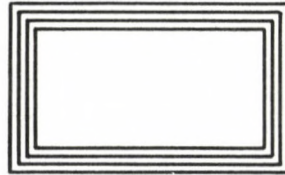


Fig. 16.

2.3.2 Stresses in the box beam of thick walled cross section, subjected to antisymmetric load

Let us build in some box beams of thin walled cross section of different size but with the same centroids into each other (Fig. 16). Formula (2.3.1) is valid to each of these boxes, but with different values of θ . If, however, the structural arrangement prevents the neighbouring walls to

slide on each other, even the values of θ are the same for the box beams.

If, due to the structural arrangement, there is no relative slide along the neighbouring walls, the system of thin-walled box beams built into each other can be replaced by a single thick-walled box beam. It follows that formula (2.3.1) derived for antisymmetric load is also valid to this thick-walled box beam. In the following, we shall analyse the stresses and strains on the basis of (2.3.1).

2.3.3 Relations for the normal stresses

The distribution of the normal stresses corresponding to formula (2.3.1) is shown in Fig. 17/a. This stress diagram can also be obtained by

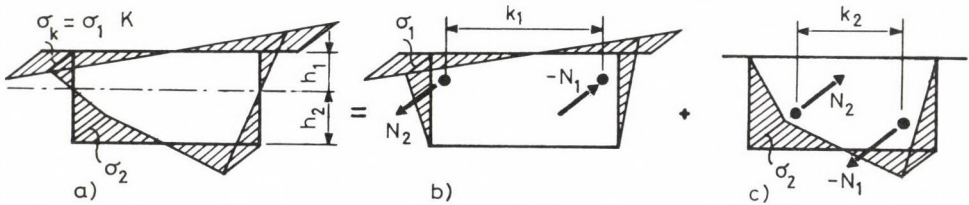


Fig. 17.

superimposing the diagrams in Figs 17/b. and 17/c.

The resultants of the tensile and compressive stresses in Fig. 17/b and in Fig. 17/c are forces $+N_1$ and $-N_1$ and forces $+N_2$ and $-N_2$, respectively.

The figures also yield

$$N_1 = \mu_1 \sigma_1 \quad , \quad (2.3.2)$$

$$N_2 = \mu_2 \sigma_2 \quad ,$$

where μ_1 and μ_2 are constants which only depend on the size of the cross section.

Forces $+N_1$ and $-N_1$ form the couple $N_1 k_1$ and forces $-N_2$ and $+N_2$ form the couple $-N_2 k_2$. Since the load is antisymmetric, the moment of the normal stresses σ acting on the cross section equals zero, i.e. we have

$$N_1 k_1 - N_2 k_2 = 0 \quad , \quad (2.3.3)$$

from which, by making use of (2.3.2), we obtain

$$\frac{N_1}{N_2} = \frac{k_2}{k_1} = \frac{\mu_1 \sigma_1}{\mu_2 \sigma_2} . \quad (2.3.3/a)$$

Constants k_1 , k_2 , μ_1 and μ_2 only depend on the size of the cross section of the box beam, so the ratio

$$\frac{\sigma_1}{\sigma_2} = \frac{\mu_2 k_2}{\mu_1 k_1} = \frac{h_1}{h_2} \quad (2.3.4)$$

also depends only on the size of the cross section. It follows that, knowing stress σ_1 , stress σ_2 can be determined.

Based on the foregoing, we can make some important statements on the normal stresses in the hinged box beam subjected to antisymmetric load.

1. The principle of superimposition holds. This follows from basic assumption No 8 in section 1.3.

2. Because of the symmetrical cross section and the antisymmetrical load, the vertical axis of symmetry coincides with the neutral axis of the normal stresses σ .

3. The position of the neutral axis of the horizontal stresses only depends on the geometrical characteristics of the cross section. Formula (2.3.4) clearly shows the validity of this statement.

4. The neutral axes belonging to the vertical and the horizontal antisymmetric loads coincide since, according to (2.3.4), the ratio σ_1/σ_2 does not depend on the load but only on the symmetrical characteristics.

5. If we know the value of the normal stress at an arbitrary point of the cross section (except at a point on the neutral axis), the stress diagram can be obtained.

6. The moment of the normal stresses on one side of the symmetry axis around the symmetry axis is equal to zero. This statement can be proved by dividing Eq. (2.3.3) by two:

$$N_1 \frac{k_1}{2} - N_2 \frac{k_2}{2} = 0 . \quad (2.3.5)$$

7. The horizontal neutral axis is the centroidal axis of the parts of the half of the cross section weighted by $(x/k)^2$. This statement can be proved as follows.

According to Eq. (2.3.5), the moment of the normal stresses around the symmetry axis is zero, i.e.

$$\int_F x dF = 0 .$$

Making use of formula (2.3.1) and denoting the compression area by 1 and the tensile area by 2, we obtain

$$\theta \int_{F_1} x^2 y dF - \theta \int_{F_2} x^2 y dF = 0 . \quad (2.3.6)$$

Dividing Eq. (2.3.6) by θk^2 , we arrive at

$$\int_{F_1} y \left(\frac{x}{k}\right)^2 dF = \int_{F_2} y \left(\frac{x}{k}\right)^2 dF . \quad (2.3.6/a)$$

With regard to the analogy with the following formulae, we shall take quantity k as equal to the distance between the stress axes of the vertical walls.

2.4 Analogy between the hinged beam and the bent beam

We shall determine the stresses and deformations in the hinged beam subjected to antisymmetric vertical and horizontal loads using formulae similar to those of the simply supported beam. First, however, we shall show that the relationship

$$\int_0^{\ell} g''^2 dz = \int_0^{\ell} g^{IV} g dz \quad (2.4.1)$$

holds for any function $g=g(z)$ if the boundary conditions

$$g = g'' = 0 \quad (2.4.2)$$

are satisfied at $z=0$ and $z= \ell$.

By applying Eq. (2.4.2)

$$\begin{aligned} \int_0^{\ell} g''^2 dz &= \int_0^{\ell} g'' g'' dz = [g' g'']_0^{\ell} - \int_0^{\ell} g' g'''' dz = \\ &= - \int_0^{\ell} g' g'''' dz = - [g g'''']_0^{\ell} + \int_0^{\ell} g g^{IV} dz = \int_0^{\ell} g g^{IV} dz . \end{aligned} \quad (2.4.1/a)$$

ANALYSIS OF SINGLE-CELL BOX BEAMS

which shows that Eq. (2.4.1) holds.

2.4.1 Formulae for the hinged beam subjected to antisymmetric vertical load

Let the simply supported hinged beam with constant cross section be subjected to the antisymmetric vertical load g^{IV} and $-g^{IV}$. The cross section is shown in Fig. 18.

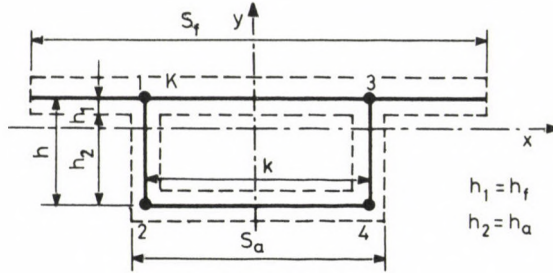


Fig. 18.

As with the bent beam, let us express the normal stresses σ_1 , at point K=1 of the cross section by the formula

$$\sigma_1 = - \frac{g'' h_1}{I_b} , \quad (2.4.3)$$

where I_b is the substitute moment of inertia of the vertical wall with the adjoining horizontal walls and h_1 is the distance between the neutral axis and the point marked with 1 in the case of vertical load. Both I_b and h_1 are yet unknown. In the following, we shall not take into consideration the negative sign in formula (2.4.3).

Formula (2.3.1) also yields the normal stress at point 1 as

$$\sigma_1 = \theta \frac{k}{2} h_1 , \quad (2.4.4)$$

from which, making use of (2.4.3), we obtain

$$\theta = \frac{2}{k I_b} g'' . \quad (2.4.5)$$

Substituting this into formula (2.3.1) we arrive at

$$\sigma = \frac{2}{kI_b} g'' \times y \quad , \quad (2.4.6)$$

or, making use of (2.4.3) once again,

$$\sigma = \frac{2}{kh_1} \times y \quad \sigma_1 \quad , \quad (2.4.7)$$

which can also be obtained directly from (2.3.1).

The vertical translation caused by normal stresses σ is obtained from

$$\eta_{\sigma} = \iint_0^Z \frac{\sigma_1}{E h_1} dz dz = \frac{1}{E h_1} \iint_0^Z \sigma_1 dz dz \quad . \quad (2.4.8)$$

By making use of (2.4.3), this formula can be written as

$$\eta_{\sigma} = \frac{1}{EI_b} \iint_0^Z g'' dz dz = \frac{g}{EI_b} \quad (2.4.9)$$

again a similar formula to the one belonging to the bent beam.

Taking into consideration the translation caused by the normal stresses and making use of Eq. (2.4.9), the external work of the antisymmetric vertical forces g^{IV} and $-g^{IV}$ acting on the two vertical walls can be given as

$$L_e = 2 \int_0^{\ell} g^{IV} \eta_{\sigma} dz = \frac{2}{EI_b} \int_0^{\ell} g g^{IV} dz \quad , \quad (2.4.10)$$

Eq. (2.3.1) yields the internal work as

$$L_i = \int_0^{\ell} \left[\int_F \frac{\sigma^2}{E} dF \right] dz = \frac{1}{E} \int_0^{\ell} \left[\int_F \theta^2 x^2 y^2 dF \right] dz \quad , \quad (2.4.11)$$

which, making use of formula (2.4.5) leads us to

$$L_i = \frac{1}{E} \frac{4}{k^2 I_b^2} \int_0^{\ell} g''^2 \left[\int_F x^2 y^2 dF \right] dz = \frac{4}{EI_b^2 k^2} \left[\int_F x^2 y^2 dF \right] \int_0^{\ell} g'' dz \quad (2.4.12)$$

Formulae (2.4.10) and (2.4.12) must be equal to each other and, making use of (2.4.1) and taking into consideration the fact that condition (2.4.2) is

satisfied, we arrive at the substitute moment of inertia as

$$I_b = \frac{2}{k^2} \int_F x^2 y^2 dF . \quad (2.4.13)$$

2.4.2 Formulae for the hinged beam subjected to horizontal antisymmetric forces

In the case of the antisymmetric load system g^{IV} and $-g^{IV}$, the normal stresses at points 1 and 2 (Fig. 18) can be expressed by the formulae

$$\sigma_1 = \frac{Mk}{2I_f} = -\frac{g''k}{2I_f} , \quad (2.4.14)$$

and

$$\sigma_2 = -\frac{Mk}{2I_a} = \frac{g''k}{2I_a} , \quad (2.4.15)$$

The above formulae are similar to formula (2.4.3), where I_f and I_a are the substitute moments of inertia of the upper and lower walls in the case of horizontal, antisymmetric forces. By combining formulae (2.4.14) and (2.4.15), we obtain

$$\frac{\sigma_1}{\sigma_2} = \frac{I_a}{I_f} . \quad (2.4.16)$$

The horizontal translation of the hinged beam subjected to the horizontal antisymmetrical load system g^{IV} and $-g^{IV}$ can easily be derived. A derivation, similar to the one carried out in the case of the vertical antisymmetric load system, results in the formulae

$$\eta_{\sigma f} = \frac{g}{EI_f} , \quad (2.4.17)$$

and

$$\eta_{\sigma a} = \frac{g}{EI_a} . \quad (2.4.18)$$

The above formulae are identical to formula (2.4.9).

Figure 17 shows that the ration

$$\frac{\sigma_1}{\sigma_2} = \frac{h_1}{h_2} \quad (2.4.19)$$

holds which, introducing (2.4.16), yields

$$\frac{I_a}{I_f} = \frac{h_1}{h_2} \quad (2.4.20)$$

for the ratio of the substitute moments of inertia of the horizontal walls. Combining formulae (2.4.4) and (2.4.14) we arrive at

$$\theta = \frac{1}{h_1 I_f} g'' \quad , \quad (2.4.21)$$

Taking into consideration the translation caused by the normal stresses developed by the external forces, the formula of the external work assumes the form

$$L_e = \int_0^{\ell} g^{IV} (\eta_{\sigma a} + \eta_{\sigma f}) dz = \int_0^{\ell} g g^{IV} \left(\frac{1}{EI_a} + \frac{1}{EI_f} \right) dz \quad , \quad (2.4.22/a)$$

which, making use of relation (2.4.20) and $h=h_1+h_2$, can be rewritten as

$$L_e = \frac{1}{EI_f} \int_0^{\ell} \left(1 + \frac{h_2}{h_1}\right) g g^{IV} dz = \frac{h}{EI_f h_1} \int_0^{\ell} g g^{IV} dz \quad . \quad (2.4.22)$$

If we use formula (2.4.21), we can obtain the internal work of the normal stresses as

$$L_i = \frac{1}{E} \int_0^{\ell} \theta^2 \left[\int_F x^2 y^2 dF \right] dz = \frac{1}{E h_1^2 I_f^2} \int_0^{\ell} \left[\int_F x^2 y^2 dF \right] g''^2 dz \quad (2.4.23)$$

This formula is similar to formulae (2.4.11) and (2.4.12).

The external work must be equal to the internal work so formulae (2.4.22) and (2.4.23) yield the substitute moment of inertia of the upper horizontal wall as

$$I_f = \frac{1}{h h_1} \int_F x^2 y^2 dF \quad . \quad (2.4.24)$$

Combining (2.4.13) and (2.4.24) we arrive at

$$I_f = \frac{k^2}{2 h h_1} I_b \quad , \quad (2.4.25)$$

and

$$I_a = \frac{k^2}{2 h h_2} I_b \quad . \quad (2.4.26)$$

We shall prove the general validity of the above formulae in Section 2.6.

2.5 Displacements and stresses in the walls of the hinged beam

2.5.1 Deformation caused by the normal stresses developed by the vertical load

The stresses in the outer fibres of the hinged beam subjected to vertical forces are given by (2.4.3) as

$$\sigma_1 = \frac{h_1}{I_b} g'' \quad (2.5.1)$$

and, on the basis of formulae (2.4.8) and (2.4.9), the vertical displacement of the vertical walls is given as

$$\eta_{vv} = -\frac{1}{Eh_1} \int\int_0^Z \sigma_1 dz dz = \frac{g}{EI_b} \quad , \quad (2.5.2)$$

The relative displacement of the vertical walls is determined by the formula

$$\eta_{rvv} = \frac{g}{EI_v} \quad (2.5.3)$$

where we have

$$I_v = \frac{I_b}{2} \quad (2.5.4)$$

In making use of (2.4.3) and (2.4.19), we arrive at the horizontal displacement of the upper and lower horizontal walls as

$$\eta_{vf} = -\frac{2}{kE} \int\int_0^Z \sigma_1 dz dz = \frac{2h_1}{k} \frac{g}{EI_b} \quad , \quad (2.5.5)$$

and

$$\eta_{va} = -\frac{2}{kE} \frac{h_2}{h_1} \int_0^Z \int \sigma_1 dz dz = \frac{2h_2}{k} \frac{g}{EI_b} . \quad (2.5.6)$$

2.5.2 Deformation caused by the normal stresses developed by horizontal load

Stresses σ_1 and σ_2 in the outer fibres caused by horizontal forces can be determined by making use of formulae (2.4.14), (2.4.25) and (2.4.15), (2.4.26) as

$$\sigma_1 = \frac{hh_1}{k} \frac{g''}{I_b} , \quad (2.5.7)$$

and

$$\sigma_2 = \frac{hh_2}{k} \frac{g''}{I_b} , \quad (2.5.8)$$

Formula (2.4.8) yields the vertical displacement of the vertical walls as

$$\eta_{HV} = -\frac{1}{Eh_1} \int_0^Z \int \sigma_1 dz dz = \frac{h}{k} \frac{g}{EI_b} . \quad (2.5.9)$$

The relative displacement of the vertical walls assumes the form

$$\eta_{rHV} = 2 \eta_{HV} = \frac{g}{EI_{HV}} , \quad (2.5.10)$$

where

$$I_{HV} = \frac{k}{2h} I_b . \quad (2.5.11)$$

In a similar way, we obtain the horizontal displacement of the upper and lower walls as

$$\eta_{Hf} = \frac{2}{kE} \int_0^Z \int \sigma_1 dz dz = \frac{2hh_1}{k^2} \frac{g}{EI_b} , \quad (2.5.12)$$

and

$$\eta_{Ha} = \frac{2hh_2}{k^2} \frac{g}{EI_b} . \quad (2.5.13)$$

Formulae (2.5.5), (2.5.6) and (2.5.10) show that the relative vertical displacement of the vertical walls caused by horizontal forces and the relative horizontal displacement of the horizontal walls caused by vertical forces are the same. In other words, if we denote the relative horizontal displacement caused by vertical forces by η_{VH} and the relative vertical displacement caused by horizontal forces by η_{HV} , then the relationship

$$\eta_{VH} = \eta_{HV} = \frac{2h}{k} \frac{g}{EI_b} \quad (2.5.14)$$

holds. The relative displacement of the horizontal walls is given by

$$\eta_H = \eta_{Ha} + \eta_{Hf} = \frac{g}{EI_H}, \quad (2.5.15)$$

where, on the basis of formulae (2.4.25), (2.4.26), (2.4.17) and (2.4.18), we have

$$I_H = \frac{k^2 I_b}{2 h^2}. \quad (2.5.16)$$

2.5.3 Deformation caused by shearing forces in the cross section

In the case of a vertical antisymmetric load system, the vertical walls cannot transfer horizontal forces to the unloaded horizontal walls because the walls are assumed to have no torsional resistance. Thus the horizontal walls are not subjected to horizontal forces and therefore no shearing force component develops in the cross section of the horizontal walls (shearing stresses do develop but their resultant vanishes). In a similar way, in the case of a horizontal load system, the shearing force component also vanishes in the cross section of the vertical walls.

Let us now cut out a section of thickness dz of the hinged beam. Figure 19 shows that shearing stresses τ and normal stresses σ develop on the adjacent sections. The difference of the normal stresses acting on the sections is

$$d\sigma = \frac{\delta\sigma}{\delta z} dz. \quad (2.5.17)$$

Neglecting the initial angular displacement, the displacement of the vertical wall caused by the shearing forces developed by the vertical antisymmetric load system assumes the form

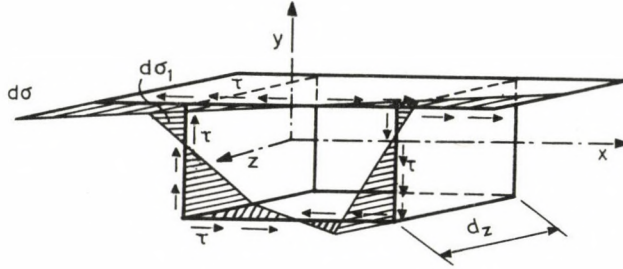


Fig. 19.

$$\eta_{V\tau} = \int_0^Z \frac{R_V}{GF_V} dz \quad , \quad (2.5.18)$$

where F_V represents the substitute cross sectional area of the vertical wall and R_V stands for the cross sectional resultant of the vertical forces.

The horizontal wall develops no translation due to the shearing stresses since $R=0$ holds in the horizontal wall so we have

$$\eta_{VH\tau} = 0 \quad . \quad (2.5.19)$$

In a similar way, we obtain the horizontal translations caused by the shearing forces developed by the horizontal antisymmetric forces as

$$\eta_{f\tau} = \int_0^Z \frac{R_H}{GF_f} dz \quad , \quad (2.4.20)$$

and

$$\eta_{a\tau} = \int_0^Z \frac{R_H}{GF_a} dz \quad , \quad (2.5.21)$$

where F_f and F_a represent the substitute cross sectional area of the upper and lower horizontal walls. In the case of horizontal antisymmetric forces, the vertical translation of the vertical walls caused by the shearing stresses vanishes, i.e.

$$\eta_{HV} \tau = 0 \quad (2.5.22)$$

holds.

We point out here that during the above derivation we have not restricted analysis to single-cell box beams so the formulae obtained are also valid for multi-cell box beams provided the distribution of the normal stresses defined by (2.3.1) is acceptable.

2.6 Generalization of the analogy

The above derivation demonstrates that an analogy exists between the formulae for the deformations and stresses of the hinged beam and those of the bent beam.

When deriving formulae (2.4.13), (2.4.24) and (2.4.25) for the substitute moment of inertia we assumed that the cross section of the beam was constant and that the boundary conditions were those of the simply supported beam.

In the following, we shall present the generalization of the analogy.

Let us consider a hinged beam and only assume that its section of thickness dz is of constant cross section. The upper flange of the half-section transfers shearing force $t_f dz$ to the vertical wall along their line of intersection (Fig. 20). Similarly, the lower flange transfers shearing

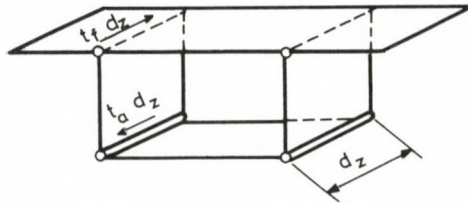


Fig. 20.

force $t_a dz$. Making use of (2.4.7), the equilibrium of the normal stresses and the shearing forces on the upper flange (Fig. 21) yields

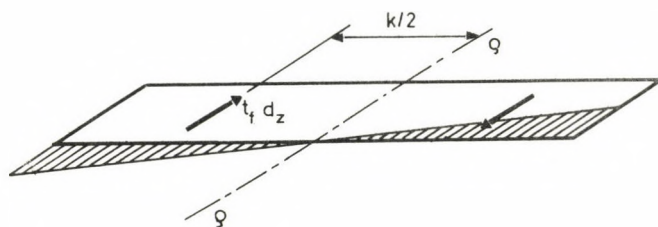


Fig. 21.

$$t_f k dz = \int_{\text{upper flange}} \frac{\delta \sigma}{\delta z} dz \times dF = \frac{\delta \sigma_1}{\delta z} dz \frac{2}{k h_1} \int_{\text{upper flange}} x^2 y dF . \quad (2.6.1)$$

Similarly, the equilibrium of the lower flange yields

$$t_a k dz = \frac{\delta \sigma_1}{\delta z} dz \frac{2}{k h_1} \int_{\text{lower flange}} x^2 y dF . \quad (2.6.2)$$

The external moment $\frac{\delta M}{\delta z} dz$ acting on the half-section is equal to the sum of the moments of the normal stresses $\frac{\delta \sigma}{\delta z} dz$ and the shearing forces t_f and t_a on the vertical wall to axis x :

$$\frac{\delta M}{\delta z} dz = \int_{\text{vertical wall}} \frac{\delta \sigma}{\delta z} dz y dF + t_f h_1 dz + t_a h_2 dz . \quad (2.6.2/a)$$

Making use of equations (2.4.7), (2.6.1) and (2.6.2), the above equation takes on the form

$$\frac{\delta M}{\delta z} dz = \frac{\delta \sigma_1}{\delta z} dz \left\{ \frac{2}{k h_1} \int_{\text{vertical wall}} x^2 y dF + \frac{2 h_2}{k^2 h_1} \int_{\text{lower flange}} x^2 y dF + \frac{2}{k^2} \int_{\text{upper flange}} x^2 y dF \right\} . \quad (2.6.3)$$

The term in braces in the right-hand side of this equation only depends on the cross section and therefore the relationship between the moment and the normal stress is independent of the other cross sectional characteristics and the boundary conditions of the beam. It follows that the formulae derived for the special case are of general validity.

2.7 Supporting frames

When analyzing the basic system of the statically indeterminate box beam, we assumed that the hinged beam was supported at its four corner points by densely placed supporting frames of unit thickness (Fig. 12).

Let us define frame-rigidity as the horizontal force A_q . The couple of zero-value of the two forces

$$A = A_q \sqrt{\frac{h^2 + k^2}{k^2}} \quad (2.7.1)$$

acting at the opposite corner points of the supporting frame causes the

$$\beta_A = \frac{1}{h} \quad (2.7.2)$$

change in the angle of the straight lines connecting the corner points of the supporting frames as in Fig. 22.

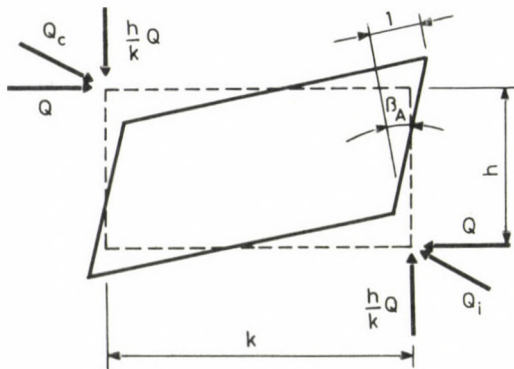


Fig. 22.

In the case of a horizontal force Q , the change in the angle of the frame is determined by

$$\beta_t = \frac{Q}{hAq} \quad (2.7.3)$$

Making use of the formulae presented in Sections 2.5.1 – 2.5.3 and of Fig. 22, the change in the angle i.e. the deformation of the cross section of the hinged beam is determined by

$$\beta_t^* = \frac{\eta_{rvv} + 2 \eta_{v\tau} + \eta_{rHV}}{k} + \frac{\eta_{vf} + \eta_{va} + \eta_{f\tau} + \eta_{a\tau} + \eta_H}{h} \quad (2.7.4)$$

The deformation of the hinged beam (2.7.4) and the supporting frame (2.7.3) must be the same, i.e. we have

$$\beta_t = \beta_t^* \quad (2.7.5)$$

Equality (2.7.5) and formulae (2.7.3) and (2.7.4) make it possible to obtain the reactive forces of the frame. Details of this calculation will be published in our following papers /6/, /7/.

REFERENCES

1. Wlassow, W.S.: Dünnwandige elastische Stäbe (Berlin, Bauwesen, 1964)
2. Florin, G.: Vergleich verschiedenen Theorien für den Verdrehung beanspruchten Kastenträger (Der Staalbau, 1963)
3. Richmond, B.: Twisting of twin-walled Boxgirders (ICE Journal, 1966)
4. Wright, R.N., Abdel Samad S.R., Robinson A.R.: Beam on Elastic Foundation Analogy for Analysis of Box Girders (Proc. ASCE Journal Struct. Div., 1968)
5. Maisel, B.J., Roll, F.: Methods of Analysis and Design of Concrete Box Beams (Cement and Concrete Association Technical Report, 1974)
6. Szidarovszky, J.: Cross sectional characteristics of single-cell box beams with a cross section of rectangular elements. Acta Technica Hung. 99 (1985)
7. Szidarovszky, J.: Exact analysis of single-cell box beams. Acta Technica 100.
8. Szidarovszky, J.: Generalization of the analysis of single-cell box beams. Acta Technica Hung. 100.

CROSS SECTIONAL CHARACTERISTICS OF SINGLE-CELL BOX BEAMS WITH A
CROSS SECTION OF RECTANGULAR ELEMENTS

J. Szidarovszky*

(Received: 25 June 1985)

For the analysis of single-cell box beams formulae of general validity for the cross sectional characteristics were given in our previous paper. This paper presents closed formulae for the cross sectional characteristics of single-cell box beams with a cross section made up from rectangular elements.

NOTATION

A	spring constant at a support,
A_r	frame-rigidity (the lateral stiffness of the supporting frame),
a_i	length of section i ,
b_f	width of the upper flange of the beam substituting the vertical wall,
b^a	width of the lower flange of the beam substituting the vertical wall,
E^a	modulus of elasticity,
F	substitute cross sectional area,
d_f	thickness of the upper horizontal flange plate,
d^a	thickness of the lower horizontal flange plate,
d^v	thickness of the vertical web plate,
h^v	distance between the stress axes of the two horizontal walls (flange plates) (Fig. 5),
$h_1 = h_f$	perpendicular distance between the upper stress axis and the neutral axis (Fig. 5),
$h_2 = h_a$	perpendicular distance between the lower stress axis and the neutral axis (Fig. 5),
I	moment of inertia (second moment of area of the cross sectional area) about the axis perpendicular to the plane of bending,
i	nodal point, boundary of a section or reference to a section,
I_b	substitute moment of inertia of the vertical wall with the horizontal walls,
I_f	substitute moment of inertia of the upper horizontal flange plate,
I^a	substitute moment of inertia of the lower horizontal flange plate,
$I^a = I_b/2$	
Q^v	horizontal component of the frame reactive force,
k	distance between the stress-axes of the vertical walls (webs) (Fig.5),
ℓ	length of the beam,
p	external vertical distributed load,
P	external vertical concentrated force,
q	horizontal component of the distributed frame reactive force,
R	resultant/shearing force,
s_f	width of the upper horizontal flange plate,
s^a	width of the lower horizontal flange plate,
t^a	shearing force,
x	vertical co-ordinate perpendicular to the axis of the beam,

*Dr. J. Szidarovszky, H-1089 Budapest, Bíró Lajos u. 42, Hungary

y	horizontal co-ordinate perpendicular to the axis of the beam,
z	co-ordinate along the axis of the beam,
w	warping,
α	angular displacement,
β	change in angle of the supporting frame,
η	displacement,
κ	built in change in angular displacement,
σ	normal stress,
τ	shearing stress,
ξ	abscissa,
\underline{E}	unit matrix.

Subscripts

0	refers to place $z=0$ or $n=0$
z	refers to place z,
ℓ	refers to place $z = \ell$,
i	refers to a section or to the boundary of a section,
n	refers to the last section or to the end of the beam or to the boundary of the last section,
κ	refers to the cause of the built in angular displacement
r	refers to an elastic support,
σ	refers to normal stress,
τ	refers to shearing stress,
v	refers to vertical direction, force or wall,
a	refers to lower horizontal wall (flange plate),
f	refers to upper horizontal wall (flange plate),
h	refers to horizontal direction, force or wall,
p	refers to external vertical force,
q	refers to frame-reaction.

1. INTRODUCTION

This paper is to present practical formulae for the calculation of the cross sectional characteristics of single-cell box beams with a cross section consisting of rectangular elements.

We shall analyse simply supported single-cell box beams subjected to antisymmetric load with a cross section consisting of perpendicular walls and having a vertical symmetry axis. Apart from the assumptions given in detail in Section 1.3 in /1/, we shall also assume as Assumption No 10 that the walls of the cross section are of rectangular cross section (Fig. 1).

The physical model and the mathematical methods for the analysis are given in detail in /1/.

The stresses and deformations developing in the individual walls can be determined by the formulae of general validity presented in Section 2.5

CHARACTERISTICS OF SINGLE-CELL BOX BEAMS

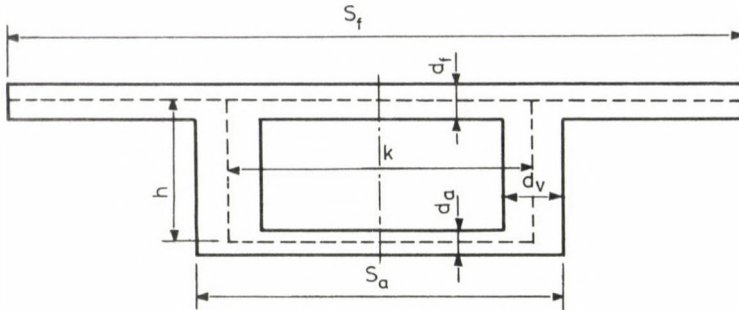


Fig. 1.

in /1/. The cross sectional characteristics for the rectangular cross section needed for the analysis shown in Fig. 1, however, can also be calculated in a simpler, more expressive way. It goes without saying that the two procedures lead us to the same result.

2. THE FRAME RIGIDITY

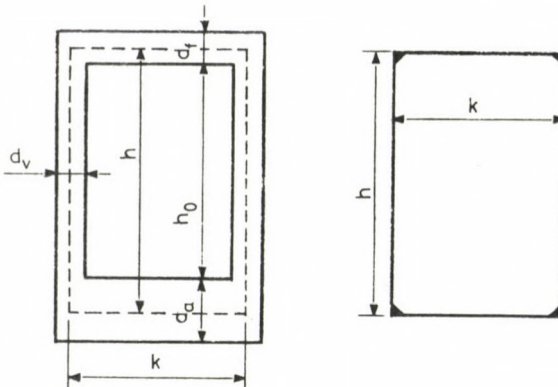


Fig. 2.

Figure 2 shows the geometrical characteristics of the supporting frame per unit length. If the closed frame supported below its columns is subjected to a horizontal force in the axis of its upper horizontal beam, the upper horizontal beam undergoes translation. By neglecting only insignificant terms, we obtain the frame rigidity /2/ as

$$q_A = \frac{S}{T}, \quad (2.1)$$

where

$$S = 2 d_V^3 \left\{ \frac{h_0}{d_V^3} + \left(\frac{k - d_V}{k} \right)^2 \frac{k - d_V}{6} \left(\frac{1}{d_f^3} + \frac{1}{d_a^3} \right) \right\} E,$$

and

$$T = h^2 \left\{ \frac{h_0^4}{h^2 d_V^3} + \left(\frac{(h_0 - d_f/2)^3}{d_f^3} + \frac{(h_0 - d_a/2)^3}{d_a^3} \right) \left(\frac{k - d_V}{k} \right)^2 \frac{2k}{3h^2} + \frac{(k - d_V)^6 d_V^3}{3k^4 d_f^3 d_a^3} \right\}$$

3. THE EFFECT OF VERTICAL ANTISYMMETRIC LOAD ON THE HINGED BEAM

In this section we shall determine the size of two vertical I-beams which, subjected to antisymmetric load, develop the same stresses and vertical displacements as the hinged beam subjected to the same antisymmetric load. The upper flange, the lower flange and the thickness of this I-beam are denoted by b_f , b_a and f_v , respectively as in Fig. 8 and the depth and the thickness of the flanges of the I-beam coincide with the depth and the thickness of the horizontal plates of the hinged beam.

Similarly, we can substitute the hinged beam subjected to horizontal antisymmetric load for two horizontal beams (Fig. 11).

The moment of inertia of the substitute beam introduced according to the foregoing coincides, as a special case, with the moment of inertia derived in Section 2.4 in /1/.

3.1 Equivalent flange-width of the vertical wall

We assume that the torsional rigidity of the individual walls is negligible and therefore the vertical walls cannot transfer horizontal forces P_x to the horizontal walls at the hinges (Figs 3 and 4). It follows that the upper horizontal wall of the hinged beam subjected to vertical load is not subjected to horizontal load and the sum of stress differences $\Delta \sigma$ transmitted to the horizontal wall of unit thickness is balanced by the shearing forces at the joint of the vertical wall (Figs 3 and 6).

CHARACTERISTICS OF SINGLE-CELL BOX BEAMS

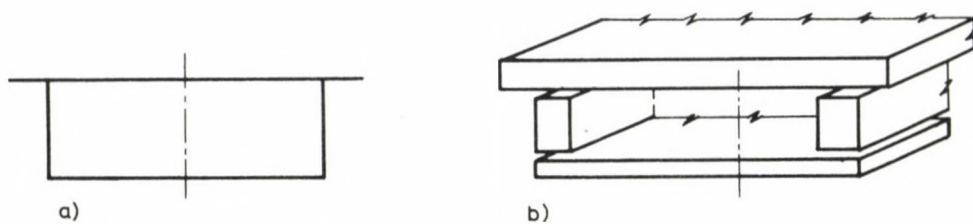


Fig. 3.

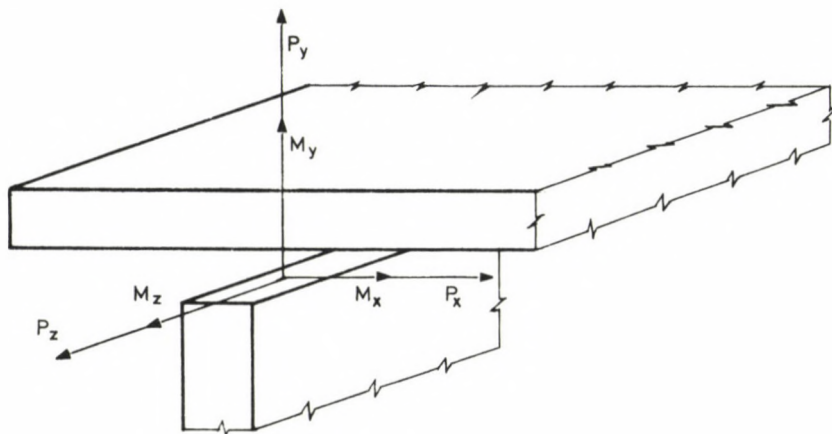


Fig. 4.

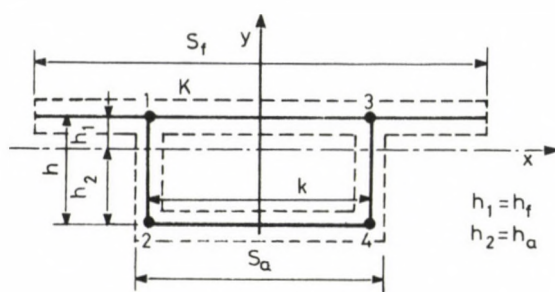


Fig. 5.

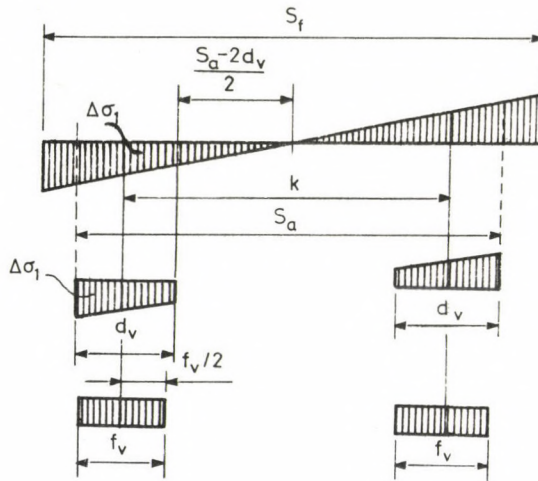


Fig. 6.

Moment equilibrium on the upper horizontal plate of unit thickness results in (Fig. 6)

$$tk = 2 \left(\frac{S_f}{2} \Delta \sigma_1 \frac{S_f}{k} \right) - \frac{2 S_f}{2} \frac{1}{2} = \frac{S_f^3}{6k} \Delta \sigma_1 ,$$

from which we obtain

$$t = \frac{S_f^3}{6k^2} \Delta \sigma_1 , \tag{3.1}$$

where factor k is yet unknown and the other factors are explained in Fig. 5. The same force t is transmitted from the two symmetrically placed plates of width b_f subjected to the stress difference $\Delta \sigma_1$, i.e. we have

$$t = b_f \Delta \sigma_1 , \tag{3.2}$$

from where, making use of Eq. (3.1), we obtain the equivalent flange-width as

$$b_f = \frac{S_f^3}{6k^2} . \tag{3.3}$$

CHARACTERISTICS OF SINGLE-CELL BOX BEAMS

According to the foregoing, in regard to stresses, the flange of width s_f can be substituted for a flange of width b_f . The same holds for the lower horizontal plate (Fig. 7), i.e. we have

$$b_a = \frac{s_a^3}{6k^2} \quad (3.4)$$

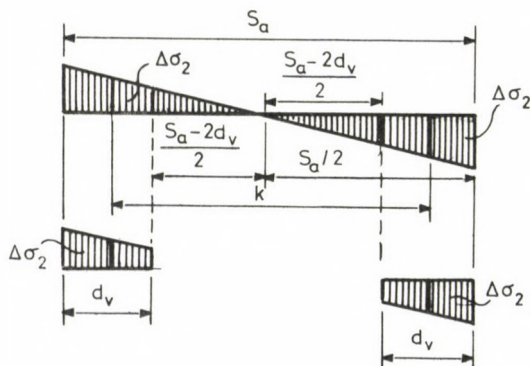


Fig. 7.

3.2 Stress axis of the vertical walls

Factor k , yet unknown, can be determined according to the following.

Shearing force t acts in the vertical plane of the resultant of stresses $\Delta \sigma$ developing in the vertical wall. Figure 7 shows that the resultant of stresses $\Delta \sigma$ acting in the left-hand wall of unit thickness assumes the form

$$\Delta R = \frac{1}{2} \frac{s_a}{k} \Delta \sigma_2 \left[\frac{s_a}{2} - \frac{1}{2} \frac{s_a - 2d_v}{k} \right] \Delta \sigma_2 \frac{s_a - 2d_v}{2} = \frac{d_v (s_a - d_v)}{k} \Delta \sigma_2 \quad (3.5)$$

The moment of stresses $\Delta \sigma$ about the symmetry axis of the cross section assumes the value

$$\begin{aligned} M &= \frac{2}{3} \frac{1}{4} \frac{s_a^3}{k} \Delta \sigma_2 - \frac{2}{3} \frac{1}{4} \frac{(s_a - 2d_v)^3}{k} \Delta \sigma_2 = \\ &= \frac{(s_a - d_v)^2 d_v + d_v^3/3}{k} \Delta \sigma_2 \quad (3.6) \end{aligned}$$

The moment of forces ΔR

$$M = \Delta R k = k \frac{d_v(s_a - d_v)}{k} \Delta \sigma_2 \quad (3.7)$$

is equal to the moment of stresses $\Delta \sigma$, so we obtain

$$k = s_a - d_v + \frac{d_v^2}{3(s_a - d_v)} \quad (3.8)$$

3.3 The equivalent web thickness of the vertical wall

Eq. (3.5) directly shows that, as regard to stresses, the vertical wall can be substituted for a wall of constant stress with thickness

$$f_v = d_v \frac{s_a - d_v}{k} \quad (3.9)$$

3.4 Shearing forces

The neutral axis of stresses σ developed by the bending moments of vertical plane coincides with the horizontal centroidal axis of the equivalent beam. Stresses σ and τ resulting from the vertical load $(p/2-h/k)q$ can be obtained on the equivalent beam.

Stresses τ in the (unloaded) horizontal wall can also be determined. On the basis of Eq. (3.1) and making use of Newton's third law (law of action and reaction), we obtain the shearing force transmitted from the vertical wall to the horizontal wall as

$$t = \frac{s_f^3}{6k^2} d_f \Delta \sigma_1 \quad (3.10)$$

The same shearing force is also given by

$$t = R \frac{S}{I_b} \quad (3.11)$$

where S represents the static moment of the upper flange of the equivalent beam about the centroidal axis. Equating formulae (3.10) and (3.11) we arrive at

$$\Delta \sigma_1 = \frac{6k^2}{s_f^3} \frac{S}{d_f I_b} R \quad (3.12)$$

CHARACTERISTICS OF SINGLE-CELL BOX BEAMS

The sum of stresses $\Delta \sigma_1$ on the half of the wall (Fig. 6) is

$$t_1 = \Delta \sigma_1 \frac{s_f}{k} \frac{s_f}{4} d_f = \frac{s_f^2 d_f}{4k} \Delta \sigma_1 \quad (3.13)$$

The difference between t and t_1 represents the shearing force per length dz in the middle of the horizontal wall. Making use of Eq. (3.12) we obtain

$$\begin{aligned} t_k = \tau d_f &= \frac{s_f^2 d_f}{4k} \Delta \sigma_1 - \frac{s_f^3 d_f}{6k^2} \Delta \sigma_1 = \\ &= \frac{s_f^2 (3k - 2s_f)}{12 k^2} d_f \Delta \sigma_1 = \frac{3k - 2s_f}{2 s_f} \frac{S}{I_b} R \quad (3.14) \end{aligned}$$

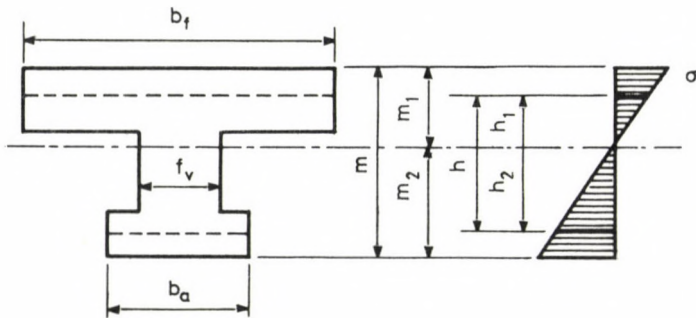


Fig. 8.

A similar procedure gives the shearing force at the outer joint of the vertical wall. The shearing force assumes the form

$$t = \tau d_f = \Delta \sigma_1 \left(\frac{s_f}{k} \frac{s_f}{4} - \frac{s_a}{k} \frac{s_a}{4} \right) d_f = \frac{s_f^2 - s_a^2}{4k} d_f \Delta \sigma_1 \quad (3.15)$$

(Fig. 6) or, making use of Eq. (3.12), we obtain

$$t = \frac{3k}{2s_f} \frac{s_f^2 - s_a^2}{s_f^2} \frac{S}{I_b} R \quad (3.16)$$

The diagram of the shearing forces is given in Fig. 9/a.

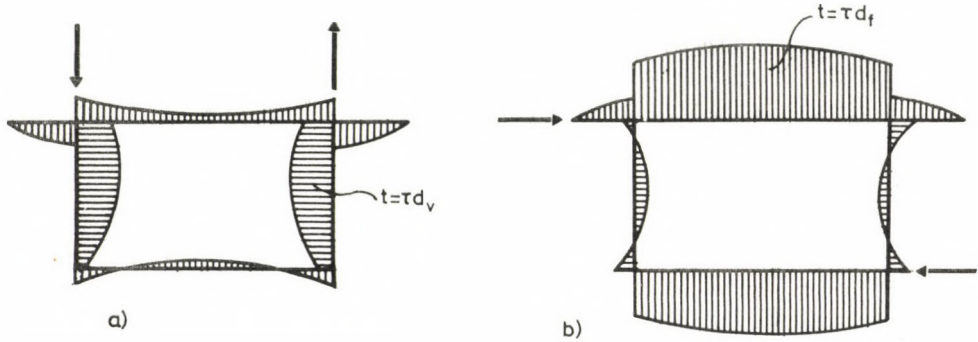


Fig. 9.

Since the vertical walls do not transmit horizontal forces to the unloaded horizontal walls, the resultant has no shearing component in the section perpendicular to the longitudinal axis of the horizontal wall. This fact is also shown in Fig. 9/a. The area of the diagram of shearing forces τd_f in the horizontal walls equals zero.

Similar reasoning shows that in the case of horizontal antisymmetric load the shearing component of the resultant equals zero in the vertical walls (Fig. 9/b).

4. THE EFFECT OF HORIZONTAL ANTISYMMETRIC LOAD ON THE HINGED BEAM

In the case of horizontal antisymmetric load, regarding normal stresses σ , the hinged beam can be substituted for two beams with horizontal axis.

4.1 Equivalent beams to the horizontal walls

The size of the equivalent beam belonging to the horizontal load will now be determined, in a similar way to the procedure used for the vertical load.

The horizontal load of the beam is represented by force q transmitted from the supporting frame (Fig. 10). With regard to stresses and deflections developed by force q , the upper flange can be substituted for a beam with web-thickness f_f and flange-width c_f . In a similar way, the lower flange can be substituted for a beam with web-thickness f_a and flange-width c_a (Fig. 11).

CHARACTERISTICS OF SINGLE-CELL BOX BEAMS

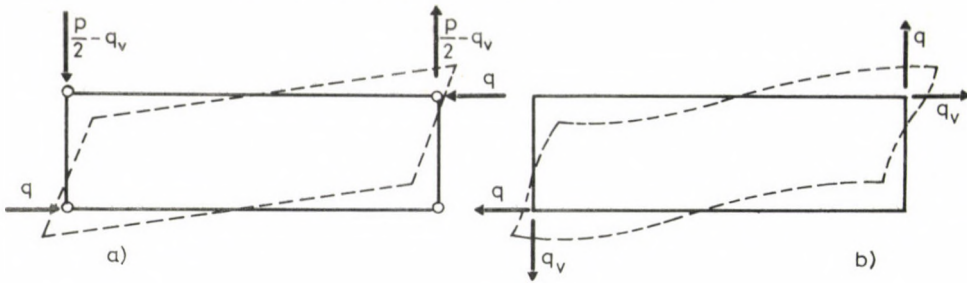


Fig. 10.

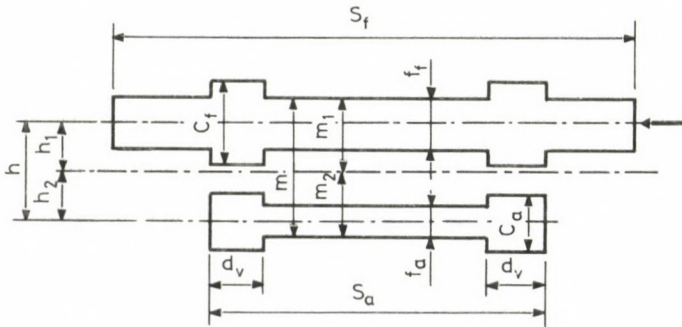


Fig. 11.

4.2 Stress axis of the horizontal walls

Formulae

$$h_1 = m_1 - \frac{d_f}{2} + \frac{d_f^2}{12 (m_1 - d_f/2)} \quad (4.1)$$

and

$$h_2 = m_2 - \frac{d_a}{2} + \frac{d_a^2}{12 (m_2 - d_a/2)} \quad (4.2)$$

similar to formula (3.8), determine the stress axis of the horizontal walls.

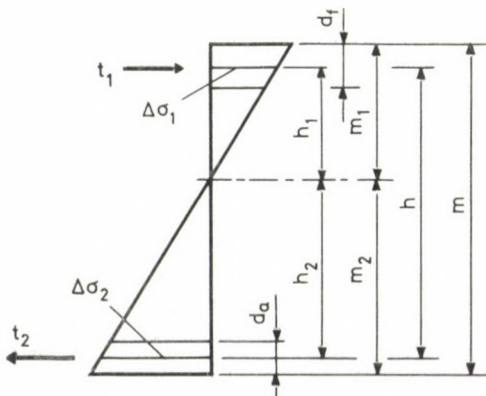


Fig. 12.

4.3 Equivalent flange-width of the horizontal walls

Proceeding as in section 3.1, moment equilibrium of the vertical wall of unit thickness (Fig. 12) results in

$$t_1 h = \Delta \sigma_1 \left[\frac{m_1}{h_1} \frac{m_1}{2} (h_2 + \frac{2}{3} m_1) + \frac{m_2}{h_1} \frac{m_2}{2} (h_2 - \frac{2}{3} m_2) \right], \quad (4.3)$$

from which we obtain the shearing force transmitted to the upper flange as

$$t_1 = \frac{\Delta \sigma_1}{2 h h_1} \left[m_1^2 (h_2 + \frac{2}{3} m_1) + m_2^2 (h_2 - \frac{2}{3} m_2) \right]. \quad (4.4)$$

Similarly, the formula for the shearing force transmitted to the lower flange assumes the form

$$t_2 = \frac{\Delta \sigma_1}{2 h h_2} \left[m_1^2 (h_1 - \frac{2}{3} m_1) + m_2^2 (h_1 + \frac{2}{3} m_2) \right], \quad (4.5)$$

Since now we have

$$C_f \Delta \sigma_1 = t_1, \quad (4.6)$$

and

$$C_a \Delta \sigma_2 = C_a \frac{h_2}{h_1} \Delta \sigma_1, \quad (4.7)$$

the formulae for the equivalent flange-width assume the form

$$C_f = \frac{1}{2 h h_1} \left[m_1^2 (h_2 + \frac{2}{3} m_1) + m_2^2 (h_2 - \frac{2}{3} m_2) \right], \quad (4.8)$$

and

$$C_a = \frac{1}{2 h h_2} \left[m_1^2 (h_1 - \frac{2}{3} m_1) + m_2^2 (h_1 + \frac{2}{3} m_2) \right]. \quad (4.9)$$

4.4 Equivalent web-thickness of the horizontal walls

The thickness of the web of the two equivalent beams are determined from

$$f_f = d_f \frac{m_1 - d_f / 2}{h_1}, \quad (4.10)$$

and

$$f_a = d_a \frac{m_2 - d_a / 2}{h_2}. \quad (4.11)$$

The above formulae are similar to formula (3.9).

CHARACTERISTICS OF SINGLE-CELL BOX BEAMS

REFERENCES

1. Szidarovszky, J.: The analysis of single-cell box beams by the hinged model. Acta Technica 99 (1985)
2. Szidarovszky, J.: Zárt hidak felső szélrácsaiban ébredő T erő meghatározása (in Hungarian), Mélyépítéstudományi Szemle, Budapest 1967. (Determination of the lateral force (T-force) in the upper lateral bracing of bridges)



RELATIONSHIP BETWEEN SAINT-VENANT'S PRINCIPLE AND BERNOULLI-NAVIER'S
THEOREM AS WELL AS BREDT'S FORMULAE AND WARPING

J. Szidarovszky*

(Received: 5 September 1985)

Saint-Venant's principle of pure torsion and Bernoulli-Navier's theorem of pure bending are based on different assumptions and seem to be independent of each other. However, each is a special case of the theory of Elasticity. The analysis of the single-cell box beam based on Bernoulli-Navier's theorem also produces Bredt's two formulae and the formula for warping (which were derived from Saint-Venant's principle), demonstrating that the two theories are not independent of each other.

NOTATION

Notation is to be found in /4/, except I which is the equivalent secondary moment of a vertical wall.

1. INTRODUCTION

The physical model of the single-cell box beam with perpendicular walls is obtained by connecting the walls by hinges at the joints - this labile structure called the "hinged beam", and the hinged beam is then supported by densely placed frameworks - the "supporting frames". Applying Bernoulli-Navier's theorem for the individual wall elements, the mathematical procedure necessary for the determination of the state of stress is presented in /1/. Formulae for the reactive forces transmitted from the supporting frames to the hinged beam are given in /3/.

According to Bernoulli-Navier's theorem, cross-sections which were plane and perpendicular to the axis of the beam before pure bending remain plane after pure bending since there are no shearing stresses. In the case of pure torsion, on the basis of Saint-Venant's principle assuming constant specific twist caused by the shearing stresses, the warping of the originally plane cross-sections can be derived. Both theories can be considered as special cases of the theory of Elasticity.

Making use of the results obtained in /1/ and /3/ based on Bernoulli-Navier's theorems, the aim of this paper is to derive Bredt's two formulae

*Dr. J. Szidarovszky, H-1089 Budapest, Bíró Lajos u. 42., Hungary

and the equation of warping which is proved on the basis of Saint-Venant's principle for pure torsion and, so demonstrate that although the two theories are based on entirely different assumptions they are not independent of each other.

1.1 Differential equation for the frame-reaction

Formula (1.2.2/b) in /3/ simplifies if the effect of the shearing forces is neglected, and so the horizontal component of the reactive force of the supporting frame is obtained from the differential equation

$$q^{IV} + 8 \frac{h^2 q_A}{k^2 EI} q = 2 \frac{hq_A}{kEI} p \quad (1.1.1)$$

with four fulfilled boundary conditions.

For a simply supported beam with a constant cross-section we have $q=0$ and $M=0$ at $z=0$ and $z=l$, so it is expedient to solve Eq. (1.1.1) by using sinus Fourier series. Let us expand the load and the frame reaction in the Fourier series

$$p = \sum_{i=1}^{\infty} p_i \sin \frac{i \pi z}{l} \quad (1.1.2)$$

and

$$q = \sum_{i=1}^{\infty} q_i \sin \frac{i \pi z}{l} \quad (1.1.3)$$

Substituting formulae (1.1.2) and (1.1.3) and the fourth derivative of the latter with respect to z into Eq. (1.1.1), after some rearrangement and the usual application of sinus orthogonality, we arrive at

$$q_i = \frac{1}{1 + \frac{i^4 \pi^4}{l^4} \frac{k^2 EI}{8h^2 q_A}} \frac{k}{4h} p_i \quad (1.1.4)$$

1.2 Deformation and state of stress for constant cross-sections

1.2.1 Deformation of the hinged beam

If the frame is infinitely flexible, i.e. $q_A=0$, then we have $q=0$. It means that the two vertical walls, together with the upper and lower flanges, take the vertical antisymmetric load $p/2$ as is presented in Section 2.5 in /1/. On the basis of formulae (2.5.2), (2.5.5) and (2.5.6) in

TORSIONAL RELATIONSHIPS

/1/, the relative vertical displacement of the vertical walls and the relative horizontal displacement of the horizontal walls are obtained from

$$\eta_{vv} = \int_0^z \int \int \int \frac{p}{EI} dzdzdzdz$$

and

$$\eta_{vh} = \eta_{vf} + \eta_{va} = \frac{h}{k} \int_0^z \int \int \int \frac{p}{EI} dzdzdzdz .$$

The rotation of the walls takes on the form

$$\beta_v = \frac{\eta_{vf} + \eta_{va}}{h} = \frac{1}{k} \int_0^z \int \int \int \frac{p}{EI} dzdzdzdz \quad (1.2.1)$$

or

$$\beta_h = \frac{\eta_{vv}}{k} = \frac{1}{k} \int_0^z \int \int \int \frac{p}{EI} dzdzdzdz \quad (1.2.2)$$

showing that the rotation of the horizontal walls and that of the vertical walls are of the same magnitude but of opposite direction (Fig. 1). It follows that the whole hinged beam subjected to antisymmetric vertical loads does not twist (only the single walls) but its cross-section undergoes a deformation.

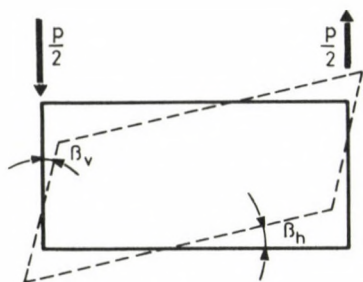


Fig. 1.

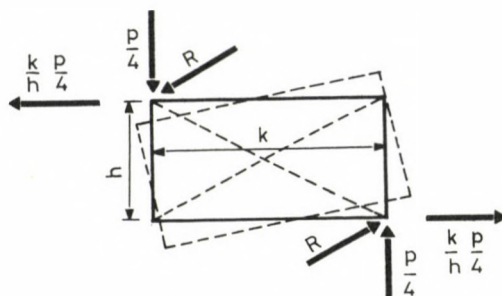


Fig. 2.

1.2.2 Normal stresses in the box beam with an undeformable cross-section

If the cross-section does not change its shape (undeformable cross-section, Fig. 2), i.e. $q_A = \infty$ holds, then we have $\beta_t = 0$ and Eq. (1.1.1) simplifies to

$$q = \frac{k}{h} \frac{p}{4} \quad (1.2.3)$$

Formula (2.214/b) in /3/ proves the validity of (1.2.3) also for the case when the effect of shearing forces are taken into account and the warping is restricted.

The normal stresses at point K=1 caused by the vertical antisymmetric forces $\pm(p/2 - (h/k)q)$ (Fig. 5) can be determined from formula (2.4.3) in /1/ as

$$\sigma_{v1} = -\frac{h_1}{2I} \left(M_p - \frac{2h}{k} M_q \right) = -\frac{h_1}{2I} \left(M_p - \frac{M_p}{2} \right) = -\frac{h_1}{4I} M_p \quad (1.2.4)$$

Making use of formulae (2.4.14) and (2.4.25) in /1/, we obtain the normal stresses caused by the horizontal antisymmetric loads as

$$\sigma_{h1} = \frac{k}{2I_f} M_q = \frac{hh_1}{kI} \frac{kM_p}{4h} = \frac{h_1}{4I} M_p \quad (1.2.5)$$

By producing the sum of the horizontal and vertical stresses, i.e. formulae (1.2.4) and (1.2.5), we arrive at the actual normal stresses in the hinged beam:

$$\sigma_1 = \sigma_{v1} + \sigma_{h1} = -\frac{h_1}{4I} M_p + \frac{h_1}{4I} M_p = 0 \quad (1.2.6)$$

The normal stresses assume zero value, showing the fact that no normal stresses develop from the antisymmetric loads if the cross-section is undeformable.

1.2.3 Internal forces and moments in the box beam with an undeformable cross-section

If the cross-section does not change its shape, then, on the basis of formula (1.2.3), we obtain the vertical antisymmetric load (Fig. 3)

$$\frac{h}{k} q = \frac{h}{k} \frac{k}{h} \frac{p}{4} = \frac{p}{4} \quad (1.2.7)$$

and the horizontal antisymmetric load

$$q = \frac{k}{h} \frac{p}{4} \quad (1.2.8)$$

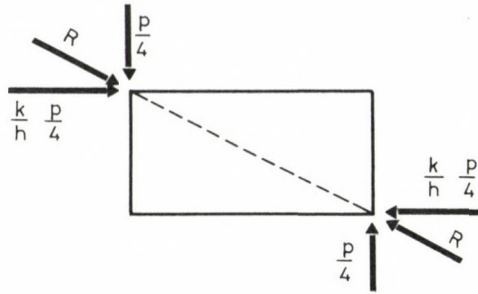


Fig. 3.

acting on the supporting frame. The resultant load acts diagonally and the ratio of the vertical and horizontal forces is

$$\frac{\frac{P}{4}}{\frac{k}{h} \frac{P}{4}} = \frac{h}{k} \quad (1.2.9)$$

The hinged beam (Fig. 2) is subjected to the vertical antisymmetrical load

$$\frac{p}{2} - \frac{h}{k} q = \frac{p}{2} - \frac{h k p}{k h 4} = \frac{p}{4} \quad (1.2.10)$$

and to horizontal antisymmetric load

$$q = \frac{k p}{h 4} \quad (1.2.11)$$

The ratio of the vertical and horizontal forces is again

$$\frac{\frac{p}{4}}{\frac{k}{h} \frac{p}{4}} = \frac{h}{k} \quad (1.2.12)$$

showing that the resultant acts along the other diagonal (Fig. 2).

In the case of an undeformable cross-section, the distributed torques caused by the vertical and horizontal loads on the hinged beam, i.e.

$$m_{tv} = -\frac{p}{4} k \quad (1.2.13)$$

and

$$m_{th} = -q h = -\frac{k}{h} \frac{p}{4} h = -\frac{p}{4} k \quad (1.2.14)$$

are equal. In other words, the distributed torque caused by the external loads is taken in an equal ratio by the horizontal and vertical walls:

$$m_t = m_{tv} + m_{th} = -\frac{p}{4} k - \frac{p}{4} k = -\frac{p}{2} k \quad (1.2.15)$$

1.2.4 Bredt's first law

Since no normal stresses develop in undeformable cross-sections — see (1.2.6) — the specific shearing forces do not vary in vertical walls, i.e. their distribution along the walls is constant.

Resultants $R_p/4$ and $(k/h)R_p/4$ caused by the vertical forces $p/4$ and by the horizontal forces $(k/h)p/4$ are distributed between the walls of height h and k . Consequently, the shearing force per unit length, i.e. the shear flow assumes the form

$$t_v = \frac{\frac{R_p}{4}}{h} = \frac{R_p}{4h} \quad (1.2.16)$$

in the vertical wall, and

$$t_h = \frac{\frac{1}{4} \frac{k}{h} R_p}{k} = \frac{R_p}{4h} \quad (1.2.17)$$

in the horizontal wall. The two formulae coincide, i.e. the shear flow is constant, as is stated in the theory of pure torsion.

The torque acting on the cross-section is obtained by integrating the distributed torque:

$$M_t = \int_0^z m_t dz = - \int_0^z \frac{k}{2} p dz \quad (1.2.18)$$

If k is constant, we have

$$M_t = -k \int_0^z \frac{p}{2} dz = k \frac{R_p}{2}, \quad (1.2.19)$$

from which we obtain R_p . Substituting R_p into formula (1.2.17), we obtain

$$t = t_v = t_n = \frac{R_p}{4h} = \frac{M_t}{2hk} \quad (1.2.20)$$

TORSIONAL RELATIONSHIPS

for the shear flow. Since the shear flow is constant, the angle of twist of a rectangular wall element is constant along the wall.

Introducing the formula

$$A_t = k h \quad (1.2.21)$$

for the area limited by the stress axes of the walls, the formula for the average shearing stress

$$\tau = \frac{t}{d} \quad (1.2.22)$$

assumes the form

$$\tau = \frac{M_t}{2 A_t d} \quad (1.2.23)$$

which, in fact, is Bredt's first law. In this formula, however, A_t is not the area limited by the centre-lines of the walls but the area limited by the stress axes. This difference is due to the fact that the membrane translation perpendicular to the cross-section is assumed to be linear along the thickness of walls through Bredt's derivation, while our derivation assumes it to be a parabola of the second order.

We shall demonstrate Bredt's second law in Section 2.

1.2.5 Resolution of the loads acting on the hinged beam

The fact that the resultant of the forces transmitted from the supporting frame to the hinged beam is parallel to the other diagonal and that the cross-section of the hinged beam is undeformable suggests that the loads on the hinged beam should be resolved into the following two parts: one part only causing angular displacements and the other part only causing twist (Fig. 1 and Fig. 2). However, it is expedient to resolve the external loads in another way.

The hinged beam is subjected to two antisymmetric loads: the vertical load $\pm(p/2 - (h/k)q)$ and the horizontal load $\pm q$. This load can also be produced as the sum of two antisymmetric loads: the one is the vertical load $\pm(p/2 - (2h/k)q)$ (Fig. 4) and the other is the vertical load $\pm(h/k)q$ and the horizontal antisymmetric load $\pm q$.

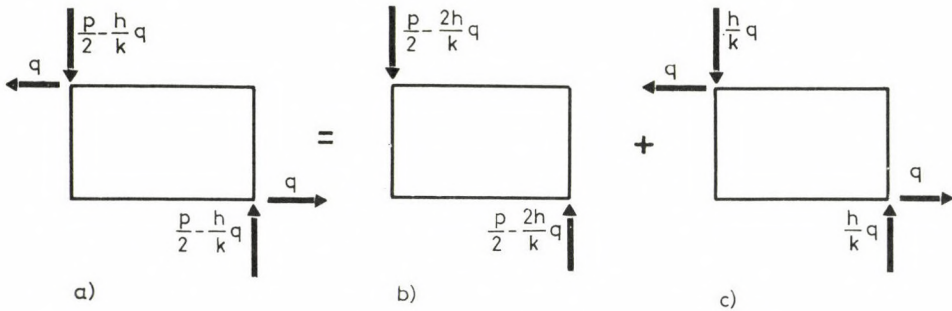


Fig. 4.

The first part causes the torque

$$M_1 = -\left(\frac{p}{2} - \frac{2h}{k} q\right) k = -\left(\frac{pk}{2} - 2 h q\right) \quad , \quad (1.2.24)$$

the second part develops

$$M_2 = -qh - \frac{h}{k} q k = -2 h q \quad . \quad (1.2.25)$$

and the sum of the two parts represents the whole torque

$$M = M_1 + M_2 = -\frac{pk}{2} \quad . \quad (1.2.26)$$

Due to the first load, the cross-section only develops deformation and the second load causes only twist. It follows that a box-beam bridge balances one part of the external torque as a hinged beam by translation and the other part as undeformable box beam by twist. In this distribution of the torque, apart from the size of the cross-section, the direction of antisymmetric load causing the torque plays an important role. If the direction of the external forces acting at the opposite corners is parallel with the diagonal connecting the other two corners (Fig. 2), the box beam balances the whole torque by twist.

By analysing the effect of torsion, the procedure presented above shows what proportion of the external torque is balanced by the box beam resisting as an undeformable twisted beam and what proportion is taken by the box beam responding as a hinged beam. It follows that the procedure is

TORSIONAL RELATIONSHIPS

also applicable to the approximate analysis of skew bridges.

Acting as an undeformable twisted beam (Fig. 4/c) the box beam takes the torque

$$M_2 = \frac{h}{k} q h + q h = 2 q h \quad (1.2.27)$$

and performing as a hinged beam (Fig. 4/b) it balances the torque

$$M_1 = \left(\frac{p}{2} - \frac{2h}{k} q \right) k = \frac{p}{2} k - 2 h q \quad (1.2.29)$$

arising from the antisymmetric vertical load

$$\pm \left(\frac{p}{2} - \frac{2h}{k} q \right) \quad . \quad (1.2.28)$$

2. TAKING INTO ACCOUNT WARPING AND THE EFFECT OF THE DEFORMATION CAUSED BY THE SHEARING FORCES

The cross-section of the box beam which is plane and perpendicular to the axis of the beam before loading does not remain plane after the antisymmetric loading and the points of the cross-section develop different axial translations i.e. the cross-section undergoes warping.

2.1 Warping - Bredt's second law

Let the tube-like cross-section be subjected to the vertical antisymmetric load $\pm(P/2 - (h/k)Q)$ and the horizontal antisymmetric load $\pm Q$ (Fig. 5).

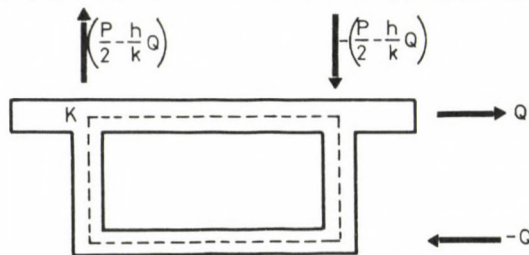


Fig. 5.

In making use of formula (1.2.23), the angular displacement of the horizontal and vertical walls caused by the shearing forces (Figs 6 and 7) is given by the formulae

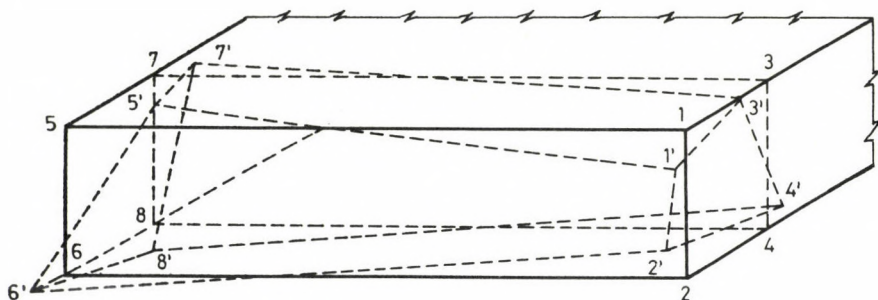


Fig. 6.

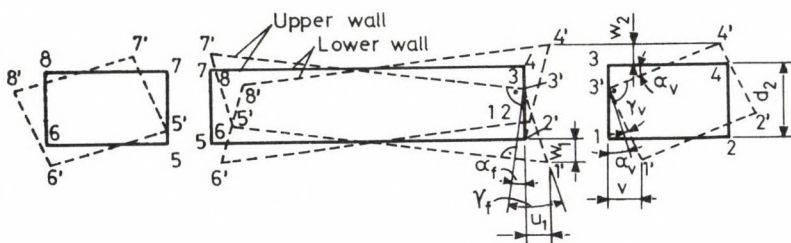


Fig. 7.

$$\gamma_f = \frac{\tau}{G} = \frac{R_q}{F_f G} \quad (2.1.1/a)$$

and

$$\gamma_a = \frac{\tau}{G} = \frac{R_q}{F_a G} \quad (2.1.1/b)$$

and

$$\gamma_v = \frac{R_p}{2} - \frac{h}{k} \frac{R_q}{F_v G} \quad (2.1.1/c)$$

Let us cut through the box beam by two planes. The planes are perpendicular to the axis of the beam and the distance between them is dz . The angular displacement of the horizontal and vertical walls in the infinitesimal element (Figs 6 and 7) is

$$\alpha_f = \frac{2 w_1}{k} \quad (2.1.2/a)$$

TORSIONAL RELATIONSHIPS

$$\alpha_a = \frac{2 w_2}{k} \quad (2.1.2/b)$$

and

$$\alpha_v = \frac{w_1 + w_2}{h} \quad (2.1.2/c)$$

The relative horizontal translations of the points marked with "1" and "2" on the two vertical sections (Fig. 7) are

$$\mu_1 = (\gamma_f - \alpha_f) dz = \left(\frac{R_q}{F_f G} - \frac{2w_1}{k} \right) dz \quad (2.1.3/a)$$

$$\mu_2 = (\gamma_a - \alpha_a) dz = \left(\frac{R_q}{F_a G} - \frac{2 w_2}{k} \right) dz \quad (2.1.3/b)$$

and

$$v = (\gamma_v + \alpha_v) dz = \left(\frac{\frac{R_p}{2} - \frac{h}{k} R_q}{F_v G} + \frac{w_1 + w_2}{h} \right) dz \quad (2.1.3/c)$$

The twist per unit length of the horizontal and vertical elements, on the basis of formulae (2.1.3/a) – (2.1.3/c), assumes the form

$$\beta_v = \frac{1}{dz} \frac{\mu_1 + \mu_2}{h} = \frac{R_q}{hG} \left(\frac{1}{F_f} + \frac{1}{F_a} \right) - \frac{2}{hk} (w_1 + w_2) \quad (2.1.4)$$

and

$$\beta_h = \frac{1}{dz} \frac{2v}{k} = \frac{R_p - \frac{2h}{k} R_q}{k G F_v} + \frac{2}{hk} (w_1 + w_2) \quad (2.1.5)$$

If we have an undeformable cross-section, the twist of the cross-section and the twist of the elements are the same and, making use of formulae (1.2.11) and (1.2.15) as well as the formulae

$$\beta = \beta_v = \beta_h \quad .$$

$$R_p = \frac{4h}{k} R_q \quad ,$$

$$M_t = \frac{k}{2} R_p$$

and

$$w = w_1 + w_2 \quad .$$

we obtain the twist per unit length as

$$\beta = \frac{\beta_v + \beta_h}{2} = \frac{M_t}{4h^2G} \left(\frac{1}{F_f} + \frac{1}{F_a} + \frac{2h^2}{k^2F_v} \right) = \frac{M_t}{4h^2k^2G} \left(\frac{k}{d_f} + \frac{k}{d_a} + \frac{2h}{dv} \right) \quad (2.1.6)$$

which is identical to Bredt's second law. If the cross-section does not keep its shape, i.e. we have a deformable cross-section, then the deformation per unit length of the cross-section is

$$\frac{\beta_t}{dz} = \beta_h - \beta_v$$

or, making use of formulae (2.1.4) and (2.1.5),

$$\frac{\beta_t}{dz} = \frac{R_p}{kF_vG} - \frac{R_q}{Gh} \left(\frac{1}{F_a} + \frac{1}{F_v} + \frac{2h^2}{k^2F_v} \right) + \frac{4}{hk} w \quad , \quad (2.1.7)$$

from which we obtain warping as

$$w = \frac{hk}{4} \frac{d\beta_t}{dz} + \left(\frac{F_f + F_a}{F_f F_a} + \frac{2h^2}{k^2F_v} \right) \frac{k}{4G} R_q - \frac{h}{4F_vG} R_p \quad . \quad (2.1.8)$$

If the upper horizontal flange extends beyond the vertical walls, then, in the case of pure torsion, no normal stresses develop in the overhanging sections so the effect of the shearing stresses is negligible. It follows that there must be a break point in the diagram of warping (Fig. 8). The angle at the break point is

$$\gamma = \frac{\tau}{G} = \frac{t}{d_f G} = \frac{R_q}{k d_f G} \quad . \quad (2.1.9)$$

TORSIONAL RELATIONSHIPS

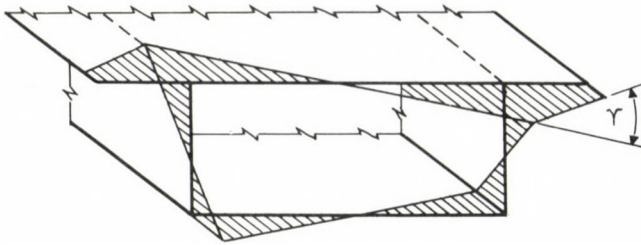


Fig. 8.

The warping developing on the hinged beam supported by the supporting frames (Eq. 2.1.8) can also be interpreted as the sum of two parts: warping on the hinged beam and warping on the undeformable cross-section.

According to Section 1.2.5, the vertical antisymmetric load $\pm(P/2 - (h/k)Q)$ and the horizontal antisymmetric load $\pm Q$ acting on the hinged beam are equivalent with the vertical load $\pm(P/2 - (2h/k)Q)$ on the hinged beam and the sum of the vertical load $\pm(h/k)Q$ and the horizontal load $\pm Q$ acting on the beam of undeformable cross-section.

If the hinged beam is subjected to the antisymmetric vertical load $P/2 - (2h/k)Q$ (Fig. 4/b), then, due to the shearing forces, the vertical wall on the left-hand side translates downwards, the one on the right-hand side translates upwards and the horizontal walls do not undergo angular displacement, they only twist. It follows that no warping occurs. This fact is descriptively shown if we develop the walls into a plane. This load only develops bending of the vertical walls and so also warping of bending nature ("bending" warping from now on).

If the beam is subjected to the antisymmetric vertical load $\pm(h/k)Q$ and the antisymmetric horizontal load $\pm Q$ (Fig. 4/c), then, because of the constant nature of the shear flow, all four walls, as plane structures, develop distortion in such a way that the distortion of the opposite walls is of opposite direction. That is why generally warping develops, which is shown in Fig. 6 and in Fig. 7 where the four walls are developed into the same plane.

Due to the vertical antisymmetric load $\pm(P/2 - (2h/k)Q)$, only "bending" warping w_a develops and the vertical antisymmetric load $\pm(h/k)Q$ and the horizontal antisymmetric load $\pm Q$ only cause "shearing" warping w_b (warping

of shearing nature). As opposed to "shearing" warping, in the case of "bending" warping, there is no sudden change in the warping diagram at concentrated forces or at places where the cross-section changes. It follows that, at concentrated forces and at changes in the cross-section, the diagram of warping w_b presents sudden changes but that of warping w_a does not.

If the hinged beam is subjected to the vertical antisymmetric load $\pm(P/2 - (2h/k)Q)$ (Fig. 4/b), we obtain warping from formula (2.1.8) as

$$w_a = \frac{hk}{4} \frac{\beta t}{dz} - \frac{h}{4F_V G} R_P + \frac{4h}{4F_V G} \frac{h}{k} R_Q \quad (2.1.10)$$

According to formulae (1.2.3), the vertical antisymmetric load $P = (4h/k)Q$ acting on the beam with an undeformable cross-section develops force Q in the horizontal walls of the hinged beam and force

$$\frac{1}{2} P - \frac{h}{k} Q = \frac{h}{k} Q \quad (2.1.11)$$

in the vertical walls.

The non-restricted warping caused by the vertical antisymmetric load $\pm(h/k)Q$ and horizontal antisymmetric load $\pm Q$ acting on the undeformable beam (Fig. 4/c) is given by formula (2.1.8) as

$$w_b = \left(\frac{F_f + F_a}{F_f F_a} + \frac{2h^2}{k^2 F_V} \right) \frac{k}{4G} R_Q - \frac{h}{4F_V G} \frac{4h}{k} R_Q = \left(\frac{F_f + F_a}{F_f F_a} - \frac{2h^2}{k^2 F_V} \right) \frac{k}{4G} R_Q \quad (2.1.12)$$

since we have $\beta_t = 0$ in this case (undeformable cross-section). The sum of formulae (2.1.11) and (2.1.12) gives the whole warping represented by formula (2.1.8).

The fact that warping can be presented in two parts makes it possible to introduce the equivalent areas F_V , F_f and F_a .

Due to the vertical antisymmetric load $\pm(P/2 - (2h/k)Q)$, no shearing forces develop in the horizontal walls and the sum of the shearing stresses is zero. At the vertical walls, as with I-beams, we have

TORSIONAL RELATIONSHIPS

$$F_v = d_v h \quad (2.1.13)$$

as a good approximation for the equivalent area.

The vertical shearing force caused by the vertical antisymmetric load $\pm(h/k)Q$ and the horizontal antisymmetric load $\pm Q$ is balanced on the area

$$F_v = d_v h \quad (2.1.14)$$

and the horizontal shearing force caused by the same load is balanced on the area

$$F_f = d_f k \quad (2.1.15)$$

and on

$$F_a = d_a k, \quad (2.1.16)$$

because of the constant nature of the shear flow.

In the case of an undeformable cross-section, we have $\beta_t=0$ and, making use of formulae (1.2.3) and (2.1.8) we obtain

$$w = \frac{k}{4G} \left(\frac{F_f + F_a}{F_f F_a} - \frac{2 h^2}{k^2 F_v} \right) R_q \quad (2.1.17)$$

which is identical to the formula presented in /2/.

In applying Bernoulli-Navier's theorem we arrived at the fact that the shear flow is of constant nature. We also obtained Bredt's first (1.2.23) and second formula (2.1.6) as well as the formula for warping for pure torsion (2.1.13). These formulae were derived from Saint-Venant's principle. It follows that Navier's theorem and Saint-Venant's principle are not independent of each other.

REFERENCES

1. Szidarovszky, J.: The analysis of single-cell box beams by the hinged model. Acta Technica Hung. 99 (1985)
2. Timoshenko, S.P., Goodier, J.N.: Theory of Elasticity, McGraw-Hill, New York, 1951
3. Szidarovszky, J.: Exact analysis of single-cell box beams. Acta Technica Hung. 100 (1986)
4. Szidarovszky, J.: Cross sectional characteristics of single-cell box beams with a schematic cross-section. Acta Technica Hung. 99 (1985)

DESIGN OF STEEL FRAMES BY MULTICRITERION OPTIMIZATION

A. Vásárhelyi^{*} - J. Lógó^{**}

(Received: 5 September 1986)

The scalar optimization method of multicriterion optimization is presented for the design of steel frames. The stress and buckling conditions are satisfied according to the Hungarian Standards (which are similar to DIN). The effect of using different objective functions was considered. Numerical examples show that from the point of view design it is not successful if all the boundary conditions are taken into consideration as objective functions at the same time.

1. INTRODUCTION

The basic idea of multicriterion optimization is very close to the process of structural design. In this paper the connection between these professional domains is presented. The cross-sectional dimensions of steel frames are designed by multicriterion optimization taking into consideration the stress, buckling and lateral buckling criteria. Numerical examples illustrate how the dimensions of the cross-sections are influenced by different objective functions.

The problem is solved by an interactive program system which contains different mathematical methods (weighting objective methods, Guddat's method and scalarization with parametrical levels).

2. APPLIED MATHEMATICAL METHODS

Only there are several methods in our interactive program system. From among the available methods, scalarization with parametric levels is presented here because other methods (weighted objectives /3/, /5/, goal programming /6/ and scalarization of Guddet /3/ are known from the literature, and because of, this method is best suited to solve our problem.

For linear vector optimization problems Brosowski /2/ investigated a scalarization which led to the following scalar problem:

^{*} A. Vásárhelyi, Dept. Mathematics, Technical University, Budapest, Hungary

^{**} J. Lógó, Dept. Mechanics, Technical University, Budapest, Hungary

$$\min \left\{ t \mid t \in \mathbb{R}, g_i(\underline{x}) \leq 0, i = 1, \dots, n, h_j(\underline{x}) = 0, \right. \\ \left. j = 1, \dots, \ell, p_k(\underline{x}) - t \leq y_k, \right. \\ \left. k = 1, \dots, m \right\} \quad (2.1)$$

where:

- t - a scalar,
- \underline{x} - vector of unknown,
- $g_i(\underline{x})$ and $h_j(\underline{x})$ - functions,
- n, ℓ, m - number of inequalities, equalities and objective functions respectively,
- $p_k(\underline{x})$ - the k -th objective function,
- y_k - is the demanded level of the k -th objective function.

By minimizing t in (2.1) such a feasible point \underline{x} is looked for which these levels can be chosen as "minimum". A slight generalization of the problem (2.1) is the following scalar problem:

$$\min \left\{ t \mid t \in \mathbb{R}, g_i(\underline{x}) \leq 0, i = 1, \dots, n, h_j(\underline{x}) = 0, \right. \\ \left. j = 1, \dots, \ell, p_k(\underline{x}) \leq \underline{y}_k + t\underline{z}_k, \right. \\ \left. k = 1, \dots, m \right\} \quad (2.2)$$

where:

- $\underline{y} \in \mathbb{R}^m$ and $\underline{z} \in \mathbb{R}^m$ (\mathbb{R}^m is the space of objective functions)
- $\underline{z} > 0$, \underline{y} and \underline{z} are chosen by the user.

The program system produces the vectors \underline{y} and \underline{z} automatically /1/.

A feasible point is selected from the calculated feasible points for each objective function in which the value of the objective function is minimum among the feasible solutions.

Let these points be s_1, \dots, s_k .

Choose \underline{y} and \underline{z} vectors automatically as follows:

$$y_i = p_i(s_i), i = 1, \dots, k, z_i = \frac{1}{k} \sum_{i=1}^k p_i(s_i) - y_i, i = 1, \dots, k \quad (2.3)$$

This choice has two advantages:

- the scalarization can be used easily,
- \underline{y} and \underline{z} are independent of the scale of the objective functions.

The Powell-algorithm was used to solve the above scalarization problem /7/.

OPTIMIZATION OF STEEL FRAMES

3. DESIGN OF STEEL FRAMES

At our University a series of experiments were run for steel frames. Data on structure and loads can be seen on Fig. 1. According to the experiments the load carrying capacity of the frame is $8 \times 33 \text{ kN} / 4 /$. The balks and pillars are supported by purlins.

According to the above method this structure has been computed with different choices of objective functions.

Assuming that – the material is homogeneous, isotropic and linear elastic, ideal plastic; – the static loads are acting on the nodes; – the frame is a planar structure. The structure was divided into 12 members.

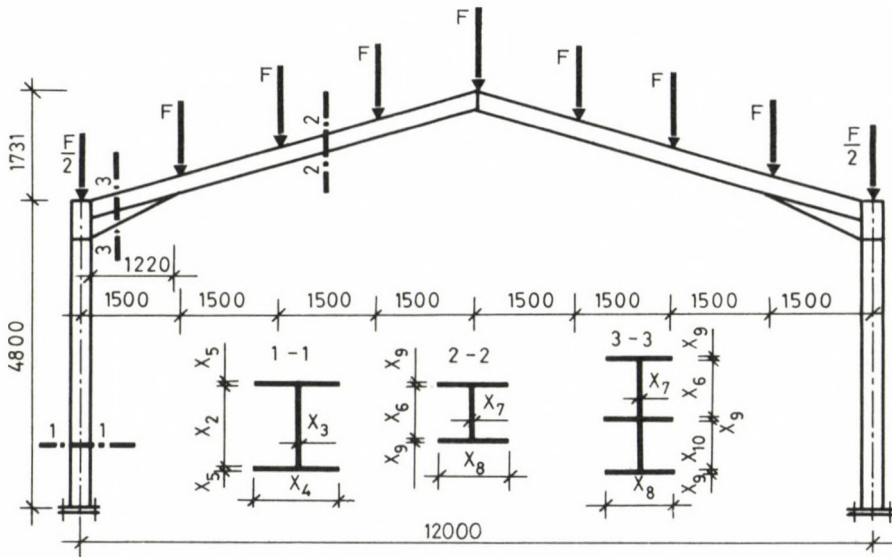


Fig. 1.

The internal forces are determined according to the force method.

The unknowns are:

- x_1 – redundant force
- $x_2 \dots x_{10}$ – the dimensions of cross-sections (Fig. 1.)

Each section of the members satisfies the equilibrium equations the compatibility and the linear plastic yield conditions:

$$\underline{G}^* \underline{s} + \underline{q} = \underline{0} \quad (3.1)$$

$$\underline{G}^* \underline{u} + \underline{F} \underline{s} = \underline{0} \quad (3.2)$$

$$\underline{N}^* \underline{s} - \underline{k} \leq \underline{0} \quad (3.3)$$

where:

- \underline{G} — geometric matrix,
- \underline{s} — vector of internal forces,
- \underline{q} — load vector,
- \underline{u} — displacement vector,
- \underline{F} — flexibility matrix,
- \underline{N} — matrix of yield conditions,
- \underline{k} — plastic limit stress.

The following conditions of stability have to be satisfied:

$$\frac{N_i}{N_L} \leq \phi_x \quad i = 1, \dots, 12 \quad (3.4)$$

$$\frac{N_i}{N_L} + \Psi_x \frac{\epsilon_x M_i}{1,1 M_L} \leq 1 \quad i = 1, \dots, 12 \quad (3.5)$$

$$\frac{N_i}{N_L} + \Psi_y \frac{\epsilon_y M_i}{1,1 M_L} \leq \phi_y \quad i = 1, \dots, 12 \quad (3.6)$$

where:

- N_i, M_i — normal force and bending moment at the i -th member, respectively,
- N_L, M_L — limit normal force and limit bending moment respectively,
- Ψ_x, Ψ_y — functions of second order effects in the plane of structure and in normal direction to the structure respectively,
- ϵ_x, ϵ_y — proportional factors depending on the internal forces,
- ϕ_x, ϕ_y — buckling functions.

$\Psi_x, \Psi_y, \epsilon_x, \epsilon_y, \phi_x, \phi_y$ are presented in the Hungarian Standards which are similar to DIN. Conditions (3.1), (3.2), (3.3) were substituted into conditions (3.4), (3.5), (3.6). The geometrical dimensions of the cross sections were limited by minimal values. In the majority of the cases, there are two objective functions: the volume of the structure (C1) and the minimum shear forces at the supports (C2).

OPTIMIZATION OF STEEL FRAMES

$$C1: \sum_{i=1}^{12} \ell_i^* A_i \rightarrow \min \quad (3.7)$$

$$C2: \sum_{i=1}^2 T_i^2 \rightarrow \min \quad (3.8)$$

where:

ℓ_i^* , A_i — length and cross-section of the i -th member respectively,
 T_i — shear force.

In Table 1 one can see which functions were taken into consideration as an objective function. In every case the constraints are (3.1), (3.2), (3.3), (3.4), (3.5), (3.6) and the geometrical limit.

CONCLUSIONS

The choice of the objective functions influences substantially the dimensions of cross-sections. Taking the stability conditions as objective functions the dimensions were close to the experimental ones. If the structure was designed for minimal volume, the same load carrying capacity was assigned by less volume than at the experimental structure. It is not a good practice to take too many objective functions into consideration at the same time.

REFERENCES

1. Bernau, H.: Interactive Methods for Vector Optimization. Proceedings of the Conference "Methoden und Verfahren der mathematischen Physik". Oberwolfach 1985.
2. Borosowski, B.: A Criterion of Efficiency and some Applications. Preprint.
3. Guddat, J. — Guerra, F. — Tammer, K. — Wendler, K.: Multi-objective and Stochastic Optimization Based on Parametric Optimization. Akademie-Verlag, Berlin 1985.
4. Iványi, M.: Load-deformation Relationships for Simple Steel Frames with unstable Elements. Periodica Polytechnica, Civ. Eng. 29. (1985), Nos 3-4, 1985.
5. Jahn, J.: Scalarization in Vector Optimization. Math. Progr. 19 (1984), 203-218.
6. Osyczka, A.: Multicriterion Optimization in Engineering with FORTRAN Programs. Ellis Horward Lim. Publ. Chichester 1984.
7. Powell, J.M.D., VMCWD: A FORTRAN Subroutine for Unconstrained Optimization. Report DAMTP NA4, University of Cambridge, 1982.

Table 1

obj. funct.	un- knowns	C1	C1, C2	C1, C2 3.4	C1, C2, 3.5	C1, C2, 3.6	C1, C2, 3.5 3.6	3.4 3.5 3.6	Exp. data
x_2 (mm)		354	354	345	330	347	344	355	340
x_3 (mm)		6	6	8	6	8	8	9	8
x_4 (mm)		181	175	173	189	173	178	182	170
x_5 (mm)		10	10	10	10	10	10	10	10
x_6 (mm)		281	300	283	288	288	288	270	280
x_7 (mm)		5	5	5	6	6	6	6	6
x_8 (mm)		140	155	152	152	153	154	140	150
x_9 (mm)		10	9	9	10	10	10	9	10
x_{10} (mm)		340	330	340	338	338	338	345	335
C1 (cm ³)		105932	108022	114168	116588	122132	122045	116948	118714

BOOK REVIEWS

Kálmán Z. Horváth: The selection of load-bearing structures for buildings. Akadémiai Kiadó Budapest – Elsevier Science Publishers B.V. Amsterdam 1986, 380 pages, 196 figures, 20 tables, subject index.

This book is the English version of the Hungarian book on the same subject published in 1982 by the Műszaki Könyvkiadó. Its aim is to present the creating process of structure design in detail and to represent the considerations that have to be taken into account in selecting the most appropriate load-bearing structure for the purpose of the building.

The introductory part of the book presents the different types of load-bearing structures, sometimes denoting the individual structures by novel names differing from the ones used by the technical literature. It describes in detail the equilibrium of forces in the different structure types, and also the structural and technological problems in connection with their realization. After systematizing the various types of load-bearing structures it deals with the executional and operational requirements taking into consideration the aesthetic, tectonic, static and physical demands.

The next part analyses the designing problem of the load-bearing structure. The standpoints of the expedient selection of the structure are shown in a separate chapter for three different tasks, namely for a hall for industrial or agricultural purposes, for a single-level one-family house, and for a factory building. The next chapter represents the whole designing process of the project plan step by step in ten concrete examples and then continues with the various tasks to be solved when completing the technical plan and the working drawings in the cases of the same buildings. The last chapter deals with the structural solution of eleven special buildings in detail. One part of them has been realized as a result of the author's original architectural work, the second one has been accomplished on the basis of the author's structural design activity. Among the examples discussed in detail the presentation of the design and construction problem of the load-bearing structures of the indoor swimming pool in Szombathely, the city office building in Budapest, Roosevelt square, the educational block of the Technical College of Traffic and Telecommunication at Győr and the hotel MALÉV-HYATT in Budapest is worthy of special interest. The Wine Museum in Budapest is also an interesting task.

BOOK REVIEWS

Throughout the book it is emphasized that a good building can only be created by an effective cooperation of all partners involved. Besides the many other related questions the author deals in detail with the advantage resulting from the application of mushroom floors and with the possibilities arising from the utilization of structures having larger span than the usual ones. Beside the main structure the complementary and junction structures are also examined. The problems of reinforcement of buildings, the question of dilatation gaps, the problem of hinges and concols and also the expert solution of isolation tasks are dealt with thoroughly. The various tasks of building engineering, the diversified problems of the construction itself have got a high significance through the discussion.

The author's experiences collected during his long professional activity of three decades are summarized successfully in this work. He presents his observations in an exciting and convincing way demonstrating them with valuable illustrations, colouring the discussion several times by witty quotations.

The wealthy treasury of his experiences is valuable not only for the specialists dealing with the design of load-bearing structures, but also for those working in other fields of architectural engineering.

P. Csonka

Gy. Márkus: Kreis- und Kreisringplatten unter periodischer Belastung. (Periodically loaded circular and annular.) Akadémiai Kiadó Budapest – Werner-Verlag Düsseldorf 1986. 415 pages, 224 Figures, 115 Tables

In structural building, problems are often encountered where determination of the strain and the cross-sectional forces of circular or annular plates is required. These problems are usually rather complex problems, and no direct aid to solve them, or if indeed at all, then only in the simplest cases, is found in the literature. In engineering practice, technical books presenting data in the form of a repertory or tables for use by the designing engineer are therefore rather valuable. The author's two earlier books have been designed for this very purpose, one titled 'Theorie und Berechnung rotations-symmetrischer Bauwerke' 1967, 1976, 1978 (Theory and calculation for rotationally symmetric structures) dealing with loads of different types acting upon circular and annular plates while another work titled 'Kreis- und Kreisringplatten unter antimetrischer Belastung' 1973 (Antimetrically loaded circular and annular plates) discussing antimetrically loaded circular and annular plates. A recently issued monograph of large format (21x23 cm) of the author is a valuable aid in solving problems concerning periodically loaded circular and annular plates.

In this book, discussion is based on the well-known Kirchhoff theory of plates. The Kirchhoff formulae as well as the solution of problems discussed in the book are presented in a dimensionless polar co-ordinate system by the author. Included in the discussion are the different types of load and support important from a practical point of view, among them the problems where the loads are acting only upon some parts of the surface, or some line sections, or only upon some points, of the plate.

Described in the book after preface and introduction are the different symmetric, antimetric, and simple trigonometric load systems taken into consideration, and then the periodical load systems that can be described by infinite trigonometric series. The author gives a particular solution of the differential equation of the circular plate for these load systems, com-

BOOK REVIEWS

pleted with appropriate independent solutions of the homogeneous differential equation to produce a general solution of the inhomogeneous differential equation. The solutions presented contain the formulae for strain and cross-sectional forces of the circular plate.

Utilizing all these results, the author gives actual examples for circular and annular plates which are important from a practical point of view. From among the rotationally symmetric problems, he deals only with the force uniformly distributed in the central area and/or with the case of plates loaded by concentrated force while concerning other types of load, reference is made to the author's earlier works, similarly to the case of antimetric load where only the case of concentrated couple acting upon the central area is discussed. A detailed analysis of the periodically loaded circular plate case is given for types of load that can be described by a trigonometric function, and the accurate and/or approximate solution for the different types of load is presented in the form of infinite and/or finite Fourier series. The same method is applied also to the case of circular and annular plates as well circular sector shaped and annular sector shaped plates periodically loaded along the periphery. The problem of circular and annular plates periodically loaded along the periphery including, among others, plates upon which a concentrated force or couple is acting in an arbitrary point is discussed separately. The discussion is extended to the problem of circular plates combined with the supports in a cantilever-type structure upon which a concentrated force or couple is acting in an arbitrary point. Also the dynamic behaviour of the circular plate supported in three points is thoroughly studied for the different types of load.

In simpler cases, strain and cross-sectional force formulae ready for use in the discussed problem are presented while in other cases, the integration constants required to determine them and in more complicated cases, equations that can be used to determine the constants are given in the book. The discussion is backed up by curves indicating the changes of cross-sectional forces as well as with Figures illustrating the strains. In case of complex problems, Figures showing the superposition of the different steps of calculation picture the calculation procedure demonstratively.

In the book, the Tables containing ready solutions worked out for the different problems are rather practicable. Tabulated in them are data of strain, and values of moments, of the plate in radial and arc direction in four subsequent rows each. The layout of the Tables is identical, permitting the complex problems to be discussed as a combination of the different partial problems.

The book with its rich content, clear-cut treatment of the problems, and valuable Tables is a fundamental work for engineering practice. To write it, and to work out the rather involved formulae and the Tables (the latter containing more than 60 000 numerical data), the author had to take an arduous work in hand, to make rather sophisticated calculations and to work out different computer programs. Success attended all these efforts: the book was a significant contribution to international literature on plates.

Edition of the book also in English would be desirable.

P. Csonka

G. Reinelt: 'The Linear Ordering Problem: Algorithms and Applications', volume 8 within series 'Research and Exposition in Mathematics', 160 pages, has been issued by Heldermann, Berlin, in English language.

BOOK REVIEWS

In optimization theory, one of the most difficult problems is to find some integer solution and within this, a solution of value 0-1. Combinatorial optimization with linear ordering is a method suited to solve problems like this.

Using the graph theory, the linear ordering problem of combinatorial optimization can be formulated, as follows: for given directed complete graph of weighted edge, a non-circuital spanning 'tournament' has to be defined.

A number of practical problems can be treated as a linear ordering problem. Such a problem is scheduling a machine with restrictions concerning priority in activities organisation, investigation of individual interests in market research, triangulation of input-output matrices in economics, ranging combined comparisons on sociology, evaluation of results of single combats in sports.

In G. Reinelt's monography, first a brief mathematical introduction is given (graph, polyeder, and complexity theory), and then the use of a polyedric combinatorial method to solve the linear ordering problem is recommended. On the basis of recent results of investigation of polytope plane structure assigned to the problem, after introduction of the notion of hyperplane defined by the system of inequalities of the linear ordering polytope, the algorithm of the intersecting planes can be produced. With this embedded in a ramification and separation process tree, a computer-aided solution applicable to the actual triangular problem dissimilarly to earlier approaches can be given.

Also different examples are given in the book, among others, for beer popularity investigations, for evaluation of the results of a football championship with a higher accuracy than usually.

The book has been designed for use in different fields of sciences where the apparatus of applied mathematics is used, first of all for economists.

I. Vágó

Gy. Vértes: Structural Dynamics. Akadémiai Kiadó, Budapest, 1986

The author wrote a book consisting of an introductory chapter and two additional chapters worked out in detail.

In Chapter 1, the different dynamic loads and impacts are defined, and then the effect of dynamic load on the physical properties of steel, concrete, and reinforced concrete is briefly analyzed.

In Chapter 2, first the one-degree-of-freedom system is studied. Discussed in this relation are the free and excited vibrations, both damped and undamped. In the discussion of excited vibration, the author deals with excitation by harmonic forces, vibration due to pulse, and excitation by forces of arbitrary time function. Included in the discussion of damping are viscous damping (damping proportionally to velocity) and the method of taking into consideration frequency-independent internal friction. Also an example for the vibration of the one-degree-of-freedom system of nonlinear rigidity and nonlinear damping (non-proportional to velocity), and another example for calculation of the elasto-plastic one-degree-of-freedom system for impulsive load are given in the book.

After the one-degree-of-freedom system, the two-degree-of-freedom system is studied and formulae are found for calculation of the natural angu-

BOOK REVIEWS

lar frequencies and vibrational modes. Also excited, undamped vibration of the system of two degrees of freedom is discussed by the author.

Multimass systems are studied in the same Chapter. For a system with discrete mass points (diagonal matrix), free vibration is investigated, with also the orthogonal properties of eigenvectors included in the investigation to show how the system can be decomposed into one-degree-of-freedom subsystems in the knowledge of the eigenvectors. Excitation by harmonic forces is discussed, then directions to take into consideration viscous damping are given. Also the effect of internal friction is studied.

Vibrations studies of a beam of constant cross section, considered to be a continuum, and the use of energy methods for vibrations studies are then presented. Example is given for the use of the Rayleigh and Rayleigh-Ritz method. From among methods available for the investigation of dynamic systems, the method of transfer matrices and its application to both free vibration and excitation by harmonic forces is discussed, then the author changes over to bar structure studies, discussing the use of the matrix-displacement method for calculation. The consistent mass matrix of bar structures, derived with the bending inertia taken into consideration, is presented.

Chapter 3 of the book deals with dynamic calculations for structures. Calculation models are shown to calculate the natural frequencies associated with horizontal vibrations for tower houses with frame and reinforcement wall as well as with a mixed supporting structure.

The problem of testing of structures for aerodynamical effects is briefly treated. The author deals with aerodynamical instability and speaks of what has to be known on Kármán's vortices.

In the book, the reader can read of vibrations dangerous to the building as well as on the effect of vibrations on human organism.

In the different chapters, the author gives first the fundamental relationships and elements before going into detailed discussion. Thus the book is a practicable aid in university studies and for engineers involved in dynamic problems. At the same time, the book offers aid also in practical problems. References to literature contribute to a thorough study of the different problems.

J. Györgyi

PRINTED IN HUNGARY
Akadémiai Kiadó és Nyomda, Budapest

NOTICE TO CONTRIBUTORS

Papers in English* are accepted on condition that they have not been previously published or accepted for publication.

Manuscripts in two copies (the original type-written copy plus a clear duplicate one) complete with figures, tables, and references should be sent to

Acta Technica
Münnich F. u. 7. I. 111 A
Budapest, Hungary
H-1051

Although every effort will be made to guard against loss, it is advised that authors retain copies of all material which they submit. The editorial board reserves the right to make editorial changes.

Manuscripts should be typed double-spaced on one side of good quality paper with proper margins and bear the title of the paper and the name(s) of the author(s). The full postal address(es) of the author(s) should be given in a footnote on the first page. An abstract of 50 to 100 words should precede the text of the paper. The approximate locations of the tables and figures should be indicated on the margin. An additional copy of the abstract is needed. Russian words and names should be transliterated into English.

References. Only papers closely related to the author's work should be referred to. The citations should include the name of the author and/or the reference number in brackets. A list of numbered references should follow the end of the manuscript.

References to periodicals should mention: (1) name(s) and initials of the author(s); (2) title of the paper; (3) name of the periodical; (4) volume; (5) year of publication in parentheses; (6) numbers of the first and last pages. Thus: S. Winokur, A., Gluck, J.: Ultimate strength analysis of coupled shear walls. *American Concrete Institute Journal* 65 (1968), 1029-1035.

References to books should include: (1) author(s) name; (2) title; (3) publisher; (4) place and year of publication. Thus: Timoshenko, S., Gere, J.: *Theory of Elastic Stability*. McGraw-Hill Company, New York, London 1961.

Illustrations should be selected carefully and only up to the necessary quantity. Black-and-white photographs should be in the form of glossy prints. The author's name and the title of the paper together with the serial number of the figure should be written on the back of each print. Legends should be brief and attached on a separate sheet. Tables, each bearing a title, should be self-explanatory and numbered consecutively.

Authors will receive proofs which must be sent back by return mail.

Authors will receive 50 reprints free of charge.

*Hungarian authors can submit their papers also in Hungarian.

Periodicals of the Hungarian Academy of Sciences are obtainable
at the following addresses:

AUSTRALIA

C.B.D. LIBRARY AND SUBSCRIPTION SERVICE
Box 4886, G.P.O., *Sydney N.S.W. 2001*
COSMOS BOOKSHOP, 145 Ackland Street
St. Kilda (Melbourne), Victoria 3182

AUSTRIA

GLOBUS, Höchstädtplatz 3, *1206 Wien XX*

BELGIUM

OFFICE INTERNATIONAL DES PERIODIQUES
Avenue Louise, 485, *1050 Bruxelles*
E. STORY-SCIENTIA P.V.B.A.
P. van Duyseplein 8, *9000 Gent*

BULGARIA

HEMUS, Bulvar Ruszki 6, *Sofia*

CANADA

PANNONIA BOOKS, P.O. Box 1017
Postal Station "B", *Toronto, Ont. M5T 2T8*

CHINA

CNPICOR, Periodical Department, P.O. Box 50
Peking

CZECHOSLOVAKIA

MAD'ARSKA KULTURA, Národní třída 22
115 66 Praha
PNS DOVOZ TISKU, Vinohradská 46, *Praha 2*
PNS DOVOZ TLAČE, *Bratislava 2*

DENMARK

EJNAR MUNKSGAARD, 35, Nørre Søgade
1370 Copenhagen K

FEDERAL REPUBLIC OF GERMANY

KUNST UND WISSEN ERICH BIEBER
Postfach 46, *7000 Stuttgart 1*

FINLAND

AKATEEMINEN KIRJAKAUPPA, P.O. Box 128
00101 Helsinki 10

FRANCE

DAWSON-FRANCE S.A., B.P. 40, *91121 Palaiseau*
OFFICE INTERNATIONAL DE DOCUMENTATION ET
LIBRAIRIE, 48 rue Gay-Lussac
75240 Paris, Cedex 05

GERMAN DEMOCRATIC REPUBLIC

HAUS DER UNGARISCHEN KULTUR
Karl Liebknecht-Straße 9, *DDR-102 Berlin*

GREAT BRITAIN

BLACKWELL'S PERIODICALS DIVISION
Hythe Bridge Street, *Oxford OX1 2ET*
BUMPUS, HALDANE AND MAXWELL LTD.
Cowper Works, *Olney, Bucks MK46 4BN*
COLLET'S HOLDINGS LTD., Denington Estate,
Wellingborough, Northants NN8 2QT
WM DAWSON AND SONS LTD., Cannon House
Folkstone, Kent CT19 5EE
H. K. LEWIS AND CO., 136 Gower Street
London WC1E 6BS

GREECE

KOSTARAKIS BROTHERS INTERNATIONAL
BOOKSELLERS, 2 Hippokratous Street, *Athens-143*

HOLLAND

FAXON EUROPE, P.O. Box 167
1000 AD Amsterdam
MARTINUS NIJHOFF B. V.

Lange Voorhout 9-11, *Den Haag*
SWETS SUBSCRIPTION SERVICE
P.O. Box 830, *2160 Sz Lisse*

INDIA

ALLIED PUBLISHING PVT. LTD.
750 Mount Road, *Madras 600002*
CENTRAL NEWS AGENCY PVT. LTD.
Connaught Circus, *New Delhi 110001*
INTERNATIONAL BOOK HOUSE PVT. LTD.
Madame Cama Road, *Bombay 400039*

ITALY

D. E. A., Via Lima 28, *00198 Roma*
INTERSCIENTIA, Via Mazzè 28, *10149 Torino*
LIBRERIA COMMISSIONARIA SANSONI
Via Lamarmora 45, *50121 Firenze*
SANTO VANASIA, Via M. Macchi 58
20124 Milano

JAPAN

KINOKUNIYA COMPANY LTD.
Journal Department, P.O. Box 55
Chitose, Tokyo 156
MARUZEN COMPANY LTD., Book Department
P.O. Box 5050 Tokyo International, *Tokyo 100-31*
NAUKA LTD., Import Department
2-30-19 Minami Ikebukuro, *Toshima-ku, Tokyo 171*

KOREA

CHULPANMUL, *Phenjan*

NORWAY

TANUM-TIDSKRIFT-SENTRALEN A.S.
Karl Johansgata 43, *1000 Oslo*

POLAND

WĘGIERSKI INSTYTUT KULTURY
Marszałkowska 80, *00-517 Warszawa*
CKP I W, ul. Towarowa 28, *00-958 Warszawa*

ROUMANIA

D. E. P., *Bucuresti*
ILEXIM, Calea Grivitei 64-66, *Bucuresti*

SOVIET UNION

SOYUZPECHAT — IMPORT, *Moscow*
and the post offices in each town
MEZHDUNARODNAYA KNIGA, *Moscow G-200*

SPAIN

DIAZ DE SANTOS Lagasca 95, *Madrid 6*

SWEDEN

ESSELTE TIDSKRIFTSCENTRALEN
Box 62, *101 20 Stockholm*

SWITZERLAND

KARGER LIBRI AG, Petersgraben 31, *4011 Basel*

USA

EBSCO SUBSCRIPTION SERVICES
P.O. Box 1943, *Birmingham, Alabama 35201*
F. W. FAXON COMPANY, INC.
15 Southwest Park, *Westwood Mass. 02090*
MAJOR SCIENTIFIC SUBSCRIPTIONS
1851 Diplomat, P.O. Box 819074,
Pallas, Tx. 75381-9074
READ-MORE PUBLICATIONS, INC.
140 Cedar Street, *New York, N. Y. 10006*

YUGOSLAVIA

JUGOSLOVENSKA KNJIGA, Terazije 27, *Beograd*
FORUM, Vojvode Mišića 1, *21000 Novi Sad*